Sub-Regimes of Vertical Two Phase Annular Flow

by

John Robert Nichol

A thesis submitted in partial fulfillment of the requirements for the degree of

Doctor of Philosophy

in

Petroleum Engineering

Department of Civil and Environmental Engineering
University of Alberta

Abstract

A convenient method to calculate pressure drop in wells producing natural gas with some water or hydrocarbon liquids is desired in order to design the initial well completion and to consider the technical and economic benefits of a subsequent intervention to extend the operating life of the well. In a laboratory flow loop, air and water have been used as fluid proxies to study two-phase behaviour.

Concurrent upward air-water flow has been measured in a 26.1mm internal diameter vertical test section at standard conditions over a range of superficial air and liquid velocities. Several sub-regimes of annular flow were newly observed or refined (pulse/disturbance wave, ripple-wave, partial-wetting, and rivulet) with both still and high speed video images recorded externally. The pressure gradients measured were consistent with previous work under similar conditions.

The liquid film within the pipe was examined through Planar Laser Induced Fluorescence (PLIF) imaging, measuring film thickness over a selected range of air and water flow rates. In addition, the onset of droplet entrainment has been observed directly. This data has enabled a new detailed map of sub-regime boundaries to be proposed. Most models for annular flow incorporate a single correlation for interfacial friction without regard to the annular sub-regimes. By observation of computed friction factor and relative roughness data, it is found that the annular region can be represented with three zones of distinct behaviour.

In non-entrained flow at high superficial gas Reynolds numbers (Re_{sg} >35,000) and laminar superficial liquid Reynolds number (Re_{sl} <250) the liquid film exhibits constant relative roughness for a given liquid input. A correlation was derived for superficial gas friction factor as a function of Re_{sl} alone. For entrained flow with Re_{sg} >35000 and Re_{sl} > 250, the film shows relative roughness decreasing as gas rate increases. Another correlation for superficial gas friction factor were derived as a function of both Re_{sl} or Re_{sg}. Pressure gradients calculated with the new correlations compared well against the experimental database as well as with applicable published data. A third zone (Re_{sg} <35,000), close to churn flow regimes, was not amenable to this approach.

Preface

Some of the results in Section 5 were originally presented at the 10th North American Conference, Multiphase 2016 in Banff, Alberta as “Observations of Sub-Regimes in Vertical Annular Flow” by J.R. Nichol and E. Kuru.

Dedication

This work is dedicated to my wife Tanice, who is waiting very patiently for the completion of this work!

Acknowledgements

"I love deadlines. I love the whooshing sound they make as they go by."

Adams, D. (2002). *The salmon of doubt : Hitchhiking the galaxy one last time*. New York: Harmony Books.

This journey began in 2009 when as a part-time student I took the course PET E 632, Multiphase Flow taught by Dr. Petre Toma. Although the journey itself has been most enjoyable, after receiving two extensions the Faculty of Graduate Studies and Research has reminded me on several occasions that reaching a destination is also important.

Thanks are due to Dr. Ergun Kuru both in his role as academic supervisor and as mentor throughout the duration of this research program.   Dr. Kuru supported the equipment modifications and purchases necessary to complete this work. I am also very grateful for the early encouragement of Dr. Petre Toma during our "cappuccino conferences."

The support of Mr. Todd Kinnee was essential in this program, without whom the flow loop modifications and repairs would not have happened.

Thanks to my research cohort in the lab: Dozhan Mamedulanov first conducted PLIF studies on the vertical loop and shared his insights into the equipment setup. Advice was also shared by Majid Bhirani, and Hossein (Zane) Zeinali out of their horizontal flow loop experience. Thanks as well to Sumanth Arnipally for allowing me to observe his experiments and for coordinating the shared laser and camera equipment. Dr. Aziz Rahman, and Dr. Sina Ghaemi have provided invaluable advice on PLIF methods.

Finally, I am grateful for the assistance of a cadre of enthusiastic student volunteers: Jae Cheol Lee, Khalid Ahmad, Jad Faddoul, Joseph Odugbesan, and Jackie Zhang.

Table of Contents

List of Tables

List of Figures

List of Symbols and Abbreviations (with nominal units)

A	Cross-sectional area [m^2]
d	pipe diameter [m]
E, FE	entrainment fraction
f	friction factor
g	gravity [9.8065m/s^2]
G	mass velocity [kg/m2-s]
H	holdup
i.d.	inside diameter [m]
j	velocity [m/s]
j*	dimensionless velocity
L, l	length [m]
m	mass [kg]
$\dot{m}$	mass flow rate [kg/s]
M	molecular weight [kg/kg-mol.]
mscfd	thousand standard cubic feet per day
Re, N_{Re}	Reynolds number
P, p	pressure [Pa or kPa or kPaa]
p*	dimensionless pressure
Q, q	volumetric flow rate [m^3/s]
r	radius [m]
R	universal gas constant [8.3145 kPa m^3/kg-mole K]
S	saturation, perimeter [m]
T	temperature [K or °C]
U, v	velocity [m/s]
V	volume [m^3]

Greek Symbols

δ	liquid film thickness [m]
ε	pipe absolute roughness [m]
μ	viscosity (dynamic) [Pa-s]
ν	viscosity (kinematic) [m^2/s]
ξ	insitu gas fraction
ρ	density [kg/m^3]
σ	interfacial tension, [N/m or dyne/cm]
τ	shear stress [Pa/m]

Subscripts

A, air	air
c	core
f	film, fluid
F	Fanning
G, g	gas
i	interfacial
L, l	liquid
LC	liquid in core
LF	liquid in film
m	mixture
M	Moody
p	pipe
SG, sg	superficial gas
SL, sl	superficial liquid
TP	two phase
w	water, wall
wirr	water, irreducible

1 Introduction

1.1 The Thesis

A simplified method can be devised to calculate pressure gradient in vertical wells producing gas with liquids.

1.2 Overview

In the province of Alberta alone, approximately 78% of ultimate conventional natural gas reserves have already been produced, leaving 49 standard billion cubic feet (BCF) for future production and discovery (AER, 2017.) There are becoming fewer discoveries among conventional gas pools and these are coming from smaller gas pools (Fig. 1.1.)

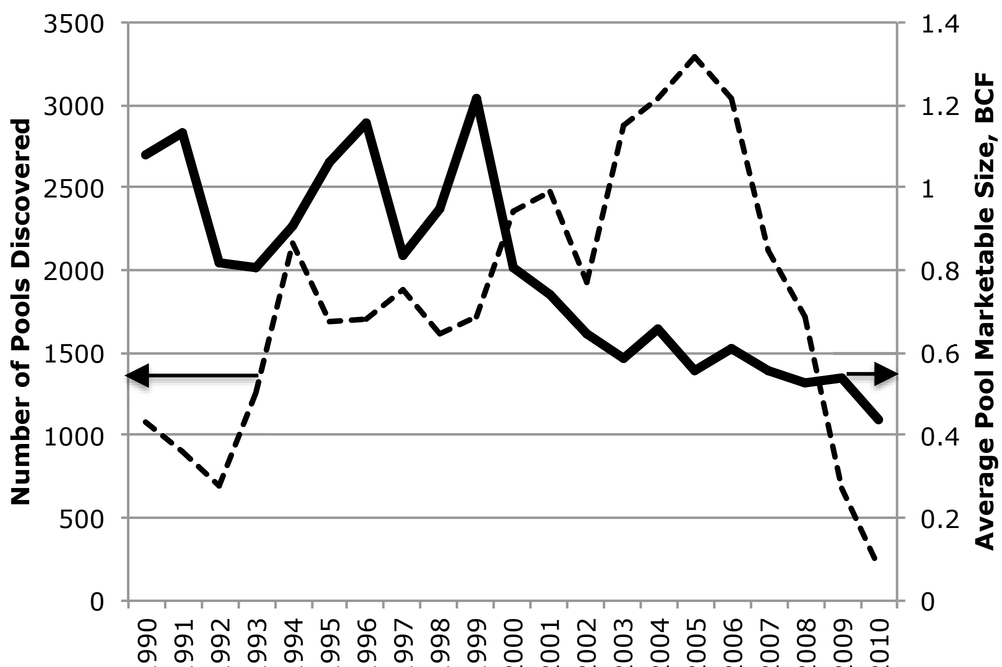

Figure 1.1 Conventional Natural Gas Discoveries in Alberta.

Then energy industry now turns its attention to the tight and unconventional gas resources, including coalbed methane and shale, whose in-place resource is estimated to be 3406 trillion cubic feet (TCF), subject to some uncertain recovery factors.

However, many of these wells will be producing some liquids with the gas. The chief sources of liquid production are:

a) Connate water migration.

b) Water breakthrough or coning.

c) Condensed water or hydrocarbon vapour.

d) Mobile liquid hydrocarbon.

If connate water saturation, S_w, is significantly higher than irreducible water saturation, S_{wirr}, in a reservoir, it is potentially mobile and may be drawn into the wellbore as gas is produced. At high gas rates, the additional drag of turbulent flow may also cause increased water production. Water breakthrough is also a consequence of high production rates: as flowing wellbore pressure is lowered, the pressure gradients in the reservoir may favour movement of water from lower water saturated zones into the wellbore. Fractured formations provide additional flow paths for movement of bottom water. At initial reservoir conditions, water vapour is in equilibrium with the formation gas. As reservoir pressure decreases with production, the amount of water vapour (as measured in water mass per unit standard volume of gas) increases; some of this water vapour condenses as the production stream cools on its way to the surface.

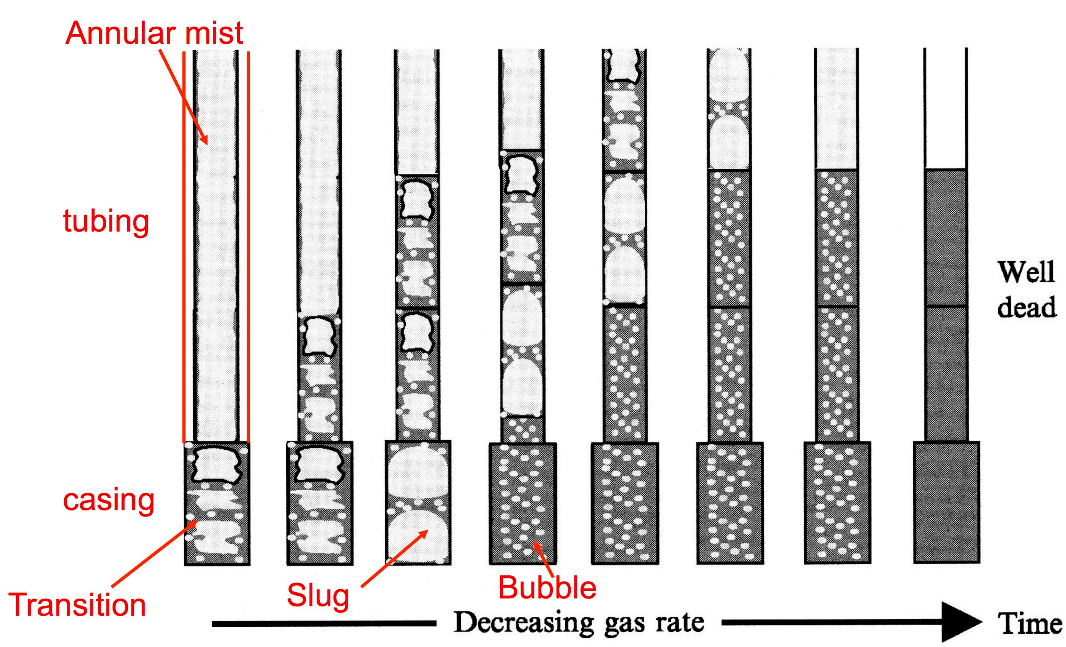

Figure 1.2 Life Cycle of a Gas Well Showing Progression of Flow Regimes.

The presence of liquids in the production string can impair the recovery of gas, in what is commonly referred to as liquid loading. With liquid loading the static and frictional pressure losses in the production tubing increase often resulting in the well "dying" as reservoir pressure declines, as shown in Fig. 1.2, adapted from Lea, Nickens, and Wells (2003). With liquids production, some of the operational responses are illustrated in Fig. 1.3. The path taken will be subject to economic analysis.

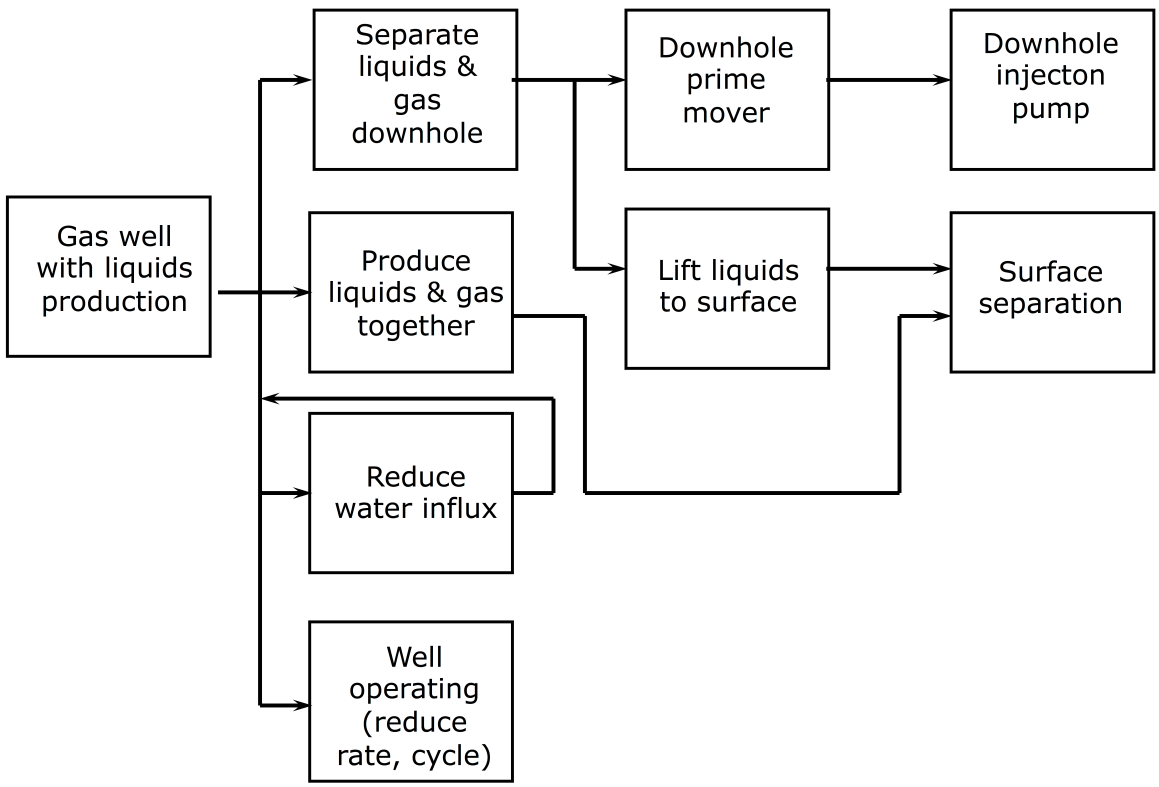

Figure 1.3 Liquid Management Options for Gas Wells.

Downhole separation of gas and water requires a suitable disposal zone and therefore is not widely applicable (Radwan, 2017.) Reducing water influx by deliberately reducing the gas rate is not economically appealing. Another approach is to introduce a viscous material into the reservoir to block the water path, however these treatments can be short lived (Wawro, Wassmuth, and Smith, 2000.) Most operators will implement some form of lift to bring the liquids to surface, especially if hydrocarbon liquids are present, for example:

a) Plunger lift in conventional gas (Ozkan, Keefer and Miller, 2003)

b) Electrical Submersible Pump (ESP) in coalbed methane (Kraweic, Finn, and Cockbill, 2008.)

c) Foam Lift in shale gas (Farina et al., 2012.)

d) Plunger Lift in shale gas (Nascimento, Becze, Virues, and Wang, 2015.)

In order to design an appropriate well completion and to anticipate the onset of liquid loading, the production engineer makes use of software tools to calculate the initial gas flow rate of the well and its decline rate. An incorrect assessment of initial production rate will have immediate economic consequences; it may result in selection of undersized production tubing (which will constrict production rate, hence cash flow) or oversized tubing (unnecessary capital cost.) A reliable decline rate is necessary to determine when liquid loading problems require a change to the well design.

1.3 The Problem

Well behaviour is commonly assessed with nodal analysis, where the inflow characteristics of the reservoir are compared with the outflow of the production tubing. The intersection of the two defines the operation point (flow rate, and bottomhole flowing pressure) of the well. Calculations of pressure gradient in two phase flow are obviously more complex than those for a single phase fluid. A number of correlations are available for the two phase calculation, however their results are far from consistent. For example, Fig. 1.4 shows a typical nodal analysis result generated with the commercially available software SNAP by the Ryder Scott Company. A constant water-gas ratio has been used. Three popular correlations were used to calculate the bottomhole pressure in the production tubing as a function of gas flow rate:

a) Gray (API, 1978)

b) Ansari, Sylvester, Sarica, Shoham, and Brill (1994)

c) Chokshi (1996) and Chokshi, Schmidt and Doty (1996)

In Fig. 1.3 observe that the three outflow correlations give different solutions for the initial gas flow rate. This presents the production engineer with a dilemma. Which correlation is to be believed? What is the uncertainty of the result from a selected correlation?

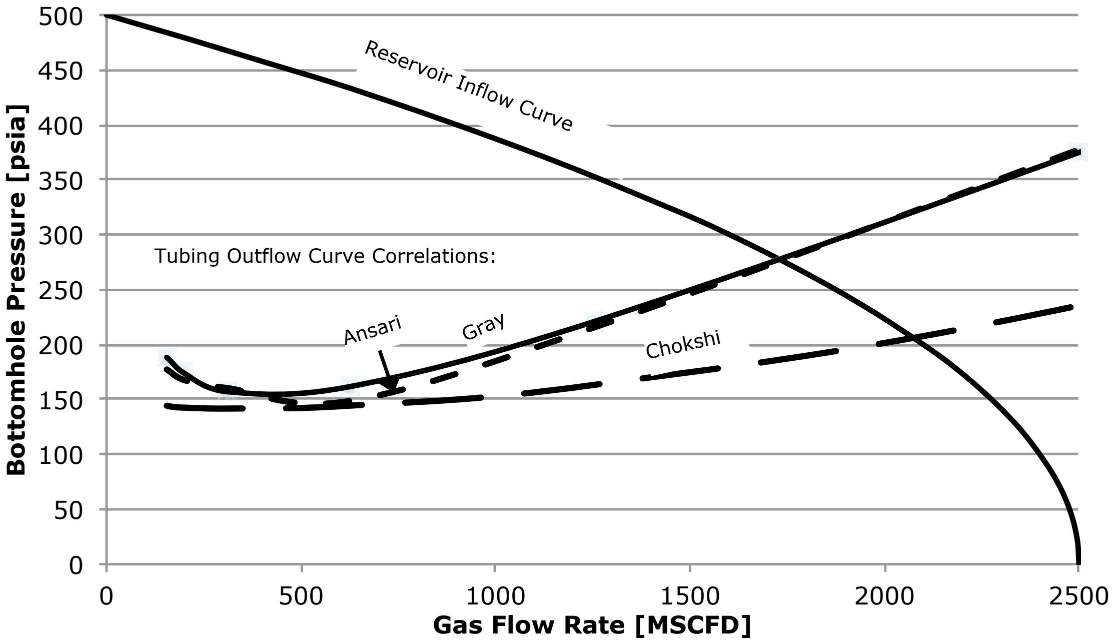

Figure 1.4 Example Nodal Analysis of Gas Well With Different Outflow Correlations.

The differences among the correlations is emphasized in Fig. 1.5. Gray (API, 1978) is excluded because it is very close to the Ansari et al. (1994) results. The range of initial operating rate is between 1730 and 2060 thousand standard cubic feet per day (MSCFD) depending on which model is selected. The SNAP software also calculates the minimum flow rate for liquid loading, which is usually considered to be the minima of the tubing outflow curve. Here the solutions range between 189 and 242 MSCFD. However those two rates will occur at different times in the life of the well and the production engineer must know when to schedule an intervention, such as a workover to install artificial lift. The importance of improving the accuracy of the multiphase correlation and the calculated point of liquid loading is now evident.

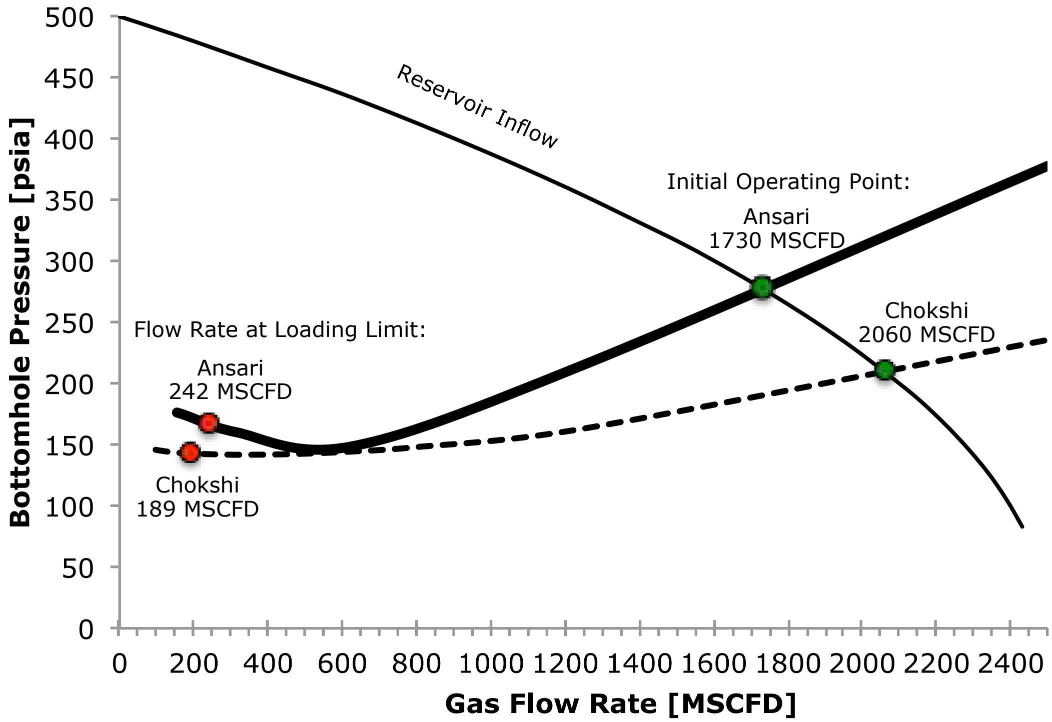

Figure 1.5 Example Nodal Analysis with Initial Operating Point and Loading Limit.

1.4 The Hypothesis

Examining the sub-regimes of annular flow in detail, along with published experimental results will provide insights that lead to new set of predictive models for pressure gradient.

1.5 Scope of Research

Initial work first determined distinct sub-regimes of annular flow vertical wells, based on the possible flow patterns of gas and liquid.

Laboratory experiments with a vertical two phase flow loop will measured a variety of parameters (differential pressure, gas flow rate, liquid flow rate, liquid velocity profile) for a test matrix of gas and liquid rates sufficient to explore each of the posed sub-regimes. The existing flow loop at the University of Alberta was modified to accommodate this work. This flow loop was originally used by Becaria (2004) and Vargas (2006) to study slug to annular transitions in small diameter tubes. The work considered the behaviour of air-water systems at standard conditions. Extensions to the program with different liquids and at elevated pressures is possible.

1.6 Structure of this Thesis

This Section has set out the need for a better understanding of two phase vertical flow. Section 2 delves into the historical work on this issue. In Section 3 the experimental apparatus is described and its operation is outlined in Section 4. The results of the experimental programs are presented in Section 5 along with detailed analysis. A description of new correlations to calculate pressure gradient is presented in Section 6. Section 7 then summarizes the contributions of the work with the requisite recommendations for further work. The Appendices contain supplementary information as required.

2 Background

2.1 Historical Studies of Two-Phase Flow

Historically, the study of two-phase fluid flow has included both qualitative (visualizing the flow patterns of the fluids) and quantitative (pressure, velocity, film thickness, entrainment, etc.) measurements.

Different flow patterns were recognized early on by Versluys (1932) who summarized his notion of multiphase flow that ranges from a continuous liquid phase (the "foam condition," which we would now term bubble flow) to a continuous gas phase (the "mist condition.") His concepts are presented in Fig. 2.1; the dark portions represent liquid and the light portions represent gas.

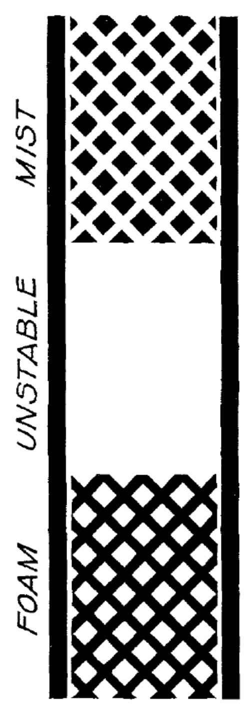

Figure 2.1 Conceptual Depiction of Multiphase Flow in Vertical Pipe.

Versluys also hinted at the structure of an intermediate region, which he considered to be unstable, "The drops or the bubbles are evenly distributed... when they become larger…the shape of a jelly-fish is approached." This is a very clear description of slug flow! Versluys also noted the difference in velocity between the gas and liquid (slip) and the importance of knowing the insitu proportions of the phases (holdup.)

An early combined quantitative and visual study of two-phase flow was performed by Gosline (1938.) Air and water pumping experiments were conducted with a 26 foot long, 1 inch i.d. glass tube. Gosline observed, "As the rate of air flow increased the unsteadiness decreased and finally the flow became quite steady. This steady motion, however, was accompanied by a change in the admixture of air and fluid. The fluid was [then] present in the tube as an annular ring in contact with the tube wall and air moved up through the central portion." This was a description of slug-to-annular flow transition, which was indicated in a graphical presentation of his laboratory measurements as the dashed line (Fig 2.2) The lines indicate conditions of constant submergence ratio, R_s, where,

$$R_s = \frac{liquid\_level\_in\_tube}{liquid\_level\_in\_tube + lift\_height} \tag{2.1}$$

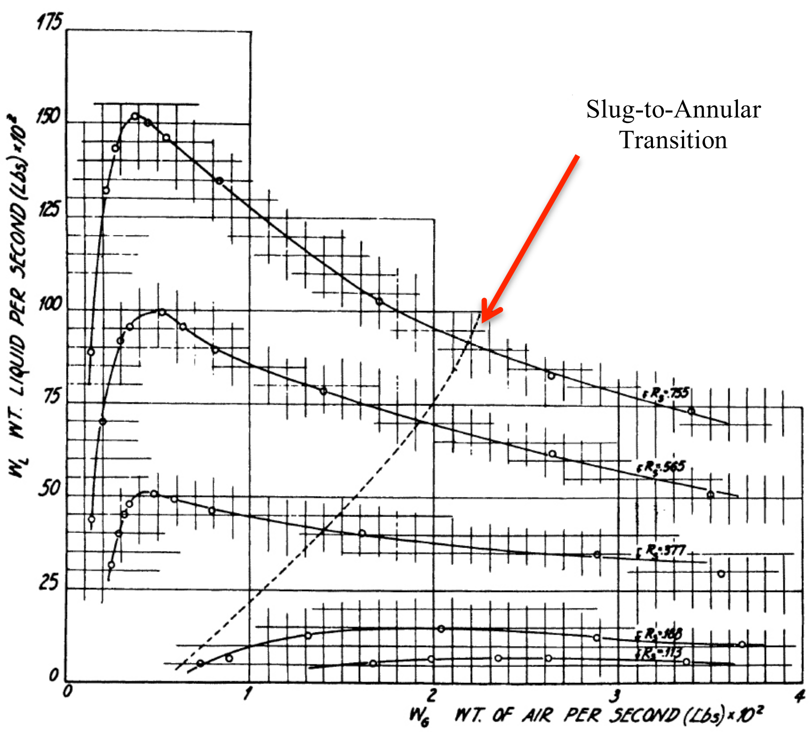

Figure 2.2 Early Quantitative Measurement of Vertical Upward Air-Water Flow. With Flow Pattern Transition Indicated.

Vertical annular flow was also observed and photographed by Cromer and Huntington (1938) through a two foot section of glass pipe atop a suspended 98 foot iron production string. At high air flow rates they observed that, "…the water rippled upward along the sides of the flow tube in the annular ring reported by Gosline." In Fig. 2.3, this annular flow is recorded in a photograph – the glass tube is between two steel supports.

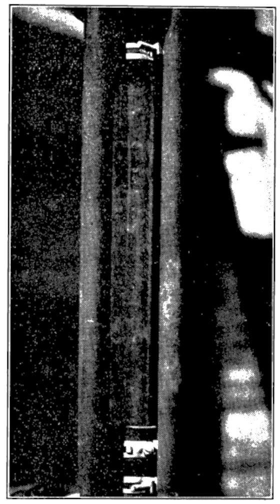

Figure 2.3 Photograph of Annular Flow from Cromer and Huntington (1938).

From their flow loop observations, Calvert and Williams (1955) were able to organize the various two-phase vertical flow patterns by appearance (Fig. 2.4.) These have been refined only slightly over the years. However,he terminology has changed: "bubble" is used instead of "aerated"; "slug" instead of "piston"; and "annular-mist" instead of "drop entrainment."

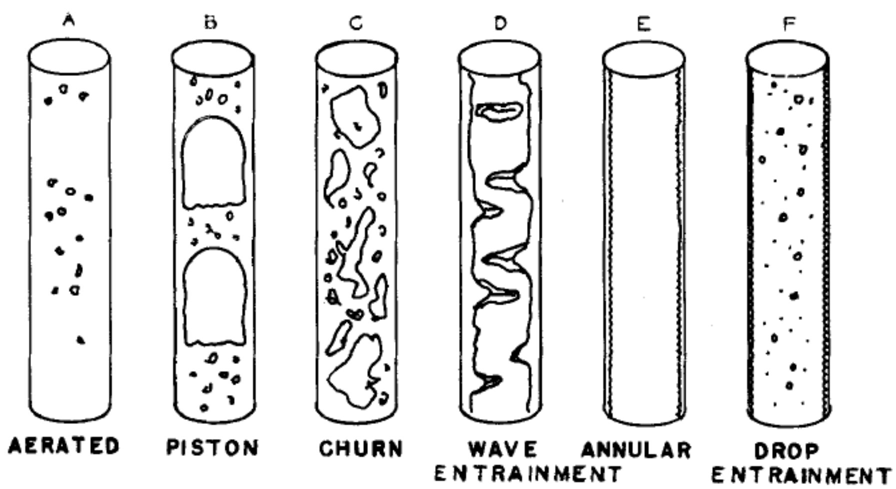

Figure 2.4 Sketch of Vertical Two Phase Flow Patterns from Calvert and Williams (1955).

In Fig 2.4 the annular flow regime is portrayed in two sub-regimes: a true annular arrangement with liquid film and gas core (E); and an entrained configuration with some of the liquid contributing to the gas core (F). Fig 2.5, also from Calvert and Williams (1955) the authors acknowledged the work of Radford (1949) in which established that the pressure gradient could be associated with flow regime transitions. The transition to annular flow in the figure is indicated to occur at approximately at point E, the minima in measured pressure gradient (at a constant water flow rate.)

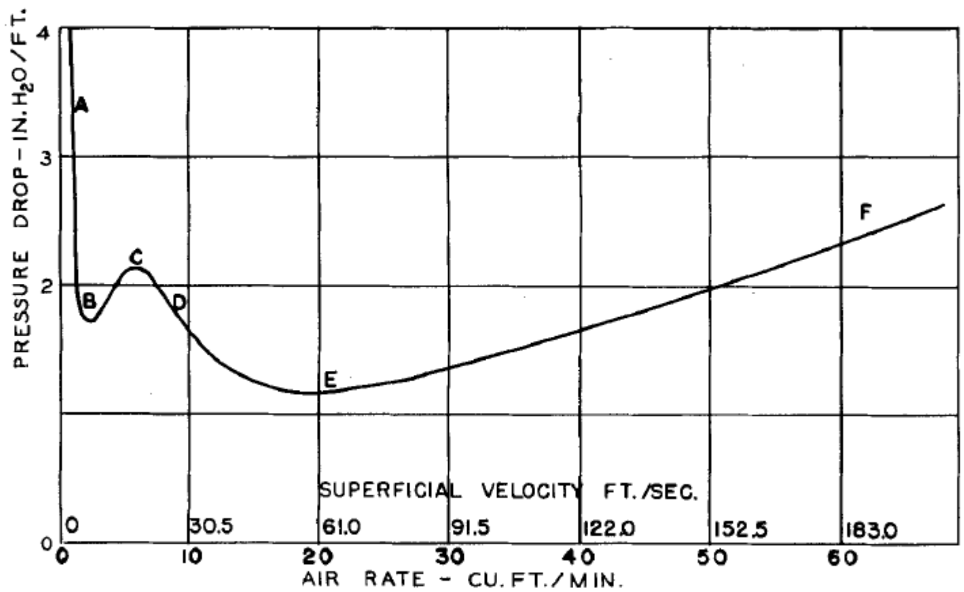

Figure 2.5 Pressure Gradients Associated with Flow Patterns in Fig. 2.4

Advancements in flow visualization have included high-speed motion pictures. Steen and Wallis (1964) photographed annular flow (in the downward direction) to obtain images of the air-water interface. It is notable that their apparatus was designed so that "the air-water interface could be viewed without looking through a water film, a principal difficulty with still films." At the interface they observed "ripple" waves at moderate air flow and then at high air rates, superimposed "roll" waves were seen.

ey associated the appearance of the "roll" waves with the onset of liquid entrainment in the central gas core. In Fig. 2.6, taken at about 2000 frames per second, a roll wave yields a filament of liquid, about to become an entrained droplet. To "see" inside the film itself, early workers employed dye tracers.

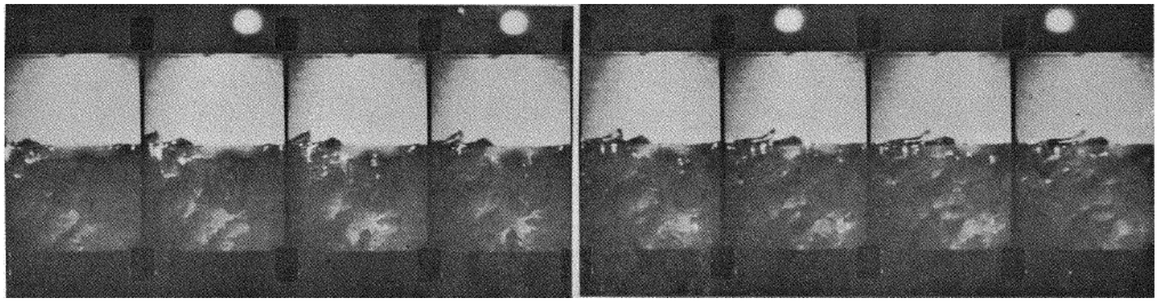

Figure 2.6 High Speed Film of Air-Water Interface.

Ho and Hummel (1970) were able to visualize and quantify a velocity profile of a vertically falling film inside a 28.4mm i.d. glass tube over a range of flow rates. Different alcohol-based fluid mixtures were used. In Fig. 2.7 the dye trace between the inside wall and the air-film interface indicates the velocity profile under laminar conditions. The film Reynolds number is defined as,

$$N_{\mathrm{Re}F} = \frac{4Q}{\nu} \tag{2.2}$$

where Q is volumetric flow rate per unit of wetted perimeter. Photographs of the dye traces were analyzed to obtain velocity distribution within the film itself. The non-linearity at the air-fluid interface was attributed to the influence of surface waves.

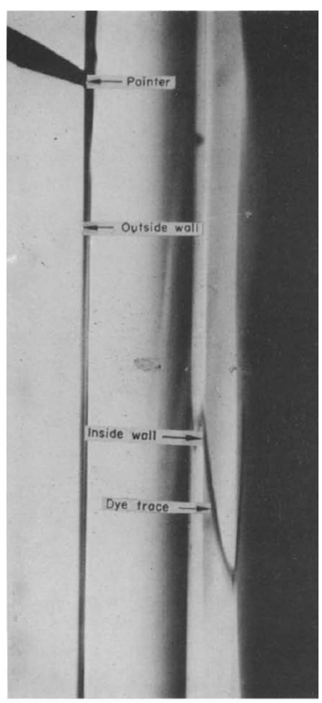

$N_{Re} = 354$

Figure 2.7 Image of Laminar Velocity Profile in Falling Liquid Film.

Later, Hewitt, Jayanti, and Hope (1990) used similar methods obtain a qualitative impression of a developing velocity profile of the liquid film. In a horizontal flow segment, dye was added to the liquid phase. Then laser light was used to illuminate the dye and photograph the gas-liquid interface. While this work was focused on studying the wavy nature of the liquid film, the dye traces also provided the information on the velocity profile within the film itself (Fig. 2.8.)

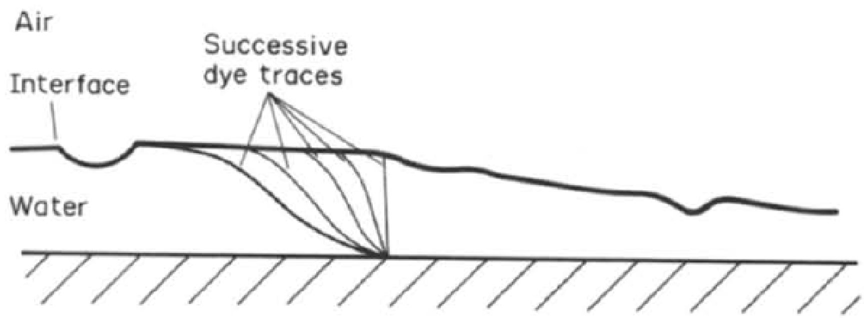

Figure 2.8. Sketch of Liquid Film Velocity Profile.

More recently, the ability to "see through" the liquid film has been enabled through use of a transparent pipe in an optically compatible fluid with using particle image velocimetry (PIV) and planar laser-induced fluorescence (PLIF) techniques. Kopplin (2004) measured the velocity profile within the liquid film in a horizontal annular flow loop with PIV (Fig. 2.9.)

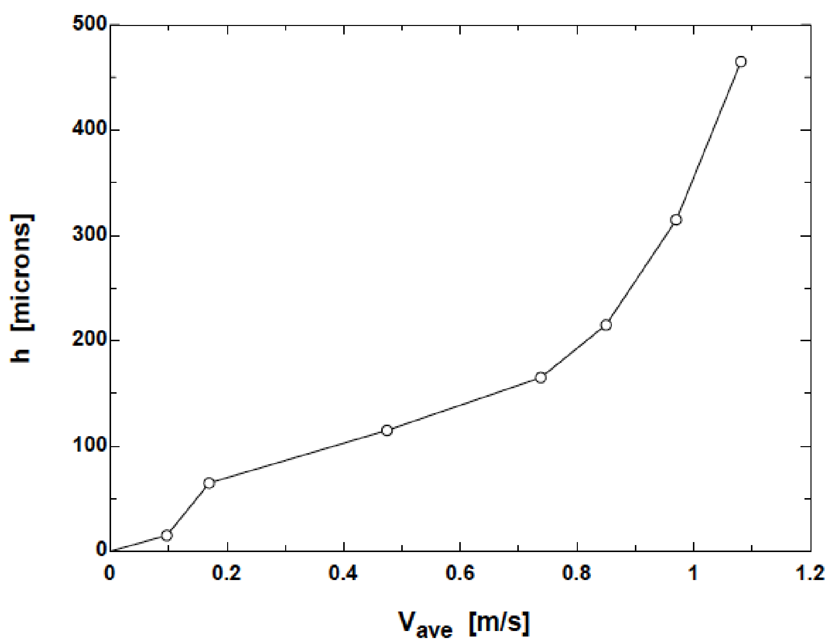

Figure 2.9 Measured Velocity Profile in Horizontal Annular Flow (Bottom of Pipe.)

Employing PLIF, Schubring (2009) was able to trace the surface of the liquid film in upward vertical pipe, as shown in Fig. 2.10 (the liquid film is lighter in colour.) In the figure there are four traces, with the bottom one measured at the highest gas flow rate (and exhibiting the thinnest film.) The window size is about 4mm wide by 0.4mm high.

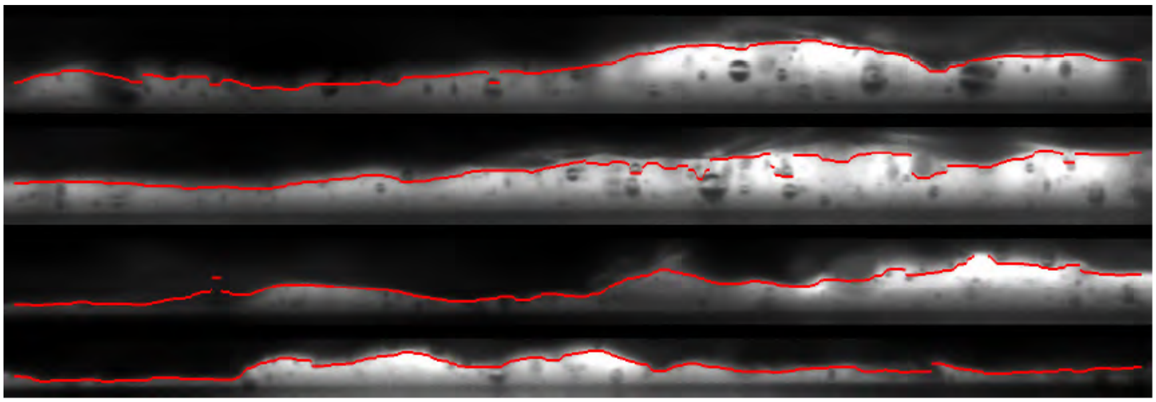

Figure 2.10 Traces of Base Liquid Film in Vertical Annular Flow.

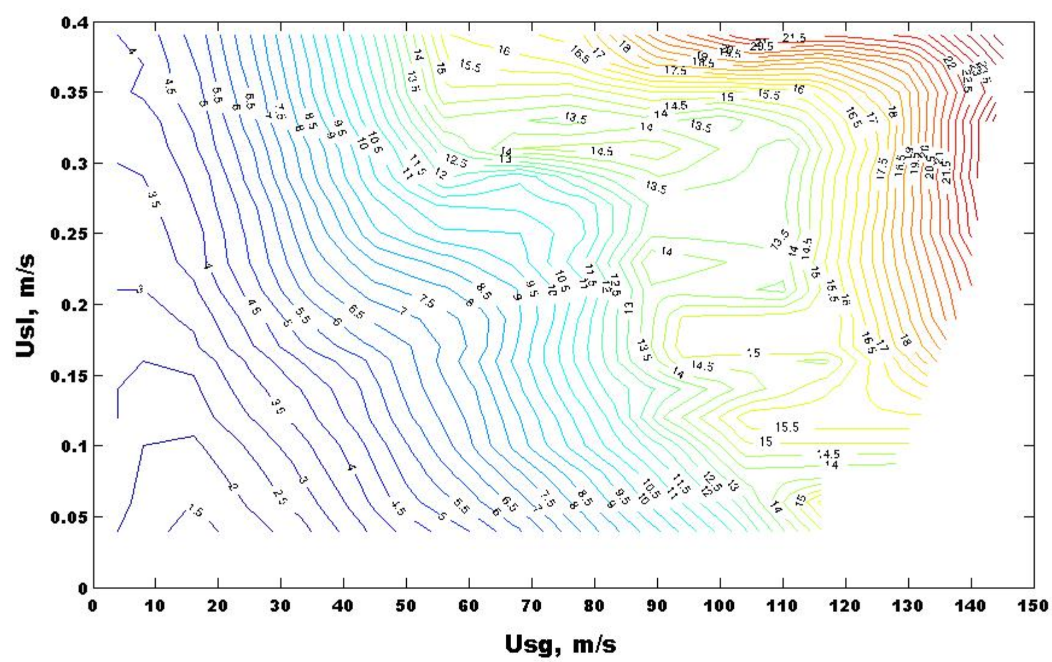

Figure 2.11 Pressure Gradient as a Function of Superficial Velocities.
from Ashwood's data (contour interval 0.5 kPa/m.)

Ashwood (2010) also employed botj PIV and PLIF techniques to measure film thickness and pressure drop in vertical air-water flow with a 23.4mm i.d. quartz tubing. A contour plot of Ashwood's (2010) data, showing the pressure gradient as a function of superficial velocities in vertical tubing is presented in Fig. 2.11. Note that the minimum superficial liquid rate measured by Ashwood (2010) was 0.4 m/s, which therefore does not include the sub-regimes identified by Nedderman and Shearer (1963) or Hall Taylor, Hewitt and Lacey (1963.).

2.2 Flow Regimes

The flow patterns presented by Taitel, Barnea and Dukler (1980) (Fig 2.12) differ very little from those proposed 25 years earlier by Calvert and Williams (1955) in Fig. 2.4.

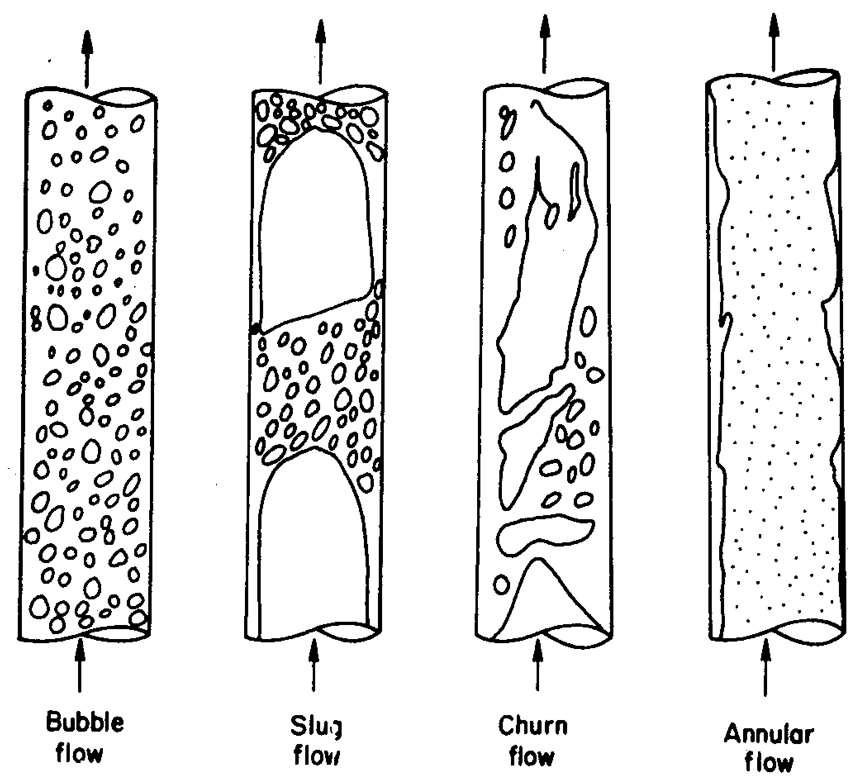

Figure 2.12 Flow Patterns from Taitel, Barnea and Dukler (1980).

Determination of flow regime is through calculated maps, such as that one shown in Fig. 2.13 from Barnea (1987.) This figure is especially useful as it closely the matches the expected conditions for the current work.

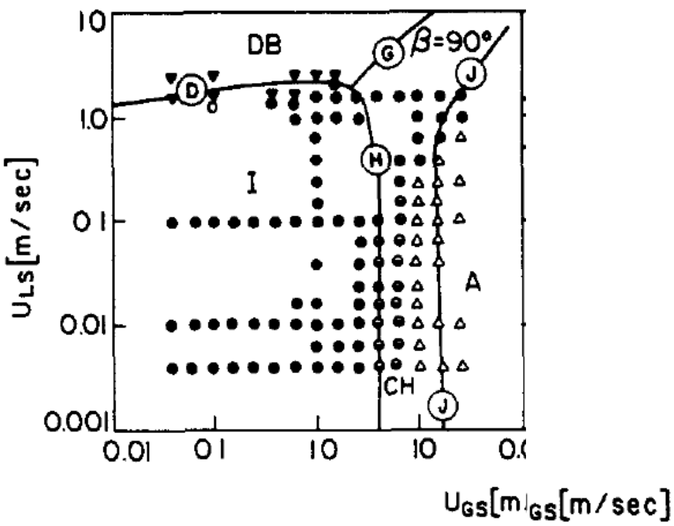

Figure 2.13 Flow Regime Map for Upward Vertical Flow of Air-Water in 2.54cm dia. Tube. at Standard Conditions.

The region of interest in the current work is that of annular flow (the region to the right of transition J in Fig. 2.13.) Transition J is adopted from Turner, Hubbard, and Dukler (1969) (in consistent units):

$$V_{crit} = 5.46\left[\frac{\sigma(\rho_l - \rho_g)}{\rho_g^2}\right]^{1/4} \tag{2.3}$$

At standard conditions for air and water, the Turner et al. (1969) equation (without the recommended 20% upwards adjustment from Coleman, Clay, McCurdy, and Norris (1991)) gives a gas velocity of 14.6 m/s (47.9 ft/s) to commence annular flow. Note that the curvature of Transition J at high superficial liquid velocity is an adjustment proposed by Barnea (1987) to account for film bridging in smaller diameter pipe.

However, the annular flow regime is not amorphous. Hall Taylor et al. (1963) observed several sub-regimes of annular flow in 31.8mm i.d. vertical pipe; their data is redrawn in terms of superficial velocities in Fig. 2.14. The onset of annular flow is about 12 m/s in this case. Note the relatively sparse data collected at low liquid velocity.

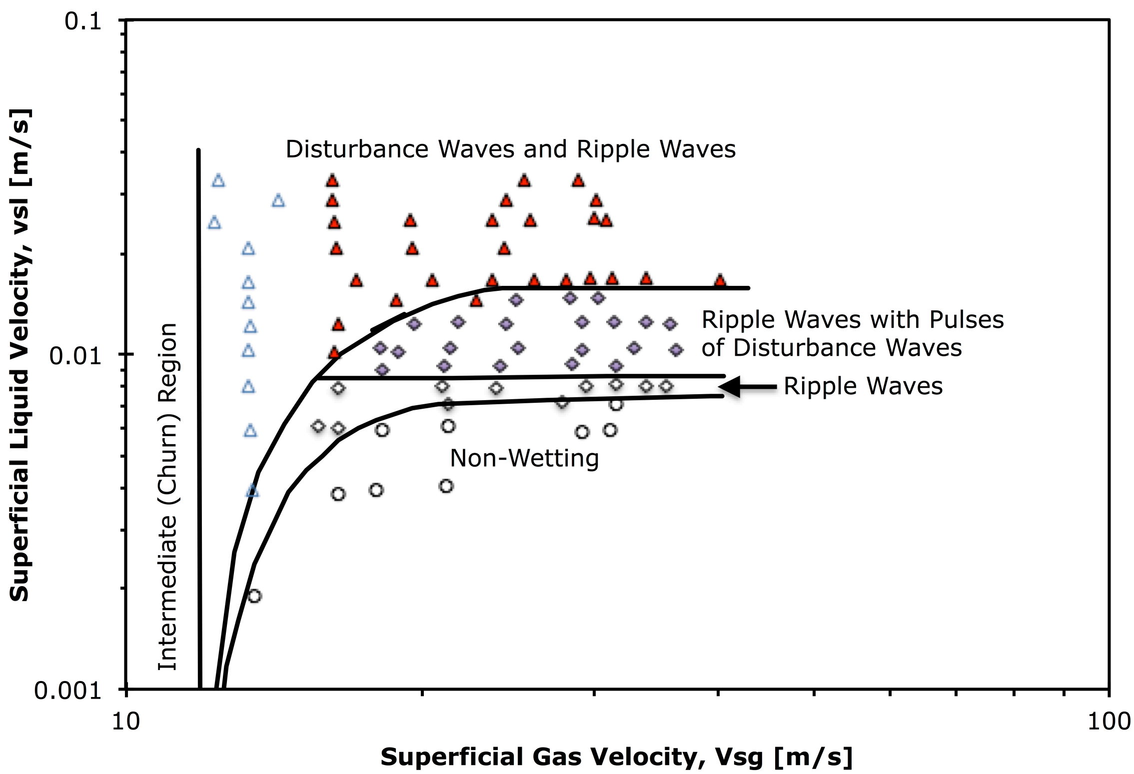

Figure 2.14 Annular Flow Sub-Regime Map of Hall Taylor et al. (1963).

Nedderman and Shearer (1963) defined three annular sub-regimes during experiments near standard conditions with the same pipe size (Fig. 2.15):

a) De-wetted (100% entrainment.)

b) Small ripple waves.

c) Large disturbance waves.

Note in Fig. 2.15 the onset of "de-wetted" flow is read from the graph to be about 48 ft/s, which is the same as to the 14.6 m/s given by the Turner et al. (1969) equation. The condition for small to large ripple wave transition was found to be about the same as given by Hall Taylor et al. (1963). However, the transition to non-wetted flow was different; this was attributed to the differences in wettability to the pipe wall.

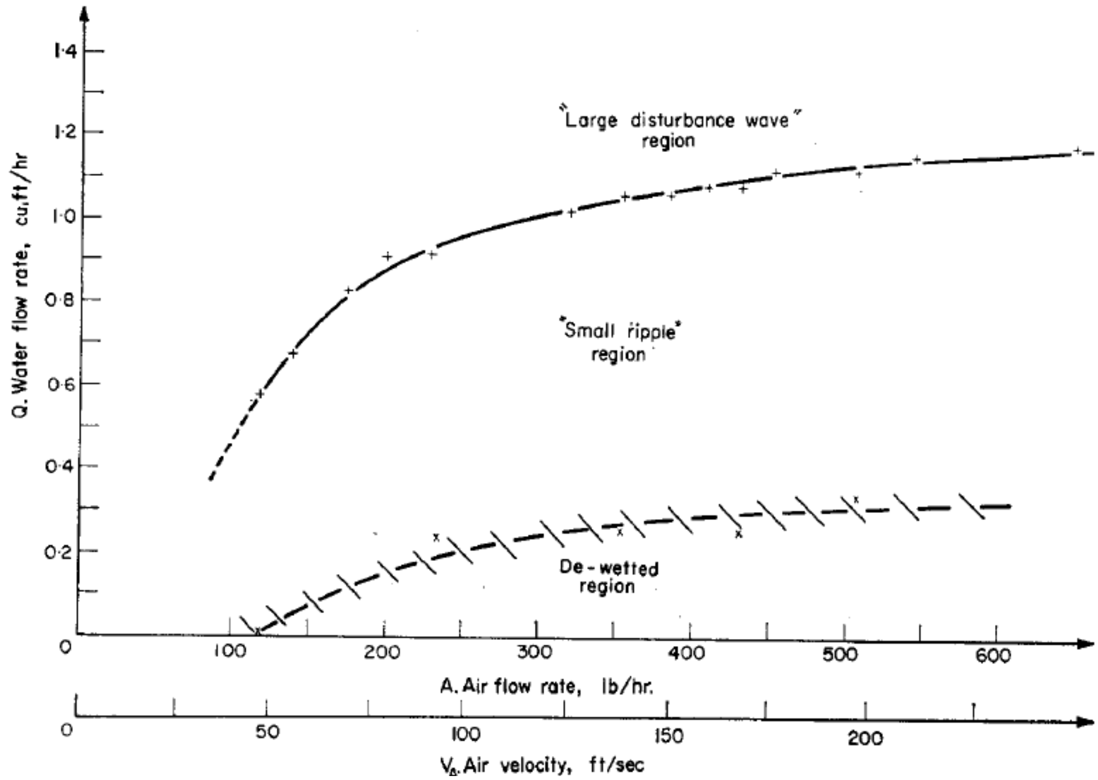

Figure 2.15 Annular Flow Sub-Regime Map of Nedderman and Shearer (1963).

Another example of annular flow sub-regimes is given by Woods, Spedding, Watterson, and Raghunathan, (1999) in Fig. 2.16, based on air-water experiments in 26mm pipe at assumed standard conditions. The initiation of annular flow is given by the equation,

$$[-(H-0.04]\sqrt{V_{sl}}+\sqrt{V_{sg}}=1.48\left[\frac{(g\sigma(\rho_L-\rho_G))^{1/4}}{\rho_g^{1/2}}\right]^{1/2} \tag{2.4}$$

Where H is a Heaviside step function (=0 if V_{sl} is negative, =1 if V_{sl} is positive.) Note the inclusion of a liquid rate term not found in the Turner equation. At very low liquid flow ($V_{sl} << V_{sg}$) the equation simplifies (in consistent units) to a form identical to equation 2.3:

$$V_{sg}=1.48^2\left(\frac{g\sigma(\rho_L-\rho_G)}{\rho_g^2}\right)^{1/4}=3.88\left(\frac{\sigma(\rho_L-\rho_G)}{\rho_g^2}\right)^{1/4} \tag{2.5}$$

The resulting superficial gas velocity at standard conditions with air-water becomes 10.4 m/s.

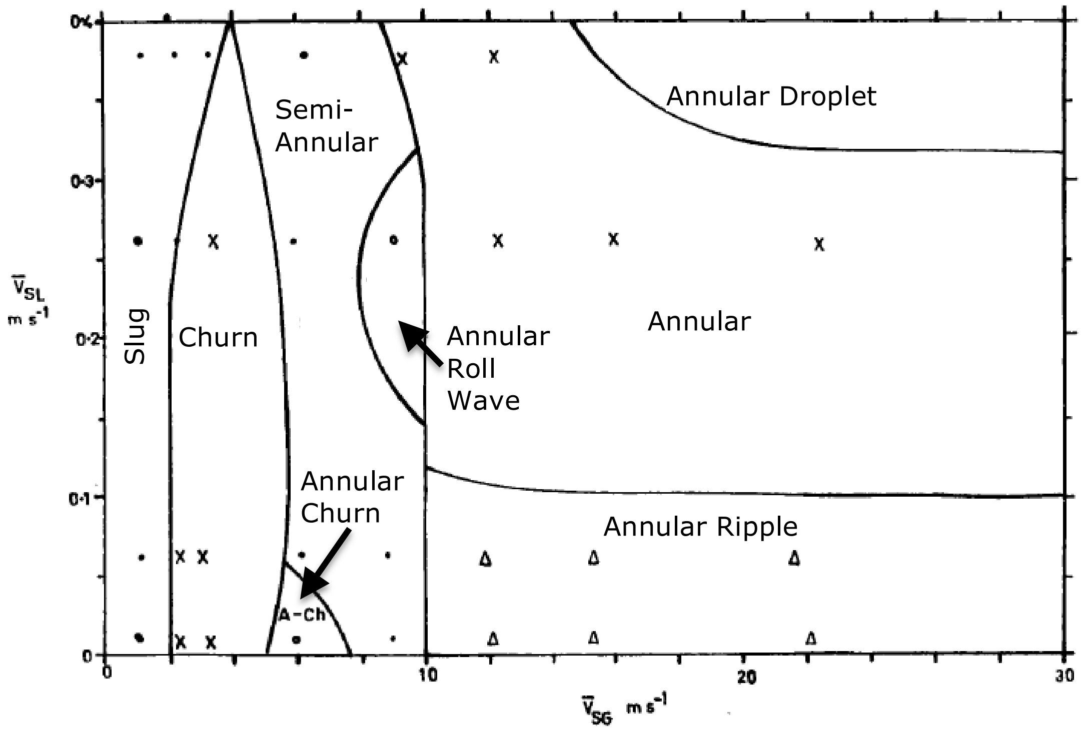

Figure 2.16 Annular Flow Sub-Regime Map of Woods Spedding, Watterson, and Raghunathan (1999).

Note that the maximum superficial liquid velocity explored in Fig. 2.16 is considerably higher than that of Nedderman and Shearer (1963) or Hall Taylor et al. (1963).

2.3 Two-Phase Flow Models

Modelling methods for multiphase flow can be classified very roughly as either homogeneous or mechanistic. In the nodal analysis example presented in Section 1.2, the Gray correlation (API, 1978) is homogeneous, in that no particular flow regime is considered. It has been found to be best suited to vertical natural gas wells producing hydrocarbon liquids (condensate.) The general solution for pressure gradient is

$$\frac{dp}{dl} = g\left[\xi\rho_g + (1-\xi)\right] + \frac{f_{tp}G^2}{2d\rho_m} + \frac{G^2 d}{\rho_m dl} \quad (2.6)$$

where the terms on the right hand side of the equation represent static, frictional and kinetic energy losses respectively. To solve for pressure gradient empirical relationships derived from field data are required first to obtain a value for insitu gas fraction, ξ.

For annular flow, an upward moving film wetting the pipe wall is assumed. It is interesting to note that this was described mechanistically as early as 1955 by Calvert and Williams, as depicted in Fig. 2.17.

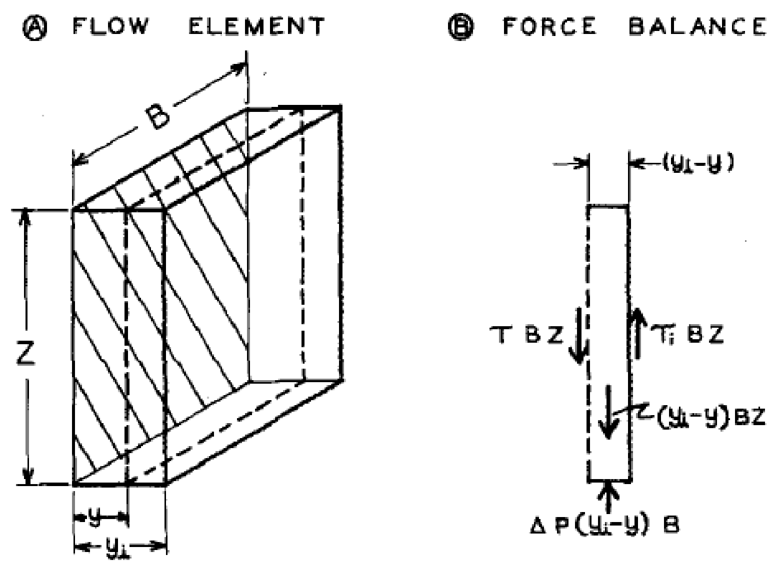

Figure 2.17 Force Balance on Element of Liquid Film in Vertical Annular Flow.

Examples of mechanistic models in use in the petroleum industry are Ansari et al. (1994) and Chokshi et al. (1996). They are part of a progression of models, developed at the University of Tulsa. In chronological order they are: Yao and Sylvester (1987) solving for gas core only; Alves, Caetano, Minami and Shoham (1991), Ansari et al. (1992), Chokshi et al. (1994), and Gomez et al. (1999).

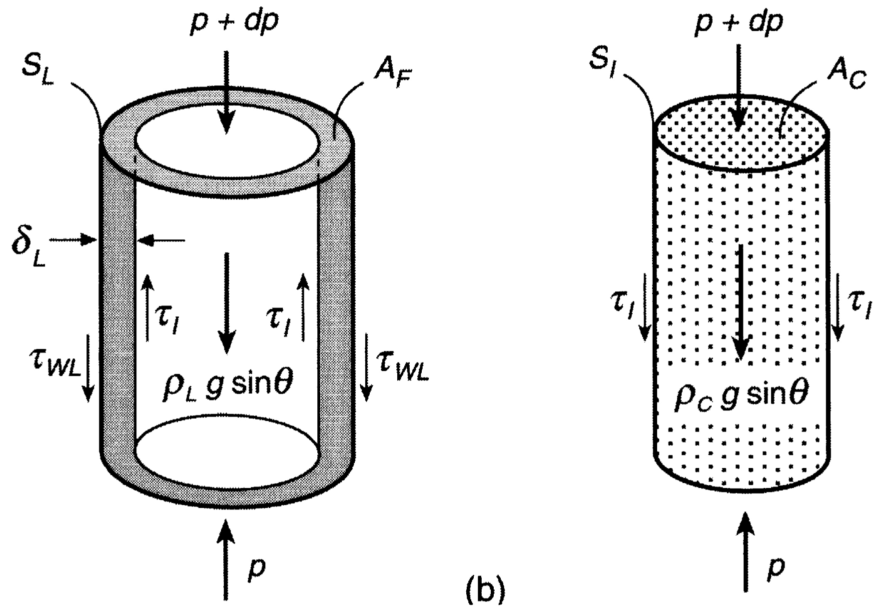

Figure 2.18 Force Balances on of Liquid Film (left) and Gas Core (right) in Vertical Annular Flow.

Typically, the force balance is applied to the gas core in addition to the film, as shown in Fig. 2.18 from Shoham (2006.) From this assumption of annular flow geometry, the force balance equations are derived for core and film respectively:

$$A_c\left(\frac{dp}{dL}\right)_c - \tau_i S_i - \rho_c A_c g = 0 \qquad (2.7)$$

$$A_F\left(\frac{dp}{dL}\right)_F + \tau_i S_i - \tau_F S_F - \rho_L A_F g = 0 \qquad (2.8)$$

With these auxiliary equations, for perimeter and cross-sectional area,

$$S_F = \pi d \qquad (2.9)$$

$$S_i = \pi(d - 2\delta) \qquad (2.10)$$

$$A_F = \frac{\pi}{4}\left(d^2 - (d - 2\delta)^2\right) \qquad (2.11)$$

$$A_c = \frac{\pi}{4}\left(d - 2\delta\right)^2 \qquad (2.12)$$

We can construct energy equations for core and film (simplified by neglected the kinetic component and interface velocity),

$$\left(\frac{dp}{dL}\right)_c = \frac{f_i \rho_c v_c^2}{2\left(d-2\delta\right)} + \rho_c g \tag{2.13}$$

$$\left(\frac{dp}{dL}\right)_F = \frac{2\mu_F v_F d}{\delta^2\left(d-\delta\right)} - \frac{f_i \rho_f v_c}{2\delta\left(d-\delta\right)} + \rho_F g \tag{2.14}$$

where average fluid velocities are given by

$$v_F = \left(1-FE\right)v_l = \frac{q_L\left(1-FE\right)}{A_F} \tag{2.15}$$

$$v_c = v_g + FE \times v_l = \frac{q_g + FE \times q_L}{A_c} \tag{2.16}$$

It is common to assume no-slip conditions in the gas core. However, experimental work by Fore and Dukler (1995) measured the slip in the entrained gas droplets and found that “the droplets at the centerline [of the pipe] are travelling, on average, at 80% of the local mean gas velocity.”

The gas-liquid interface differs from a pipe wall in that it has some velocity and its roughness may vary. While the mechanistic models developed by Ansari et al. (1994) and Chokshi (1994) assumed the interface velocity to be much smaller than core velocity, Alves (1991) accounted for it, so that the core velocity term became v_c - v_F. where v_F is average film velocity. Strictly speaking, the relative velocity of the gas core should be expressed as $v_c - v_i$, with v_i being the interface velocity, i.e. the velocity of the surface in contact with the core. Proper evaluation of v_i requires knowledge of the velocity profile in the liquid film.

Solution of equations 2.13 and 2.14 for pressure gradient requires knowledge of,

a) film thickness, δ

b) entrainment fraction, FE

c) interfacial friction factor f_i

The solution is obtained iteratively by assuming an initial value of film thickness and setting the pressure gradients in the film and core equal to each other. However, empirical correlations for liquid entrainment and interfacial friction are required. Hence this is often termed as a *semi*-mechanistic approach.

For entrainment, the correlation by Wallis (1968, 1969) has been used almost exclusively. It was presented originally in graphical form (Fig. 2.19.) The correlating parameter is dimensionless gas velocity, termed π_2 by Wallis,

$$\pi_2 = \frac{V_{sg}\mu_g}{\sigma_L}\left(\frac{\rho_g}{\rho_l}\right)^{1/2} \tag{2.17}$$

Note that Wallis' correlation is a function of gas velocity but not liquid velocity.

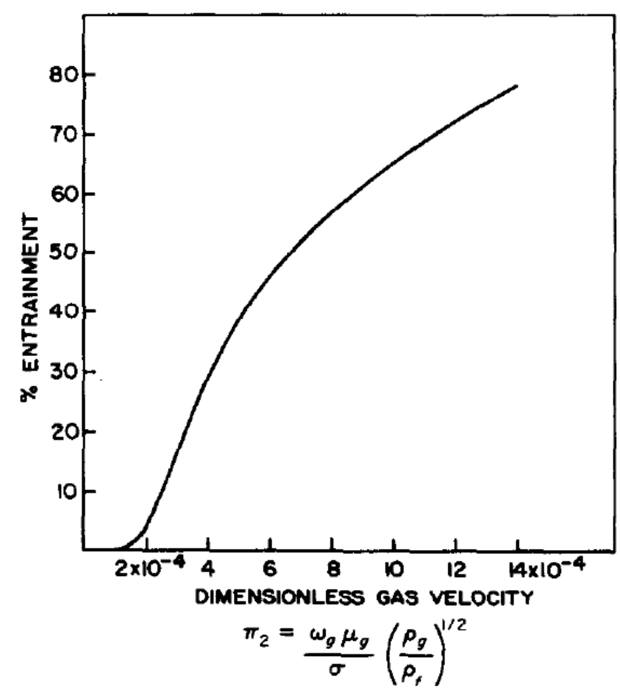

Figure 2.19 Wallis' Correlation for Liquid Entrainment in Annular Flow.

For numeric and iterative solutions, the curve of Wallis has been approximated by the equation,

$$FE = 1 - \exp\left[-0.125(v_{crit} - 1.5)\right] \tag{2.18}$$

where,

$$v_{crit} = 10000 \times \pi_2 \tag{2.19}$$

Wallis' correlation shows a threshold or critical gas velocity that must be achieved before entrainment of the liquid film occurs. By inference there is a condition of annular flow for which there is no entrainment. Examination of the original dataset (Fig. 2.20, digitized from a graph in Steen and Wallis (1964)) used to construct this correlation shows some scatter, creating some uncertainty about the point of onset of entrainment.

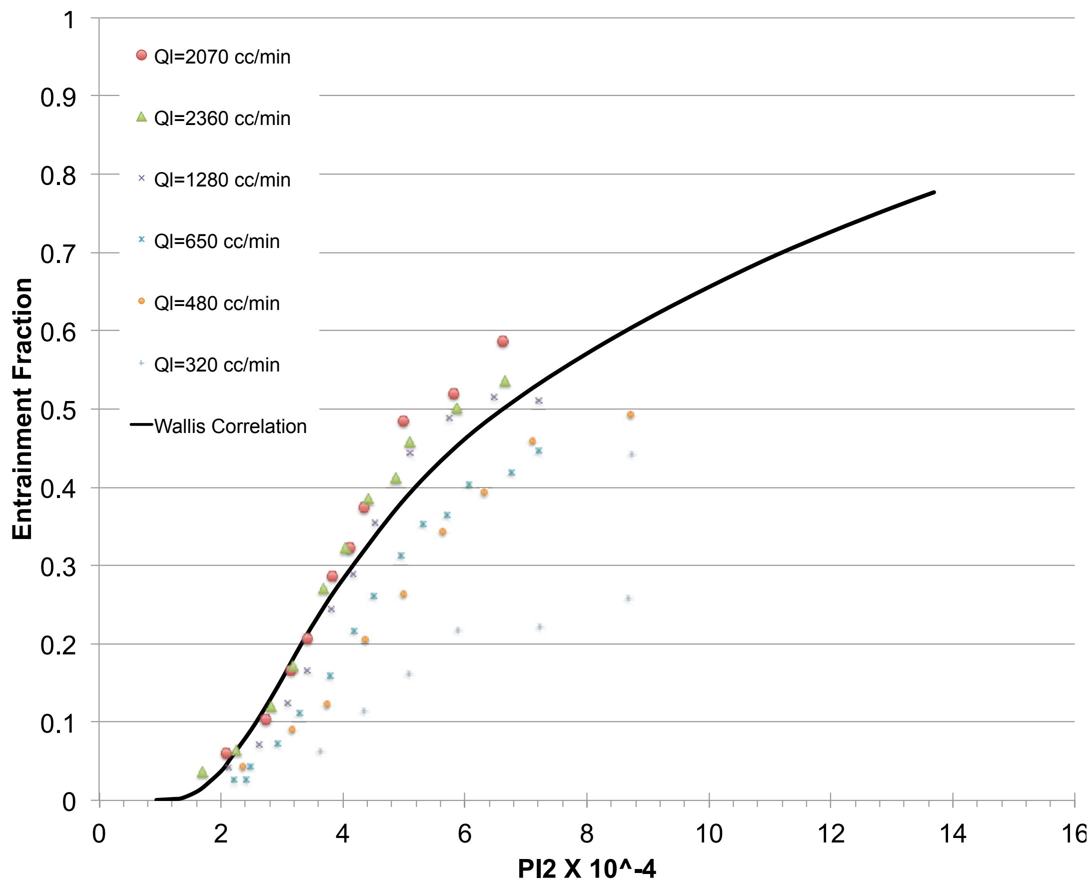

Figure 2.20 Data Used to Construct Wallis' Correlation for Liquid Entrainment in Annular Flow.

When other flow loop data of Steen and Wallis (1964) is used, the result is less pleasing: Fig. 2.21 represents air-water tests between 1 and 4 atm.

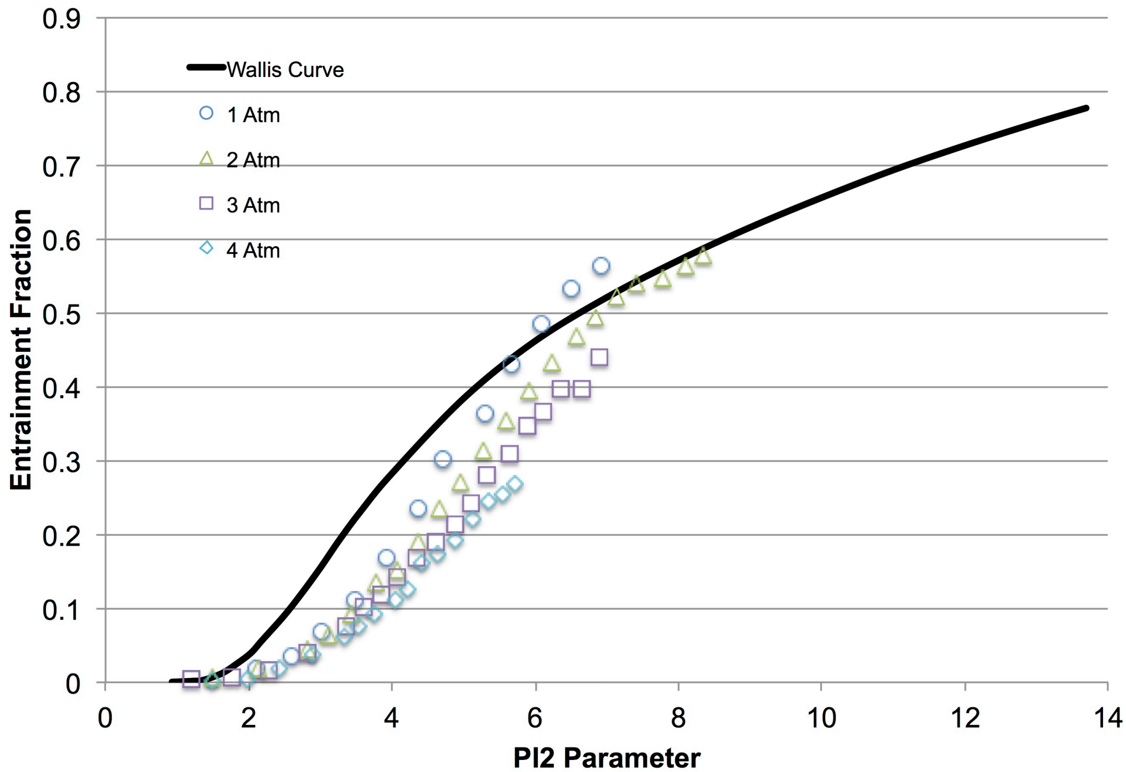

Figure 2.21 Wallis' Correlation for Liquid Entrainment Compared with Air-Water Data.

The correlation for interfacial friction (in Moody form) is taken from Wallis (1969) for "thin" liquid films,

$$f_i = 0.02\left(1 + 300\frac{\delta}{d}\right) \tag{2.20}$$

This equation is based on an approximation of the Nikuradse [(NACA 1950) relationship for friction factor under fully turbulent conditions (i.e. not a function of Reynolds number). Ansari et al. (1994) interpreted "thin" films to be an entrainment fraction (FE) >90% in their mechanistic implementation of annular flow:

$$f_i = f_{SC}\left(1 + 300\frac{\delta}{d}\right) \tag{2.21}$$

Where f_{sc} is the friction factor evaluated with superficial parameters. For "thick" films (FE<90%) the correlation of Whalley and Hewitt (1978) is suggested,

$$f_i = f_{sc}\left[1 + 24\left(\frac{\rho_l}{\rho_g}\right)^{1/3}\frac{\delta}{d}\right] \tag{2.22}$$

When equation 2.21 is tested against the data reported by Asali (1984), the result is given in Fig. 2.22.

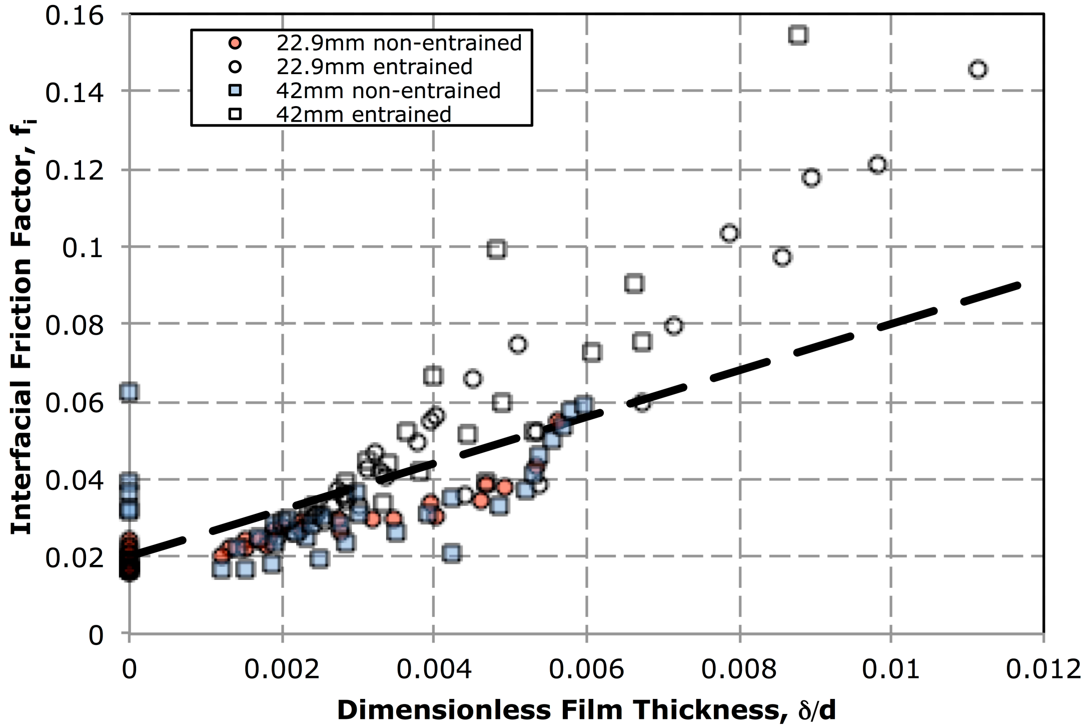

Figure 2.22 Interfacial Friction Calculated with Asali (1984) vs. Wallis (1969) correlation.

Many variants of the interfacial friction factor have been proposed. For example, Ashwood (2010), based on her data found that a better relationship for interfacial friction factor is found when a dependency on gas Reynolds number is introduced,

$$f_i = \mathrm{Re}_g^{-0.25}\left(1+\frac{900\delta}{d}\right) \tag{2.23}$$

Another approach by Spedding et al. (1998) was to consider the friction factor as function of Re_{sl} and Re_{sg}. Their data analysis resulted in a parametric equation,

$$\left.\frac{dP}{dl}\right|_{TP} = \left[1.5457\times10^{-4}\,\mathrm{Re}_{sl}^{3.5683}\mathrm{Re}_{sg}^{(-0.6315\log\mathrm{Re}_{sl}+3.1909)}\right]\times\phi\left(\frac{0.0317}{d}\right)^3 \tag{2.24}$$

The friction parameter, ϕ, is given graphically as a function of the superficial velocities in Fig. 2.23. While this method does free the pressure gradient solution from the need to determine entrainment and film thickness, it is limited to relatively high gas rates only ($Re_{sg} > 8 \times 10^4$.)

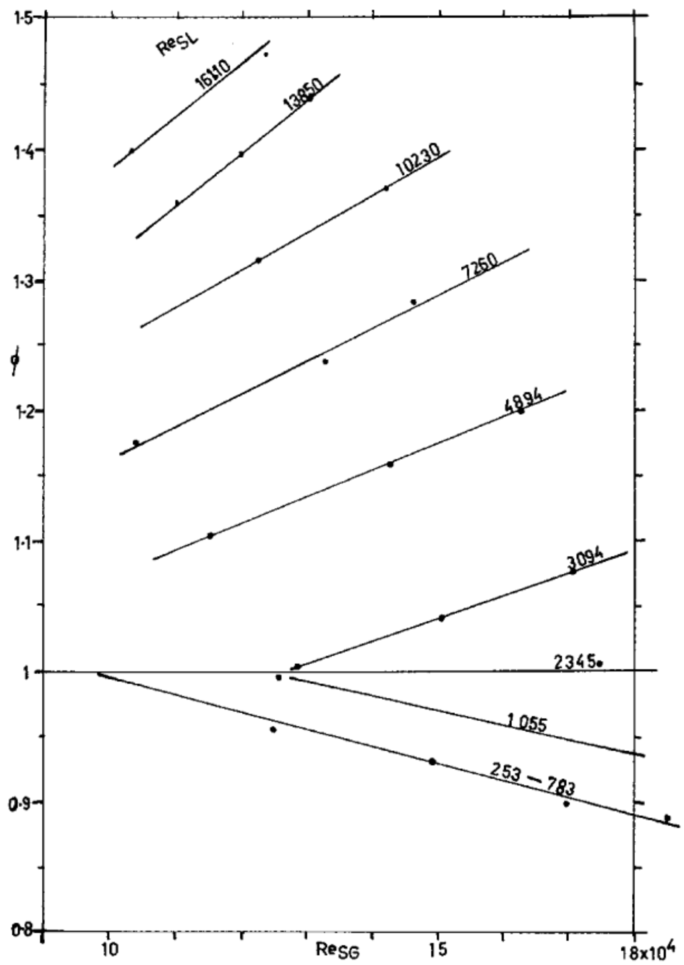

Figure 2.23 Friction Parameter ϕ in Spedding et al. (1998a) Pressure Gradient Correlation.

In summary, mechanistic models still require correlations for both entrainment and friction factor. Comparisons with experimental data show that these correlations do not always provide a good prediction.

3 The Experimental Apparatus

A vertical flow loop at the University of Alberta, has been modified from previous work. The loop is instrumented to record pressure and temperature continuously while metered air and water is flowing. Still and video cameras can observe the flow externally. Additional equipment is installed to measure liquid film thickness using the Planar Laser Induced Fluorescence (PLIF) method. Initial evaluation has established a performance envelope for the system.

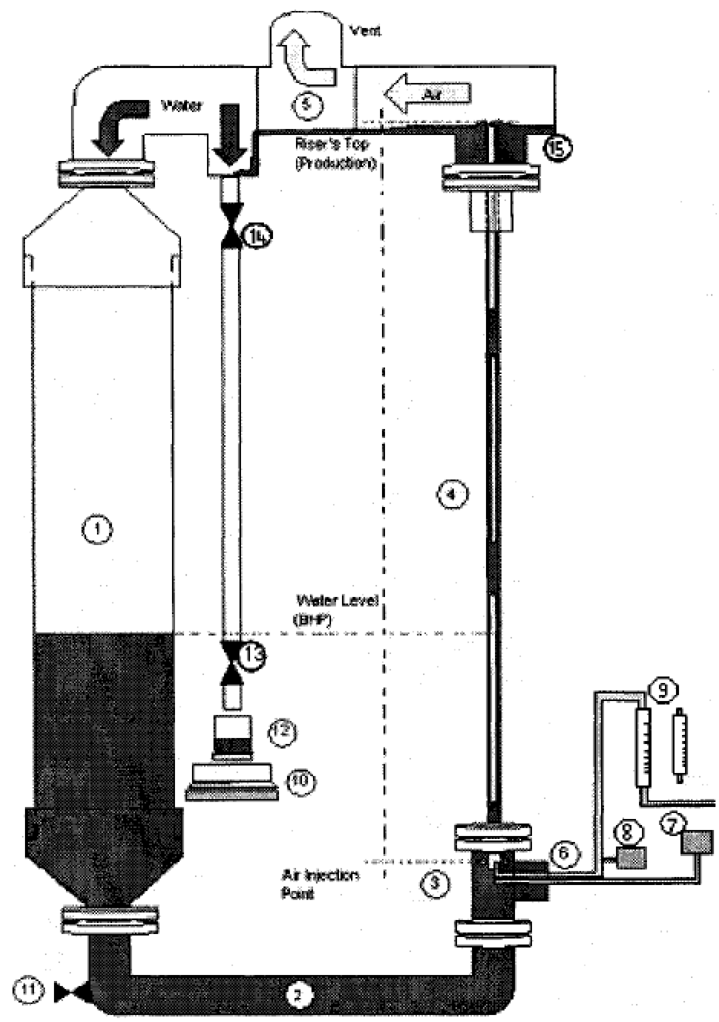

Figure 3.1 Original Flow Loop Before Modifications.

3.1 Flow Loop Construction

The original vertical flow loop at the University of Alberta, as used by Becaria (2004) and Vargas (2006) for studies of slug to annular transitions, is shown in Figure 3.1. Airflow was measured with a rotameter and liquid rate was obtained by weighing the water stream returned to a bypass line.

Modifications to the loop began in 2012 to prepare it for this current program, and one to be conducted concurrently by Mamedulanov (2016.) The major changes are:

a) The vertical test section of the loop now consists of a 31.8 mm o.d. by 26.1mm i.d. (average of two orthogonal measurements) cast acrylic pipe to allow for visual observation of the two phase flow. Cast acrylic has better optical clarity than extruded acrylic. Also, this also allows direct comparison with some previously published results, which use the same size tubing.

b) The test section has been lengthened to 3.65 m (two sections chemically welded together) to minimize the impact of entrance effects.

c) A viewing section has been fashioned from acrylic sheet material and installed near the top of the vertical section; this can be filled with glycerol for annular film imaging during PLIF experiments.

d) The supply hose from the building compressed air outlet has been upgraded in order to reduce line losses and to ensure that flow velocities are well into the annular regime with the larger diameter test section.

e) A manually operated valve has been added downstream of the liquid rotameters to provide adjustment to the input water rate.

f) A manifold has been installed to accommodate three new rotameters to measure a wide range of liquid flow rates.

g) A mist pad is added at the air vent to capture any droplets entrained during startup conditions.

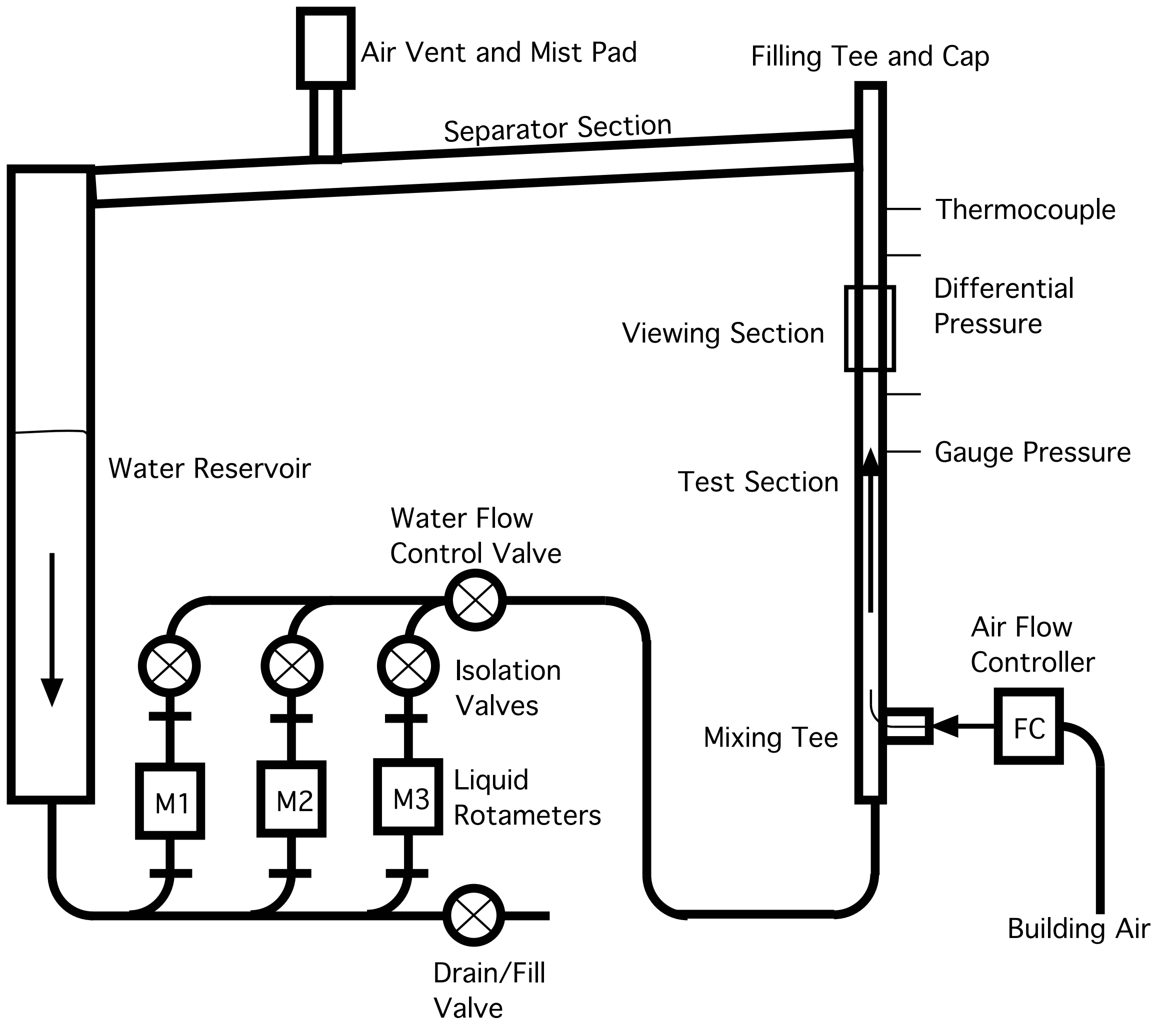

Figure 3.2 Schematic of Vertical Flow Loop

Within a mixing tee at the bottom of the test section, compressed air is supplied to a short centralized stainless tube of approximately 6 mm i.d., which is perforated along its length and capped at the end. Water is gravity fed from the nominal 152 mm diameter reservoir section through one of the three selected rotameters mounted in parallel (Fig. 3.2.) The air and water mixture flows upwards through the 26 mm test section until it reaches a larger diameter (50 mm) horizontal separator section at the top of the loop. This 50mm pipe is set approximately at a 2° downward slope to encourage segregated flow; air exits the upper vent through a mist pad while water returns to the reservoir.

Guidance for this setting angle was taken from Barnea (1987) for air-water at standard conditions in a 51mm i.d. pipe at 1° downward from horizontal. When the flow loop performance envelope (with velocity re-calculated at the 51mm i.d. pipe diameter) is superimposed upon Barnea's flow regime map (Fig 3.3) observe that flow conditions in the separator section are expected to be either segregated-smooth (SS) or segregated wavy (SW) over the expected performance envelope of the loop. This indicates that the air and water will separate with the water returning to the reservoir.

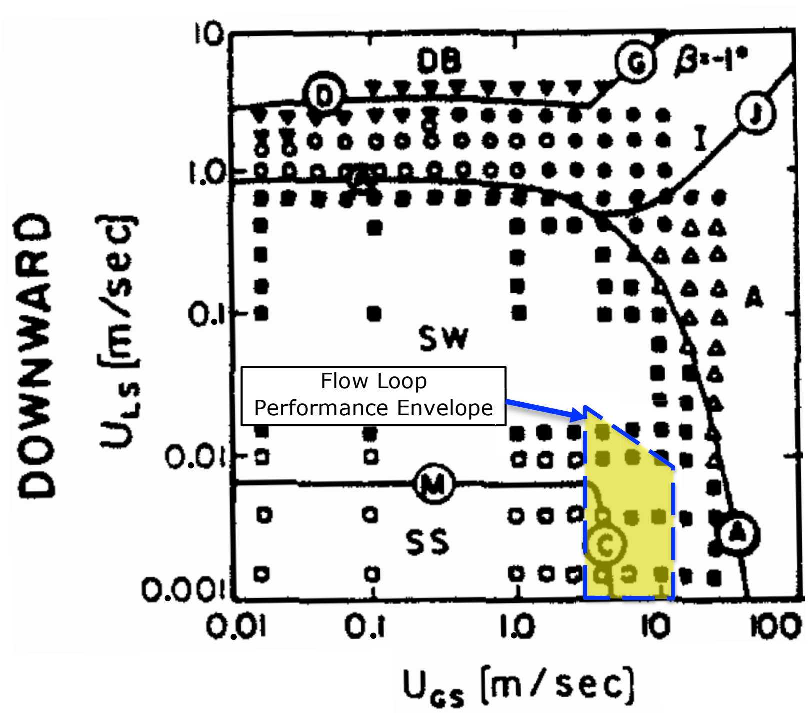

Figure 3.3 Barnea's Horizontal Flow Regimes in 51mm i.d. Pipe.
with Performance Envelope of University of Alberta Vertical Loop Superimposed.

Uniquely this flow loop does not feature a water pump. The reservoir maintains a nearly constant fluid head, which is sufficient to feed liquid back into the mixing section at a constant rate. Taps are mounted near the top of the test section to allow as much development length as possible before measurements are taken (Fig. 3.4). Differential pressure is measured over a 762 mm vertical interval, which is a compromise between achieving developed flow as high as possible at the top of the pipe and obtaining sufficient signal amplitude. The midpoint of the differential measurement segment is 2.8 m above the mixing tee, giving a development length to diameter ratio, *L/d*, of approximately 108. Since the thermocouple protrudes slightly into the test section, the tap for temperature measurement is downstream of the differential pressure taps to avoid disturbing the measured flow stream (Fig. 3.5.)

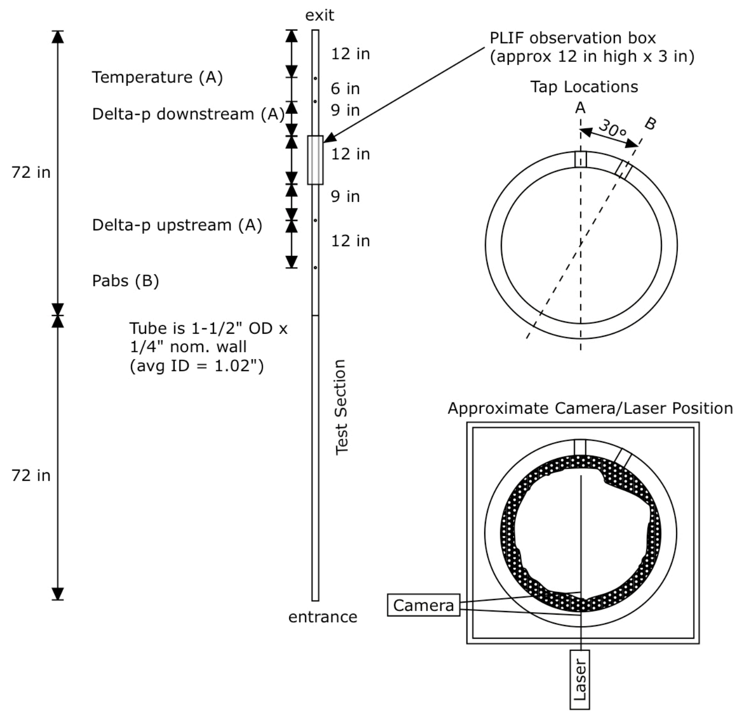

Figure 3.4 Vertical Flow Loop Taps and Instrumentation Locations.

Figure 3.5 Test Section Thermocouple Tap (Top) and Downstream Differential Pressure Tap (Below.)

3.2 Flow Loop Instrumentation and Measurement

Instrumentation mounted to the test section itself is as follows (Manufacturer data sheets for key instrumentation are provided in Appendix 2):

a) Type K thermocouple

b) Gauge pressure transducer (Omega PX419-2.5GI, S/N426582, +/-0.08% of full scale accuracy) calibrated to 2.5psi (17.24 kPa) full scale (Figure 3.6.)

Figure 3.6 Gauge Pressure Transducer.

c) Differential pressure transducer (Omega PX2300-1DI, s/n 5119830, +/-0.25% of full scale accuracy) calibrated to 1.0 psi (6.895 kPa) full scale (Figure 3.7.)

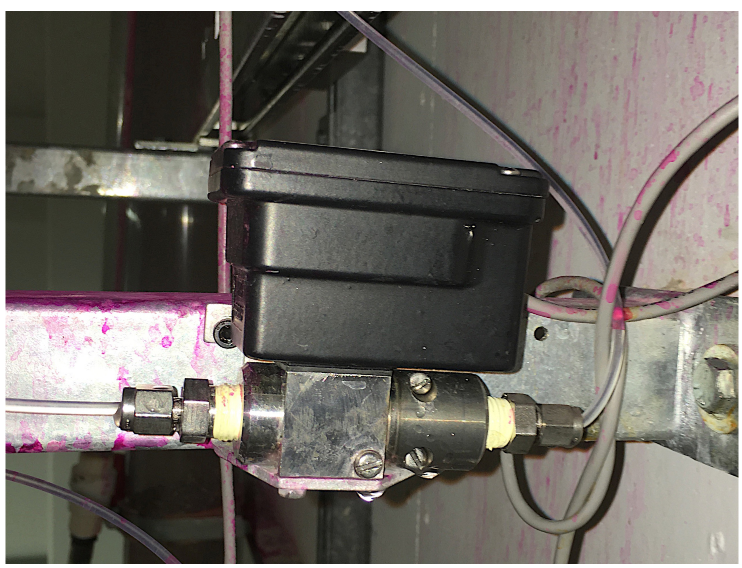

Figure 3.7 Differential Pressure Transducer with Taps Upstream (L) and Downstream (R.)

The pressure transducers, which are mounted well below their corresponding taps, are connected by 1.5mm i.d. perfluoroalkoxy (PFA) tubing. Signal wires from the transducers are connected to a terminal box where they are converted from a standard 4-20 ma to a 1-5v signal with a precision 250 ohm resistor. The analog signals are then sent to a data acquisition board on a PC, which has 16-bit resolution. Data is sampled and recorded using SignalExpress™ software by National Instruments, a simplified version of their LabView™ application. Figure 3.8 shows an example of the display when the system is operating.

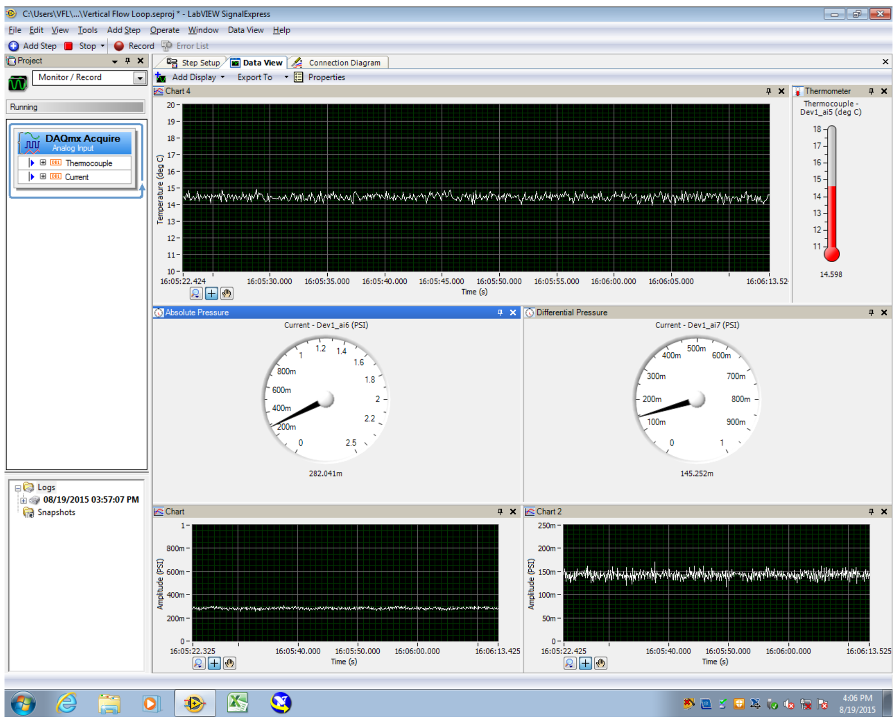

Figure 3.8 Screenshot of SignalExpress Software.

The pressure transducers were initially calibrated with a precision tester, and a calibration curve entered into SignalExpress (Figure 3.9.) During the course of the pressure gradient program, the calibration was checked directly by comparing the displayed pressure against a several different heights of static water column in the test section (Figure 3.10.) This confirmed the linearity of the pressure transducers but also revealed a small overall scale error along with a small offset error at very low pressure. This allowed further corrections to be made to the raw data. With a 30 inch (76.2cm) spacing between differential taps and a maximum pressure differential of 1 psi, the maximum pressure gradient that can be measured is about 9 kPa/m.

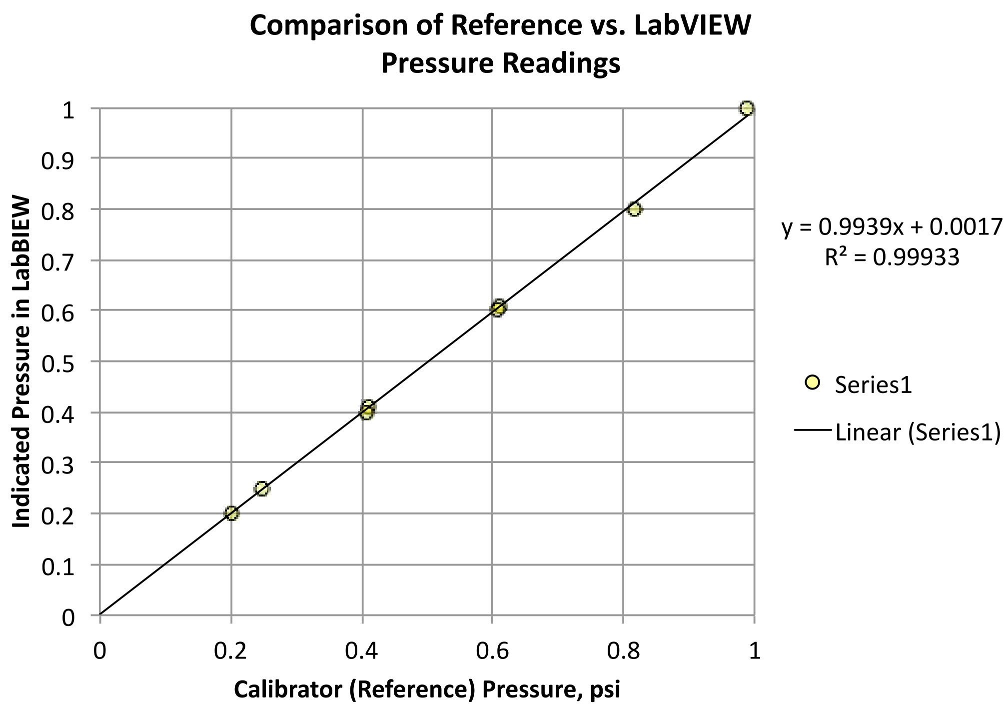

Figure 3.9 Original Pressure Calibration Curve for Differential Pressure Transducer.

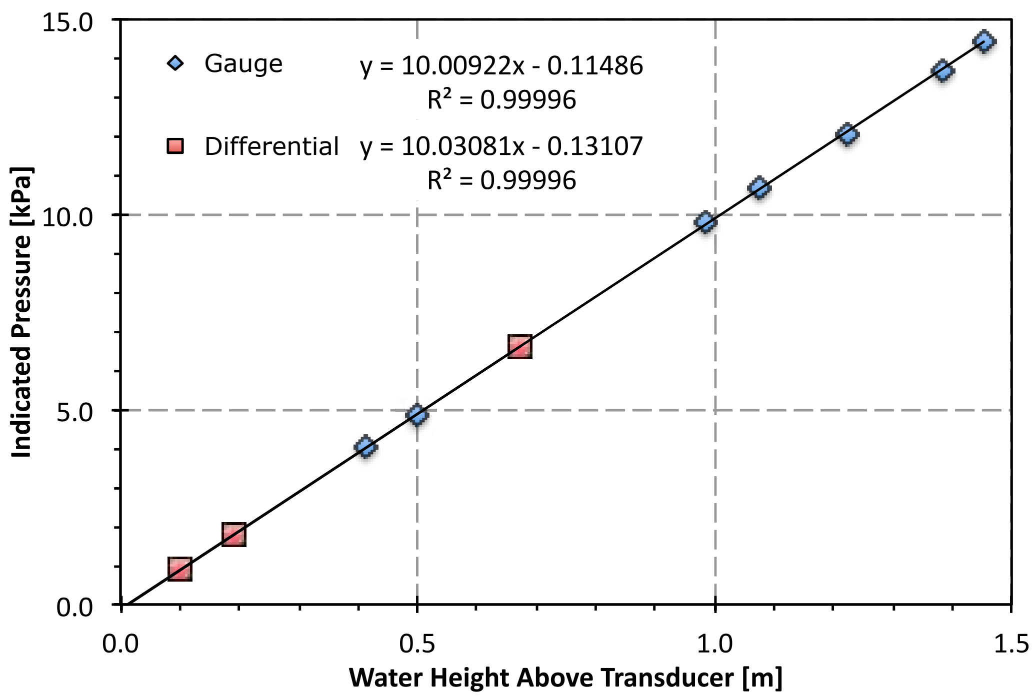

Figure 3.10 Measured Fluid Level to SignalExpress Displayed Pressure.

Liquid flow is read manually through one of three high accuracy (+/- 1% of full scale) glass Kobold KDV series rotameters with ranges 2-20 standard litres per hour (SLPH), 16-160 SLPH and 100-1000 SLPH respectively (Fig. 3.11.) (See Appendix 4 for their corresponding calibration sheets.)

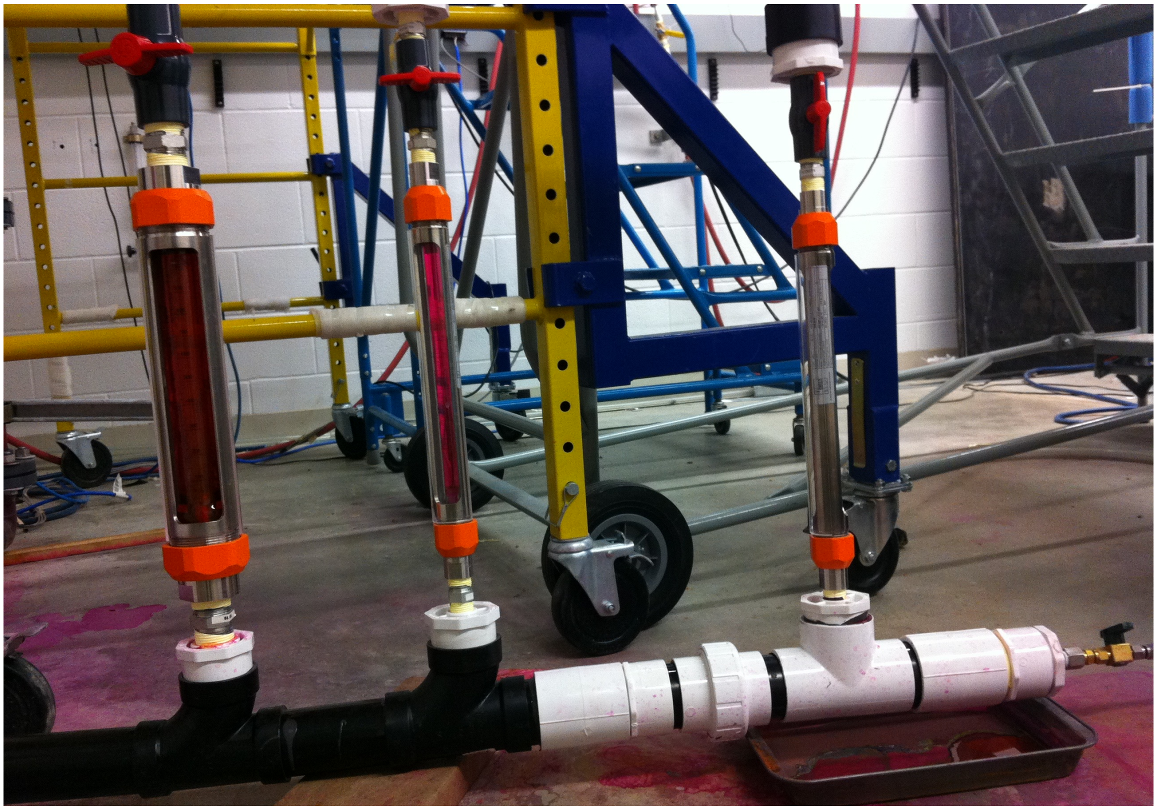

Figure 3.11 Three Water Rotameters with Isolation Valves.

Air flow was initially measured with a Cole-Parmer direct-reading rotameter, with a 30-300 standard litres per minute (SLPM) range on a 100mm scale. This was soon found to be unsuitable for experimental work because:

a) The claimed accuracy for this rotameter is relatively coarse, only +/-3% of full scale.

b) The scale is calibrated only for a standard condition specified by the manufacturer (14.7 psia, 70°F); for other conditions, the indicated flow rate must be calculated (see Appendix 5.)

c) A total of three manual readings (with a corresponding number of potential reading errors) are required to calculate a flow rate: the rotameter scale reading, air temperature and gauge pressure.

A mass flow controller (Omega FMA 2621A, serial #105116) with a claimed accuracy of +/- 0.2% of full scale was added in series with the air rotameter (Fig. 3.12.) The controller has a maximum flow capacity of 1500 SLPM. Comparison of the two devices on two separate occasions (Figure 3.13) shows that while they are in good agreement at low flow rates, the rotameter overestimates flow rate compared with the mass flow controller at higher rates.

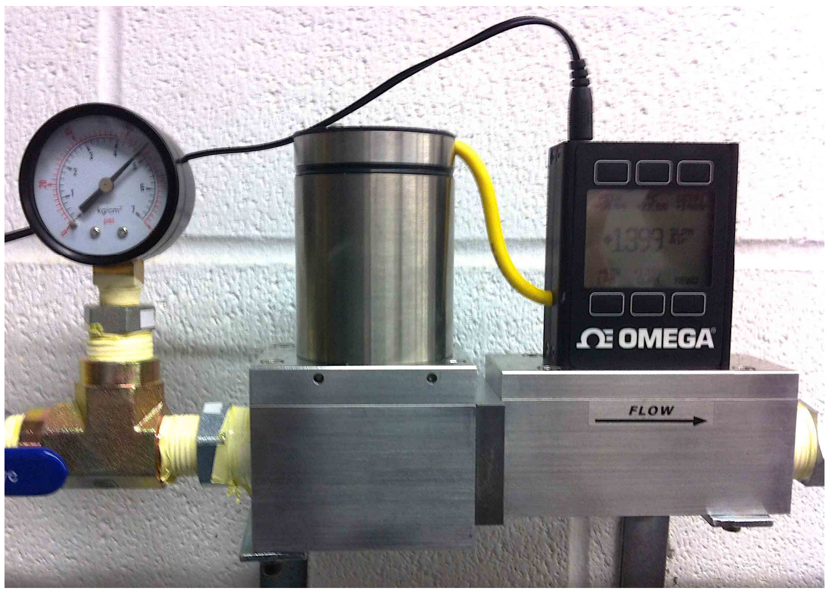

Figure 3.12 Mass Flow Controller for Air.

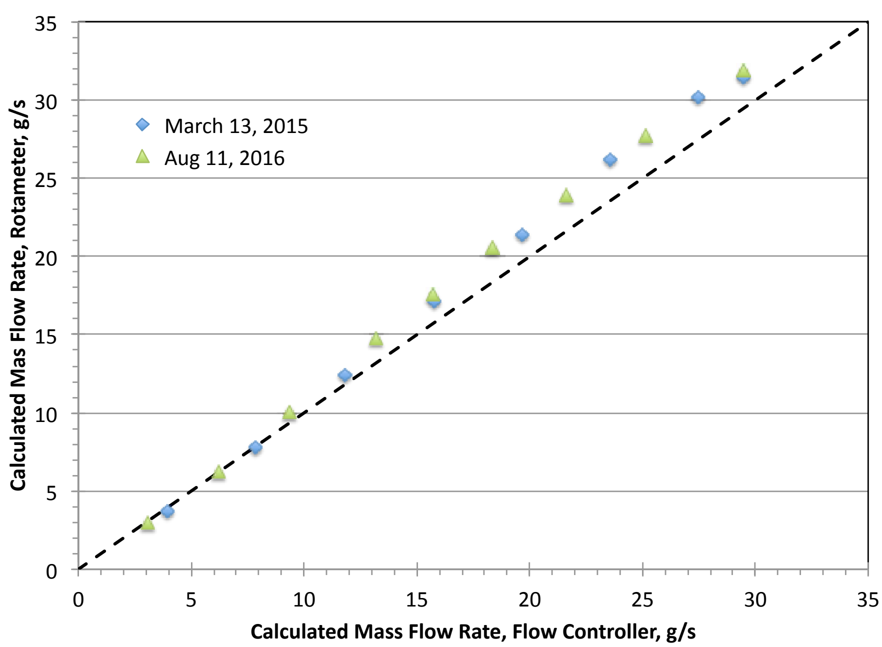

Figure 3.13 Comparison of Original Air Rotameter with Mass Flow Controller.

Flow rate data for air and water are adjusted and recorded manually. In addition, cameras are placed near the top of the test section (at approximately L/d = 128) for external observation and image taking. For high-definition video and stills, an Olympus OM-D M10 with an M.Zuiko Digital 14-150mm *f*1.4 lens is used. High-speed videos are taken with an iPhone 6s set to 240 frames/second at 720p resolution (Fig 3.14.)

Figure 3.14 iPhone 6s (L) and Olympus DSLR (R) Mounted for Imaging.

For the subsequent PLIF work, a Newwave Solo III laser and LaVision Imager Intense CCD camera (1376 x 1040 pixel) are employed (Fig. 3.15), in a configuration similar to that described by Mamedulanov (2016). This equipment has also been used by Zeinali (2012) and Bizhani (2013) in a horizontal loop located in the same lab. A diffuser changes the linear laser into a light "sheet." The laser and camera are controlled by a PC specially configured by LaVision Inc. and running their proprietary DaVis 8.3 software.

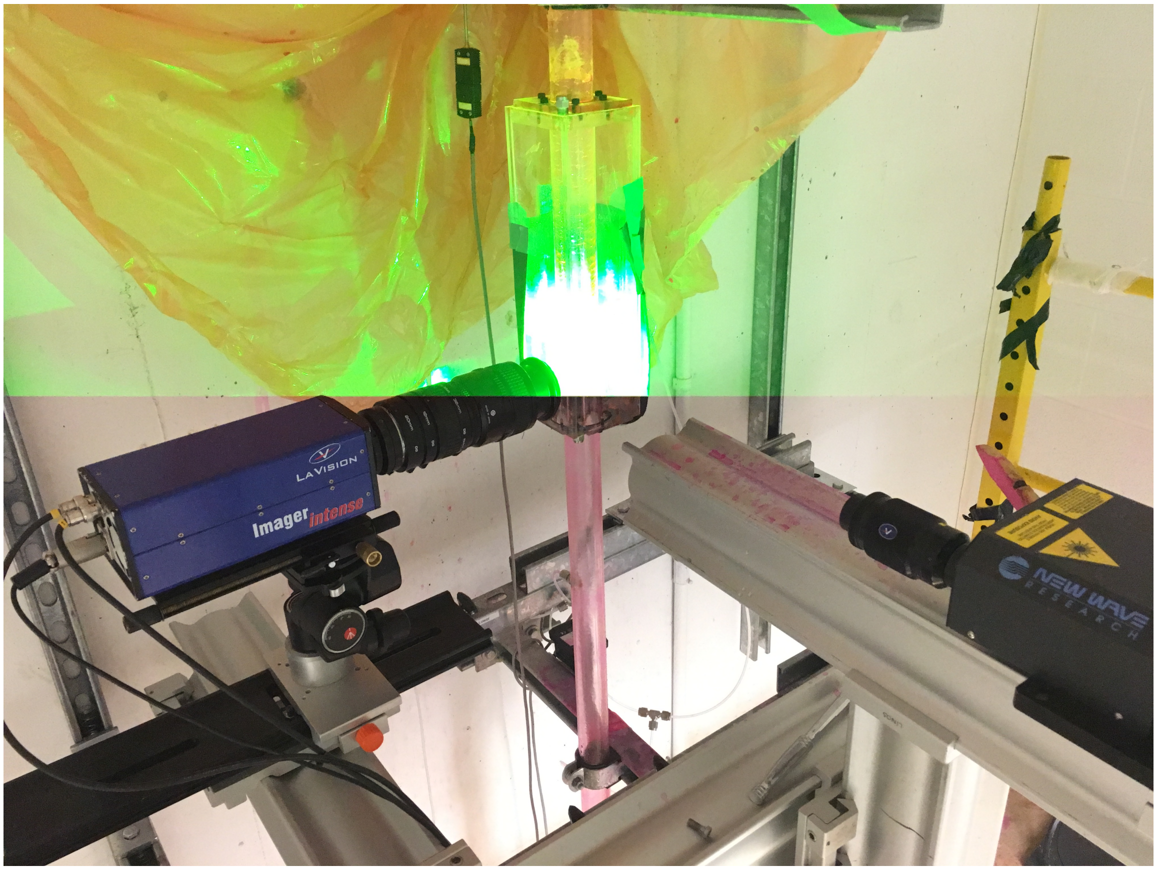

Figure 3.15 CCD Camera (L) and Laser (R) Acquiring Image Through Viewing Section.

Runs are to be conducted largely in the annular regime where liquid film is expected to be relatively thin. The laser sheet (about 0.5mm to 1mm width) is set at the centerline of the pipe. The camera is offset horizontally so that a portion of the pipe wall is included to provide a reference line; laser and camera are at zero angle of incidence to the viewing box sides to minimize refractive distortion. This arrangement is similar to that employed by Schubring (2009) and Zadrazil, Matar, and Markides (2014.) However for some work, Mamedulanov (2016) also located the laser laterally from the pipe centre line "in order to reduce obstruction of liquid film image by rough surface of the film and increasing air bubble concentration in the film with increasing liquid and gas flow rates." The camera employs a Nikor 65 mm f2.8 Micro lens with three extension tubes (total length 68mm) to give a small, high resolution window about the liquid film. An aperture setting of *f*16, is found to minimize the effects of ambient light in the lab. The laser/camera combination is located near the bottom of the viewing section where L/d is approximately 104.

The viewing box in the test section is filled with 99.5% glycerol (Sigma-Aldrich product G7893) which has a refractive index of 1.474 at 20°C (Hoyt, 1934.) which closely matches the refractive index of 1.49 for the acrylic of the test section pipe and the viewing box material. This is intended to further minimize image distortion. During image acquisition the back planes of the viewing box are covering in matte black construction paper to reduce stray reflections.

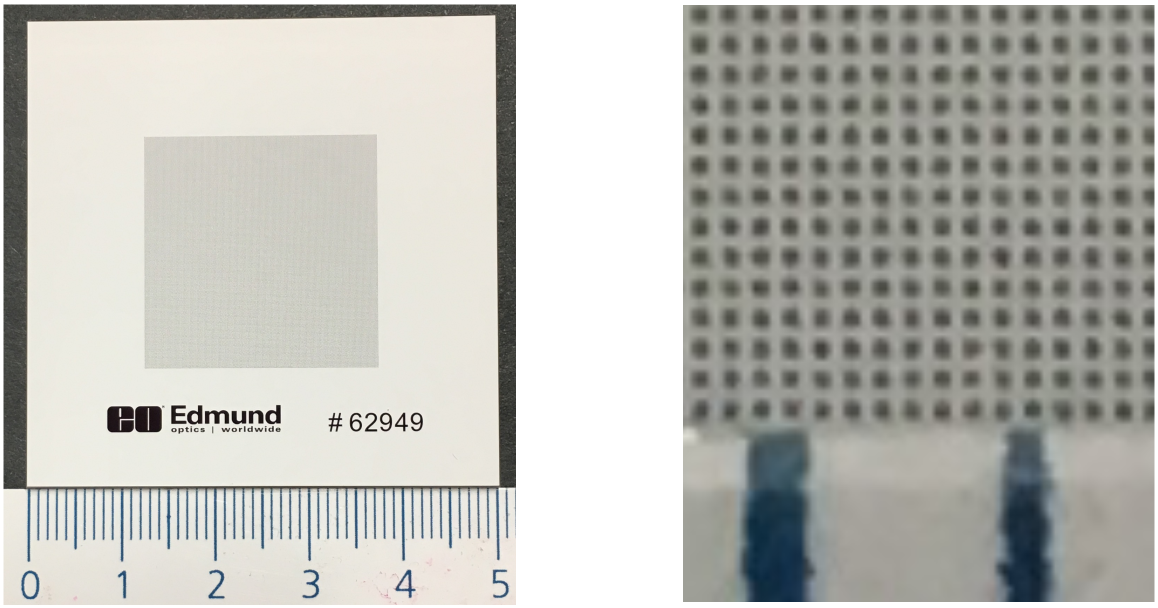

Figure 3.16 Calibration Target Before Trimming (L) and Closeup of Dot Pattern (R.) with 1mm Scale Markings Below.

For PLIF image calibration, a precision grid distortion target (Figure 3.16) was selected. The target has uniform dots of 0.0625mm diameter, spaced on 0.125mm apart. This is an improvement over the 0.5mm spacing target used by Mamedulanov (2016.) The target has been trimmed to fit the same target holder as used by Mamedulanov (Figure 3.17.) The target holder consists of a 150mm long half-cylinder constructed of nylon and semi-circular cross-section to fit tightly within the test section pipe. A bolt threaded into the top allows it to be lowered by string through the filling tee into the viewing box for calibration. It has three magnets installed to allow manipulation from the outside. With adhesive material, the face of the target is at the centerline of the test section pipe when installed for calibration.

Figure 3.17 Calibration Target Mounted to Target Holder.

The laser emits a green light at a wavelength of 532 nm. In order to obtain a bright image of the film over a narrow cross section, Rhodamine B dye (Acros #132311000) is added to the distilled water in the loop. The dye absorbs light energy from the laser and emits light (fluoresces) at a slightly higher wavelength (see Figure 3.18 from Kristofferson, Erga, Hamre, and Frette (2014) and well within the spectral range of the camera (290-1100 nm.). This dye has been used in several similar experiments, although the concentration has varied widely The current experiments followed those of Mamedulanov (2016) who used an initial Rhodamine-B dye concentration of 150mg/l.

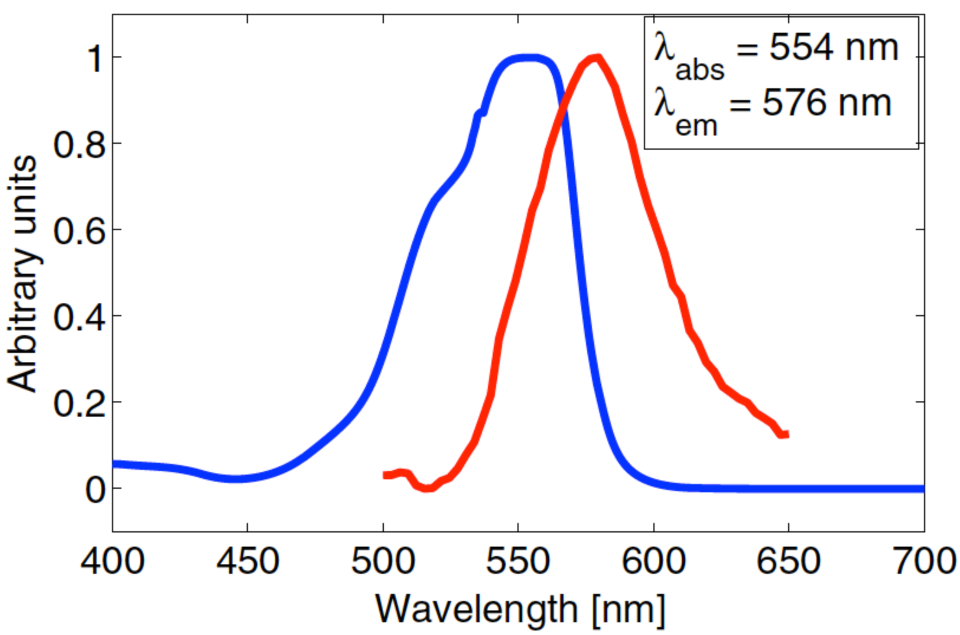

Figure 3.18 Light Response of Rhodamine B in Water.

However, during the course of this work, system fluid losses (e.g. evaporation, leakage) required additional distilled water to be added to the reservoir. To estimate the current dye concentration, several reference mixtures were prepared in concentrations of 150, 120, 100, 80, 60, 40, 20 and 10 mg/l; these were compared with samples taken from the bottom of the rotameter section of flow loop (Figure 3.19) Two cleanup samples from the flow loop were intended to flush any accumulated solids and corrosion products before taking two "clean" samples. When illuminated from behind, the colour of the samples was compared against the reference mixtures to obtain an estimate of concentration in the flow loop.

Figure 3.19 Comparison of Flow Loop Rhodamine Sample vs. Prepared Concentrations. (Flow loop sample is marked with black plastic on top.)

In a more quantitative approach, the photograph was analyzed to establish a correlation between grey-scale image intensity of each known sample intensity and its corresponding dye concentration (Fig. 3.20.) For the grey-scale intensity, an average of a rectangle located in the centre of the sample image was calculated NIH ImageJ software. The grey-scale value of the flow loop samples was then fit to the curve; this yielded an estimated dye concentration of 40 mg/l. To account for uneven background illumination, the value from sample 2, which was placed closer to reference samples of the same concentration, was considered more accurate.

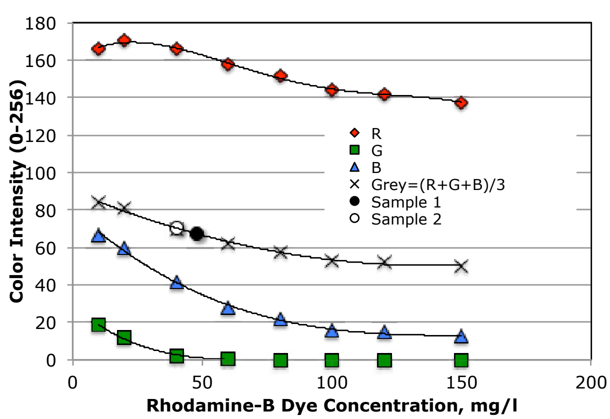

Figure 3.20 Colour Intensity Response of Rhodamine B Concentrations.

3.3 Flow Loop Performance Envelope

During functional testing of the flow loop, the air flow rate was set at intervals from 350 SLPM to 1500 SLPM. This covered the range from just below churn-annular transition to the maximum possible with the flow controller. For each air flow rate, the water flow was adjusted from the maximum stable rate to the minimum readable on the smallest rotameter (2 SLPH.) However, it was found that for the higher air rates, a high liquid feed caused considerable instability in the loop. This was attributed to the air feeding back into the liquid rotameters when the water head in the reservoir was too low. As a result, the reservoir was filled to a maximum safe level (about 2m), based on internal pressure and weight of the water. The resulting stable performance envelope of the apparatus was found, as shown in Figure 3.21.

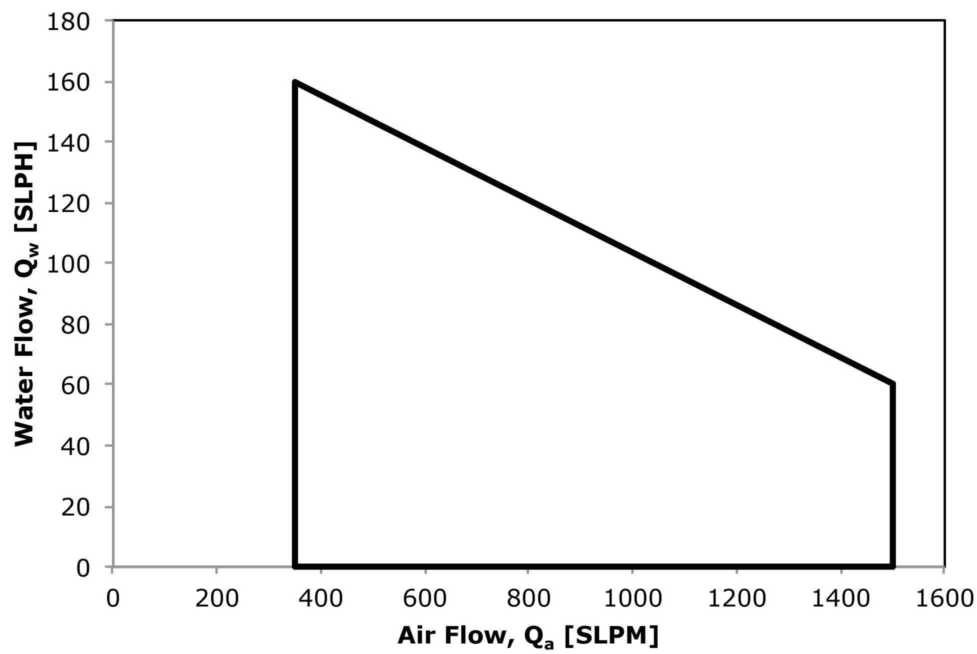

Figure 3.21 Flow Loop Performance Envelope.

3.4 Flow Loop Teething Problems

Initial runs were made over the period December 4, 2014 to October 8, 2015. These early data were not used for further analysis because:

a) A rotameter was used initially for air flow measurement, with the accuracy concerns described earlier.

b) Initial pressure offsets were not recorded.

c) Poor cable shielding caused extremely high noise levels in temperature and pressure transducer signals.

d) Pressure taps were not consistently purged before starting measurement runs.

e) Municipal (hard) water was used at first. Scale buildup started to obscure viewing of flow regimes as well as potentially increasing the surface roughness of the pipe wall; attempts to clean with various solvents, such as acetic acid contributed to stress cracking and the test section had to be replaced in April, 2015.

4 The Experimental Programs

Two experimental programs were conducted. The first sought to collect finely-spaced measurements of pressure gradients within the performance envelope. In addition, images were taken externally to help identify sub-regimes of annular flow. Imaging took the form of high shutter speed stills, high resolution video and slow motion video.

In the second program the PLIF technique was used to capture internal images of the liquid film itself at various sample points within the test matrix. The objective was to measure average film thickness over a range of air and water flow rates and to observe the onset of liquid entrainment.

4.1 Pressure Gradient Program

To ensure consistent pressure measurements, the following preparation procedure was followed before beginning a series of runs:

a) Ensure water level in the reservoir is close to the highest marked level.

b) Close the water flow control valve to isolate the test section from the reservoir.

c) Add demineralized water to the test section through the filling tee until the pressure taps are covered.

d) After allowing time for any entrained air bubbles to rise and clear, drain the tap lines at the pressure transducers to remove any air bubbles.

e) Purge the differential pressure transducer connections according to the manufacturer's instructions.

f) Open isolation valve to the selected rotameter; close remaining isolation valves,

g) Slowly open the water flow control valve to lower the liquid column in the test section, allowing the water to equalize with the level in the reservoir.

h) When liquid column in the test section is below the pressure taps, record the offset values.

i) Check that the filling tee cap is reinstalled!

For a series of measurements, the following steps were followed:

a) Turn on power to the air flow controller, and set flow rate to less than 100 SLPM.

b) Slowly adjust air rate on the controller in 100 SLPM increments until reaching desired rate (maximum is 1500 SLPM.) This avoids a surge which would otherwise cause a slug of water to "burp" out the air vent.

c) Adjust the water flow control valve to maximum stable rate (directly read from the liquid rotameter); allow several minutes for system to stabilize. This ensures the maximum film thickness at the selected air rate so as to minimize air intake into the pressure transducer tap lines.

d) In SignalExpress software, start recording of temperature, gauge pressure and differential pressure; record liquid rotameter reading.

e) Take external still and video images.

f) Stop recording and save data to MS-Excel file.

g) Adjust water flow rate to next lowest increment, according to the test matrix and repeat steps d) and e.)

h) When water rate is at 20 SLPH, take readings on the "medium" range rotameter where this rate is marked at the bottom of the scale and repeat for the "small" range rotameter where this rate is marked at the top of the scale.

Flow loop runs were conducted intermittently between Dec 4, 2014 and Dec 16, 2016. This includes additional runs conducted to fill in data gaps or to confirm repeatability. Note also, some runs were done with air only. See Figure 4.1 for a plot of the final test matrix. Note that it is presented in terms of air flow rate (SLPM) and water flow rate (SLPH) as read from the instruments. A generally orthogonal approach was used in selecting the air rate and water rate increments for the test matrix, allowing results to be plotted as a functions of gas rate or liquid rate.

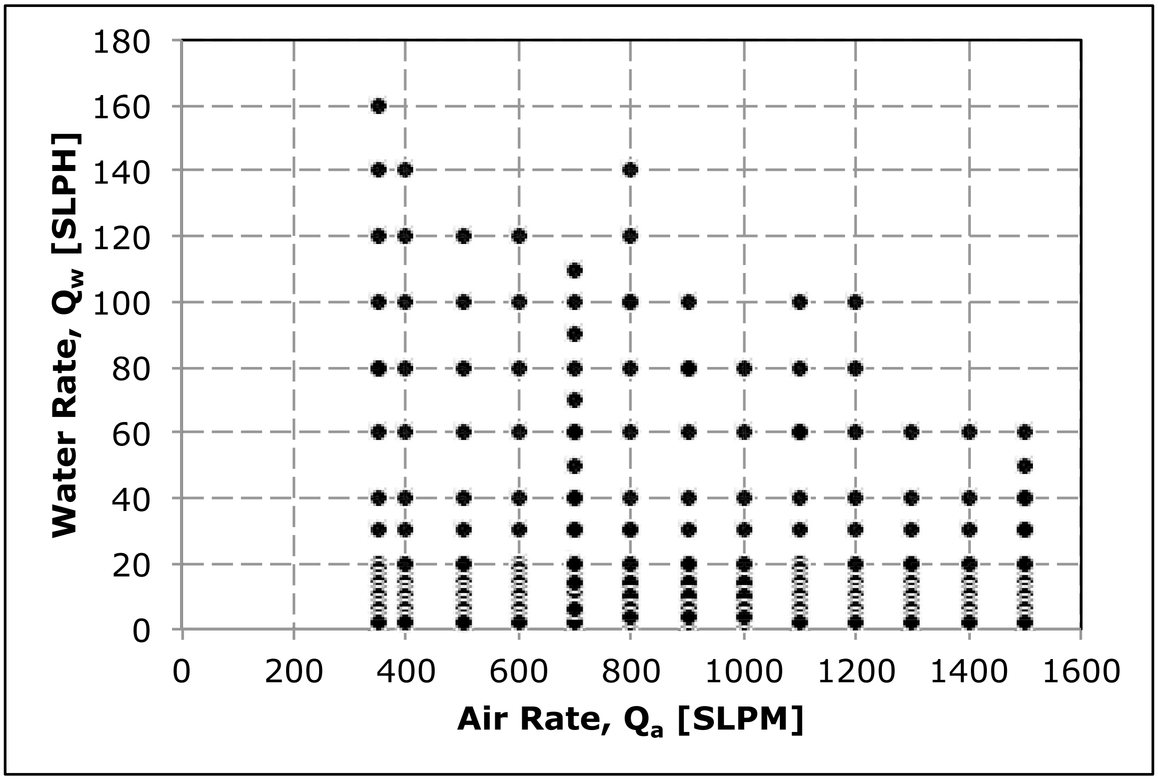

Figure 4.1 Test Matrix for Pressure Gradient Program.

The raw data collected for point of the test matrix were:

a) Date.

b) Air Flow Controller Set Point, SLPM referred to 15°C, 100 kPaa.

c) Air Flow Controller outlet pressure, psia.

d) Air Flow Controller outlet temperature, °C.

e) Controller Air Flow Pressure, psia.

f) Flow Loop Temperature, °C (input Ai5 on SignalExpress.)

g) Flow Loop Pressure, psig (input Ai6 on SignalExpress.)

h) Pressure Differential, psi (input Ai7 on SignalExpress.)

i) Rotameter Water Flow rate ,SLPH.

j) Gauge pressure Offset, psi.

k) Differential pressure Offset, psi.

l) Daily mean station pressure, kPaa.

Flow loop temperature, gauge pressure and differential pressure signals were sampled by the SignalExpress software at the highest rate possible without overloading the computer's data buffer; this was in the range of 15-25 ms between samples. After each air/water rate run, the data was transferred to an Excel spreadsheet, where a mean value and standard deviation was calculated for the first 1000 samples. All other data were recorded manually.

The University of Alberta is at 675m (2214 ft) above sea level, where the atmospheric pressure is typically lower than at the usual reference, sea level (SL). Hence assuming standard pressure for air properties (density, viscosity) would introduce a significant error. For example, when atmospheric pressure at sea level is 101.7 kPaa, the true atmospheric pressure (also called station pressure) in Edmonton is only 94 kPaa. Station pressure data from Edmonton City Centre Airport (Blatchford Field), elevation 671m (2202ft) was obtained from https://edmonton.weatherstats.ca/charts/pressure_station-daily.html (last accessed August 16, 2017.) Figure 4.2 shows an historical comparison between the commonly reported sea level adjusted pressure and the actual barometric pressure for Edmonton for a period covering the pressure gradient program.

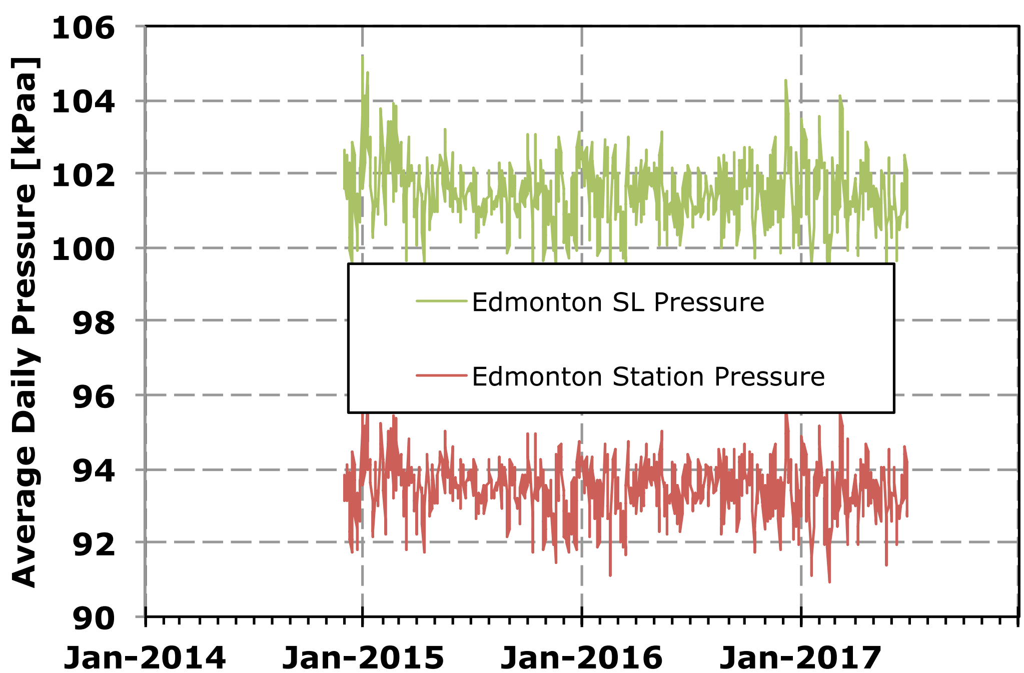

Figure 4.2 Edmonton Station Pressure (True Atmospheric) and Sea Level Reference Pressure.

For further analysis, the following were calculated from the raw data:

a) Air Mass Flow Rate, g/s. The air flow controller was programmed to display air rate referenced to 15°C and 100 kPaa. For use at the slightly varying conditions in the flow loop test section, it was convenient to first calculate a mass flow rate by rearranging the ideal gas equation thus:

$$\dot{m}_{air} = \frac{P_{std} Q_{air} M_{air}}{RT_{std}} = \frac{100 \times Q_{air} \times 28.9625}{8.3451 \times (273.15 + 15)} \times 1000 \tag{3.1}$$

where Q_{air} is in units of m^3/s.

b) Corrected pressure differential, psi. At low flow rates, the offset error becomes significant. Therefore the averaged differential pressure was corrected by adding the offset pressure reading recorded under static conditions before commencing a series of runs. The offset was also recorded after a series of runs and in many cases was found to have changed because a small amount of air had intruded into the tap tubing. If the discrepancy was large, repeat runs were conducted. Observe in Figure 3.10 that the pressure gradients (slopes) are greater than the water density at nominal lab temperature of 21°C which is 9.8745 kPa/m. Therefore the indicated differential pressure is adjusted as follows:

$$\Delta P_{diff\_corrected} = \left(\Delta P_{diff} - P_{diff\_offset} \right) \times \frac{9.8745}{10.03081} \tag{3.2}$$

c) Corrected gauge pressure, psi. In a similar fashion, the indicated gauge pressure is adjusted as:

$$\Delta P_{gauge\_corrected} = \left(\Delta P_{diff} - P_{gauge\_offset} \right) \times \frac{9.8745}{10.00922} \tag{3.3}$$

d) Corrected absolute pressure at P_0. To account for the flow loop lab's elevation above sea level, the daily mean station pressure (actual barometric pressure) is added to the corrected gauge pressure.

e) Corrected pressure gradient, psi/ft and Pa/m. The spacing between differential pressure transducers is 30 inches (0.762m). Therefore,

$$\frac{dP}{dl} = \frac{Corrected\_Differential\_\Pr essure}{30/12}\frac{[psi]}{[ft]} \times \frac{6895}{3.28}\frac{[Pa]}{[m]} \tag{3.4}$$

f) Water density, g/cc. Based on average measured temperature and differential section average pressure, water density was calculated with a correlation by McCain, Spivey, and Lenn (2011). For convenience, this correlation was implemented in an Excel spreadsheet as a Visual Basic for Applications (VBA) function macro (see Appendix 7 for VBA source code.)

g) Water volumetric flow rate, m3/s.

h) Superficial liquid velocity, m/s or cm/s. Calculated as:

$$V_{sl} = \frac{Q_w}{A_p} \tag{3.5}$$

i) Pressure at P_1 (beginning of differential pressure section), kPaa. Fluid properties were calculated for conditions at the mid-point of the differential pressure taps. The pressure at the beginning of the differential section (Fig. 4.3) was calculated by assuming the measured pressure gradient was constant in the upper portion of the test section. Since the pressure difference, ΔP, between P_1 and P_2 is measured, we can develop:

$$\frac{\Delta P}{L_2} = \frac{P_0 - P_1}{L_1}$$

$$P_1 = P_0 - \frac{L_1}{L_2} \times \frac{\Delta P}{\Delta L} \tag{3.6}$$

j) Pressure at P_2 (end of differential pressure section), kPaa. Pressures P_1 and P_2 are used to calculate the kinetic energy (KE) component of pressure drop. P_2 is evaluated as:

$$P_2 = P_1 - \Delta P \tag{3.7}$$

k) Average pressure for fluid properties, kPaa. Calculated as:

$$P_{avg} = \overline{P} = P_1 + \frac{\Delta P}{2} \tag{3.8}$$

l) Average superficial air flow rate, m^3/s. Calculated from the mass flow rate and adjusted to pressure at the midpoint of differential section by rearrangement of the ideal gas law:

$$Q_g = \frac{\dot{m}_{air}}{M_{air}} \frac{RT}{\bar{P}} \tag{3.9}$$

m) Average superficial air velocity, m/s.

$$V_{sg} = \frac{Q_g}{A_p} \tag{3.10}$$

n) Average air density, kg/m^3 (for fluid property calculations):

$$\bar{\rho}_{air} = \frac{\bar{P} M_{air}}{RT} \tag{3.11}$$

o) Air density at P_1, kg/m^3:

$$\rho_{air}\Big|_{P_1} = \frac{P_1 M_{air}}{RT} \tag{3.12}$$

p) Air density at P_2, kg/m^3:

$$\rho_{air}\Big|_{P_2} = \frac{P_2 M_{air}}{RT} \tag{3.13}$$

q) Superficial air velocity at P_1, m/s

$$V_{sg}\Big|_{P_1=} \frac{Q_{sg}}{A_p} = \frac{\dot{m}_{air}}{M_{air}} \frac{RT}{P_1} \frac{1}{A_p} \tag{3.14}$$

r) Superficial air velocity at P_2, m/s

$$V_{sg}\Big|_{P_2=} \frac{Q_{sg}}{A_p} = \frac{\dot{m}_{air}}{M_{air}} \frac{RT}{P_2} \frac{1}{A_p} \tag{3.15}$$

s) Average air viscosity, μ_a, Pa-s. Calculated with T and P_{avg} from correlations published by Kadoya, Matsunaga, and Nagashima (1985). VBA code is provided in Appendix 7.

t) Average water viscosity, Pa-s. Calculated with T and P_{avg} from correlations published by McCain et al. (2011.)

u) Water density, g/cc. Based on average measured temperature and test section average pressure, water density was calculated with a correlation by McCain et al. (2011.)

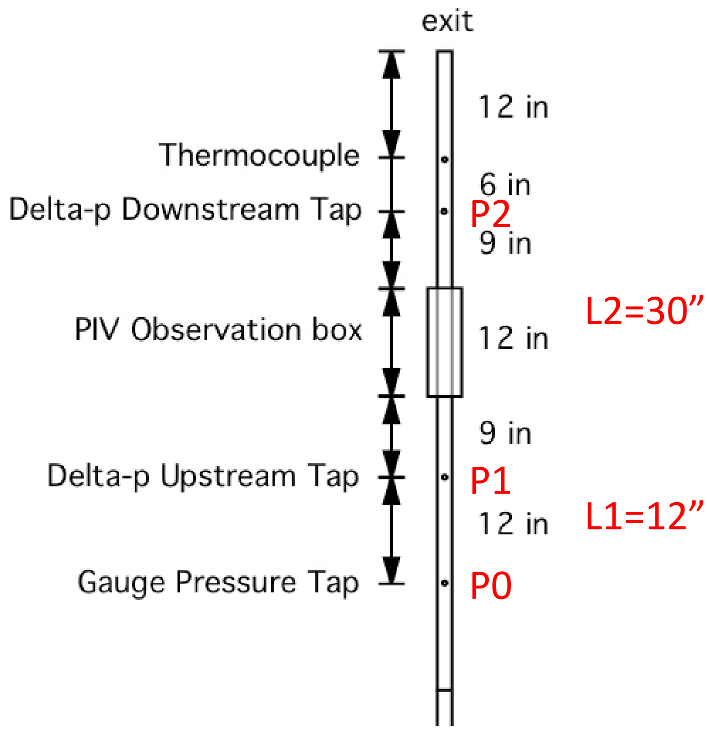

Figure 4.3 Details of Pressure and Temperature Taps in Test Section.

4.2 PLIF Program

The pressure gradient program, with its external observations, provided data to construct a preliminary map of annular flow sub-regimes. The subsequent PLIF program, conducted March 24-28, 2017, aimed to obtain data otherwise not possible with external images, namely film thickness and onset of droplet entrainment. Air and water runs were conducted with a subset of the original test matrix (Figure 4.4.) No new pressure or temperature data were gathered during this phase. For the purpose of calculating superficial velocities, values matching runs during the pressure gradient program were used.

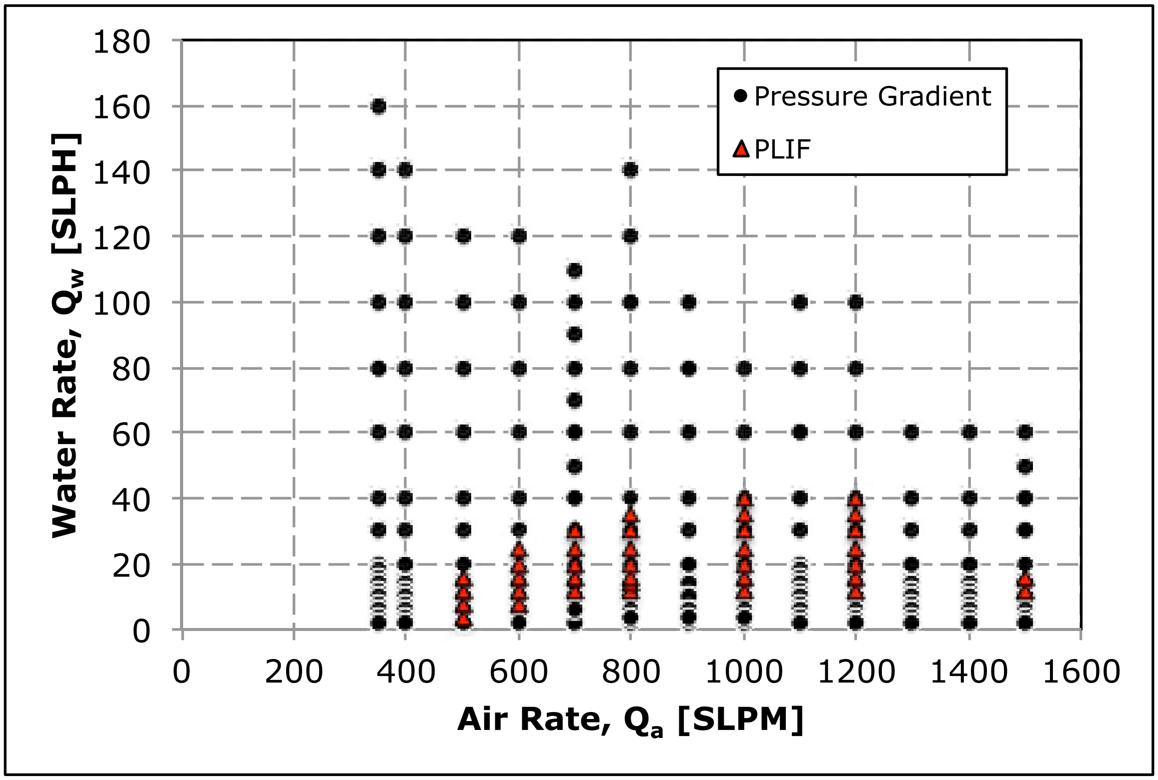

Figure 4.4 Test Matrix for PLIF and Pressure Gradient Runs.

The preparation procedure for PLIF was as follows:

e) Close the water flow control valve to isolate the test section from the reservoir.

f) Add demineralized water to the test section through the filling tee to the top of the viewing section.

g) Lower the calibration target holder through the filling tee to near the bottom of the viewing section. Illuminate with bright spotlight.

h) Ensure the viewing box is sufficiently filled with clean glycol.

i) Using magnets held externally, orient the calibration grid so that it is normal to the CCD camera lens and visible on the PC monitor with DaVis software.

j) Obtain a well-focused image as close as possible to the target, allowing a clear view of the target edge (which is the interior wall of the pipe.)

k) Perform image calibration procedure.

l) Remove calibration target and reinstall filling tee cap.

m) Establish desired air and water flow rates.

n) With DaVis software (and special safety glasses on!), energize pulsed laser and adjust light sheet to about 0.5mm width and at centerline of pipe.

o) Acquire images.

A calibration procedure is necessary to compensate for any distortions in the raw acquired image caused by curvature of the acrylic pipe. First a raw image of the target is obtained. Figure 4.5 shows an uncalibrated image of a previously used target with 0.25mm dot spacing. Observe the distortion on the right hand side of the image near the interior pipe wall. Then the DaVis software detects the dot centres and constructs a uniform grid which removes the distortion near the pipe wall (Figure 4.6.) On Figures 4.6 the horizontal and vertical scales are actually 1/10x indicated, i.e. 10mm is actually 1mm. Observe the target edge on the right side, touching the pipe wall. The image size is about 3.76 mm x 2.84 mm, with a resulting resolution of 2.73μm per pixel. For comparison, in other PLIF work Schubring (2009) with 23.4 mm quartz and 22.4 mm FEP vertical tubing, used two lenses giving resolutions of 6.5 and 3.14μm per pixel; Mamedulanov (2016) obtained a resolution of 6.45 μm per pixel. In a downward vertical annular flow study Zadrazil et al. (2014) employed a 22μm resolution in 32.4 mm tubing.

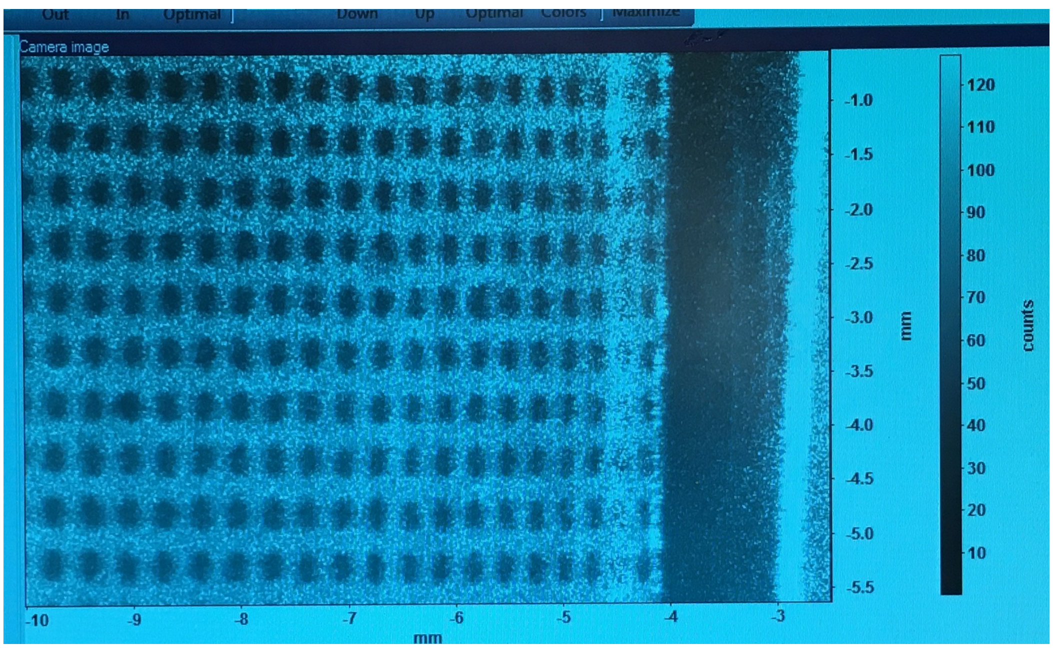

Figure 4.5 0.25 Dot Spacing Pattern Before Calibration.

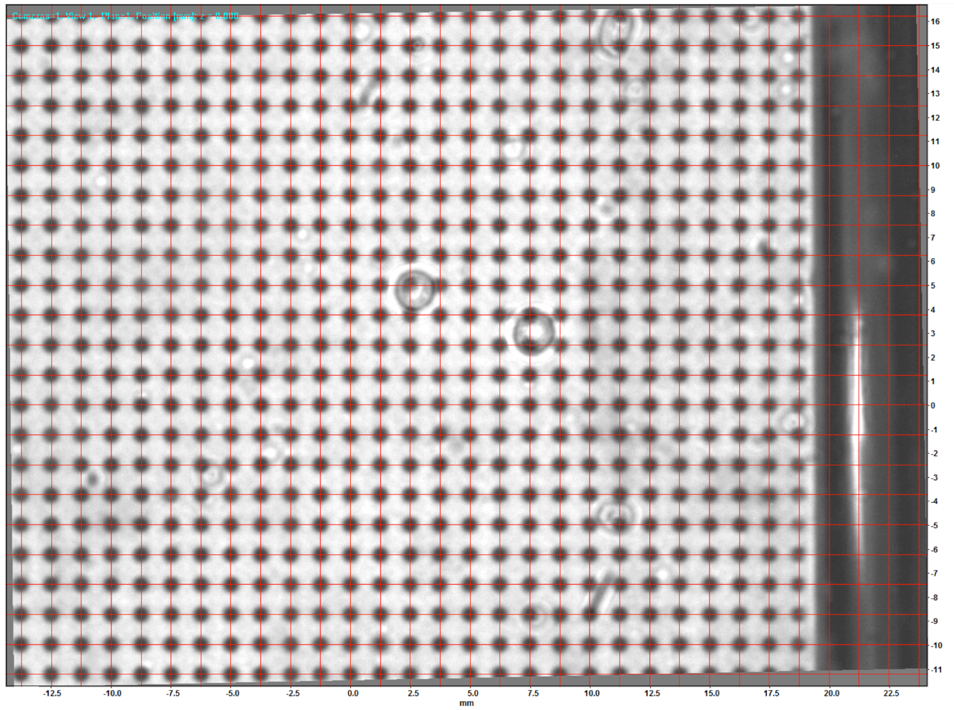

Figure 4.6 0.125 Dot Spacing Pattern After Software Calibration.

Figure 4.7 compares the PLIF imaging window of the current work with recent experiments. Since the PLIF hardware was being shared with other concurrent research projects in the lab, it was mounted on a small mobile cart. Over the course of several sessions, therefore, this setup was performed several times. This resulted in image sizes being slightly different each time.

During image acquisition, the CCD camera lens was adjusted to a small aperture, *f*16, to improve the image depth of field and minimize the influence of ambient light. For each flow rate, between 750 and 1000 images were captured at rate of 5 per second. These were then exported in BMP format with 256 grey levels. Figure 4.8 shows an example at 1000 SLPM air and 25 SLPH water, where the liquid film shows brightly from the illuminated Rhodamine B dye in solution and entrained bubbles appear as dark ovals.

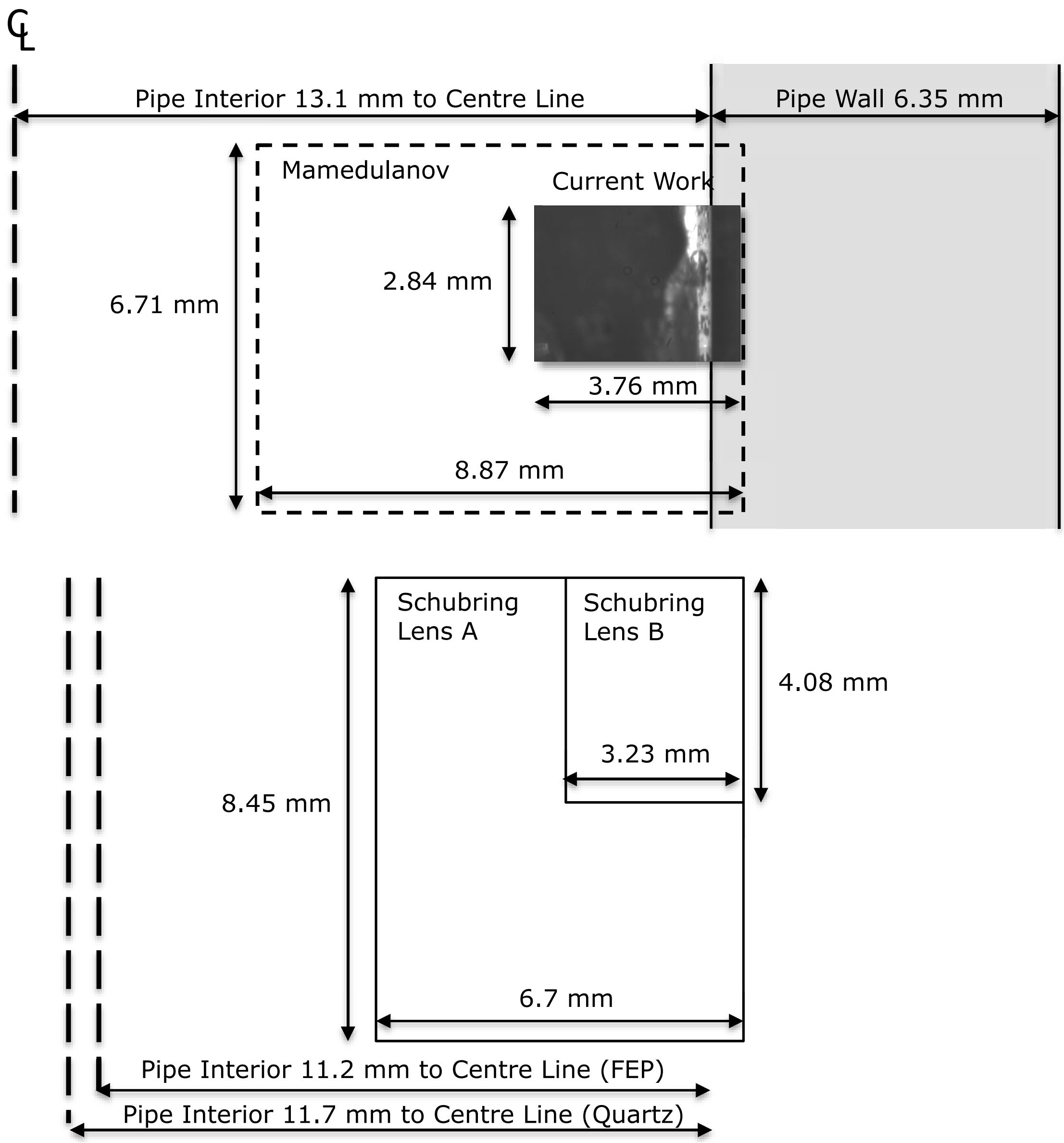

Figure 4.7 PLIF Imaging Window Sizes Compared: Current Work vs. Mamedulanov and Schubring.

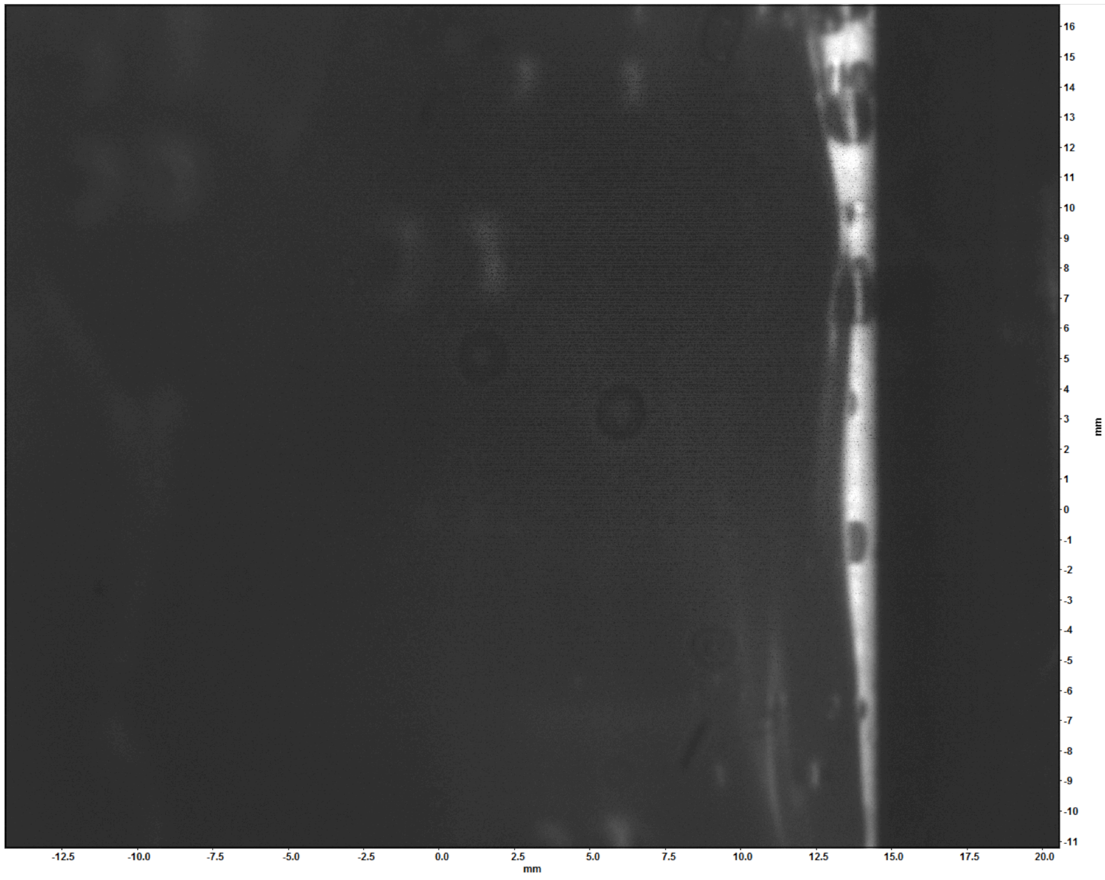

Figure 4.8 Sample PLIF Image at 1000 SLPM Air and 25 SLPH Water.

5 Experimental Results and Analysis

5.1 Test Matrix

Over the course of the pressure gradient program, some air/water rate combinations were rerun because either some essential data had been forgotten to be recorded or to check the repeatability of the system. For pressure gradients and external images 222 useable air/water rate combinations were collected, including 6 data points run with air alone. For this program, pressures in the differential section ranged from 92.4 to 96.4 kPaa with temperatures spanning 10.8 to 24.3°C. Median values for pressure and temperature were 92.9 kPaa and 18.3°C respectively. In addition the PLIF program recorded images for 37 air/water rate combinations. The final test matrix for both programs is shown in Figure 5.1 in terms of superficial air and water velocity as described in Section 4.1.

In order to validate the experimental pressure gradients, the data was compared with published results in similar flow loops under the same conditions.

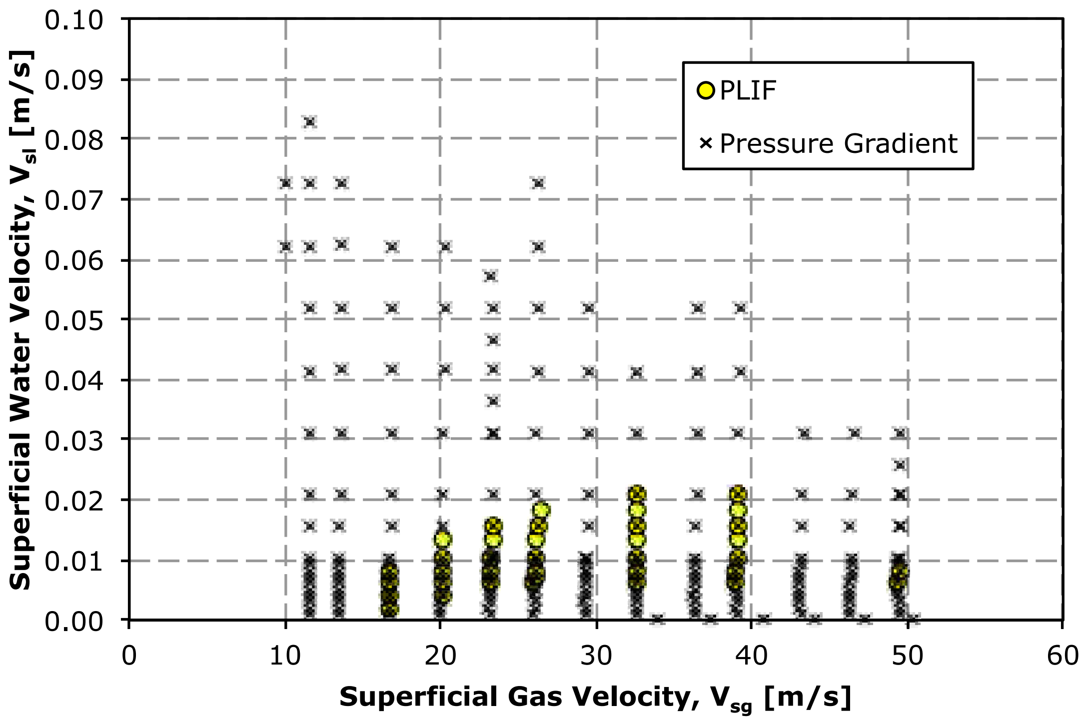

Figure 5.1 Test Matrix for Pressure Gradient and PLIF Program.

The test matrices of selected published work are given in Figure 5.2. Higher water rates studies by Radford (1949) are not included. Previous work studied the completion transition from bubble to slug to churn to annular flow. Note that while the current and previous studies have measured the nominal annular flow regime, the current work has concentrated on annular flow and has explored very low liquid rates more thoroughly.

While tabular data is preferred, some sources provide information only in graphic form. To capture this data for further analysis, the images were scanned and the data extracted. This will introduce some error, depending on the quality of the source material. See Appendix 6 for a fuller discussion.

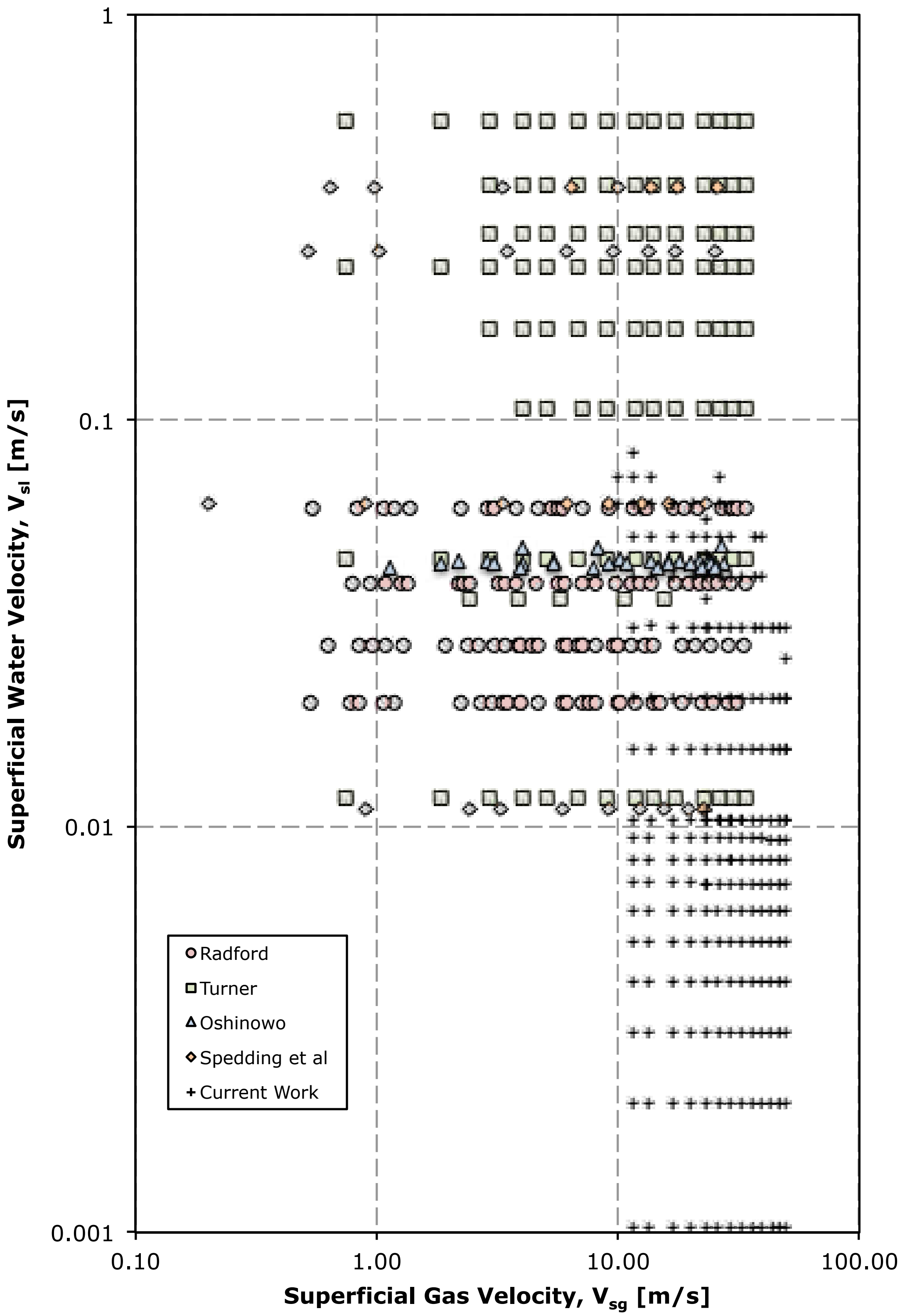

Figure 5.2 Test Matrices from Similar Pressure Gradient Experiments.

5.2 Pressure Gradients

The complete table of data from the pressure gradient program is given in Appendix 1.

Within the pressure gradient program, a series of measurements was made with air alone, which allowed a check of the combined accuracy of the instrumentation and calculations using the measured data. The corrected pressure gradient was then compared with that calculated using an explicit form of the single phase mechanical energy equation,

$$\frac{dp}{dl} = \rho_g g + \frac{f_M \rho_g v_{SG}^2}{2d} + \frac{\rho_g v \Delta v}{\alpha dl} \quad (5.1)$$

The term, α, in the kinetic term of equation 5.1 is a velocity profile adjustment, which Govier and Aziz (2008) recommend approximating to 0.5.

Examination of the literature finds that seemingly smooth surfaces do in fact possess a small but finite hydraulic roughness. In Figure 5.3 from Moody (1944) drawn (nearly smooth) tubing is assigned an absolute roughness, of 0.000006 ft (0.0015mm.) More recently McGovern (2011) appears to have inferred that the same absolute roughness applies to other materials including plastic (Table 5.1)

Table 5.1 Absolute Roughness of Various Materials.

	ϵ/[mm]
Smooth honed steel	0.00065
Drawn tubing: glass, brass, copper, lead, plastic	0.0015
Asphalted cast iron	0.12
Galvanized steel	0.15
Wood stave	0.18 - 0.91
Cast iron	0.26
Concrete	0.3 - 3
Heavy brush coat: asphalts, enamels, tars	0.45 - 0.6
General tuberculation 1-3 mm	0.6 - 1.9
Riveted steel	0.9 - 9
Severe tuberculation and incrustation	2.5 - 6.5

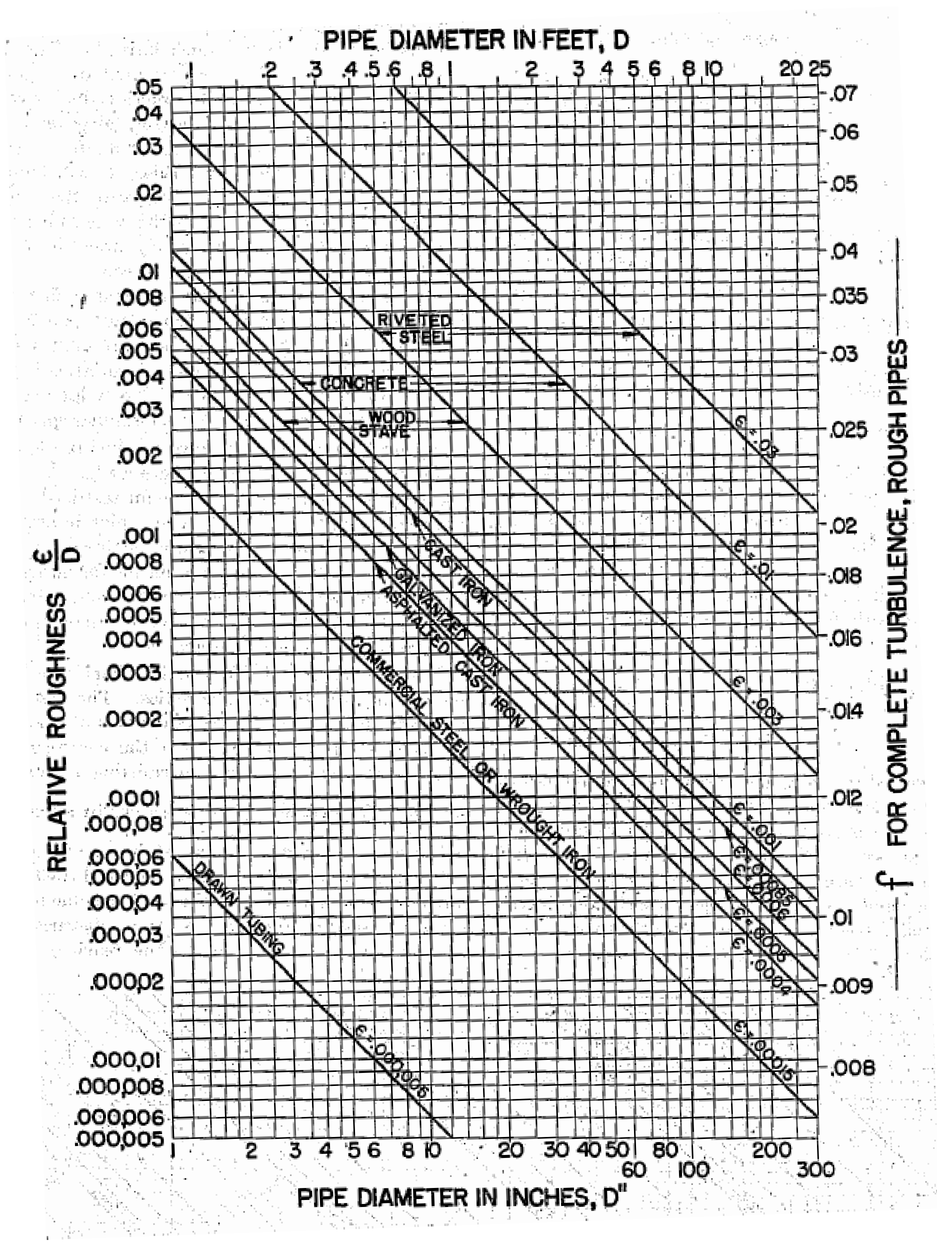

Figure 5.3 Relative Roughness for Various Materials and Dimensions of Pipe.

In another interpretation Flack and Schultz (2014) present a Moody friction factor chart with the legend indicating absolute roughness, ε, for drawn tubing and “Perspex” (plexiglass) at 0.0025mm (Fig. 5.4.)

For comparison the mass flow rate, temperature and pressure data for the air-only runs was used to calculate pressure gradient for the following cases:

a) smooth pipe, no kinetic energy term.

b) smooth pipe with kinetic energy term.

c) rough pipe (ε = 0.0025mm, as suggested by Flack and Schultz) with the kinetic energy term.

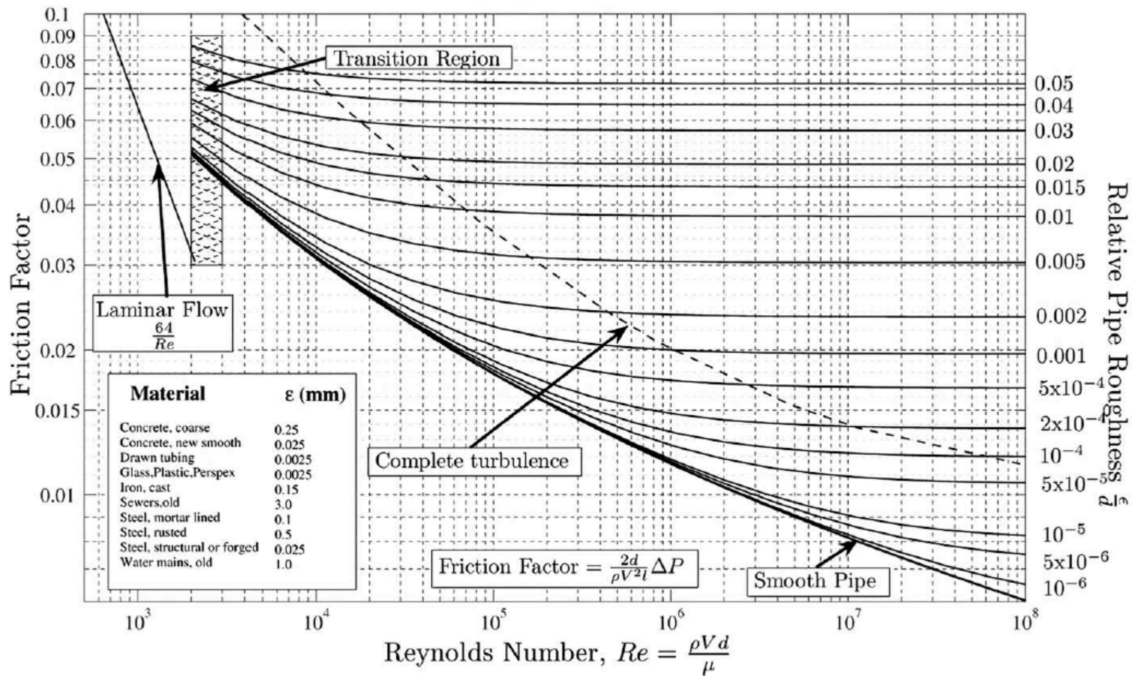

Figure 5.4 Moody Friction Factors and Absolute Roughness for Typical Materials.

For smooth pipe, the friction factor correlation of Prandtl, as given in Schlichting (1975) was used:

$$\frac{1}{\sqrt{f}} = 2.0\log\left(N_{\mathrm{Re}}\sqrt{f}\right) - 0.8 \tag{5.2}$$

Although Prandtl requires an iterative solution, it is more accurate than the Blasius equation,

$$f = \frac{0.3164}{\mathrm{R}_e^{0.25}} \tag{5.3}$$

at Reynolds numbers greater than about 10^5, according to Schlichting (1975.) To evaluate the rough pipe case, the Swamee-Jain correlation (1976) was used:

$$\frac{1}{\sqrt{f}} = 1.14 - 2\log\left(\frac{\varepsilon}{d} + \frac{21.25}{N_{\mathrm{Re}}^{0.9}}\right) \tag{5.4}$$

In calculating the kinetic energy term, the differential velocity was calculated from the terms defined in Section 4 as,

$$\Delta v = V_{sg}\Big|_{P_2} - V_{sg}\Big|_{P_1} \tag{5.5}$$

Fig. 5.5 shows the measured vs. calculated pressure gradients over the range of air-only velocities in the vertical flow loop. The pressure offset error was not recorded at the time; instead the values found to be consistent during subsequent work were used (-0.018 psi for gauge, -0.022 psi for differential.)

In comparing measured versus calculated results, it is evident from Fig. 5.5 that inclusion of the oft-neglected kinetic energy term is important, while the assumption of pipe roughness has a lesser impact on the calculated result. This is consistent with the assumption that the acrylic test section tubing is close to hydraulically smooth. For the five highest flow rates, the average absolute difference between measured and calculated with smooth pipe and KE is 2.2%. However if the pipe was assumed to be smooth with KE disregarded, the average discrepancy for the same four points becomes about 5.4%.

Note the measured pressure gradient at v_g = 34 m/s is about 15% lower than the calculated value. The measured differential pressure after correction at this rate was about 330 Pa. At about 5% of full scale of the differential pressure transducer, this is within a zone of poorer accuracy of the instrument. In addition, at lower pressure differentials the signal to noise ratio decreases, making it difficult to interpret an average value from the recorded data. If a signal to noise ratio (S/N) is defined as the ratio of the average value to the standard deviation, then for the case of air-only flow S/N declines rapidly below a corrected differential pressure of about 600 Pa (see Fig. 5.6.)

It is useful to present the two-phase pressure gradient data in graphic form. Fig. 5.7 shows pressure gradient as a function of v_{sg}, grouped by constant liquid rate. For reference, the air-only data along with theoretical air pressure gradient are included. A closeup of the more crowded data in the lower left corner of the graph is given in Fig. 5.8. The pressure gradient minima occurs at about 17 m/s. This generally reflects a transition from gravity-dominated flow at low gas velocities to friction-dominated flow at higher velocities. Increased liquid loading serves to magnify the pressure loss.

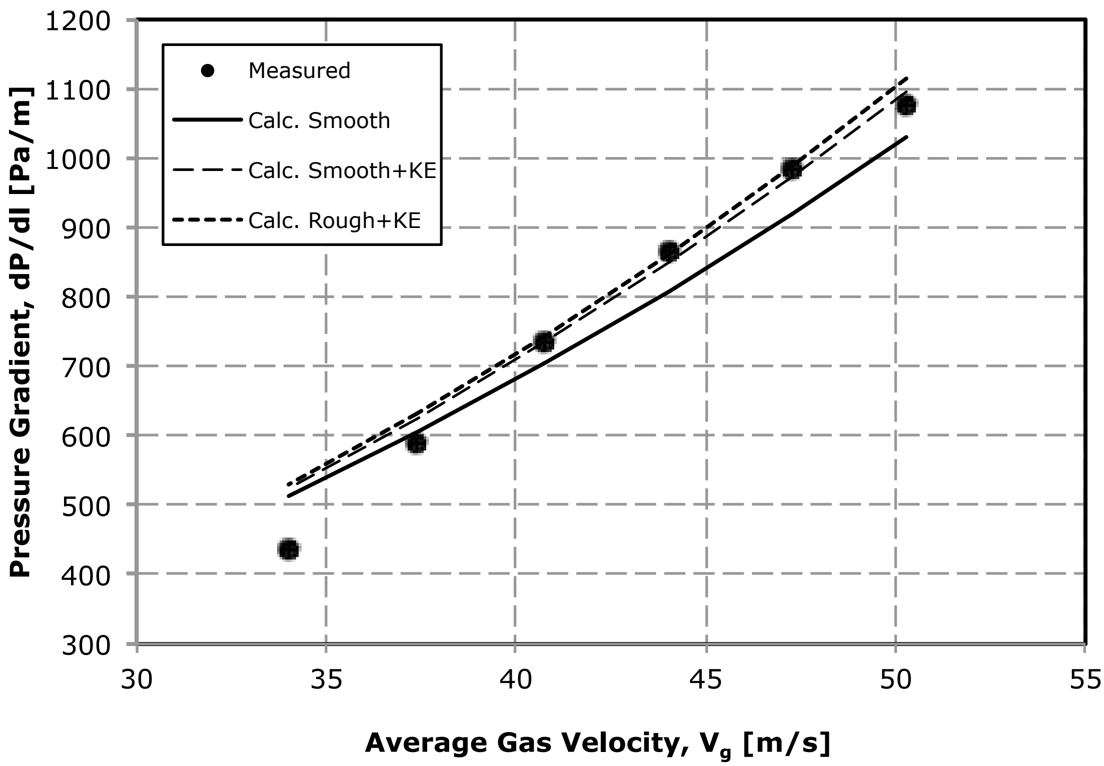

Figure 5.5 Calculated vs. Measured Pressure Gradient in Flow Loop with Air.

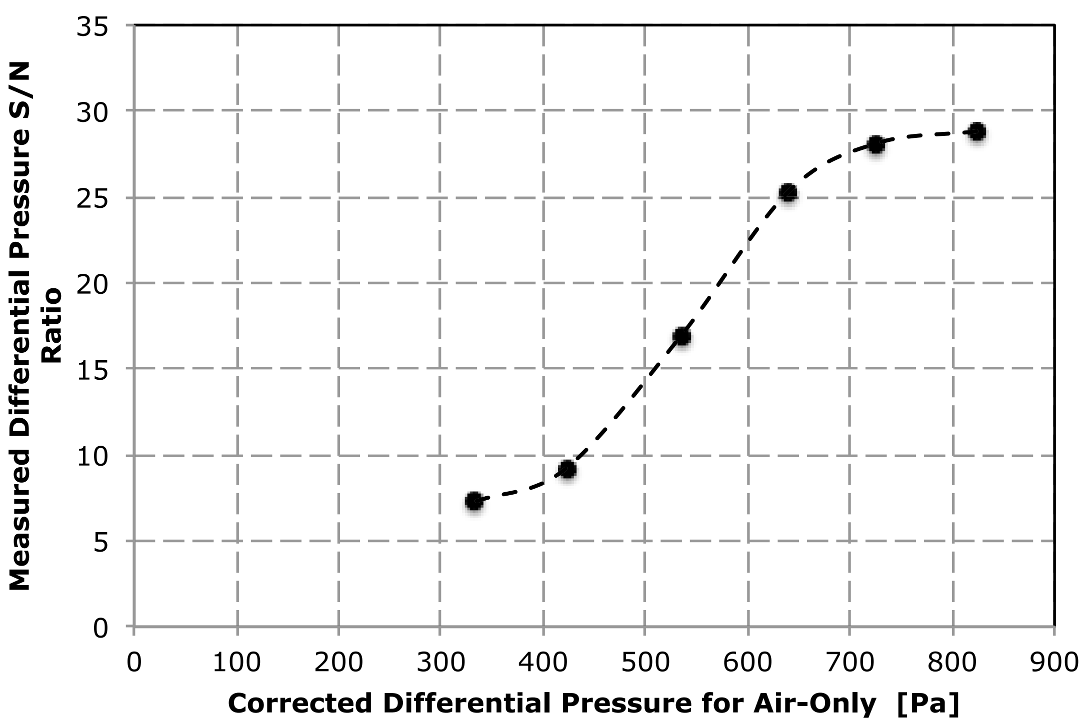

Figure 5.6 Measured Differential Pressure Error vs. Calculated Differential Pressure.

At the lowest superficial liquid rate measured (0.001 m/s) the pressure gradient asymptotically approaches air-only values as gas velocity decreases.

Figure 5.9 depicts the pressure gradients as a function of superficial liquid velocity, with Figure 5.10 providing an enlarged view for lower velocities. Note a prominent change in slope of the curves at approximately v_{sl} = 0.01 m/s.

The veracity of the two-phase pressure gradient data can also be inferred when compared with published work. These data were selected from experimental results with air and water obtained from nominal 25.4mm i.d. tubing at or near standard conditions (101.325 kPaa, 15°C.) For closely matching superficial liquid velocities, the experimental pressure gradients from the current work are very consistent with those of Radford (1949.) The greatest discrepancy is at V_{sl} =0.061 m/s , where Radford's data is about 10-15% higher (Fig. 5.11.) Pressure gradients data by Turner (1966) and Oshinowo (1971) also match very well with the current work as seen in Figs 5.12 and 5.13 respectively. Finally, the data from Spedding , Woods, Raghunathan and Watterson(1998a, 1998b) is in conformance with the current results for two different values of v_{sl} (Fig. 5.14.)

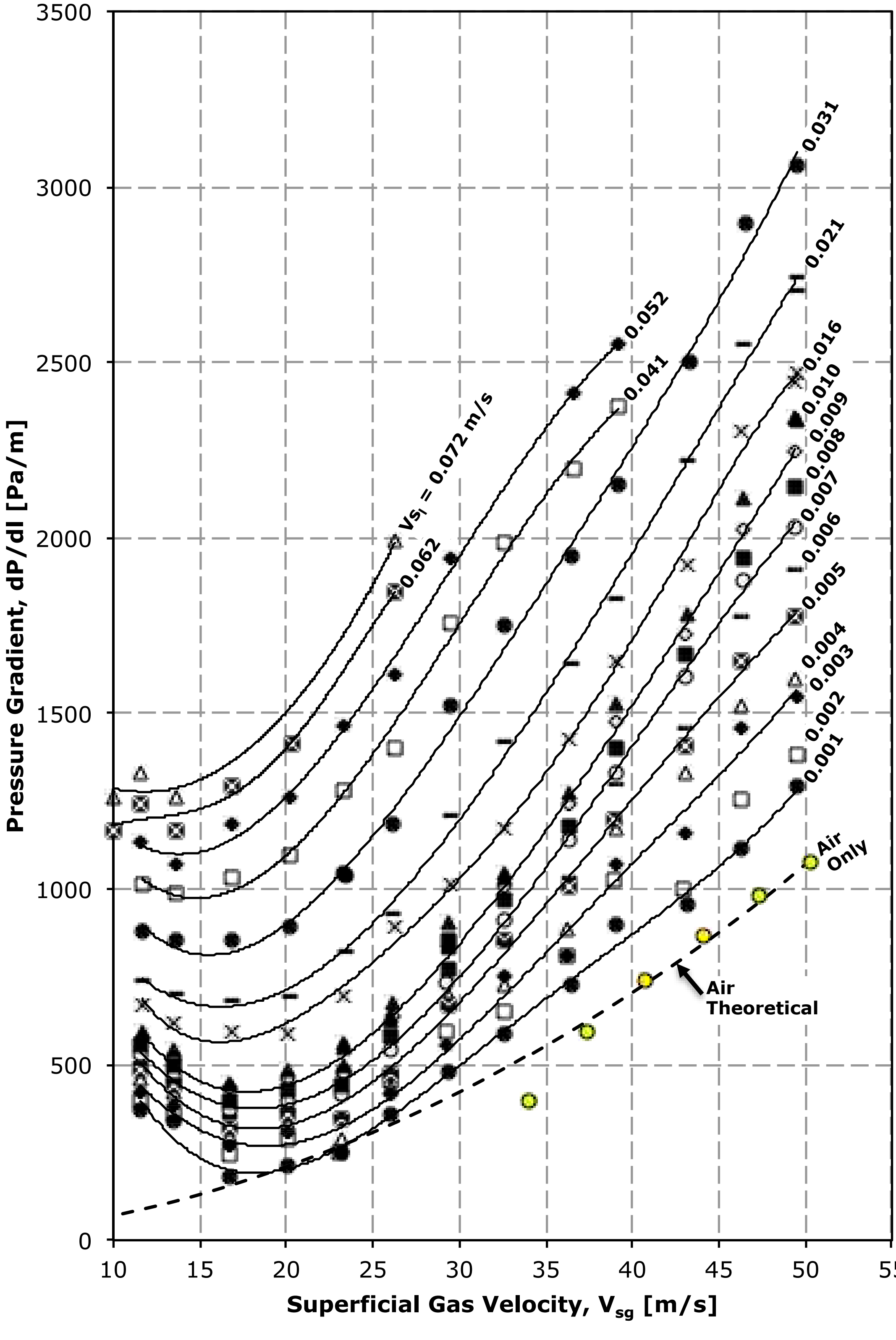

Figure 5.7 Pressure Gradient vs. Superficial Gas Velocity, Grouped by Constant v_{sl}.

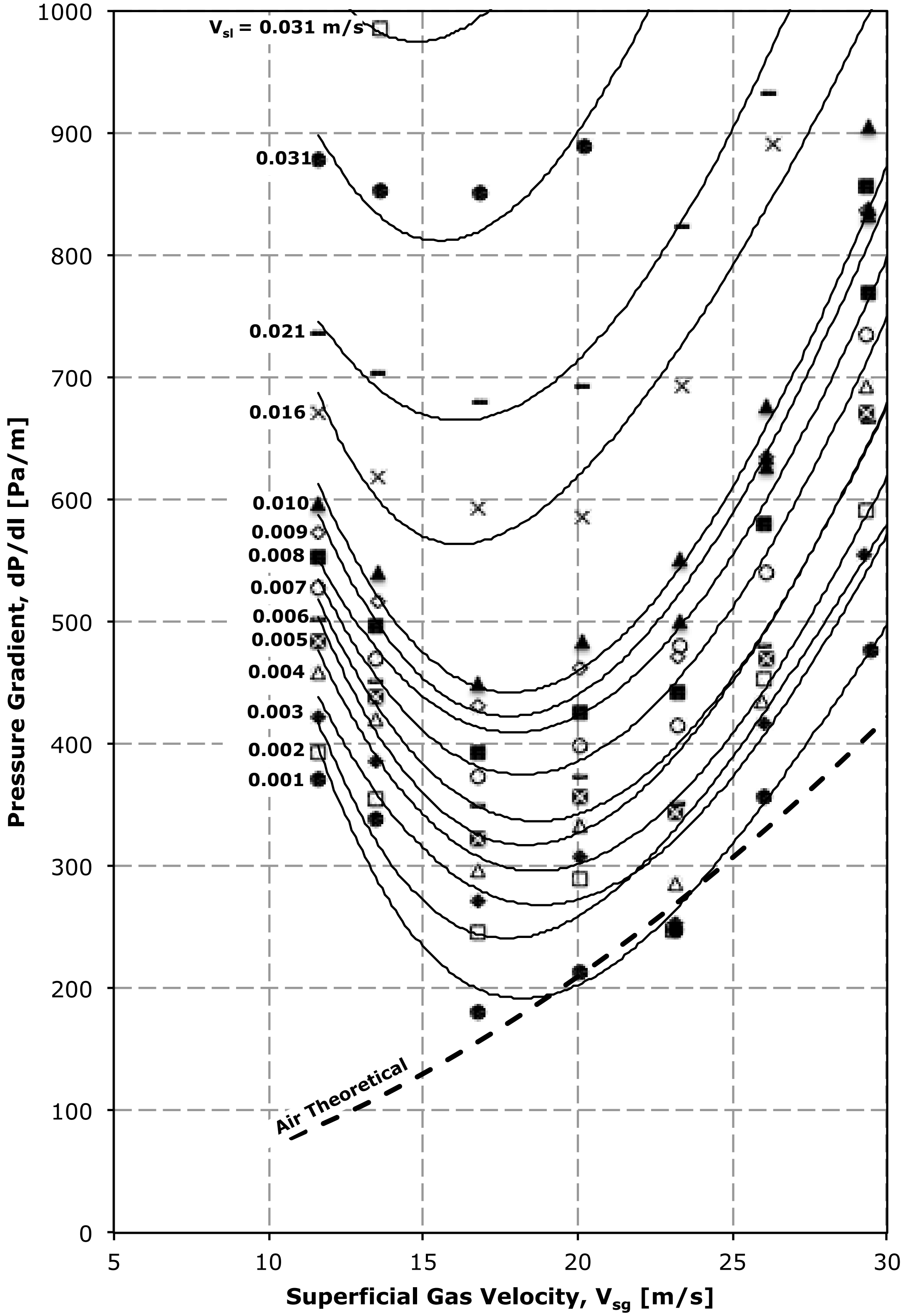

Figure 5.8 Pressure Gradient vs. Superficial Gas Velocity Grouped by Constant v_{sl} (Closeup.)

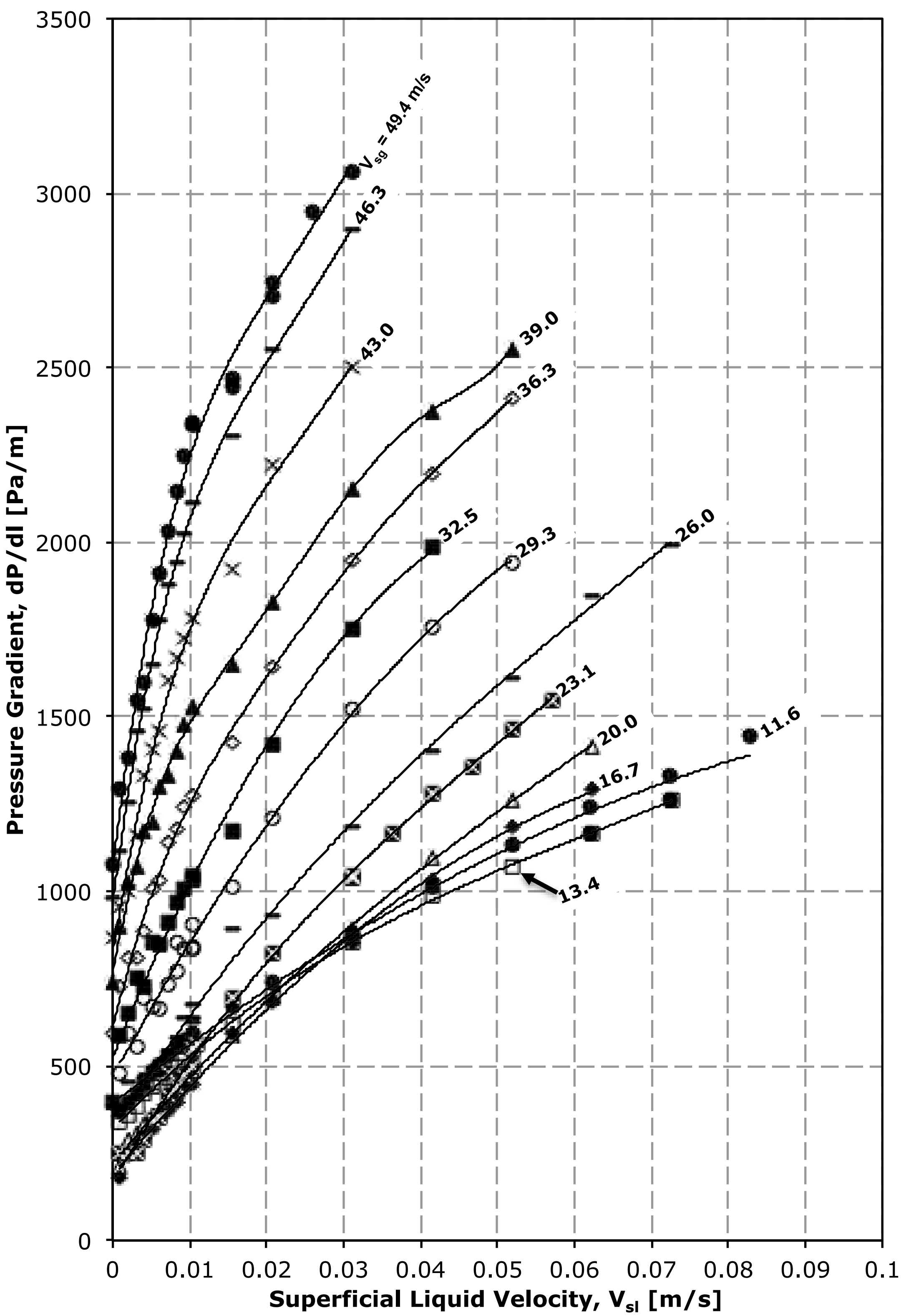

Figure 5.9 Pressure Gradient vs. Superficial Liquid Velocity, Grouped by Constant v_{sg}.

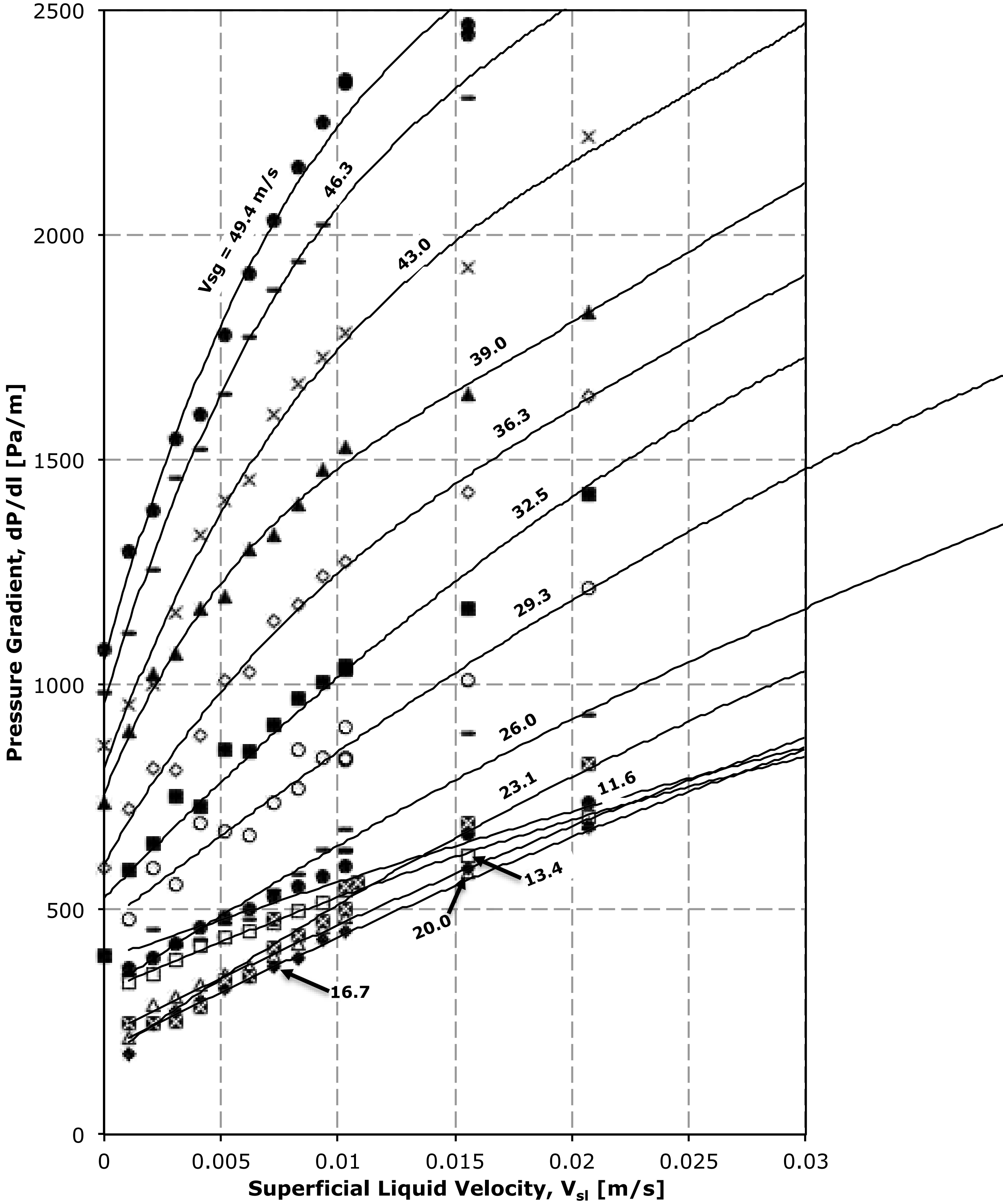

Figure 5.10 Pressure Gradient vs. Superficial Liquid Velocity, Grouped by Constant v_{sg}. (Closeup.)

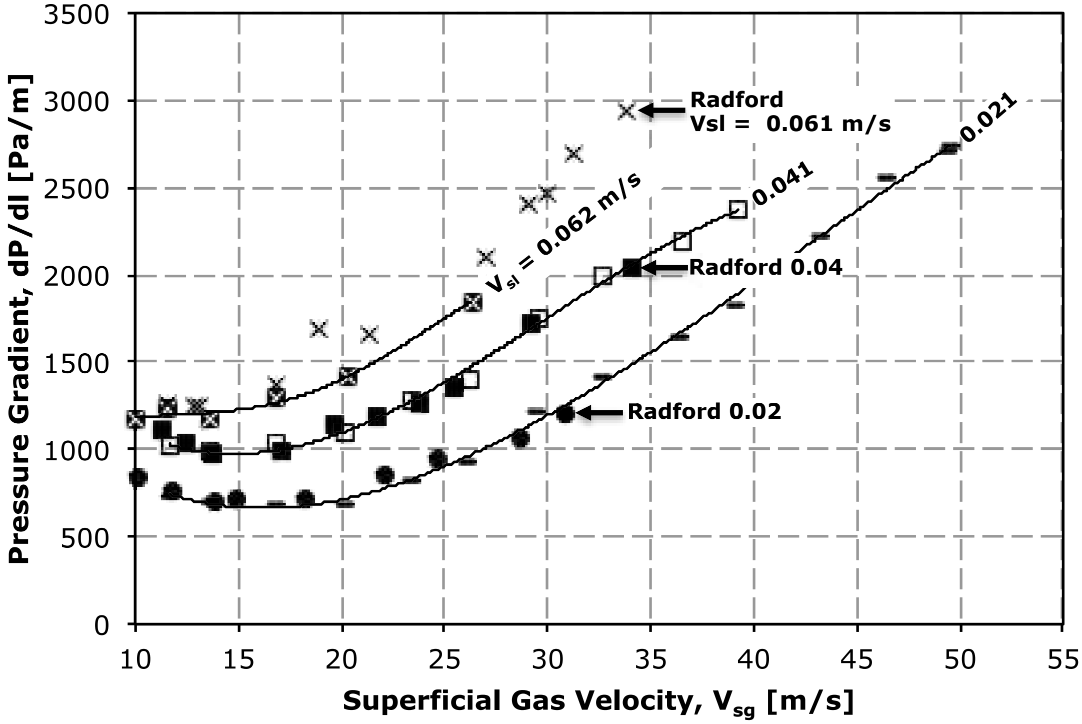

Figure 5.11 Pressure Gradients Compared: Current Work vs. Radford (1949).

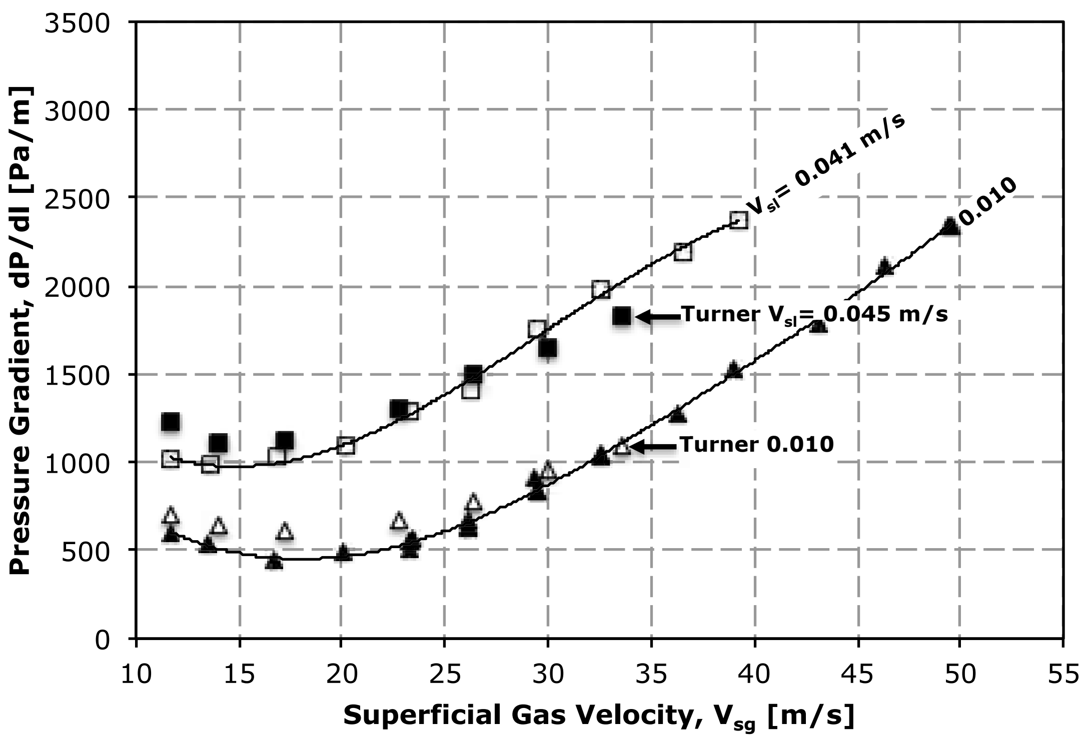

Figure 5.12 Pressure Gradients Compared: Current Work vs. Turner (1966).

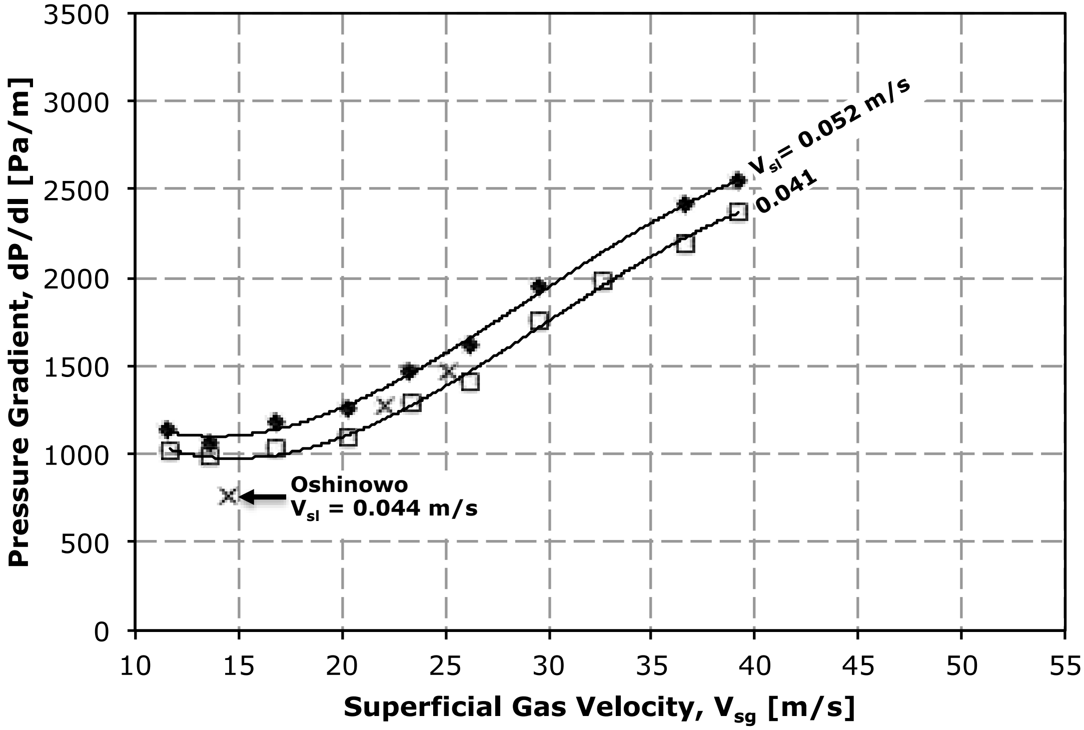

Figure 5.13 Pressure Gradients Compared: Current Work vs. Oshinowo (1971).

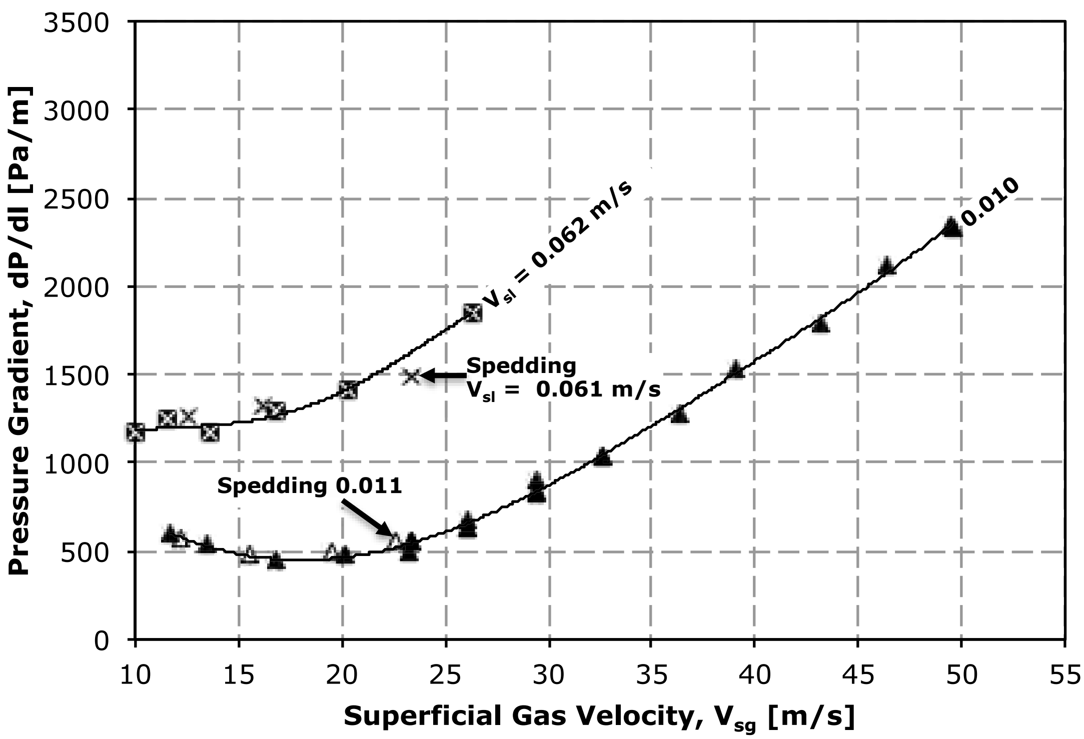

Figure 5.14 Pressure Gradients Compared: Current Work vs. Spedding et al (1998a).

5.3 Sub-Regimes of Annular Flow

For each air/water flow rate, external still images were taken at shutter speeds as high as 1/3600s sec, with video at both 30 and 240 frames per second. Based on examination of these images a number of distinct sub-regimes were observed (see Fig. 5.15, where actual size of each image is 38 x 90 mm):

a) Churn flow (CH). A chaotic mix of liquid with large entrained bubbles, and gas.

b) Churn-Ring (CH-RING). Intermittent churn or disturbance flow with large "rings" of liquid film with large entrained bubbles.

c) Annular-Ring (ARING). Slow moving "rings" of liquid with large entrained bubbles.

These first three sub-regimes are usually mapped as a single flow regime, i.e. churn. However, observation of slow motion video has allowed a finer distinction to be made. These sub-regimes are to the left of the pressure gradient minima, as depicted in Figs. 5.7 and 5.8. The increase in pressure gradient with reducing gas velocity is attributed in part to increasing liquid holdup. This in turn results in a higher static component of the pressure loss. The interval between disturbances is marked by a falling film adjacent to the pipe wall. This is evident from the motion of entrained air bubbles in the liquid film, which can be followed until a disturbance wave or ripple wave arrives to propel the majority of the liquid film upward. The churn, churn-ring and annular-ring sub-regimes still provide a net upward movement of liquid at a superficial gas velocity as low as 11.6 m/s, which is between the values calculated with the methods of Turner et al. (1969) and Woods et al. (1999). Wallis (1969) provides a description of this condition as one "in which thin liquid films flow downward while thick ones flow upward. A net upflow of liquid then occurs as a result of 'waves' of thick film riding over a smoother and thinner falling film." This was observed in the high frame rate videos of this churn region. The flow rate at which this occurs is given by eq'n 5.6a and solves to 11.4 m/s.

Within the nominal annular regime itself, the following were identified:

d) Annular Rivulet (ARIV). Liquid film moving as one or more thin bands or rivulets when liquid input is very low.

e) Annular Partial Wetting (APW). The circumferential continuity of the liquid film breaks and liquid flows upwards in wide bands, generally wetting greater than half the pipe wall circumference.

f) Annular Ripple Wave (AR). The liquid film appears as a thin continuous layer with smooth ripple-like waves; few bubbles are observed at lower gas rates. In slow motion video, distinct periodic bands appear; the varying colour of the dye indicates that these bands alternate in film thickness.

g) Annular Ripple Wave (AR-b). At higher gas rates more and more air bubbles are entrained in the liquid film.

h) Annular Pulse (AP). Liquid film with a large quantity of entrained bubbles, more variation in thickness, and frequent pulse or disturbance waves. See Fig. 5.16 for a closeup of this sub-regime.

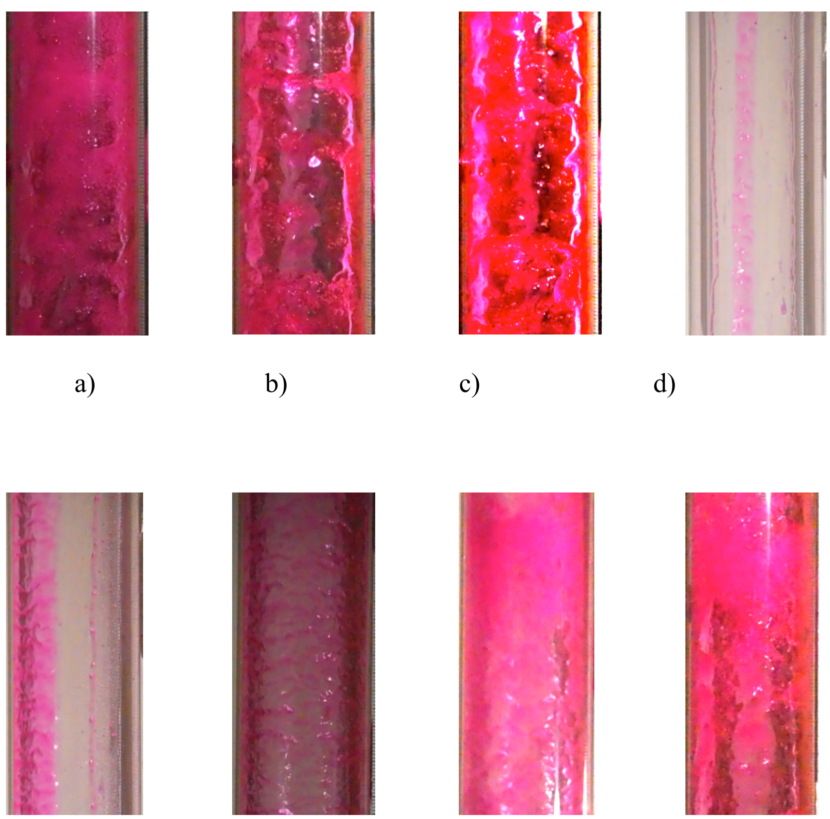

a) b) c) d)

e) f) g) h)

Figure 5.15 Example External Images of Two Phase Flow Regimes.

Based on the images obtained, each air/water rate was assigned to one of the defined flow sub-regimes. Note that the water colour is from remnant Rhodamine-B dye from the concurrent PLIF studies. There was some difficulty determining some of the sub-regime transitions. The transition from APW to ARIV was determined as follows: rivulet flow was assigned when less than about half the pipe wall was wetted with liquid. Also, the sub-regime transition from AP to AR was considered complete when the disturbance wave interval was longer than 30s apart. The annular flow sub-regimes are mapped as a function of superficial fluid velocities in Fig. 5.17. Note the transition to annular flow was observed to occur in the interval $11.5 < v_{sg} < 13.5$ m/s.

Figure 5.16 Annular Pulse (AP) Sub-Regime at v_{sg} = 16.7 m/s and v_{sl} = 0.031 m/s.

A composite of representative external images for the test matrix is provided in Appendix 8 in tabloid format (279 mm x 432 mm.)

Slow-motion video images revealed the following: The AP sub-regime exhibits air bubbles entrained in the liquid film up to a superficial gas velocity of 18 m/s. At higher gas velocity, the high frequency of disturbance waves makes it difficult to observe the film. The annular ripple wave sub-regime has two forms: entrained air bubbles are seen in the liquid film at higher water rates (AR-b) and at lower water rates, the film appears to be bubble free (AR). There is a continuum between AR and AR-b.

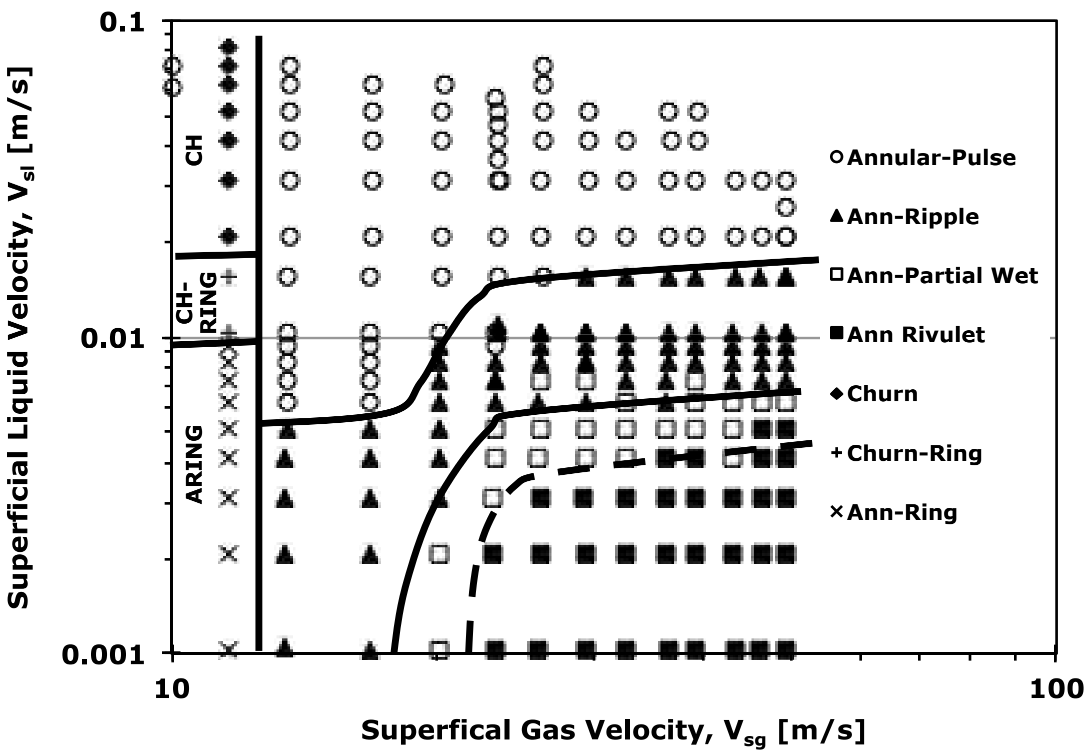

Figure 5.17 Annular Flow Sub-Regimes.

It is instructive to overlay the flow regime boundaries of Figure 5.17 onto the pressure gradient curves. In Fig. 5.18 shows that increased liquid input triggers the transition from AR to AP with a corresponding increase in pressure gradient. However, an increasing gas velocity inhibits that transition. In Figure 5.19, the boundaries between flow regimes are clearly controlled by liquid velocity.

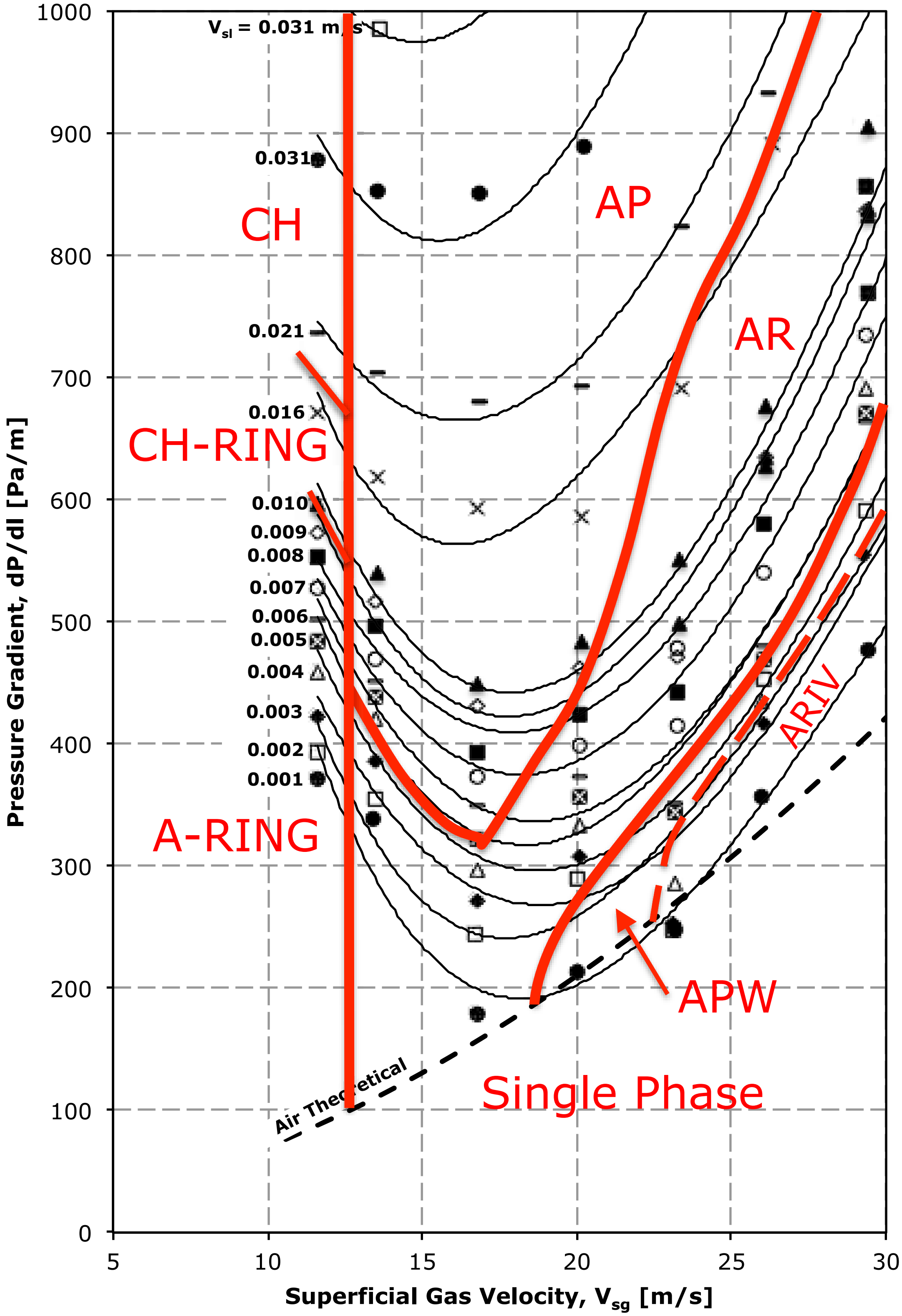

Figure 5.18 Pressure Gradient vs. v_{sg}, with Sub-Regime Boundaries.

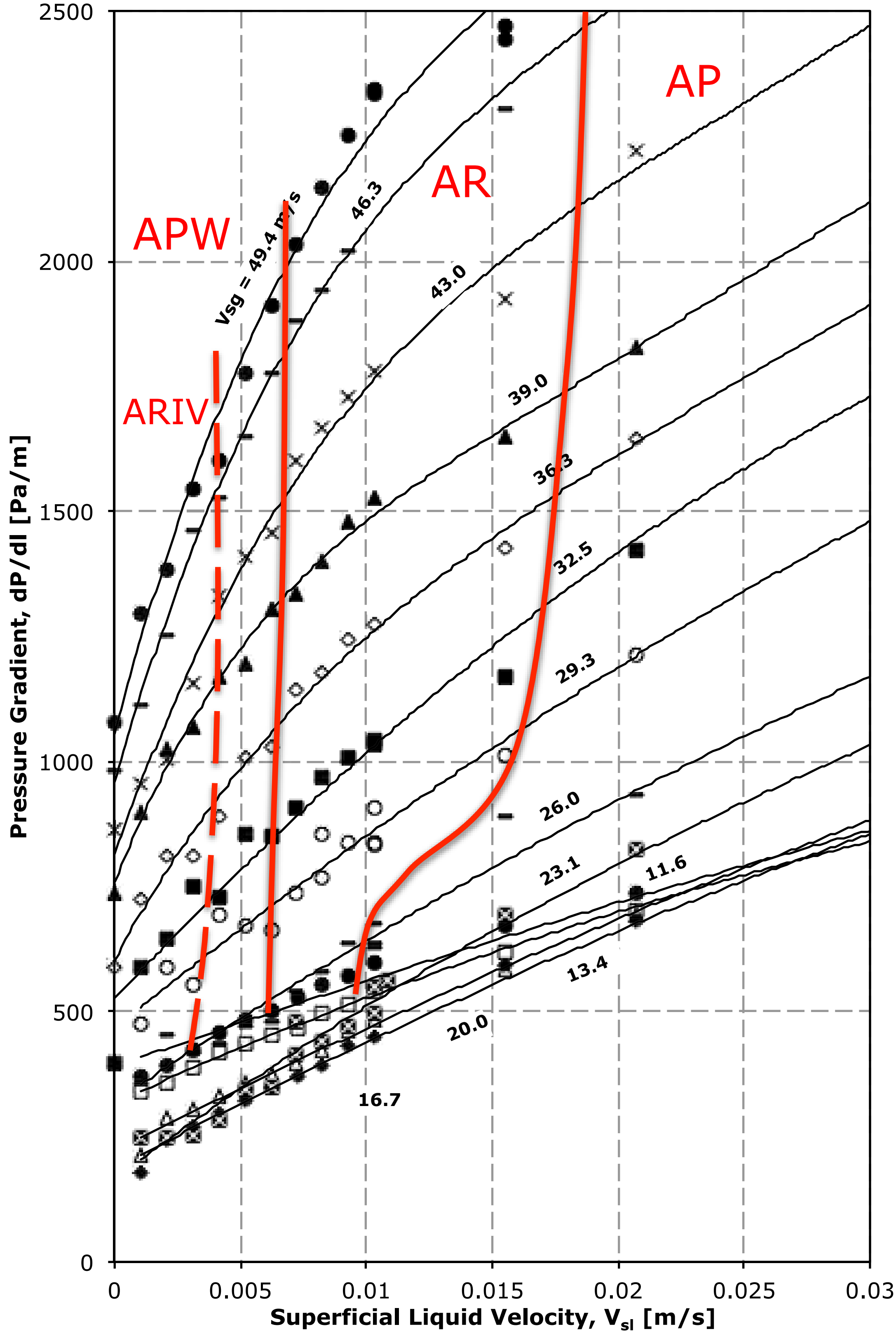

Figure 5.19 Pressure Gradient vs. v_{sl}, with Sub-Regime Boundaries.

From a conceptual standpoint, the transition to annular flow is subject to the following:

a) Upward flow of the liquid film.

b) Upward transport of any entrained liquid droplets.

c) Liquid holdup small enough to avoid bridging across the pipe.

The upward movement of the liquid film is a result of drag forces from the gas core. Wallis (1969) cited experimental work that led to an expression for minimum dimensionless gas velocity,

$$v_{sg}^{*} \approx 0.9 \tag{5.6a}$$

describing "a situation in which thin liquid films flow downward while thick ones flow upward." Furthermore, Wallis contended that in the case of laminar liquid flow, the transition would occur at

$$v_{sg}^{*} \approx 0.8 \tag{5.6b}$$

The dimensionless superficial gas velocity is defined as,

$$v_{sg}^{*} = v_{sg} \frac{\rho_g^{1/2}}{\left[gD\left(\rho_f - \rho_g\right)\right]^{1/2}} \tag{5.7}$$

With air and water properties at standard conditions in nominal 25 mm pipe, equation 5.6a gives a minimum gas velocity of 11.4 m/s while equation 5.6b solves to 10.1 m/s. This gives the range of minimum superficial velocity for net upward liquid film transport.

Recall the Turner et al. (1969) expression for annular flow based on the minimum lifting velocity (critical velocity) of liquid droplets (now showing the droplet coefficient of drag, C_D,

$$v_{crit} = 2.515\left[\frac{\sigma g\left(\rho_l - \rho_g\right)}{C_D \rho_g^2}\right]^{1/4} \tag{2.3}$$

To arrive at a tractable solution, Turner assumed the droplets are spherical and moving at very high velocity so that their drag coefficient is constant at $C_D = 0.44$. Recent work has shown that additional considerations are required to used equation 2.3 properly:

a) entrained liquid droplets can become distorted or broken up by the gas stream, therefore the spherical drag coefficient no longer applies (Wang, Bai, Zhu, Zhong, and Li, 2012).

b) At low gas flow rates, the particle Reynolds number, Re_p decreases so that the drag coefficient increases. Re_p is defined as $\rho v_p d_p/\mu$ where ρ is the fluid density, v_p is particle velocity, d_p is particle diameter and μ is fluid viscosity.

c) Equation 5.7 will result in a single value for droplet diameter, whereas a wide range of diameters has been measured experimentally (Luan and He, 2012).

In spite of these concerns, equation 5.7 persists as one of the preferred estimates of minimum lifting velocity in the petroleum industry. Using air-water properties at standard temperature and pressure (with surface tension, $\sigma = 7.2 \times 10^{-2}$ N/m) air water properties equation 2.3 solves numerically to 14.4 m/s.

In general, the bridging criterion applies to very thick films, which is not the case for the current work. Therefore the transition to annular flow can be considered to occur in two stages: initially, the gas core develops sufficient drag force to lift a liquid film upwards; then with increasing gas velocity, droplets are sheared from the liquid film and entrained in the high speed gas core. Note that the film lifting equations (5.6a, 5.6b) account for pipe diameter while the droplet equation does not. Furthermore neither equation considers the effect of liquid velocity.

The test matrix from other 25mm id work is shown in Fig. 5.20. It is apparent that previous workers wanted to study the spectrum of flow regimes from bubble to annular mist. Observe that the current work was focused on annular flow at relatively low liquid rates. The annular transitions from several published works is depicted in Fig. 5.21, most from nominal 25.4mm i.d. tubing at or near standard conditions. Included are both the Wallis (1969) criteria for film stability and the Turner (1969) criteria for droplet lifting. The transition to annular flow among different sources exhibits obvious differences. This can be explained, in part, by different definitions. For example, Radford's "wall film flow" begins within the churn regime; the "mist" regime assumes fully entrained liquid in friction dominated flow. The annular transition from Barnea (1987) is based on a reinterpretation of his own data. Spedding et al. (1998a) defined a "semi-annular" condition that appears to correspond with Radford's (1949) onset of "wall film flow." The transitions shown are:

1. Nedderman and Shearer (1963), 31.8mm pipe, dewetted region
2. Hall Taylor and Hewitt (1963), 31.8mm pipe, non-wetting
3. Radford (1949), mist flow
4. Turner et al (1969) equation 2.3, calculated for air-water in nominal 25mm i.d. pipe at standard conditions
5. Equation 5.6a from Wallis (1969)
6. Spedding et al. (1998a), annular transition
7. Barnea (1987), slug-churn transition
8. Radford (1949), beginning of wall film
9. Spedding et al. (1998a), semi-annular

Note the general agreement with the APW and ARIV sub-regimes identified in the current work.

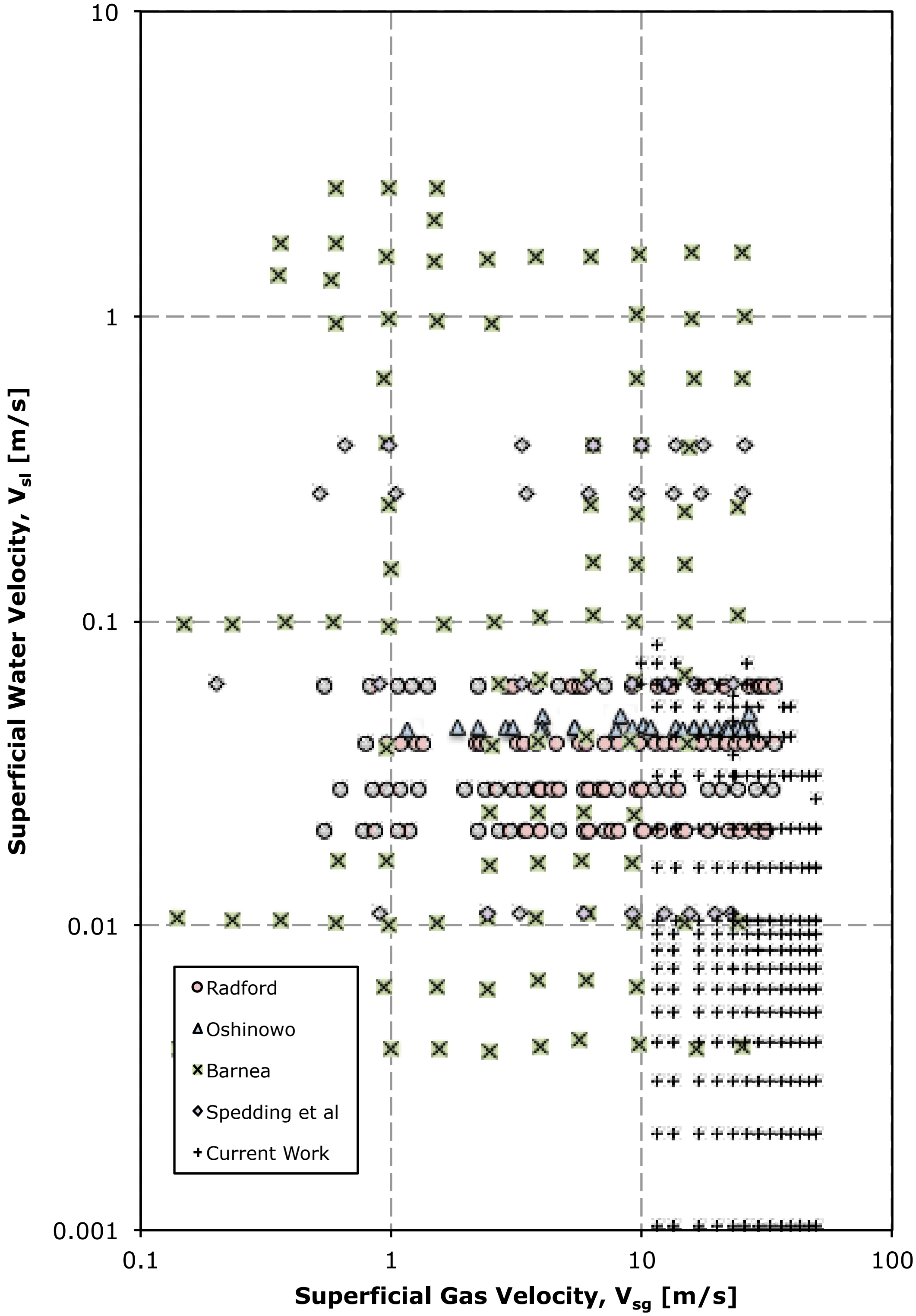

Figure 5.20 Test Matrices for Experiments in Flow Regime Identification.

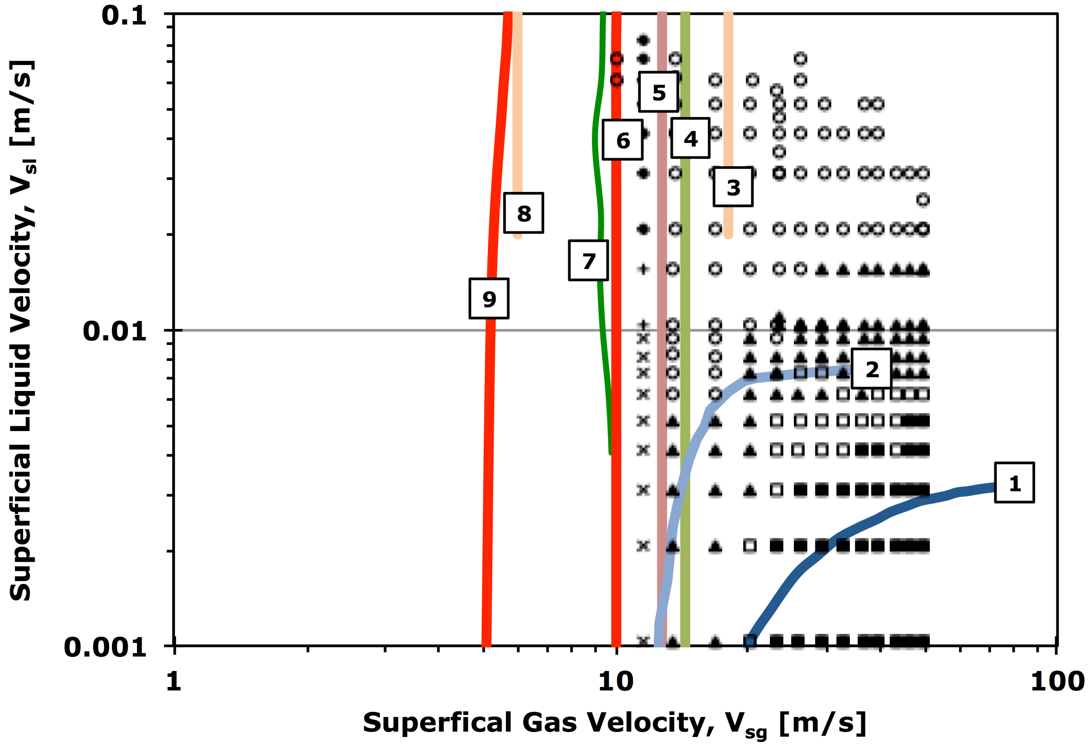

Figure 5.21 Transition to Annular Flow from Various Sources (see Legend in Fig 5.17)

5.3 Film Thickness

A limited number of PLIF runs were conducted to verify liquid film thickness (see the test matrix, Fig. 5.1.) The images were also examined for signs of liquid entrainment, something that was not possible with the external images. Previous work has used MatLab scripts to automate interpretation of large numbers of PLIF images, among them Schubring (2009), Zadrazil (2014), and Mamedulanov (2016) for vertical annular flow. The complexity of composing an intelligent script to interpret the images for all conditions let to a different approach: manually interpret a small number of images instead.

For each air/water case, the first 750 to 1000 images were exported from the DaVis software to 256-level greyscale files in BMP format. The first 50 images form each group were then imported to NIH ImageJ software (which is public domain) where it was scaled. The liquid film was identified by its brightness and then manually traced to obtain a film cross sectional area (Figure 5.22.)

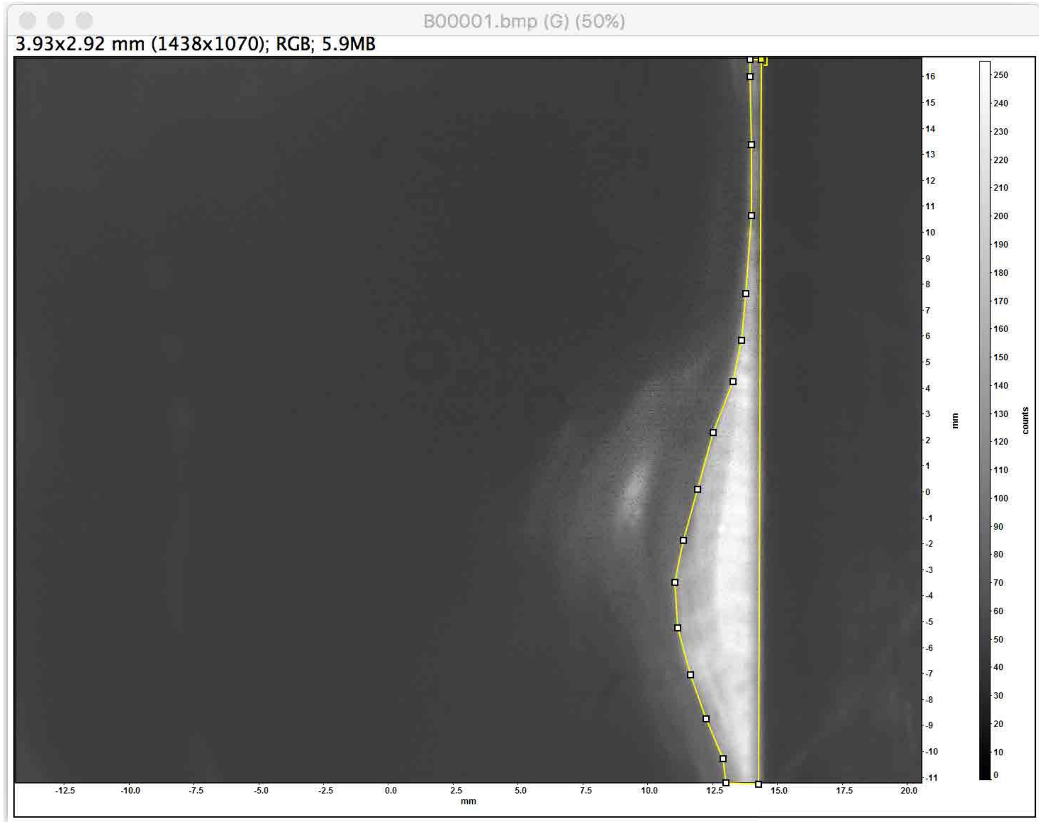

Figure 5.22 PLIF Image from v_{sg} = 26.7 m/s, v_{sl} = 0.074 m/s (1 of 50.)

The area was computed by the ImageJ software and copied to an Excel spreadsheet where the average film height was calculated. In the example in Fig. 5.22, the scale is 366 pixels per mm and the image height is 1024 pixels or 2.8mm. The film cross section area is 0.426 mm^2; therefore the average film thickness in the sample is 0.426 mm^2/2.8mm = 0.152mm. After 50 samples were processed in this fashion, a median value and standard deviation were determined. The median was used to reduce the influence of some of the extreme values obtained. A running average was calculated to check that the small number of data points would converge to a reliable value. Fig. 5.23 shows the results from a series of samples. The first data point is from Fig. 5.22. While the average film thickness varied considerably from image to image, the running average did not vary appreciably. A measure of convergence was also used, which was the percentage change in running average between samples. The results of the PLIF program are summarized in Tables 5.2 and 5.3.

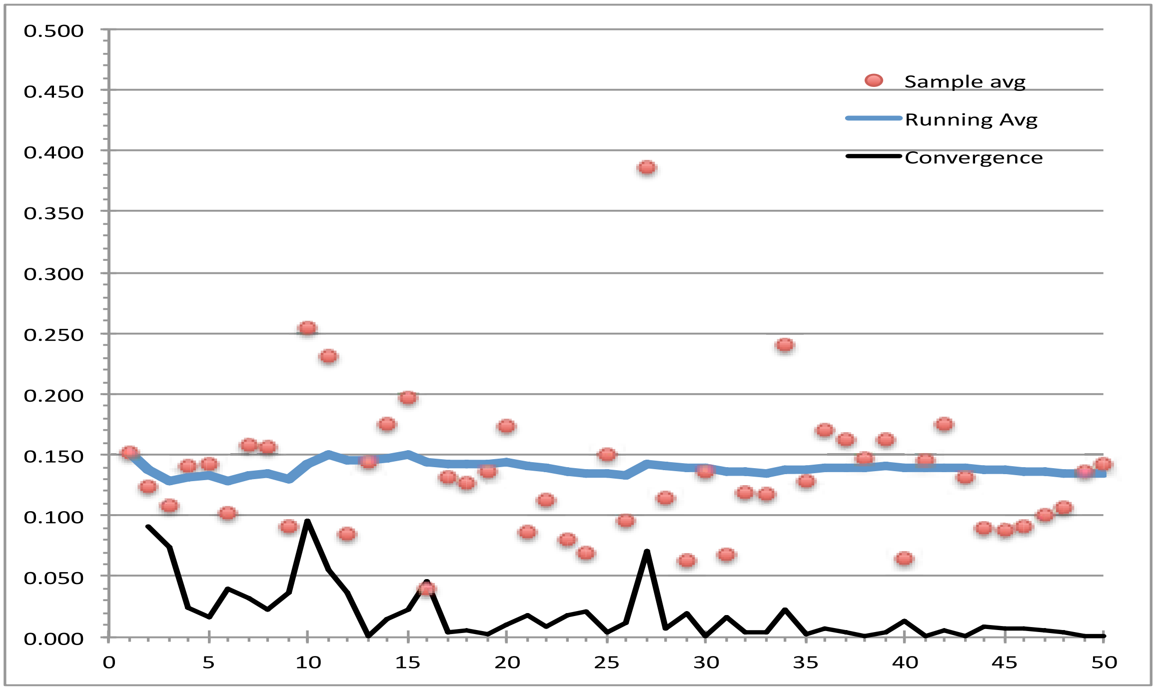

Figure 5.23 Film Thickness from PLIF Images (v_{sg} = 26.7 m/s, v_{sl} = 0.074 m/s.)

Table 5.2 Median Liquid Film Thickness in mm, from PLIF Images.

Superficial Gas Velocity, V_{sg} [m/s]	Superficial Water Velocity, V_{sl} [m/s]: 0.0021	0.0042	0.0063	0.0074	0.0084	0.0095	0.0105	0.0131	0.0158	0.0184	0.0210
16.5	0.250	0.258	0.268		0.249						
19.8		0.186	0.215		0.203		0.223	0.291			
23.1			0.167		0.200		0.216	0.185	0.171		
26.4			0.130	0.132	0.125	0.138	0.157	0.182	0.164	0.234	
33.0			0.104		0.097		0.126	0.125	0.148	0.222	
39.6			0.066		0.085		0.105	0.107	0.124	0.148	0.122
49.5			0.045		0.097						

Table 5.3 Liquid Film Thickness Standard Deviation in mm, from PLIF Images.

Superficial Gas Velocity, V_{sg} [m/s]	Superficial Water Velocity, V_{sl} [m/s]: 0.0021	0.0042	0.0063	0.0074	0.0084	0.0095	0.0105	0.0131	0.0158	0.0184	0.0210
16.5	0.126	0.172	0.155		0.238						
19.8		0.127	0.164		0.085		0.100	0.244			
23.1			0.090		0.112		0.107	0.080	0.086		
26.4			0.090	0.057	0.054	0.055	0.068	0.074	0.069	0.190	
33			0.048		0.044		0.041	0.043	0.052	0.151	
39.6			0.025		0.031		0.041	0.028	0.037	0.069	0.043
49.5			0.018		0.042						

The film thickness results are presented graphically in Figures 5.24 and 5.25.

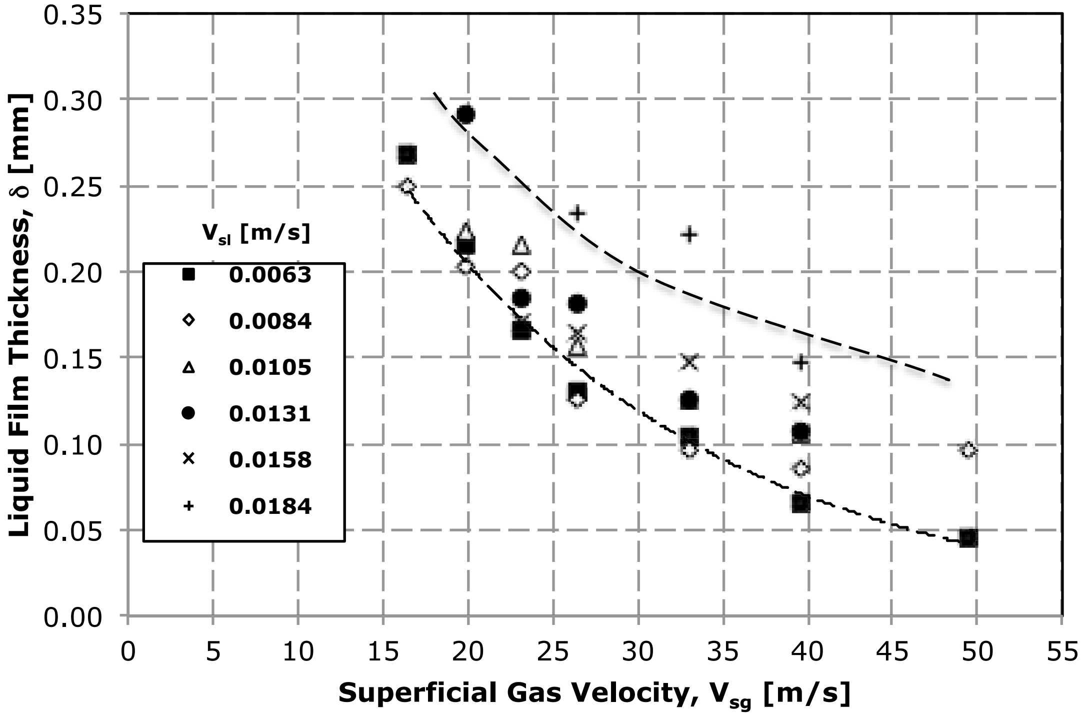

Figure 5.24 Film Thickness vs. v_{sg} from PLIF Program.

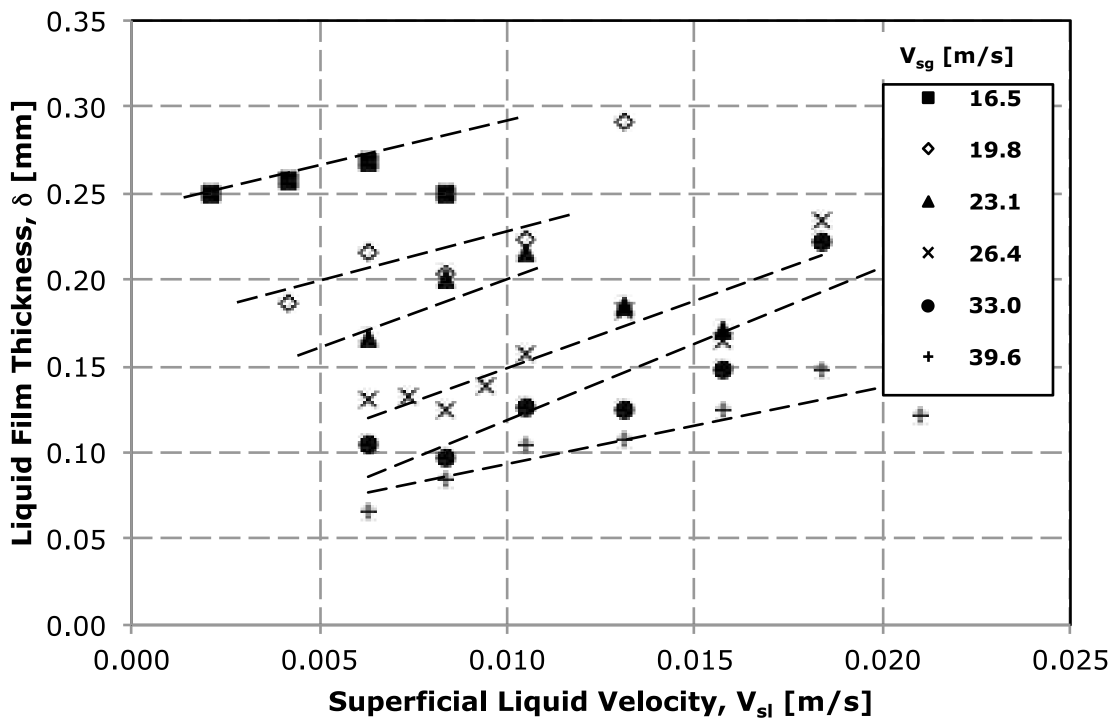

Figure 5.25 Film Thickness vs. v_{sl} from PLIF Program.

Although the relatively narrow laser beam illuminates only a sliver of liquid film cross section, image interpretation was found to be challenging. Examining an image by Hewitt and Hall-Taylor (1970) illustrates some of the difficulties in interpreting the liquid film images - Figure 5.26 is an axial view looking downward into the pipe. The authors did not provide flow rate data, only a comment that this was a disturbance wave.

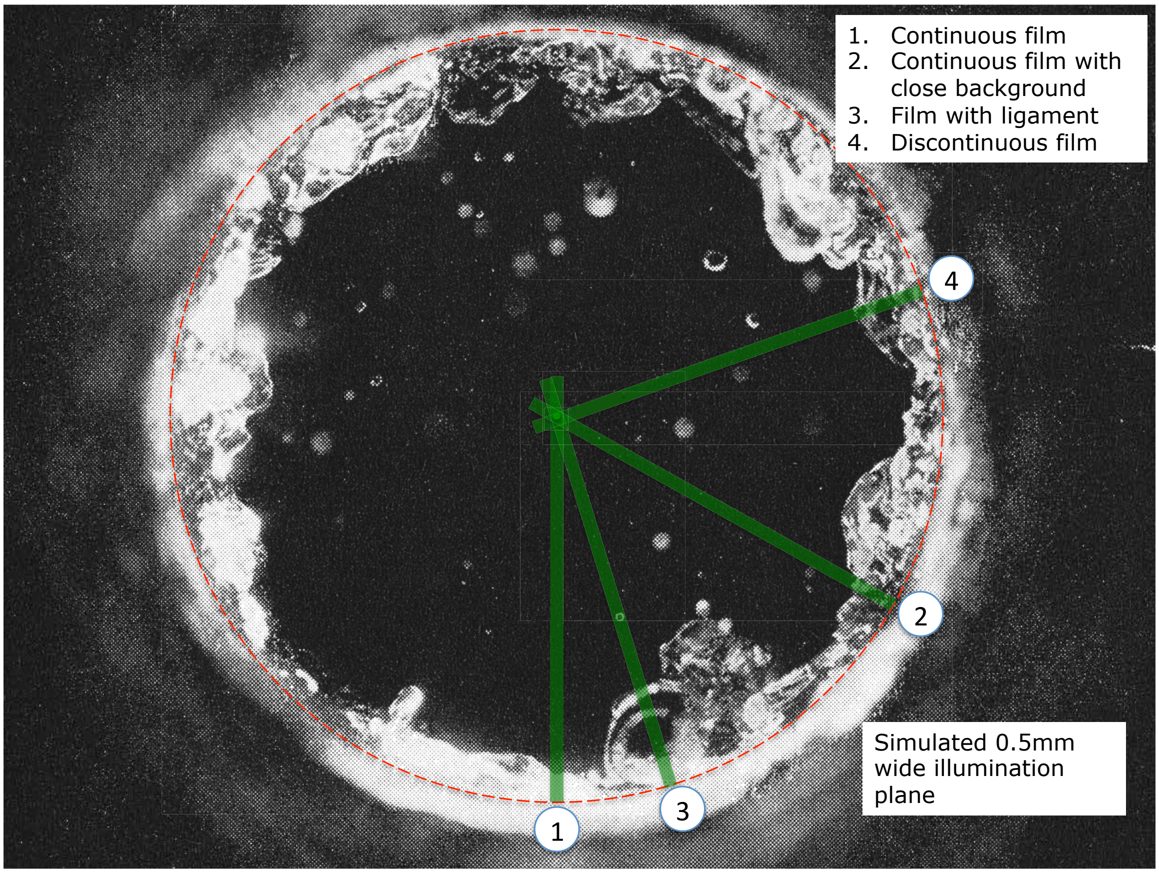

Figure 5.26 Axial View of Disturbance Wave in Annular Flow from Hewitt and Hall-Taylor (1970).

While there is considerable scatter in Fig. 5.24, a general trend is clear: the liquid film thins as gas velocity increases; and it thickens with increased liquid input. This is a result the increased gas velocity and subsequent drag causing the film velocity to increase - for a given volumetric flow rate of liquid film (as given by the area-velocity product), an increase in liquid velocity results in a decrease in area and hence thickness.

These results are compared with the work of Mamedulanov (2016), who earlier used the same apparatus. He used a MatLab script to process about 1500 images for each air/water rate, although it appears that same result would have been obtained with 600 images. Three sets of PLIF images were obtained by Mamedulanov with the laser at the centerline of the test section, the same configuration of the current work. The manual interpretation does provide a reasonable match to the more rigorous method, as illustrated in the following figures (Fig. 5.27, 5.28 and 5.29.)

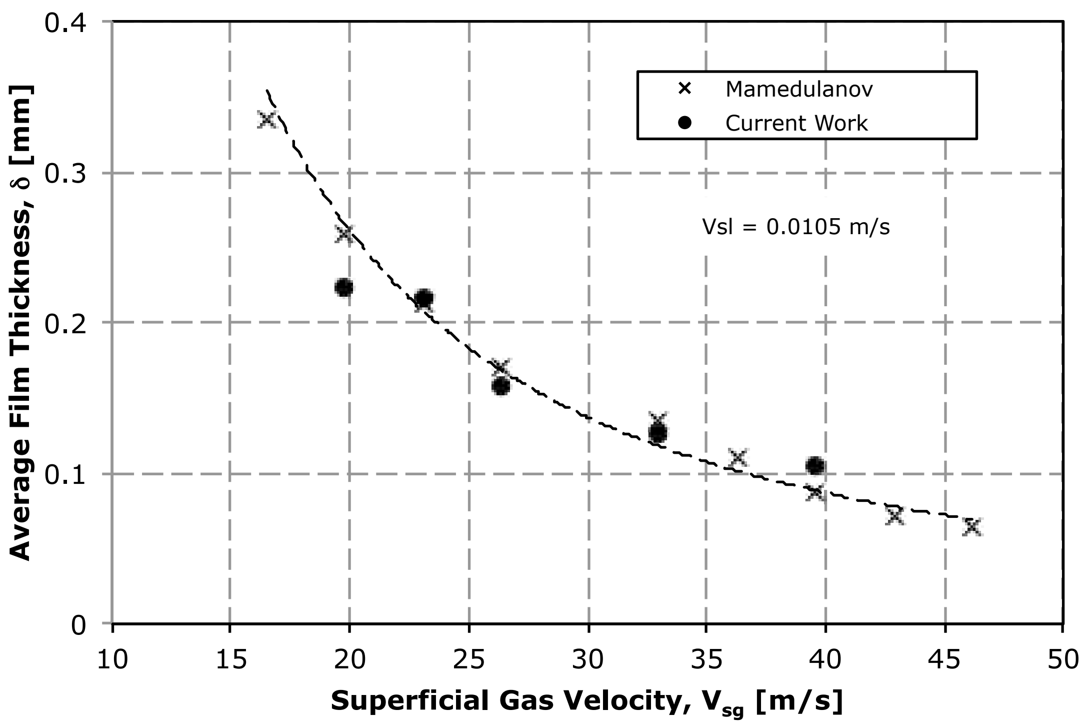

Figure 5.27 Film Thickness Results from Mamedulanov (2016) and Current Work at v_{sg}=0.0106 m/s.

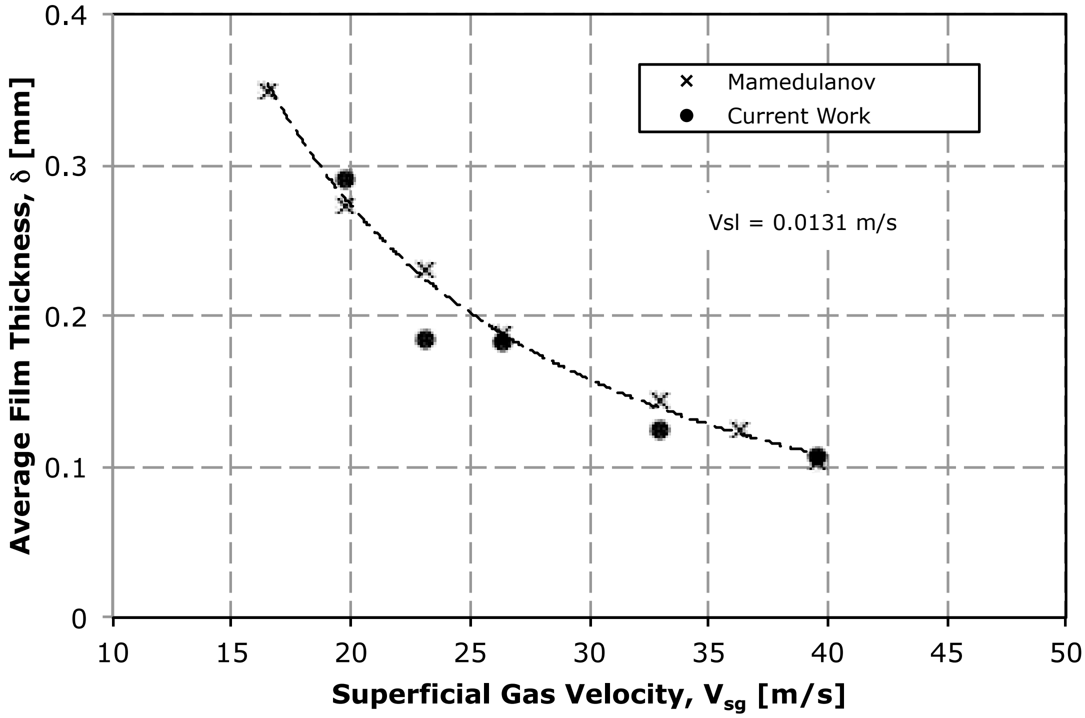

Figure 5.28 Film Thickness Results from Mamedulanov (2016) and Current Work at v_{sg}=0.0131 m/s.

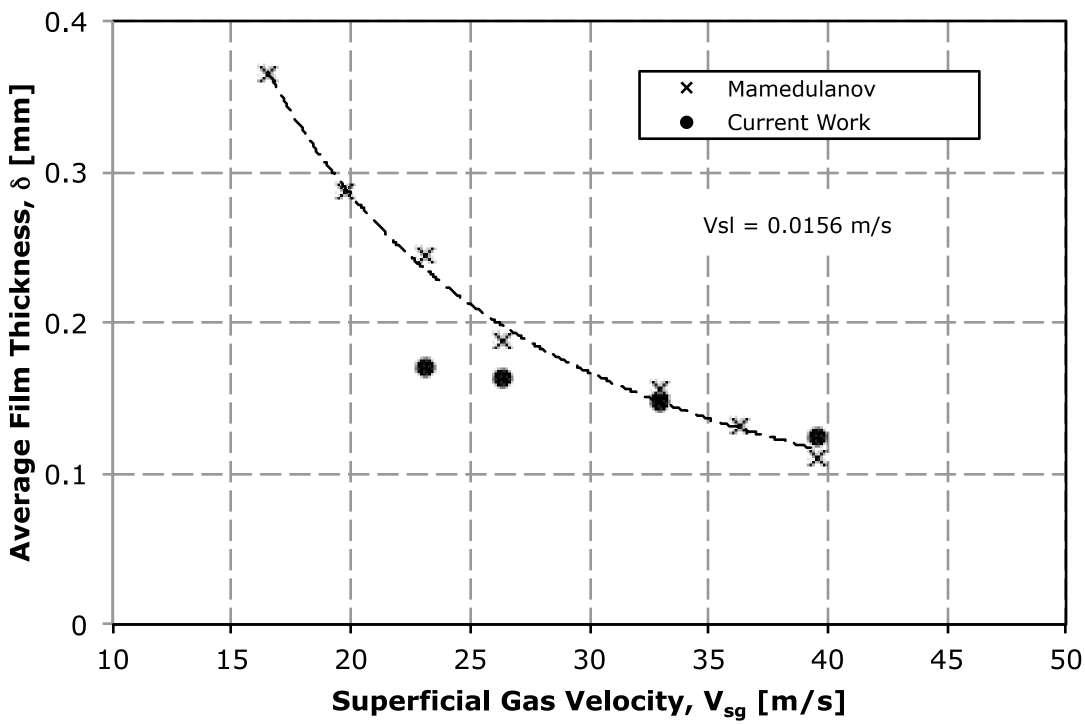

Figure 5.29 Film Thickness Results from Mamedulanov (2016) and Current Work at v_{sg}=0.0156 m/s.

5.4 Entrainment

Entrainment in two phase flow, FE, is defined as the fraction of input liquid mass flow in the gas core, or

$$FE = 1 - \frac{\dot{m}_f}{\dot{m}_l} \tag{5.8}$$

Recall the dimensionless velocity gas parameter given by Steen and Wallis (1964) in their experimental work,

$$\pi_2 = v_g \frac{\mu_g}{\sigma}\left(\frac{\rho_g}{\rho_l}\right)^{1/2} \tag{2.16}$$

To initiate entrainment of liquid from the film into droplets, Steen and Wallis proposed that π_2 must equal 2.46×10^{-4}, that is,

$$v_{crit} = 2.46 \times 10^{-4} \frac{\sigma}{\mu_g}\left(\frac{\rho_l}{\rho_g}\right)^{1/2} \tag{5.9}$$

From an examination of published work, Paleev and Filippovich (1966) correlated an entrainment-related term to another dimensionless group with data from several sources. It is notable that the data used presents considerable scatter – their original graph is given as Fig. 5.30.

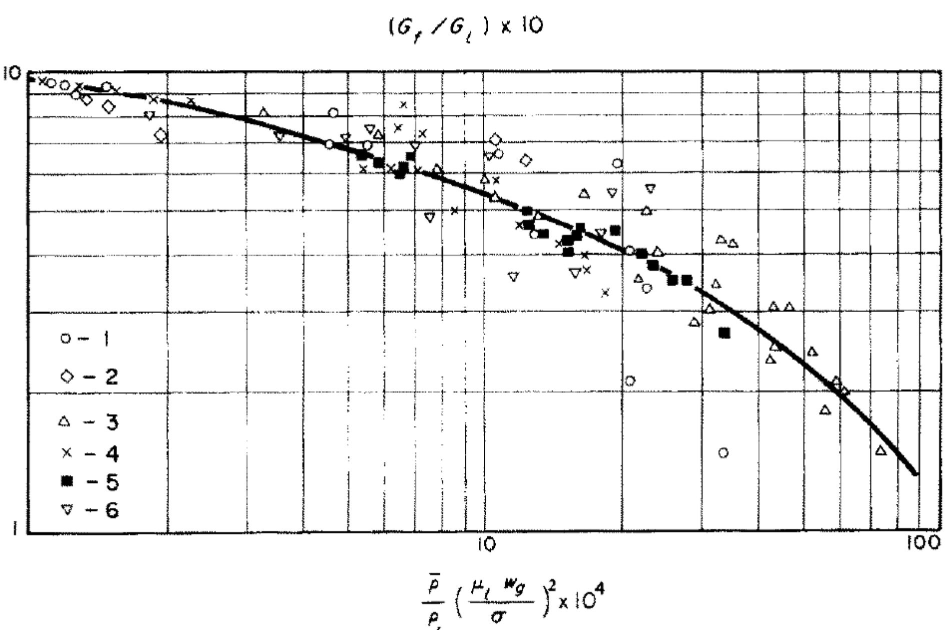

Figure 5.30 Entrainment Correlation of Paleev and Filippovich (1966).

Paleev and Filippovich fitted the data to the following equation:

$$\frac{\dot{m}_f}{\dot{m}_l} = 0.985 - 0.44\log\left[\frac{\bar{\rho}}{\rho_l}\left(\frac{\mu_l v_g}{\sigma}\right)^2 \times 10^4\right] \tag{5.10}$$

where the density of the droplet-laden gas core is related to actual gas density by,

$$\bar{\rho} = \rho_g\left[1 + \frac{\dot{m}_l\left(1 - \dot{m}_f / \dot{m}_l\right)}{A_p \rho_g v_{sg}}\right] \tag{5.11}$$

Thus the solution for $\dot{m}_f / \dot{m}_l$ is iterative. Wallis (1968) named the Pavleev dimensionless group as π_1, defined by,

$$\pi_1 = \frac{\bar{\rho}}{\rho_l}\left(\frac{\mu_l v_g}{\sigma}\right)^2 \tag{5.12}$$

which gives rise to

$$\pi_2 = \frac{\mu_g}{\mu_l}\left(\pi_1\right)^{1/2} \tag{5.13}$$

Wallis assumed that $\bar{\rho} \approx \rho_g$. An expression for liquid entrainment fraction is obtained by adapting the Paleev and Filippovich equation,

$$FE = 1 - \frac{\dot{m}_f}{\dot{m}_l} = 1 - \left[0.985 - 0.44\log\left[\frac{\bar{\rho}}{\rho_l}\left(\frac{\mu_l v_g}{\sigma}\right)^2 \times 10^4\right]\right]$$
$$FE = 1 - \left[0.985 - 0.44\log\left[\pi_1 \times 10^4\right]\right]$$
(5.14) (5.15)

Rearranging equation 5.13 in terms of $\pi_1$and substituting into 5.15 yields,

$$FE = 1 - \left[0.985 - 0.44\log\left[\left(\frac{\mu_l \pi_2}{\mu_g}\right)^2 \times 10^4\right]\right] = 1.775 + 0.88\log\left(\frac{\mu_l \pi_2}{\mu_g}\right) \tag{5.16}$$

To find the minimum velocity for entrainment set *FE* = 0 to solve first for π_2 and then v_{crit},

$$1.775 + 0.88\log\left(\frac{\mu_l \pi_2}{\mu_g}\right) = 0$$

$$\frac{\mu_l \pi_2}{\mu_g} = 10^{\frac{-1.775}{0.88}} \qquad (5.17)\ (5.18)\ (5.19)$$

$$\pi_2 = 9.62\times10^{-3}\frac{\mu_g}{\mu_l}$$

Wallis assumed air and water properties near standard conditions (probably $\mu_g = 1.9 \times 10^{-5}$ Pa-s and $\mu_l = 1.0 \times 10^{-3}$ Pa-s) so that

$$\pi_2 = \left(9.615\times10^{-3}\right)\left(1.9\times10^{-2}\right) = 1.83\times10^{-4} \qquad (5.20)$$

This value of the π_2 term is which considerably lower than originally proposed by Steen and Wallis in 1964. Further solving for $v_{crit:}$, the critical velocity to initiate droplet entrainment,

$$\pi_2 = v_{crit}\frac{\mu_g}{\sigma}\left(\frac{\rho_g}{\rho_l}\right)^{1/2} = 1.83\times10^{-4}$$

$$v_{crit} = 1.83\times10^{-4}\frac{\sigma}{\mu_g}\left(\frac{\rho_l}{\rho_g}\right)^{1/2} \qquad (5.21)\ (5.22)$$

Finally, for air-water at standard conditions, where the surface tension $\sigma = 7.2 \times 10^{-2}$ N/m, $\mu_g = 1.9 \times 10^{-5}$ Pa-s, ρ_l = 1000 kg/m3, and ρ_g = 1.22 kg/m3, the critical velocity is 19.9 m/s. Compare with Turner's result of 14.4 m/s required to lift droplets. Wallis' original correlation for entrainment in graphic form is compared with the fitted curve from equation 5.16 and 5.23 in Fig. 5.31.

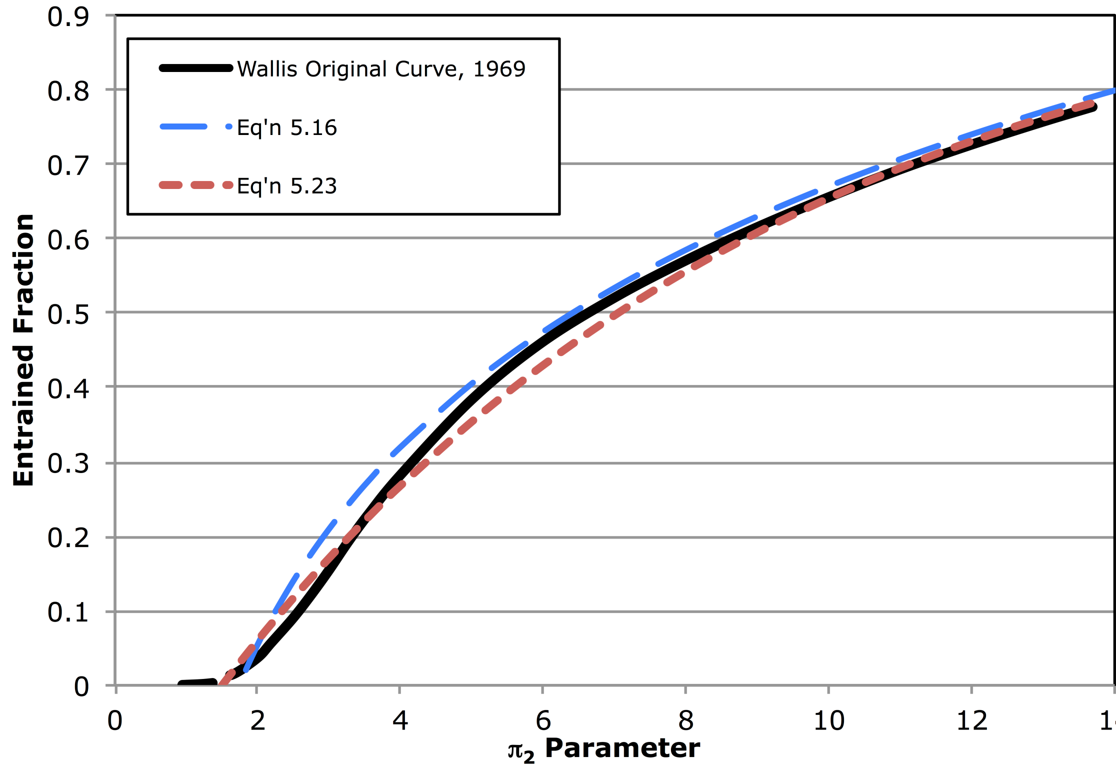

Figure 5.31 Entrainment Correlation Curve from Wallis (1969) and Fitted Curves.

While equation 5.16 is suitable to represent Wallis' entrainment correlation, a more popular fit, as used by Ansari et al. (1992) and Chokshi (1994) in their mechanistic models of annular flow is:

$$FE = 1 - \exp(-0.125(10^4 \pi_2 - 1.5)) \qquad (5.23)$$

Given the original data scatter in Figure 5.30, either equation 5.16 or 5.23 provides a reasonable representation. However, it is useful to re-examine the correlation against other experimental data. Figure 5.32 shows entrainment measurements from the data of Collier and Hewitt (1961), Asali (1984), and Schadel (1988) with air-water systems and four different pipe diameters, plotted against the Wallis correlation. Liquid input is given in terms of a superficial liquid Reynolds number, defined as,

$$\mathrm{Re}_{sl} = \frac{\rho_l v_{sl} d}{\mu_l} \qquad (5.24)$$

We see in Figure 5.32 that the Wallis correlation appears to define the *minimum* value of entrainment for a given gas velocity. Furthermore, below a given threshold liquid rate, annular flow occurs with no entrainment. A more detailed look at Asali's (1984) data from 22.9 mm i.d. pipe is given in Figure 5.33.

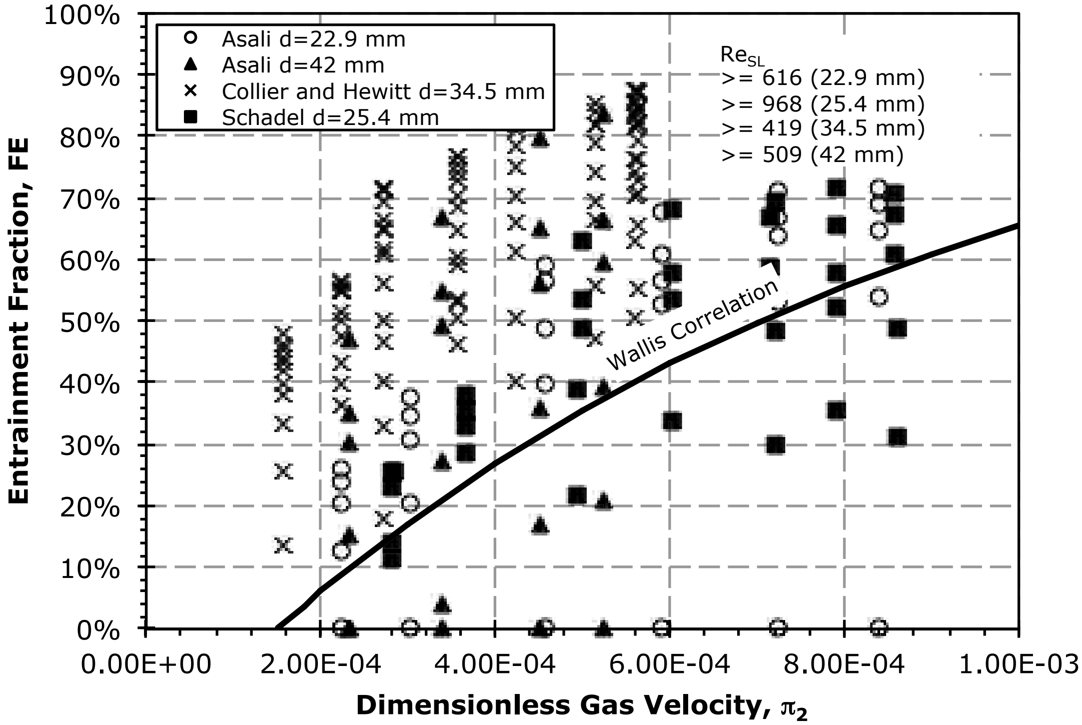

Figure 5.32 Entrainment Fraction vs. π_2 Term for Various Pipe Sizes.

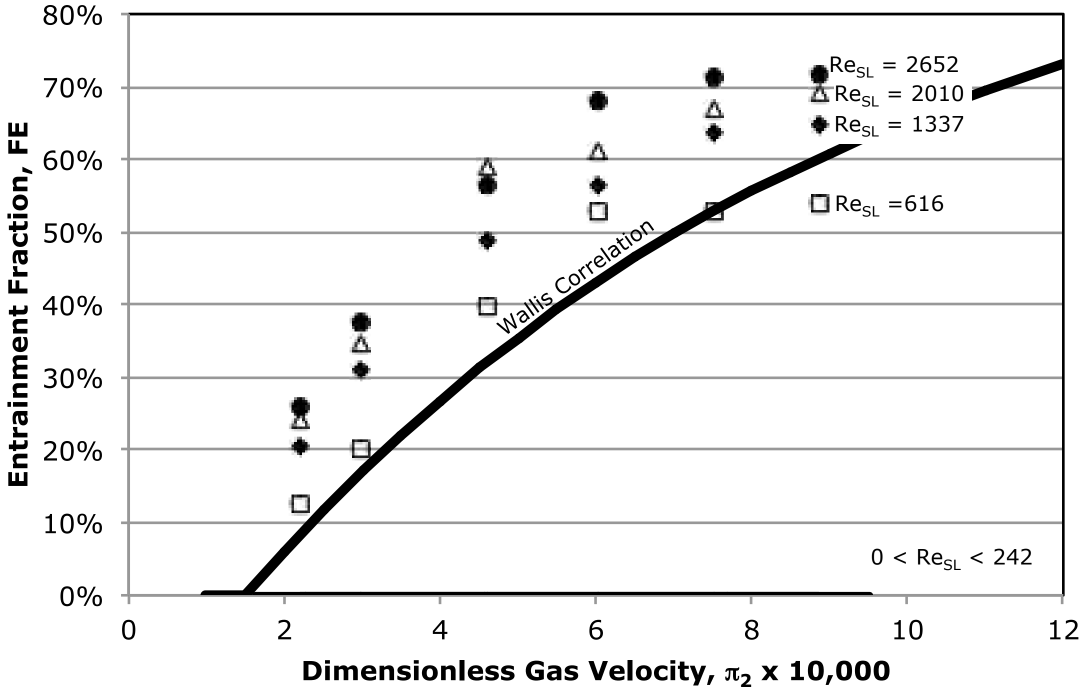

Figure 5.33 Entrainment Fraction vs. π_2 Term from Asali (1984), 22.9mm Pipe.

In Fig. 5.33, entrainment fraction increases with both gas rate and liquid rate. The entrainment values appear to converge to zero at some finite gas velocity. When replotted in terms of superficial Reynolds numbers (Fig. 5.34), it appears that the onset of entrainment occurs at about Re_{sl} = 250 for 22.9 mm pipe independent of gas rate.

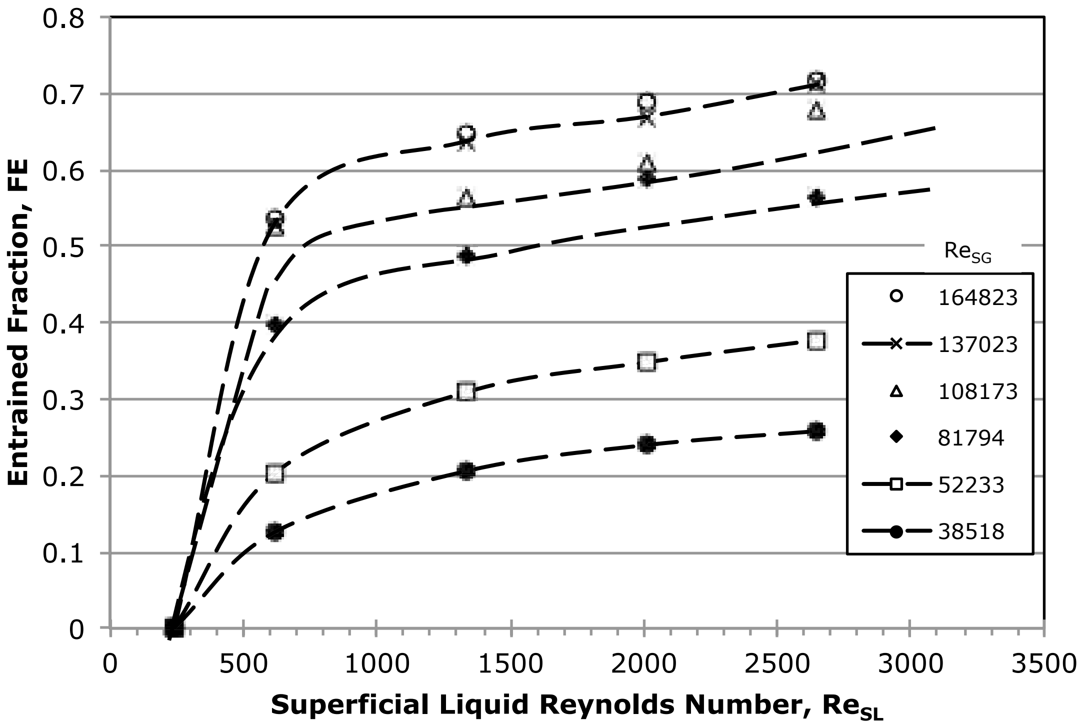

Figure 5.34 Entrainment Fraction vs. Re_{SL} for 22.9 mm Pipe, from Asali (1984).

The relationship between liquid input and entrainment was examined more closely in experiments by Schadel (1988) and reported in Schadel, Leman, Binder, and Hanratty (1990.) Those results, along with additional data from Turner (1966) and Asali (1984) are shown together Fig. 5.35. For air-water systems at or near standard conditions, the critical film Reynolds number, Re_{LFC}, to initiate droplet entrainment was found to depend on tube diameter but weakly on gas rate. Overall, however, the critical film Reynolds number is roughly 250. This effectively defines the laminar turbulent transition for the liquid film. By contrast, Lockhart and Martinelli proposed that for viscous (laminar) film and turbulent gas phase flow in horizontal pipe, the maximum liquid Reynolds number is <1000.

Based on published work, it is found that liquid entrainment in the gas core of annular flow requires two conditions to be satisfied:

a) A minimum gas velocity to lift droplets.

b) A minimum liquid velocity to supply the system.

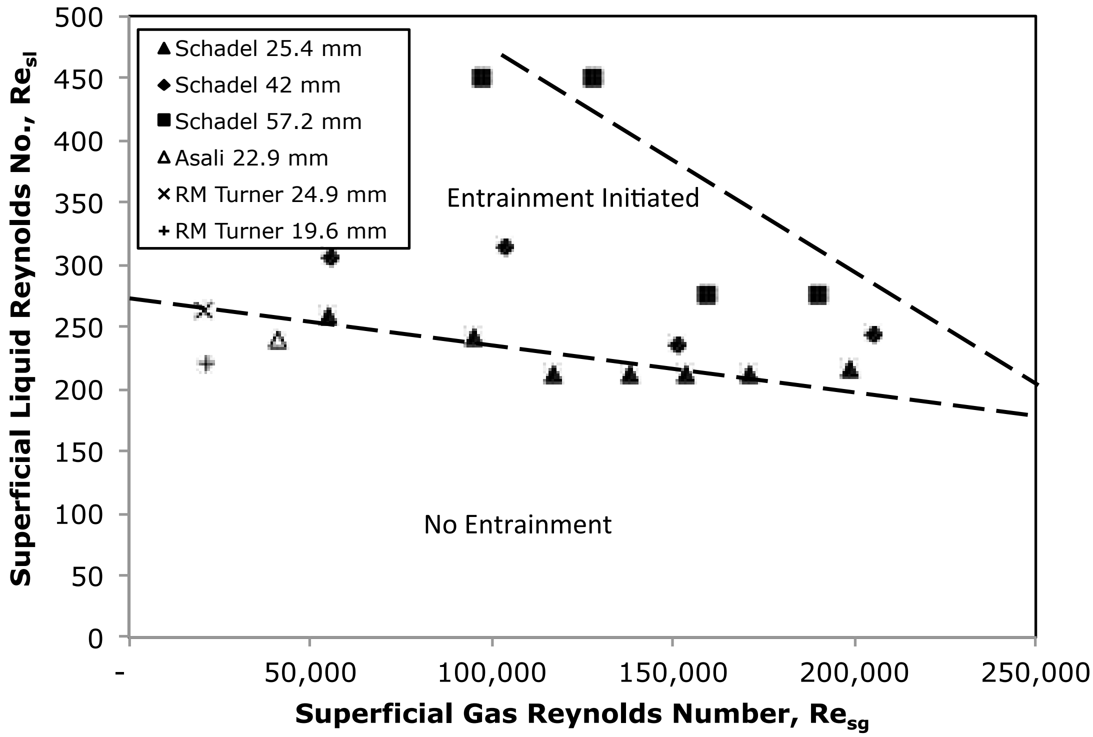

Figure 5.35 Onset of Entrainment: Experimental Results.

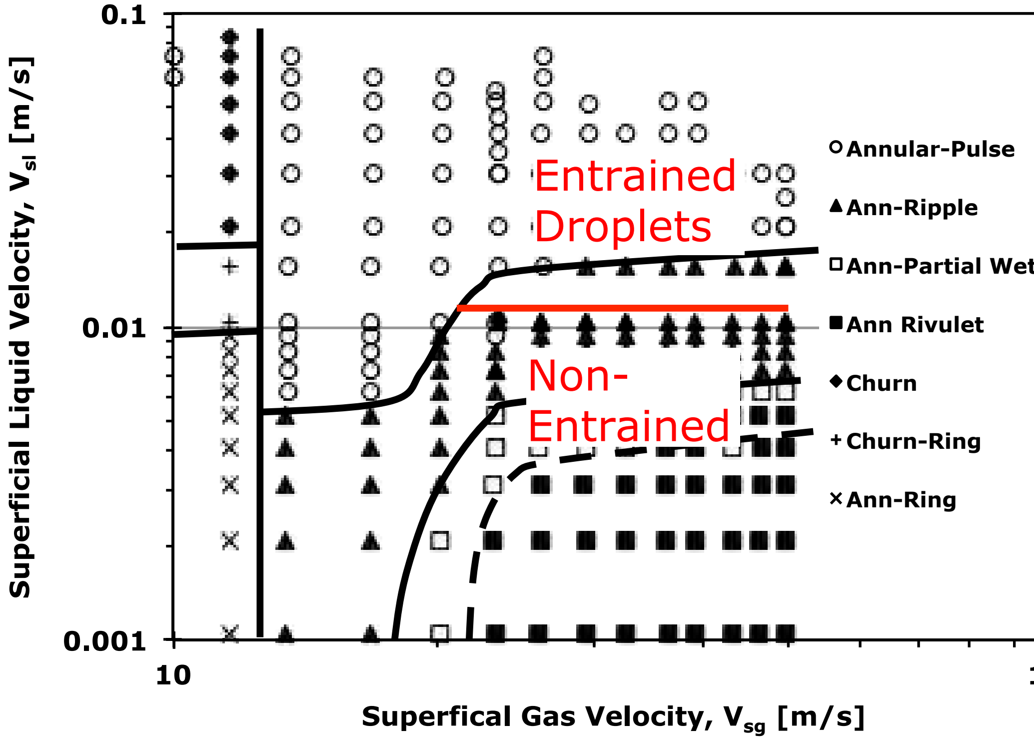

Figure 5.36 Annular Sub-Regime Map of Fig. 5.17 with Entrainment Threshold.

With respect to the current work, Re_{sl},=250 corresponds to s a superficial liquid velocity, v_{sl} of about 0.01 m/s for 26 mm nominal i.d. pipe. Therefore the flow regime mapping of the current results can be amended to include an inferred entrainment threshold – see Figure 5.36.

Another aim of the PLIF program was to confirm the onset of entrainment visually, since this was not possible from external observation. Zadrazil et al.(2014) lists five mechanisms of liquid entrainment:

a) Shearing of wave crests ("ligament breakup.)
b) Undercutting of liquid film by gas flow ("bag breakup".)
c) Bubbles bursting within the film
d) Droplets crashing into the liquid film.
e) Disturbance or pulse waves.

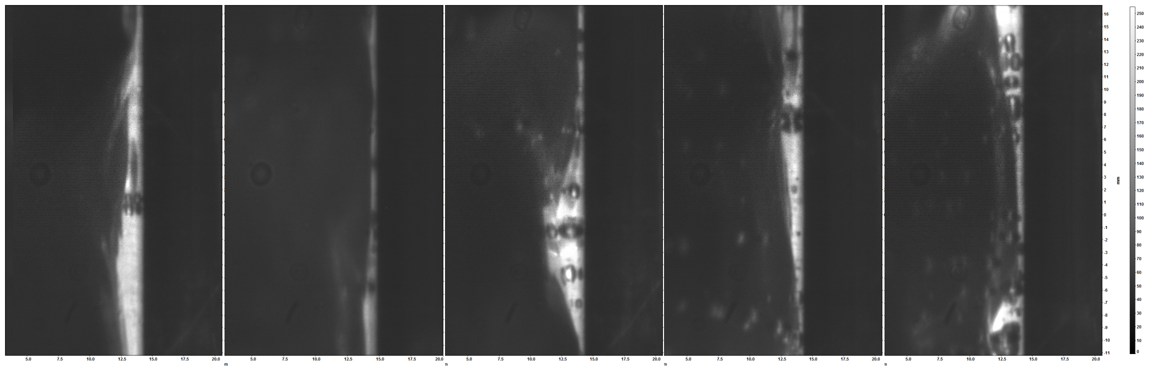

a) b) c) d) e)

Figure 5.37 PLIF Images at Vsg = 40 m/s
Vsl = a) 0.0084 m/s b) 0.0095 m/s c) 0.0105 m/s d) 0.0131 m/s e) 0.0158 m/s

Liquid becomes entrained in the gas core as a result of wave breakup. This takes the form of ligaments initially. An equilibrium between rates of entrainment and deposition sustains a droplet concentration in the core. Entrainment was evident in PLIF images as droplets illuminated by the laser along with the film itself, occurring between v_{sl} = 0.0095 and 0.0105 m/s (Fig. 5.37 b, c.) This allows the placement of an entrainment onset boundary in Fig. 5.36. Note also in Fig. 5.37 the occurrence of entrained air bubbles increases dramatically at the same time. Rodriguez (2004) listed two mechanisms for air bubble entrainment in horizontal two phase flow:

a) impact of liquid droplets onto the film surface
b) folding of air into pockets by collapsing liquid wave peaks

5.5 Interfacial Friction and Film Roughness

For single phase gas flow, the friction factor can be derived by rearranging the energy equation,

$$\frac{dp}{dl} = \rho_g g + \frac{f_M \rho_g v_g^2}{2d} + \frac{\rho_g v_g \Delta v_g}{\alpha dl} \tag{5.25}$$

to find,

$$f_M = \frac{2d}{\rho_g v_g^2}\left[\frac{dp}{dl} - \rho_g g - \frac{\rho_g v_g \Delta v_g}{\alpha dl}\right] \tag{5.26}$$

Similarly, the pressure gradient in the gas core of annular flow is given by,

$$\left.\frac{dp}{dl}\right|_c = \rho_c g + \frac{f_i \rho_c v_c^2}{2(d-2\delta)} + \frac{\rho_c v_c \Delta v_c}{\alpha dl} \tag{5.27}$$

and by a similar rearrangement, the interfacial friction factor could be found from experimental data,

$$f_i = \frac{2(d-2\delta)}{\rho_c v_c^2}\left[\frac{dp}{dl} - \rho_c g - \frac{\rho_c v_c \Delta v_c}{\alpha dl}\right] \tag{5.28}$$

However, information on film thickness and entrainment would still be required. For non-entrained two-phase flow, $\rho_c = \rho_g$, $v_c = v_g$, and $\mu_c = \mu_g$. In this case equation 5.28 could be solved if the film thickness is assumed to be very small. Now if the mechanical energy equation is cast once again in terms of superficial gas quantities:

$$\left.\frac{dp}{dl}\right|_{sg} = \rho_g g + \frac{f'_{sg} \rho_g v_{sg}^2}{2d} + \frac{\rho_g v_{sg} \Delta v_{sg}}{\alpha dl} \tag{5.29}$$

All the terms in equation 5.29 can be evaluated, save the superficial gas friction factor, f'_{sg} which must be obtain using a correlation. The superficial friction factor concept was employed by Bergelin (1949) for horizontal and downward vertical flow for the gas phase, and by Govier and Short (1958) for upward two phase flow for the liquid phase.

With sufficient experimental data, a friction factor correlation may be created from,

$$f'_{sg} = \frac{2d}{\rho_g v_{sg}^2}\left[\frac{dp}{dl} - \rho_g g\right] \tag{5.30}$$

where the kinetic energy term has been removed for simplicity. Now expanding the earlier analysis with Asali (1984) and plotting data for entrained conditions (Figure 5.38) it is found that the superficial gas friction factor appears to be a monotonically decreasing function of Re_{sg}, for a given Re_{sl}.

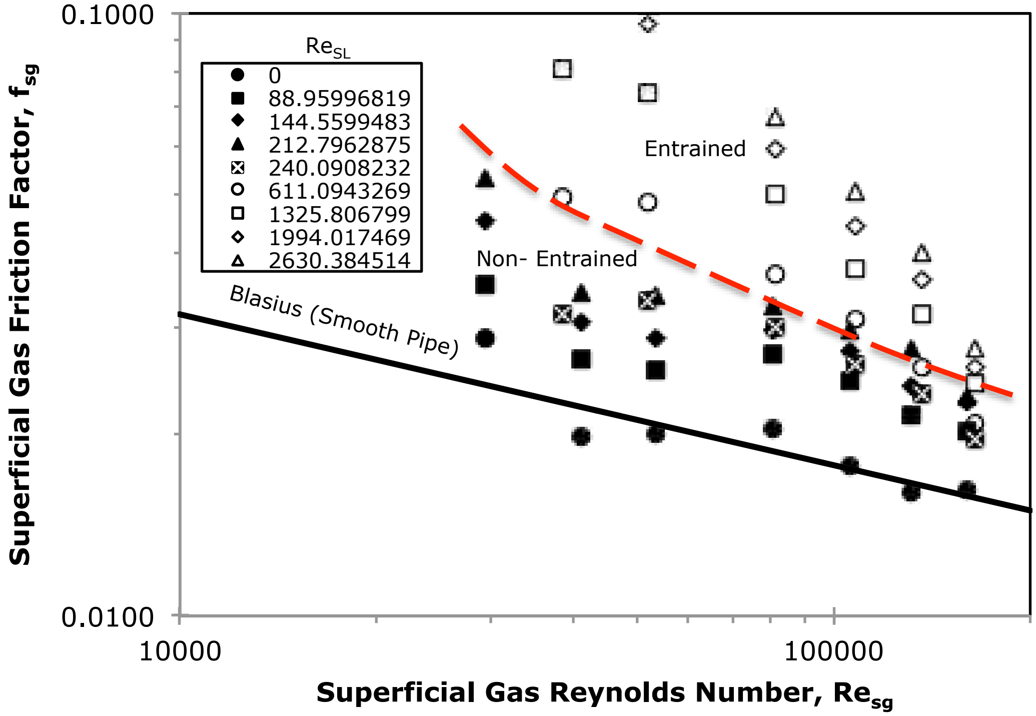

Figure 5.38 Friction Factor vs. Superficial Gas Reynolds Number for 22.9mm Tubing.

The same exercise is now performed with the higher resolution data from the current work (Fig. 5.39.) Note that there is a region of nearly constant friction factor starting at about $Re_{sg} = 35000$. This corresponds with the beginning of gas friction dominated two phase flow (i.e. the positive slope portion of Fig. 5.7). The data stops at Re_{sg}=82000 which was the upper limit of the air flow controller. The region of constant friction factor is associated with non-entrained flow. To investigate further, the effective film roughness was calculated from the friction factor by rearranging the Swamee-Jain equation (5.4) thus:

$$\frac{\varepsilon}{d} = 3.7\left(10^{-\sqrt{\frac{0.25}{f_M}}} - \frac{5.74}{\mathrm{Re}_{SG}}\right) \tag{5.31}$$

Figure 5.40 shows the effective relative roughness of the film as a function of Re_{sg}. Some data dispersion is evident at very low liquid Reynolds numbers. Some key observations from this figure are:

a) up to $Re_{sg} = 35000$ the film exhibits a decreasing relative roughness

b) about $Re_{sg} = 35000$ and below the onset of entrainment, the film has a nearly constant roughness, i.e. it is behaving as a pipe wall.

c) In the entrained region, the effective relative film roughness is monotonically decreasing with values of Re_{sg}.

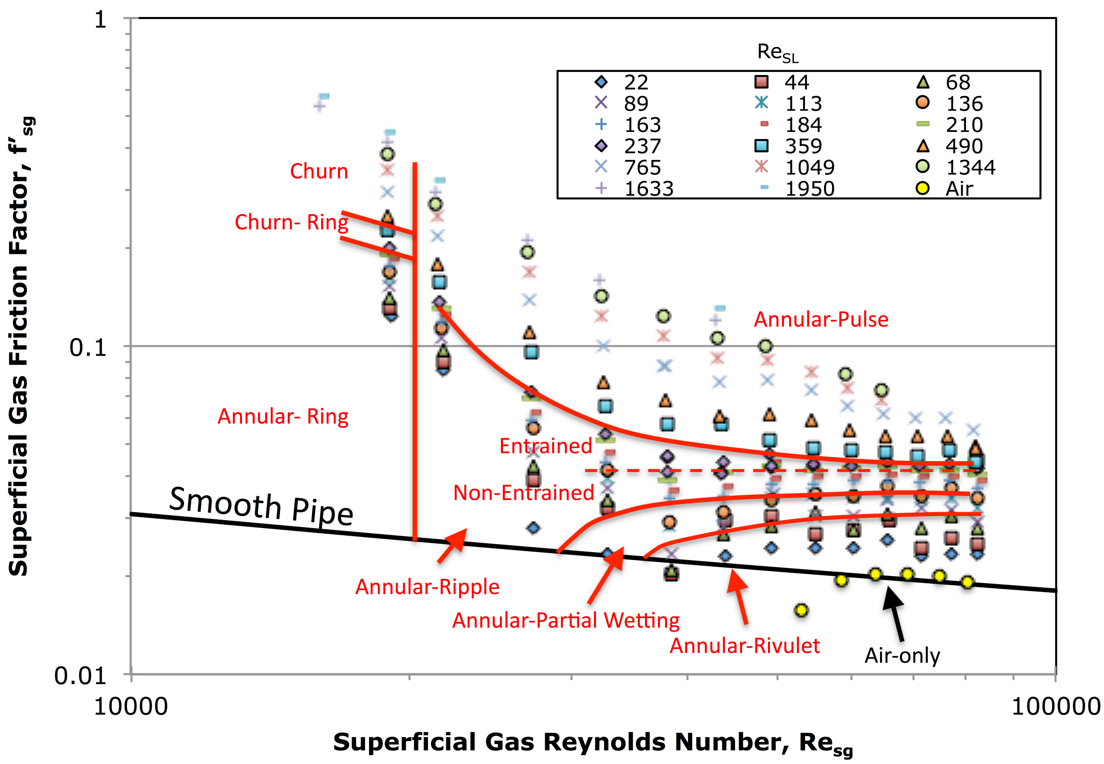

Figure 5.39 Superficial Gas Friction Factor vs. Superficial Gas Reynolds Number.

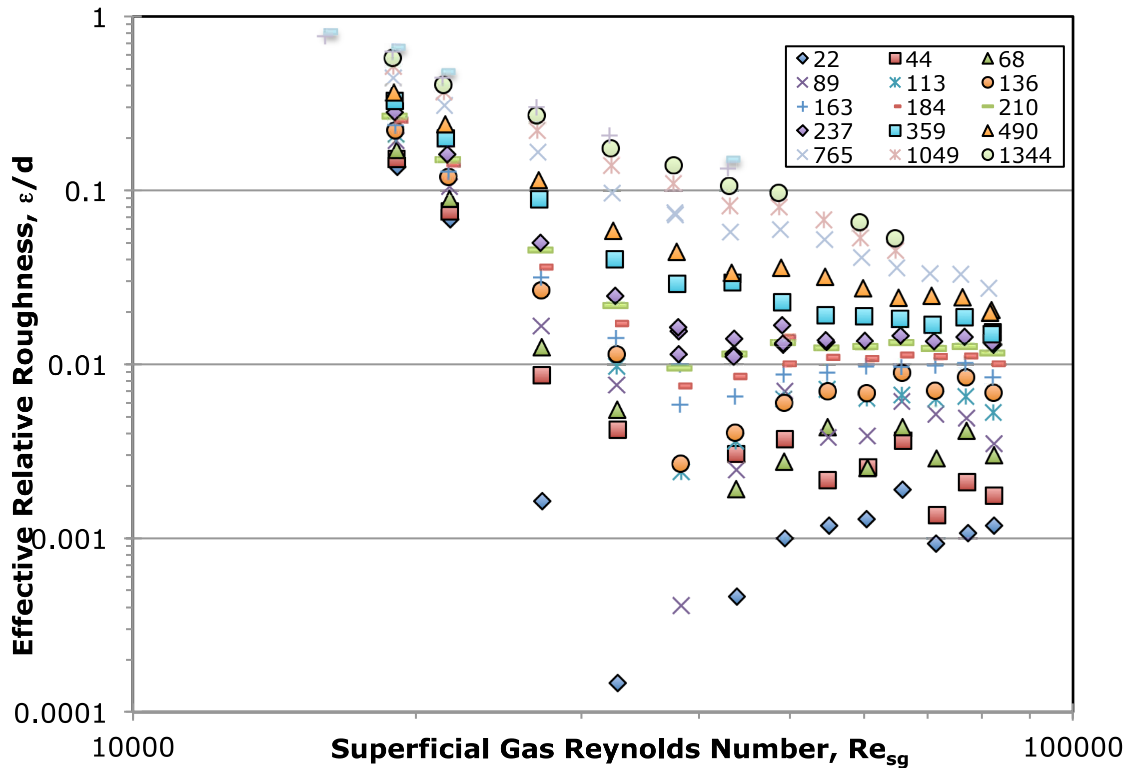

Figure 5.40 Effective Relative Roughness vs. Superficial Gas Reynolds Number.

6 New Friction Factor Correlations for Annular Flow

Semi-mechanistic models require correlations for entrainment and friction factor in order to arrive at a solution. In addition, a scheme to determine film thickness is required. Some of these correlations have been tested against published data and found to be an imperfect fit. Analysis of data from both the current experimental work and previous published results confirms that another approach is to find a correlative relationship for a superficial gas friction factor. Then pressure gradient can be solved with the superficial gas form of the mechanical energy equation. It is found that the sub-regimes of annular flow can be partitioned in to three "zones" for the purpose of finding a new friction factor:

I) constant roughness, high gas rate, no entrainment

II) variable roughness, high gas rate, entrained liquid

III) variable roughness, low gas rate

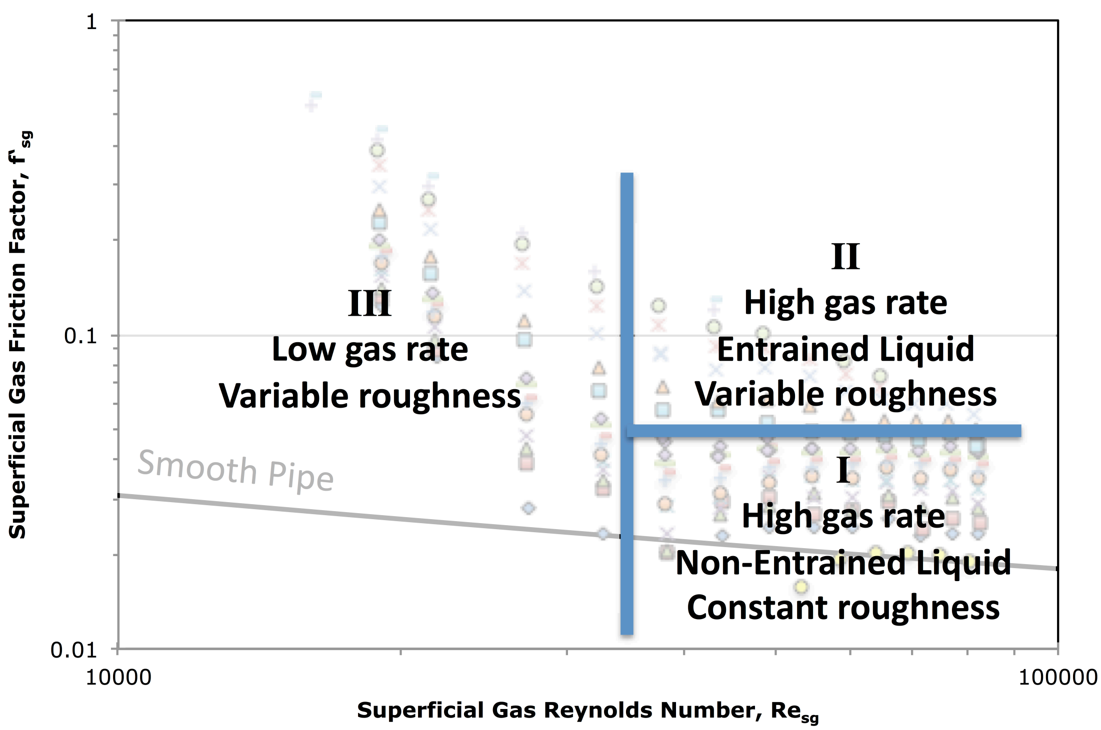

Figure 6.1 Annular Flow Zones for Pressure Gradient Calculation

6.1 Zone I Constant Roughness, High Rate, Non-Entrained Flow

This is "pure" annular flow, where the entire liquid portion flows in the film. The effective roughness of the film, and hence the friction factor are generally constant at for a given liquid input. It appears that the partial-wetting and rivulet sub-regimes exhibit similar behaviour, therefore they are included in this zone as well. From Fig. 5.41 the average friction factor in Zone I is found to be a a function of Re_{sl} only, with the resulting relationship (Fig. 6.2). It is striking that the extrapolation of the fit line to zero liquid rate has nearly the same value as originally proposed by Wallis (see equation 2.20.)

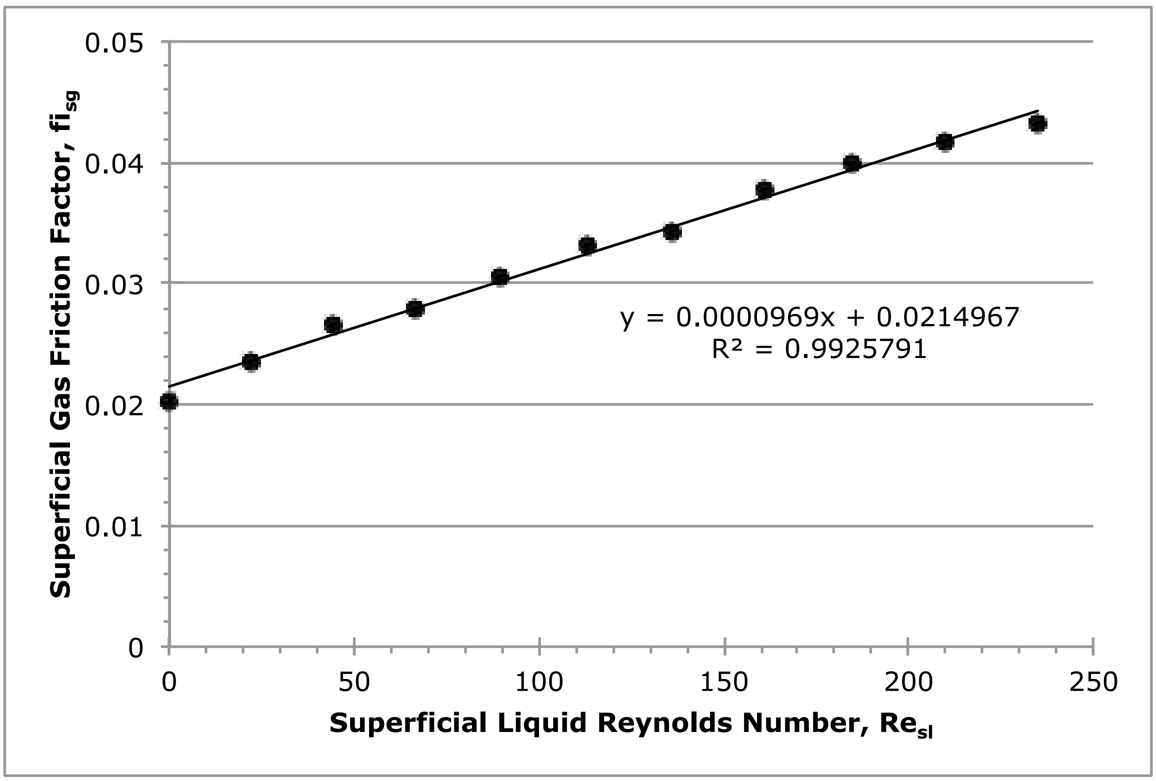

Figure 6.2 Friction Factor Correlation for Zone I.

The limits of the friction factor correlation for Zone I

$$f'_{sg} = 9.69 \times 10^{-5}\,\mathrm{Re}_{sl} + 0.0215 \qquad (6.1)$$

are: $Re_{sg} > 35000$, and $Re_{sl} < 250$.

A comparison of measured vs. calculated results from the current work is given in Figure 6.3.

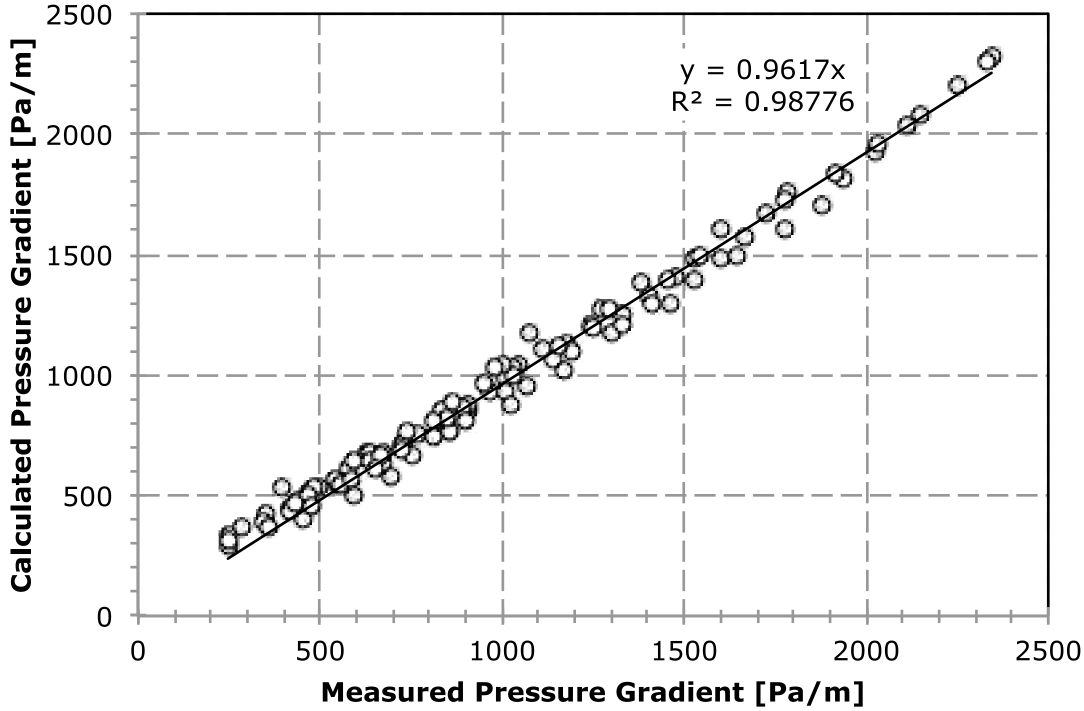

Figure 6.3 Calculated vs. Measured Pressure Gradient for Zone I.

6.2 Zone II Variable Roughness, High Gas Rate, Entrained Flow

The friction factor in Zone II is a function of both Re_{sl} and Resg. By inspection, the friction factors in Zone II demonstrate a linear trend on the log-log chart, therefore a simple linear relationship was adopted,

$$\log(f'_{sg}) = m\log(\mathrm{Re}_{sg}) + b \tag{6.2}$$

where m and b are functions of Re_{sl}. For each value of Re_{sl}, a slope was estimated for those data points. A curve found to fit well through the data points was,

$$m(\mathrm{Re}_{sl}) = -0.5583\ln(\mathrm{Re}_{sl}) + 3.0934 \tag{6.3}$$

Similarly, it was assumed that all the friction factor trends in this zone would converge with the maximum friction factor value in Zone I ($f'_{sg} = 0.045725$) at some higher value of Re_{sg}, (110000.) With this constraint, the y-intercept of equation 6.2 was determined for each Re_{sl} trend. A curve fit to those data was found to be

$$b(\mathrm{Re}_{sl}) = 2.8144\ln(\mathrm{Re}_{sl}) - 16.935 \tag{6.4}$$

These relationships are valid for: $35000 < Re_{sg} < 110000$ and $Re_{sl} > 250$. The result of the fitting for slope and intercept is given in Fig. 6.4.

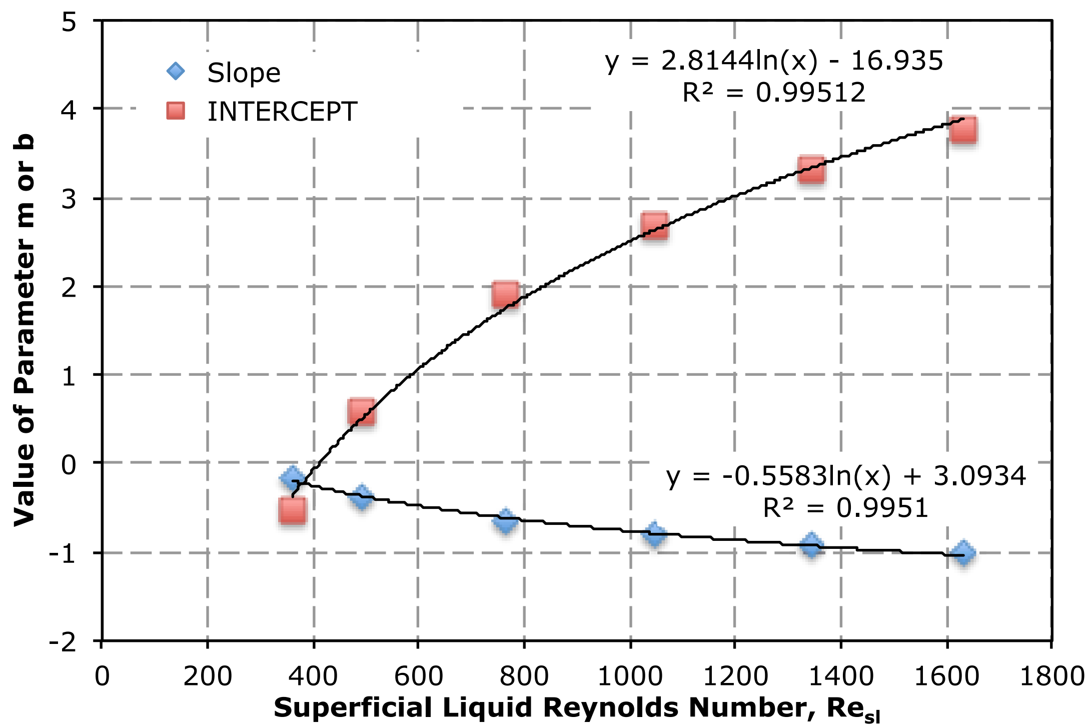

Figure 6.4 Determining Slope and Intercept Parameters for Zone II Friction Factor Correlation.

The friction factor may be determined with the following steps:

a) calculate $m(Re_{sl})$ and $b(Re_{sl})$ from equations 6.3 and 6.4

b) calculate $\log(f'_{sg})$ from equation 6.2

c) calculate $10^{\log(f'_{sg})} = f'_{sg}$.

d) insert f'_{sg} into the mechanical energy equation (5.25) and solve for pressure gradient.

A comparison of calculated vs. measured pressure gradients for Zone II is given in Fig. 6.5 using data from the current work.

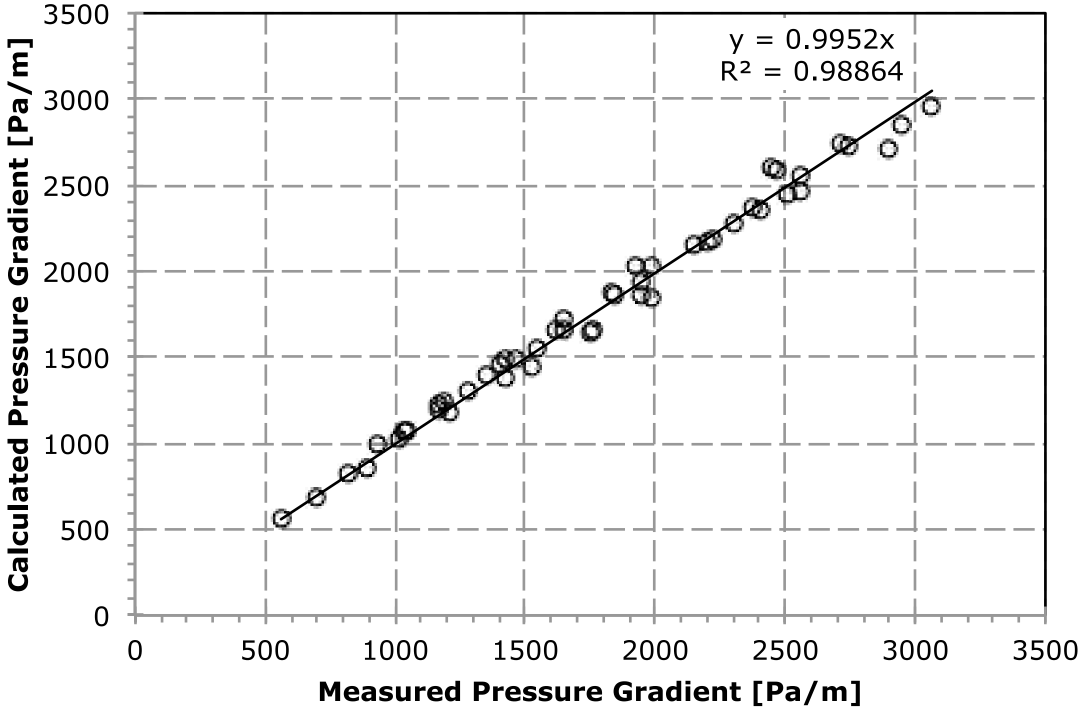

Figure 6.5 Calculated vs. Pressured Pressure Gradient for Zone II.

6.3 Zone III Variable Roughness, Low Gas Rate

Friction factors for Zone III are also expressed in the form given in equation 6.2. In addition, values of f'_{sg} must match those of the Zones I and II correlations at Re_{sg} =35000. The slope and intercept functions are given by

$$m(\text{Re}_{sl}) = -0.5583\ln(\text{Re}_{sl}) + 3.0934 \qquad (6.5)$$

and

$$b(\text{Re}_{sl}) = -1.715\times10^{-9}(\text{Re}_{sl})^3 + 6.498\times10^{-6}(\text{Re}_{sl})^2 - 9.222\times10^{-3}(\text{Re}_{sl}) + 11.098 \qquad (6.6)$$

These relationships are valid for: Resg <35000. The solution method is the same as for Zone II. Unfortunately, this model fails to match pressure gradients in Zone III (see figure 6.6)

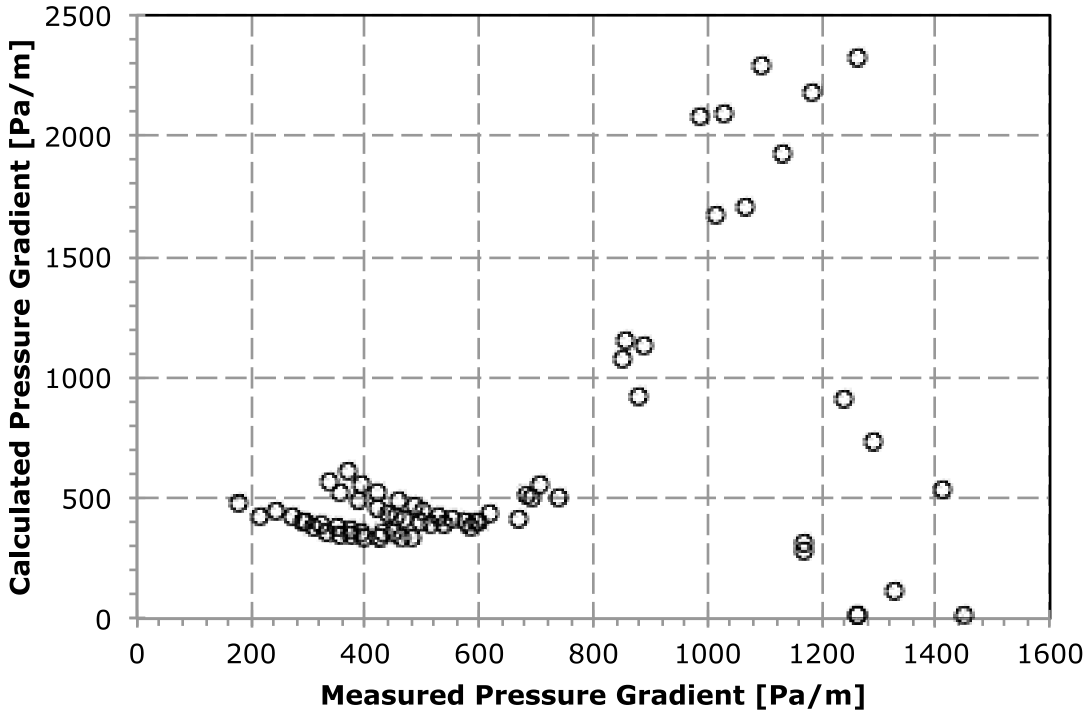

Figure 6.6 Calculated vs. Measured Pressure Gradient for Zone III.

6.4 Application of New Correlations to Published Data

Published experimental results in air-water systems with nominal 25.4mm i.d. pipe at near standard conditions are found in Radford (1949), Turner (1966) and Spedding et al. (1998a.) In addition, the results from Oshinowo (1971) were included in spite of the data being acquired at about 150 kPaa. Only two data points met the criteria for the Zone I correlation while the rest were applicable to Zone II (Figure 6.7) Note that the match is best up to about 2000 Pa/m. The highest pressure gradient measured in the current work was about 3000 Pa/m. Note that most of the data stays within an arbitrary +/-20% error cone, even beyond 3000 Pa/m.

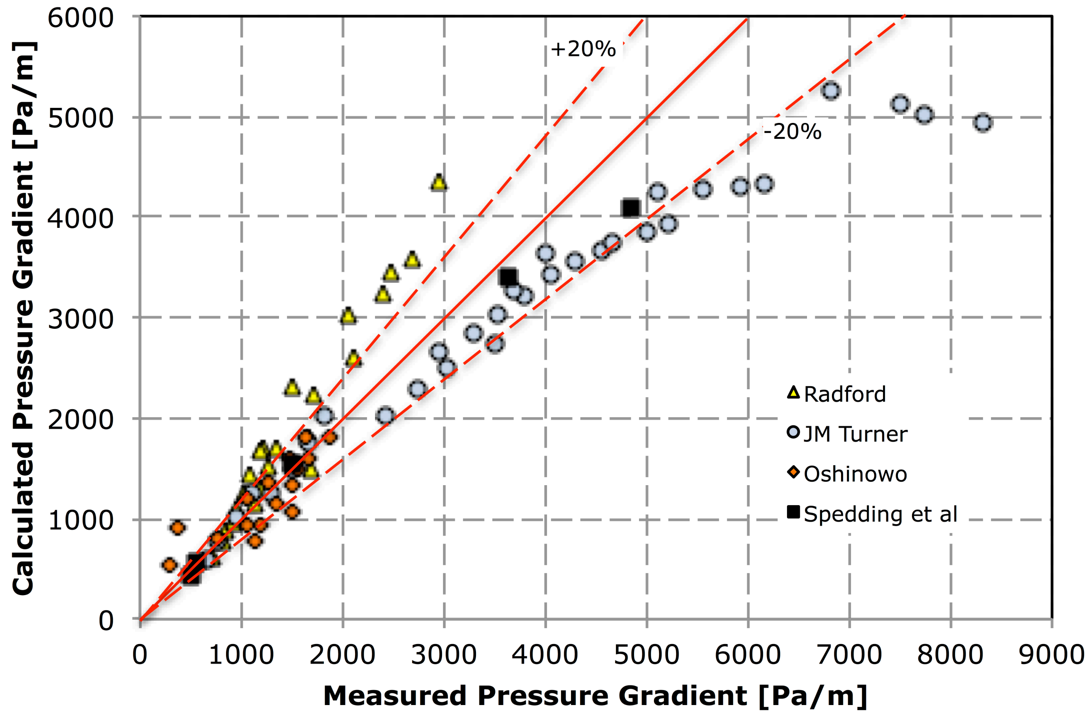

Figure 6.7 Measured vs. Calculated Pressure Gradient from Selected Published Results.

7 Conclusions, Contributions and Recommendations

7.1 Conclusions

The flow loop apparatus in the Drilling Engineering lab at the University of Alberta is capable of acquiring excellent quality pressure gradient data. Air-only gradients were consistent with calculations for single phase gas flow. The two phase data compared very well with published data from four different sources.

Several sub-regimes of annular flow were identified or confirmed by external observation, and a new flow regime map was drawn. High frame rate video was especially helpful in detecting falling film behaviour and discerning the three sub-regimes within the churn region.

Liquid lifting occurred at the lowest superficial gas rate in the test matrix (11.6 m/s), which is below that calculated with the Turner et al (1969) equation: 14.4 m/s. Although there is a net lifting of liquid, the layer next to the pipe wall is seen falling until the arrival of a strong wave.

For any given liquid input rate, the pressure gradient minima all occur at about 17m/s. It was found that the friction factor correlation worked best above this rate.

At high v_{sg}, the pressure gradient in rivulet flow is higher than for air alone. This is in spite of the liquid content being nearly undetectable at low liquid rates.

Analysis of PLIF images by manual interpretation was partially successful. Most running averages of film thickness were converging within the 50 samples analyzed. The accuracy of the method could be improved with a better interpretive guide.

The onset of entrainment indicates the liquid film in at the laminar – turbulent transition, and can be detected:

a) directly by observing a sharp increase in the number of droplets.

b) Indirectly by an increase in bubble concentration in the film

The ripple regime, which can appear smooth even in high speed video, experiences a wider range of film thickness and transient waves than originally thought.

7.2 Contributions to Knowledge

A new database has been created for vertical upward concurrent flow of air and water and near standard conditions in nominal 25mm i.d. pipe. Most of the measurements are provided in tabular form in Appendix 1. The database also includes the following:

a) A spreadsheet record of gauge pressure, differential pressure and temperature acquired at approx. 15ms intervals for each test point. This can be used for post analysis to study signal noise and spectral content.

b) Still and video images for each air/water combination. Frame-by-frame analysis could yield further refinement of sub-regime boundaries and additional information on ripple wave and pulse wave frequency.

c) PLIF images for a subset of the test matrix (see Fig. 5.1.) Improved interpretations of film thickness, wave geometry, and air entrainment are possible.

Sub-regimes of annular flow have been mapped in greater detail. Some of the results are similar to those of Hall Taylor and Hewitt (1963); however, the churn regime is found to have three visibly distinct zones and the previously named non-wetting area has been sorted into a partial-wetting and a rivulet flow sub-regime.

The quality of the pressure gradient data allowed calculations to be made of superficial gas friction factor. An examination of the behaviour of the superficial gas friction factor, f'_{sg}, revealed that the annular regime can be simplified into three zones. An attempt to produce a convenient correlation for f'_{sg} was successful for two of those zones: .

a) stable annular flow (Resg>35000) and laminar film

b) stable annular flow (Resg>35000) and turbulent film

The two correlations produced excellent predictions of pressure gradients measured with the current work, and more importantly, a reasonable match with two-phase pressure gradients with previously published data spanning several decades. The required inputs to perform a calculation of pressure gradient are easily available:

a) gas flow rate

b) liquid flow rate

c) pipe diameter

d) pressure

e) temperature

From these inputs, gas density can be calculated along with superficial gas velocity. Superficial gas Reynolds number and superficial liquid Reynolds number are then calculated to use in the correlation for the superficial gas friction factor. Finally the mechanical energy equation evaluates the pressure gradient.

7.3 Future Work – Near Term

The applicability of correlations based on specific fluids under some given condition (i.e. temperature, pressure, pipe diameter) outside their original experimental range is uncertain. To establish the robustness of any conclusions, a number of paths are possible. The most obvious is to extend the test matrix to higher air flow rates, since the annular-mist region was not explored in this work. Given the operational problems at high air rates, a pump would be required to stabilize the loop; this would also allow the evaluation of high liquid loading.

The flow loop could also, without modification, investigate the loading limits of two-phase flow. Simply operating at lower air rates, the stability limit of the liquid film could be determined.

While the air is certainly in turbulence throughout, clarification of the laminar-turbulent transition of the liquid film would yield useful information. The current work determined that the laminar-turbulent transition occurred at about $Re_{sl} = 250$. However application of PIV (Particle Image Velocimetry) could give greater detail on the change in liquid film velocity profiles. The question of whether the film surface (interface) velocity, v_i, is significant might also be answered.

New PLIF and PIV programs could be employed to investigate the influence of bubbles entrained in the liquid film. These are likely to be disruptive to the velocity distribution within the film and may also have an effect on the liquid properties (e.g. density, effective viscosity.)

7.4 Future Work – Long Term

The current work was accomplished with air and water only. Therefore the influence of other fluid properties is not known, and correlations are not likely to be universal. This was recognized by Steen and Wallis (1964) prompting them to conduct further experiments with silicone oil (different viscosity and surface tension.) They also conducted studies at elevated pressures (2 to 4 atm) to explore the effects of gas density. Given that the flow loop is located indoors, only benign fluids, such as water-glycerol mixtures, should be considered.

Another important variable has attracted less attention: pipe roughness. Virtually all laboratory flow loops have used plexiglass, glass, copper or polish stainless steel, which are effectively smooth pipes. Experiments with rough pipe, such as steel tubing, would provide better insights into two phase flow behaviour under field conditions. In addition, water wettability on a hydrophilic steel surface is quite different from wettability on plexiglass. For example Takamasa, Hazuku, and Hibiki (2008) have shown that hydrophilic pipe has a transition to annular flow at a lower velocity than with acrylic pipe.

"I took the degree of Doctor of Philosophy in 1903. The meaning of this degree is that the recipient of instruction is examined for the last time in his life, and is pronounced completely full. After this, no new ideas can be imparted to him."

Stephen Leacock in the Preface to "Sunshine Sketches of a Little Town," 1913.

References

ABB (2003). Flow products variable area flowmeters. Technical Information publication 10A-11.

AER (2017). ST98-2017: Alberta's energy reserves and supply/demand outlook, executive summary. http://www1.aer.ca/st98/data/executive_summary/ST98-2017_Executive_Summary.pdf

Alves, I., Caetano, E., Minami, K., & Shohan, O. (1991). Modelling annular flow behavior for gas wells. SPE Production Engineering, November, 435-440.

Ansari, A., Sylvester, M., Sarica, C., Shoham, O. & Brill, J. (1994). A comprehensive mechanistic model for upward two-phase flow in wellbores. SPE 20630, SPE Production and Facilities May, 143-152.

API (1978). API 14B Subsurface controlled subsurface safety valve sizing computer program.

Asali, J. (1984). Entrainment in vertical gas-liquid annular flows. Ph.D. Thesis, University of Illinois at Urban-Campaign.

Ashwood, A. (2010). Characterization of the macroscopic and microscopic mechanics in vertical and horizontal annular flow. Ph.D. Thesis, University of Wisconsin-Madison.

Barnea, D. (1987). A unified model for predicting flow-pattern transitions for the whole range of pipe inclinations. Int. J. Multiphase Flow, 13(1), 1-12.

Becaria Valero, J. (2004). Experimental observations and numerical modelling of gas lifting in small diameter pipes in view of unloading liquids from wells with low reservoir pressure. M.Sc. Thesis, University of Alberta.

Bergelin, O., (1949). Flow of gas-liquid mixtures. Chemical Engineering, May, 104-107.

Bizhani, M. (2013). Solids transport with turbulent flow of non-newtonian fluid in the horizontal annuli. M.Sc. Thesis, University of Alberta.

Calvert, S. & Williams, B. (1955). Upward cocurrent annular flow of air and water in smooth tubes," A.I.Ch.E. Journal, March, 78-86.

Chokshi, R. (1994). Prediction of pressure drop and liquid holdup in vertical two-phase flow through large diameter tubing. Ph.D. Thesis, University of Tulsa.

Chokshi, R., Schmidt, Z. & Doty, D. (1996). Experimental study and the development of a mechanistic model for two-phase flow through vertical tubing. SPE 35676.

Coleman, S., Clay, H., McCurdy, D,. & Norris III, H. (1991). A new look at predicting gas well loadup. SPE 20280, JPT March, 329-333.

Collier, J., & Hewitt, G. (1961). Data on the vertical flow of air-water mixtures in the annular and dispersed flow regions. Part II: film thickness and entrainment data and analysis of pressure drop measurements. Trans Instn. Chem. Engrs., 39, 127-136.

Cromer, S. & Huntington, R. (1938). Visual studies of the flow of air-water mixtures in a vertical pipe. AIME San Antonio Meeting, October, 79-90.

Farina, L., Passucci, C., Di Lullo, A., Negri, E., Pascolini, O., Anderson, S., & Page, S. (2012). Artificial lift optimization with foamer technology in the alliance shale gas field. SPE 160282.

Flack, K. & Schultz, M. (2014). Roughness effects on wall-bounded turbulent flows. Turbulent boundary layers on a systematically varied rough wall. Physics of Fluids 26, 101305 (2014); doi: 10.1063/1.4896280.

Fore, L., & Dukler, A. (1995). The distribution of drop size and velocity in gas-liquid annular flow. Int. J. Multiphase Flow, 21(2) 137-149.

Gomez, L., Shoham, O., Schmidt, Z., Chokshi, R., Brown, A., & Northug, T. (1999). A unified mechanistic model for steady-state two-phase flow in wellbores and pipelines. SPE 56520, 1999 SPE Annual Technical Conference and Exhibition, October 3-6,Houston, Texas.

Gosline, J. (1938). Experiments on the vertical flow of gas-liquid mixtures in glass pipes. AIME Houston Meeting, October, 56-70.

Govier, G., & Aziz, K. (2008). The flow of complex mixtures in pipes (second edition). Society of Petroleum Engineers.

Govier, G., and Short, L. (1958). The upward vertical flow of air-water mixtures. II Effect of tubing diameter on flow pattern, holdup and pressure drop. Can. J. Ch. Eng., October, 195-202.

Hall Taylor, N., Hewitt, G. & Lacey, P. (1963). The motion and frequency of large disturbance waves in annular two-phase flow of air-water mixtures. Chemical Engineering Science, 18, 537-552.

Hewitt, G., & Hall-Taylor, N. (1970). Annular two-phase flow. Permagon Press.

Hewitt, G., Jayanti, S., & Hope, C. (1990). Structure of thin liquid films in gas-liquid horizontal flow. International Journal of Multiphase Flow, 16(6), 951-957.

Ho, F. & Hummel, R. (1970). Average velocity distributions within falling liquid films. Chemical Engineering Science, 25, 1225-1237.

Hoyt, L. (1934). New table of the refractive index of pure glycerol at 20°C. Industrial and Engineering Chemistry. 26(3), 329-332.

Kadoya, K., Matsunaga, N. & Nagashima, A. (1985). Viscosity and thermal conductivity of dry air in the gaseous phase," J. Phys. Chem. Ref. Data 14(4), 948-970. doi:10.1063/1.555744.

Kopplin, C. (2004). Local liquid velocity measurements in horizontal, annular two-phase flow. M.Sc. Thesis, University of Wisconsin-Madison.

Krawiec, M., Finn, C., & Cockbill, J. (2008). Dewatering coalbed methane wells using ESPCPs. 2008-201 Canadian International Petroleum Conference, Calgary.

Kristofferson, A., Erga, S., Hamre, B., and Frette, O. (2014). Testing fluorescence lifetime standards using two-photon excitation and time-domain instrumentation: rhodamine b, coumarin 6 and lucifer yellow. J. Fluoresc. 24, 1015-1024. doi 10.1007/s10895-014-1368-1.

Lea, J., Nickens, H., & Wells, M. (2003). Gas well deliquification : Solution to gas well liquid loading problems. Burlington, MA: Gulf Professional Pub.

Luan, G. & He, S. (2012). A new model for the accurate prediction of liquid loading in low-pressure gas wells. JCPT 493-498.

Mamedulanov, D. 2016. measurement of liquid film thickness during upward annular air-water flow in vertical pipe using planar laser-induced fluorescence (PLIF) technique. M.Sc. Thesis, University of Alberta.

McCain, W., Spivey, J., & Lenn, C. (2011). Petroleum reservoir fluid property correlations. Tulsa, Okla.: PennWell Corp.

McGovern, J. (2011). Technical note: friction factor diagrams for pipe flow. Dublin Institute of Techology. Retrieved from http://arrow.dit.ie/engschmecart/28

Moody, L. (1944). Friction factors for pipe flow. Trans AIME, Nov., 671-684.

NACA (1950). Law of flow in rough pipes. technical memorandum 1292, a translation of Nikuradse, J. "stromungsgesetze in rauhen rohren," 1933.

Nascimento, C., Becze, A., Virues, C., & Wang, A. (2015). Using dynamic simulations to optimize the start-up of horizontal wells and evaluate plunger lift capability: Horn River shale gas trajectory-based study. SPE 174053-MS.

Nedderman, R., & Shearer, C. (1963). The breakdown of the liquid film in annular two-phase flow. Chemical Engineering Science, 18, 661-670.

Nichol, J., & Kuru, E. (2016). Observations of sub-regimes in vertical annular flow. Proc. 10th North American Conference on Multiphase Technology, 207-216.

Oshinowo, O. (1971). Two-phase flow in a vertical tube coil. Ph.D. Thesis, University of Toronto.

Ozkan, R., Keefer, B. & Miller, M. (2003). Optimization of plunger-lift performance in liquid loading gas wells. SPE 84135.

Radford, B. (1949). Gas-liquid flow in vertical pipes, a preliminary investigation. M.Sc. Thesis, University of Alberta.

Radwan, M. (2017). Feasibility evaluation of using downhole gas-water separation technology in gas reservoirs with bottom water. SPE 183739-MS.

Rodriguez, D. (2004). Characterization of bubble entrainment, interfacial roughness and the sliding bubble mechanism in horizontal annular flow. Ph.D. Thesis, University of Wisconsin-Madison.

Schadel, S. (1988). Atomization and deposition rates in vertical annular two-phase flow. Ph.D. Thesis, University of Illinois at Urbana-Champaign.

Schadel, S., Leman, G., Binder, J., & Hanratty, T. (1990). Rates of atomization and deposition in vertical annular flow. Int. J. Multiphase Flow, 16(3), 363-374.

Schlichting, H. (1979). Boundary-layer theory [Grenzschicht-Theorie.] (7th ed.). New York: McGraw-Hill.

Schubring, D. (2009). Behavior interrelationships in annular flow. Ph.D. Thesis, University of Wisconsin-Madison.

Shoham, O. (2006). “Mechanistic modelling of gas-liquid two-phase flow in pipes,” SPE, Richardson, Texas.

Spedding, P., Woods, G., Raghunathan, R., & Watterson, J. (1998a). Vertical two phase flow, part ii: experimental semi-annular flow & hold-up. Trans. IChemE Vol. 76 Part A, 620-627.

Spedding, P., Woods, G., Raghunathan, R., & Watterson, J. (1998b). Vertical two-phase flow part iii: pressure drop. Trans. IChemE 76, Part A 628-634.

Steen, D. & Wallis, G. (1964). The transition from annular to annular-mist cocurrent two phase downflow. Report No. NYO-3114-2, Two-Phase Flow and Boiling Heat Transfer Interim Report, June.

Swamee, P., & Jain, A. (1976). Explicit equations for pipe-flow problems. Journal of the Hydraulics Division, Proc. American Society of Civil Engineers, May, 657-664.

Taitel, Y., Barnea, D., & Dukler, A. (1980). Modelling flow pattern transitions for steady upward gas-liquid flow in vertical tubes. A.I.Ch.E. Journal, 26(3), 345-354.

Takamasa, T., Hazuku, T. & Hibiki, T. (2008). Experimental study of gas-liquid two-phase flow affected by wall surface wettability. Int. J. Heat Fluid Flow 20, 1593-1602. doi:10.1016/j.ijheatfluidflow.2008.09.001

Turner, R., Hubbard, M., & Dukler, A. (1969). Analysis and minimum flow rate for the continuous removal of liquids from gas wells. SPE 2198, JPT November, 1475-1482.

Turner. J. (1966). Annular two-phase flow. Ph.D. Thesis, Dartmouth College.

Vargas, E. (2006). Laboratory investigations on upward gas-liquid transport from low-pressure reservoir during slug-to-annular flow pattern transitions. M.Sc. Thesis, University of Alberta, Edmonton Canada.

Versluys, J. (1932). The cause of fluctuations in rising mixtures of gas and liquid. Journal of Rheology, 3(3), 3-15.

Wallis, G. (1968). Phenomena of liquid transfer in two-phase dispersed annular flow. Int. J. Heat and Mass Transfer, 11, 783-785.

Wallis, G. (1969.) One dimensional two-phase flow. McGraw-Hill, New York.

Wang, Z., Bai, H. Zhu, S., Zhong, H., & Li, Y. (2015). An entrained-droplet model for prediction of minimum flow rate for the continuous removal of liquid from gas wells. SPE 174077, SPEJ, 1135-1144.

Wawro, K., Wassmuth, F. & Smith, J. (2000). Reducing water production in a naturally fractured gas well using sequential gel/gas slug injection. SPE 59746.

Whalley, P. & Hewitt, G. (1978). The correlation of liquid entrainment fraction and entrainment rate in annular two-phase flow. AERE Report R-9187.

Woods, G., Spedding, P., Watterson, J., & Raghunathan, R. (1999). Vertical Two Phase Flow. Dev. Chem. Eng. Mineral Process, 7, 7-16. doi:10.1002/apj.5500070103

Yao S., & Sylvester, N. (1987). A mechanistic model for two-phase annular-mist flow in vertical pipes. A.I.Ch.E. Journal, 33(6), 1008-1012.

Zadrazil, I., Matar, O. & Markides, C. (2014). An experimental characterization of downwards gas–liquid annular flow by laser-induced fluorescence: Flow regimes and film statistics. IJMF 60, 87-102.

Zeinali, H. (2012). Effect of near-wall turbulence and selective removal of particles from sand beds deposited in pipelines. Ph.D. Thesis, University of Alberta.

Appendices

Appendix 1 Flow Loop Pressure Gradient Program Data

Line No.	Date	Controller Air Flow Set Point, SLPM @ 15C, 100 kPaa	Air Mass Flow Rate, g/s	Average Flow Loop Temperature, °C (Ai5)	Average Flow Loop Pressure, psig (Ai6)	Average Pressure Differential, psi (Ai7)	Kobold Rotameter Water Flow rate SLPH	Differential Pressure Correction	CORRECTED Average Pressure Differential, psi (Ai7)
1	15-12-11	700	14.1035211	15.8903047	0.17987701	0.03423117	20	-0.02235518	0.05520796
2	15-12-11	700	14.1035211	15.6378908	0.1736608	0.03108062	18	-0.02235518	0.052134152
3	15-12-11	700	14.1035211	15.2666021	0.16440215	0.02774199	16	-0.02235518	0.048876851
4	15-12-11	700	14.1035211	14.932775	0.14853438	0.0246214	14	-0.02235518	0.045832281
5	15-12-11	700	14.1035211	14.3045589	0.13466017	0.01737381	12	-0.02235518	0.038761229
6	15-12-11	700	14.1035211	13.8249607	0.12289326	0.01659065	10	-0.02235518	0.037997146
7	15-12-11	700	14.1035211	13.5330889	0.1151955	0.00995716	8	-0.02235518	0.031525248
8	15-12-11	700	14.1035211	13.0043547	0.10440436	0.00630425	6	-0.02235518	0.027961313
9	15-12-11	700	14.1035211	12.4219062	0.08926046	0.00562606	4	-0.02235518	0.027299644
10	15-12-11	700	14.1035211	13.117161	0.07931238	0.00572657	2	-0.02235518	0.027397708
11	15-12-18	700	14.1035211	19.7339138	0.30321712	0.09478214	60	-0.02409581	0.115307399
12	15-12-18	700	14.1035211	20.0974356	0.33148058	0.10777327	70	-0.02409581	0.128656872
13	15-12-18	700	14.1035211	20.4052473	0.35092064	0.12106031	80	-0.02409581	0.141620251
14	15-12-18	700	14.1035211	20.4977257	0.37123566	0.12929227	90	-0.02409581	0.149651693
15	15-12-18	700	14.1035211	20.544067	0.39731613	0.14190785	100	-0.02409581	0.161959969
16	15-12-18	700	14.1035211	20.2007942	0.41655425	0.15127555	110	-0.02409581	0.17109948
17	16-01-08	800	16.1183098	21.264194	0.50246097	0.19777299	140	-0.02766161	0.219943217
18	16-01-08	800	16.1183098	20.9095401	0.47247177	0.18165055	120	-0.02766161	0.204213505
19	16-01-08	800	16.1183098	19.8026068	0.42906266	0.15521583	100	-0.02766161	0.178422711
20	16-01-08	800	16.1183098	19.0587792	0.38196065	0.13124436	80	-0.02766161	0.155035167
21	16-01-08	800	16.1183098	18.2333673	0.32915071	0.10656872	60	-0.02766161	0.1309606
22	16-01-08	800	16.1183098	17.0675018	0.26984525	0.07804269	40	-0.02766161	0.103129434
23	16-01-08	800	16.1183098	15.3030217	0.19037801	0.0434087	20	-0.02766161	0.069339102
24	16-01-08	800	16.1183098	15.2959316	0.1930603	0.04426157	20	-0.02766161	0.070171191
25	16-01-08	800	16.1183098	14.7651079	0.17624142	0.03806022	16	-0.02766161	0.064120902
26	16-01-08	800	16.1183098	14.1421126	0.15262609	0.02670957	12	-0.02766161	0.053046744
27	16-01-08	800	16.1183098	13.4164142	0.13205413	0.02156388	8	-0.02766161	0.048026395
28	16-01-08	800	16.1183098	12.758385	0.08938805	0.01279597	2	-0.02766161	0.039472066
29	16-01-15	800	16.1183098	16.5214234	0.22476116	0.07724941	30	-0.02370879	0.098498952
30	16-01-15	900	18.1330986	18.5203024	0.45661323	0.19665006	100	-0.02370879	0.214991116
31	16-01-15	900	18.1330986	17.9184604	0.41124915	0.17542349	80	-0.02370879	0.194281604
32	16-01-15	900	18.1330986	17.0390708	0.35481316	0.14858279	60	-0.02370879	0.168094716
33	16-01-15	900	18.1330986	16.0403046	0.28641178	0.11377485	40	-0.02370879	0.134134666
34	16-01-15	900	18.1330986	15.2681455	0.24194319	0.09089874	30	-0.02370879	0.111815801
35	16-01-15	900	18.1330986	14.6088247	0.20134979	0.07128419	20	-0.02370879	0.092679038
36	16-01-15	900	18.1330986	14.3876164	0.19911912	0.07062194	20	-0.02370879	0.092032921
37	16-01-15	900	18.1330986	13.9943965	0.18333035	0.06359687	16	-0.02370879	0.085112213
38	16-01-15	900	18.1330986	13.4664589	0.15988785	0.05156697	12	-0.02370879	0.073442116
39	16-01-15	900	18.1330986	12.5963065	0.13192771	0.05469544	8	-0.02370879	0.076494375
40	16-01-15	900	18.1330986	12.9969396	0.07925264	0.03026262	2	-0.02370879	0.052656721
41	16-01-15	1000	20.1478873	16.5521501	0.44532268	0.20147077	80	-0.02370879	0.219694393
42	16-01-15	1000	20.1478873	15.972966	0.39413833	0.17488096	60	-0.02370879	0.193752293
43	16-01-15	1000	20.1478873	15.0898322	0.32302158	0.13732358	40	-0.02370879	0.157109771
44	16-01-15	1000	20.1478873	14.3702087	0.26350957	0.10894775	30	-0.02370879	0.129425151
45	16-01-15	1000	20.1478873	13.8056697	0.22310915	0.09348538	20	-0.02370879	0.11433943
46	16-01-15	1000	20.1478873	13.5108755	0.20655266	0.08599636	16	-0.02370879	0.107032839
47	16-01-15	1000	20.1478873	13.0933067	0.17893642	0.07254054	12	-0.02370879	0.093904787
48	16-01-15	1000	20.1478873	12.3917608	0.14291464	0.0586431	8	-0.02370879	0.080345878
49	16-01-15	1000	20.1478873	11.8645622	0.09350833	0.04301587	2	-0.02370879	0.065099313
50	16-01-22	1100	22.162676	19.1557923	0.54013367	0.24535491	100	-0.02770474	0.266408174
51	16-01-22	1100	22.162676	18.814483	0.49032138	0.22111091	80	-0.02770474	0.242754731
52	16-01-22	1100	22.162676	17.6253862	0.43092542	0.19279088	60	-0.02770474	0.215124557
53	16-01-22	1100	22.162676	16.2268324	0.35876104	0.15852308	40	-0.02770474	0.181691488
54	16-01-22	1100	22.162676	14.2809903	0.26276928	0.1168185	20	-0.02770474	0.141002787
55	16-01-22	1100	22.162676	15.1672019	0.30500926	0.13404062	30	-0.02770474	0.157805392
56	16-01-22	1100	22.162676	13.9912765	0.25121456	0.1130986	18	-0.02770474	0.137373507
57	16-01-22	1100	22.162676	13.6340084	0.23450866	0.10583984	16	-0.02770474	0.130291556
58	16-01-22	1100	22.162676	13.2709318	0.22308806	0.1018374	14	-0.02770474	0.126386612
59	16-01-22	1100	22.162676	12.9955654	0.1972223	0.0888995	12	-0.02770474	0.113763873
60	16-01-22	1100	22.162676	12.677008	0.18378712	0.08662917	10	-0.02770474	0.111548846
61	16-01-22	1100	22.162676	12.2127576	0.16036815	0.07302833	8	-0.02770474	0.098279306
62	16-01-22	1100	22.162676	12.1919417	0.14446766	0.06419348	6	-0.02770474	0.089659664
63	16-01-22	1100	22.162676	11.8652242	0.12875407	0.06435832	4	-0.02770474	0.089820493
64	16-01-22	1100	22.162676	12.8006389	0.10888915	0.05440561	2	-0.02770474	0.08011022

Line No.	Date	Controller Air Flow Set Point, SLPM @ 15C, 100 kPaa	Air Mass Flow Rate, g/s	Average Flow Loop Temperature, °C (Ai5)	Average Flow Loop Pressure, psig (Ai6)	Average Pressure Differential, psi (Ai7)	Kobold Rotameter Water Flow rate SLPH	Differential Pressure Correction	CORRECTED Average Pressure Differential, psi (Ai7)
65	16-01-22	350	7.05176055	19.4287376	0.46666279	0.13638336	160	-0.02770474	0.160091071
66	16-01-22	350	7.05176055	18.7742661	0.43686159	0.1228485	140	-0.02770474	0.146885901
67	16-01-22	350	7.05176055	18.5404646	0.4123126	0.11267737	120	-0.02770474	0.13696253
68	16-01-22	350	7.05176055	18.47717	0.38615132	0.10062034	100	-0.02770474	0.125199205
69	16-01-22	350	7.05176055	18.2643957	0.35169458	0.08739232	80	-0.02770474	0.112293404
70	16-01-22	350	7.05176055	17.9722817	0.31615812	0.07186342	60	-0.02770474	0.097142774
71	16-01-22	350	7.05176055	17.523887	0.28006419	0.05575291	40	-0.02770474	0.0814247
72	16-01-22	350	7.05176055	16.9979755	0.25754813	0.04832215	30	-0.02770474	0.07417495
73	16-01-22	350	7.05176055	16.7079358	0.23302342	0.03988778	20	-0.02770474	0.065946029
74	16-01-22	350	7.05176055	16.6031584	0.2281443	0.03723065	18	-0.02770474	0.063353625
75	16-01-22	350	7.05176055	16.3876986	0.21842818	0.03494225	16	-0.02770474	0.061120968
76	16-01-22	350	7.05176055	16.276455	0.21081928	0.03209987	14	-0.02770474	0.058347825
77	16-01-22	350	7.05176055	16.1319629	0.20771984	0.02917505	12	-0.02770474	0.055494253
78	16-01-22	350	7.05176055	15.9109152	0.19813362	0.02718516	10	-0.02770474	0.053552838
79	16-01-22	350	7.05176055	15.6233573	0.18914839	0.0243089	8	-0.02770474	0.050746633
80	16-01-22	350	7.05176055	15.4249235	0.17825632	0.02020331	6	-0.02770474	0.046741051
81	16-01-22	350	7.05176055	15.0759802	0.16676732	0.01690994	4	-0.02770474	0.043527911
82	16-01-22	350	7.05176055	14.7473375	0.15517511	0.01427826	2	-0.02770474	0.040960332
83	16-01-29	1300	26.1922535	17.2910688	0.51832384	0.25682235	60	-0.0267145	0.276630153
84	16-01-29	1300	26.1922535	15.8811566	0.44885779	0.22483539	40	-0.0267145	0.245422367
85	16-01-29	1300	26.1922535	15.025348	0.37608933	0.19146073	30	-0.0267145	0.212860679
86	16-01-29	1300	26.1922535	13.7849445	0.3333057	0.17504018	20	-0.0267145	0.196840119
87	16-01-29	1300	26.1922535	13.5704245	0.31877775	0.16911189	18	-0.0267145	0.191056236
88	16-01-29	1300	26.1922535	13.1725647	0.30051608	0.16229676	16	-0.0267145	0.184407121
89	16-01-29	1300	26.1922535	12.7419446	0.28080104	0.15485561	14	-0.0267145	0.17714723
90	16-01-29	1300	26.1922535	12.5670619	0.25133386	0.13825143	12	-0.0267145	0.160947513
91	16-01-29	1300	26.1922535	12.1452024	0.23372286	0.1330598	10	-0.0267145	0.155882341
92	16-01-29	1300	26.1922535	11.8039524	0.21108522	0.12429917	8	-0.0267145	0.14733512
93	16-01-29	1300	26.1922535	11.4465518	0.18730635	0.10447678	6	-0.0267145	0.127995584
94	16-01-29	1300	26.1922535	10.9704621	0.16186837	0.08688234	4	-0.0267145	0.110829721
95	16-01-29	1300	26.1922535	12.0623718	0.14405232	0.08142035	2	-0.0267145	0.105500778
96	16-01-29	1400	28.2070422	16.888886	0.5593267	0.29943616	60	-0.0286069	0.320052238
97	16-01-29	1400	28.2070422	15.1995276	0.47631269	0.26093034	40	-0.0286069	0.282484386
98	16-01-29	1400	28.2070422	13.1725647	0.41586924	0.23263352	30	-0.0286069	0.254876847
99	16-01-29	1400	28.2070422	13.487375	0.36921588	0.21071781	20	-0.0286069	0.233494985
100	16-01-29	1400	28.2070422	13.305994	0.35510191	0.20049103	18	-0.0286069	0.223517323
101	16-01-29	1400	28.2070422	13.0015173	0.33385575	0.1912971	16	-0.0286069	0.214547341
102	16-01-29	1400	28.2070422	12.7013804	0.31613541	0.18428868	14	-0.0286069	0.20770964
103	16-01-29	1400	28.2070422	12.3300042	0.29211783	0.17238294	12	-0.0286069	0.196093919
104	16-01-29	1400	28.2070422	12.004816	0.27031038	0.15811909	10	-0.0286069	0.182177522
105	16-01-29	1400	28.2070422	11.7542816	0.2432516	0.1441761	8	-0.0286069	0.168574169
106	16-01-29	1400	28.2070422	11.468863	0.21849893	0.13687659	6	-0.0286069	0.161452467
107	16-01-29	1400	28.2070422	11.1547179	0.19219365	0.11348873	4	-0.0286069	0.138634315
108	16-01-29	1400	28.2070422	10.7829452	0.17478339	0.09765937	2	-0.0286069	0.123190538
109	16-01-29	1500	30.2218309	12.8140309	0.40723316	0.23599969	20	-0.0286069	0.258161021
110	16-01-29	1500	30.2218309	13.627172	0.45414507	0.25124447	30	-0.0286069	0.27303445
111	16-01-29	1500	30.2218309	14.3770335	0.52252108	0.2820589	40	-0.0286069	0.303098274
112	16-02-06	1500	30.2218309	16.7545574	0.56483222	0.32023813	60	-0.02689	0.338672417
113	16-02-06	1500	30.2218309	16.0714245	0.53512833	0.30732462	50	-0.02689	0.326073466
114	16-02-06	1500	30.2218309	15.5187653	0.48635065	0.27983118	40	-0.02689	0.299249736
115	16-02-06	1500	30.2218309	14.6978358	0.42358369	0.25005495	30	-0.02689	0.270198834
116	16-02-06	1500	30.2218309	13.8233474	0.37986429	0.23870899	20	-0.02689	0.259129251
117	16-02-06	1500	30.2218309	13.6932259	0.3611397	0.22803436	18	-0.02689	0.248714644
118	16-02-06	1500	30.2218309	13.5336019	0.33802472	0.21649438	16	-0.02689	0.237455767
119	16-02-06	1500	30.2218309	13.2500176	0.31703436	0.20325126	14	-0.02689	0.224535234
120	16-02-06	1500	30.2218309	13.0223016	0.29440783	0.1898704	12	-0.02689	0.211480319
121	16-02-06	1500	30.2218309	12.7860195	0.26666372	0.17453084	10	-0.02689	0.196514421
122	16-02-06	1500	30.2218309	12.4962921	0.23831747	0.15443075	8	-0.02689	0.176903944
123	16-02-06	1500	30.2218309	12.2946698	0.21278291	0.14810187	6	-0.02689	0.170729229
124	16-02-06	1500	30.2218309	12.2539469	0.18424943	0.13004949	4	-0.02689	0.15311659
125	16-02-06	1500	30.2218309	12.4701372	0.16558487	0.11981612	2	-0.02689	0.143132493
126	16-02-12	1200	24.1774647	19.2504179	0.54749049	0.26013756	100	-0.02928	0.28236762
127	16-02-12	1200	24.1774647	18.7617613	0.50424599	0.23998712	80	-0.02928	0.262708027
128	16-02-12	1200	24.1774647	17.6715322	0.45024969	0.21461684	60	-0.02928	0.237955738

Line No.	Date	Controller Air Flow Set Point, SLPM @ 15C, 100 kPaa	Air Mass Flow Rate, g/s	Average Flow Loop Temperature, °C (Ai5)	Average Flow Loop Pressure, psig (Ai6)	Average Pressure Differential, psi (Ai7)	Kobold Rotameter Water Flow rate SLPH	Differential Pressure Correction	CORRECTED Average Pressure Differential, psi (Ai7)
129	16-02-12	1200	24.1774647	16.0914579	0.3723346	0.17787844	40	-0.02928	0.202112259
130	16-02-12	1200	24.1774647	15.0882582	0.30556377	0.15745181	30	-0.02928	0.182183203
131	16-02-12	1200	24.1774647	14.1829647	0.27269967	0.14365155	20	-0.02928	0.168719099
132	16-02-12	1200	24.1774647	13.9855947	0.25917711	0.13814828	18	-0.02928	0.163349886
133	16-02-12	1200	24.1774647	13.6651026	0.23989546	0.12963278	16	-0.02928	0.155041816
134	16-02-12	1200	24.1774647	13.4519112	0.219195	0.12181575	14	-0.02928	0.147415199
135	16-02-12	1200	24.1774647	13.2675384	0.21162767	0.11829296	12	-0.02928	0.143978222
136	16-02-12	1200	24.1774647	12.9991197	0.18995061	0.10616149	10	-0.02928	0.132142258
137	16-02-12	1200	24.1774647	12.9047873	0.16785735	0.10318924	8	-0.02928	0.129242416
138	16-02-12	1200	24.1774647	12.5200538	0.1429824	0.09200578	6	-0.02928	0.118331372
139	16-02-12	1200	24.1774647	12.1016086	0.12774641	0.08677324	4	-0.02928	0.113226294
140	16-02-12	1200	24.1774647	12.7047067	0.10972329	0.07230049	2	-0.02928	0.09910608
141	16-02-12	1000	20.1478873	14.4201489	0.21350973	0.09044838	20	-0.02779594	0.115363992
142	16-02-12	1000	20.1478873	14.3011722	0.20480043	0.086348	18	-0.02779594	0.111363495
143	16-02-12	1000	20.1478873	13.7624978	0.1793148	0.07518174	14	-0.02779594	0.100469236
144	16-02-12	1000	20.1478873	13.4083515	0.1426819	0.06902932	10	-0.02779594	0.094466682
145	16-02-12	1000	20.1478873	12.6940926	0.11033632	0.05722715	6	-0.02779594	0.082952
146	16-02-12	1000	20.1478873	12.8513199	0.09301978	0.04559438	4	-0.02779594	0.071602592
147	16-02-12	900	18.1330986	15.2022713	0.1992593	0.074832	20	-0.02779594	0.100128016
148	16-02-12	900	18.1330986	14.5419982	0.18309581	0.06919054	16	-0.02779594	0.09462398
149	16-02-12	900	18.1330986	14.563908	0.19138557	0.06701906	18	-0.02779594	0.092505392
150	16-02-12	900	18.1330986	14.1382317	0.16842523	0.05549724	14	-0.02779594	0.081264234
151	16-02-12	900	18.1330986	13.858018	0.14247179	0.04832467	10	-0.02779594	0.074266383
152	16-02-12	900	18.1330986	13.0648438	0.11677724	0.03504752	6	-0.02779594	0.061312651
153	16-02-12	900	18.1330986	12.9833536	0.09893033	0.0391198	4	-0.02779594	0.065285735
154	16-02-12	800	16.1183098	14.8792859	0.18039169	0.0488739	20	-0.02779594	0.074802231
155	16-02-12	800	16.1183098	14.8161102	0.17317141	0.044142	18	-0.02779594	0.070185595
156	16-02-12	800	16.1183098	14.4173511	0.1535361	0.03339446	14	-0.02779594	0.059699852
157	16-02-12	800	16.1183098	14.0709183	0.1291653	0.02541874	10	-0.02779594	0.051918421
158	16-02-12	800	16.1183098	13.5145042	0.10936808	0.01947807	6	-0.02779594	0.046122457
159	16-02-12	800	16.1183098	13.1464741	0.09531116	0.02358218	4	-0.02779594	0.050126596
160	16-02-17	700	14.1035211	19.1490906	0.29311917	0.08953639	60	-0.02807278	0.11474432
161	16-02-17	700	14.1035211	16.5530444	0.18263628	0.03553	21	-0.02807278	0.062053478
162	16-02-17	700	14.1035211	15.9947323	0.17528727	0.03434905	20	-0.02807278	0.06090129
163	16-02-17	700	14.1035211	17.6850971	0.24286486	0.06525898	40	-0.02807278	0.091058286
164	16-02-17	700	14.1035211	17.0431575	0.21542131	0.05033942	30	-0.02807278	0.076502154
165	16-02-17	700	14.1035211	15.0585367	0.15379492	0.02624232	14	-0.02807278	0.052992037
166	16-03-05	600	12.0887324	21.7472293	0.38337705	0.12880347	120	-0.03131142	0.156214639
167	16-03-05	600	12.0887324	20.6422356	0.35130274	0.11193539	100	-0.03131142	0.139757457
168	16-03-05	600	12.0887324	20.0234265	0.31975579	0.09277121	80	-0.03131142	0.121060092
169	16-03-05	600	12.0887324	19.0611117	0.27459613	0.06946129	60	-0.03131142	0.09831798
170	16-03-05	600	12.0887324	17.9267023	0.22731674	0.04717762	40	-0.03131142	0.076577119
171	16-03-05	600	12.0887324	17.14505	0.20252989	0.03495839	30	-0.03131142	0.064655541
172	16-03-05	600	12.0887324	16.4474897	0.17633255	0.02347863	20	-0.03131142	0.053455419
173	16-03-05	600	12.0887324	16.1249691	0.16935952	0.02102248	18	-0.03131142	0.051059099
174	16-03-05	600	12.0887324	15.9038211	0.16320563	0.01683613	16	-0.03131142	0.046974723
175	16-03-05	600	12.0887324	15.5631295	0.15282518	0.01384441	14	-0.03131142	0.044055881
176	16-03-05	600	12.0887324	15.3344389	0.14558988	0.01099385	12	-0.03131142	0.041274755
177	16-03-05	600	12.0887324	15.0155846	0.13728467	0.00908976	10	-0.03131142	0.039417051
178	16-03-05	600	12.0887324	14.9048559	0.13096407	0.0064547	8	-0.03131142	0.036846178
179	16-03-05	600	12.0887324	14.6142511	0.12037749	0.00349837	6	-0.03131142	0.033961858
180	16-03-05	600	12.0887324	14.2491282	0.10829139	0.0015101	4	-0.03131142	0.03202202
181	16-03-05	600	12.0887324	13.7806871	0.07423417	-0.00714424	2	-0.03131142	0.023578496
182	16-03-05	500	10.0739436	20.298886	0.37503294	0.11653382	120	-0.02975397	0.142724363
183	16-03-05	500	10.0739436	20.0893582	0.34740685	0.10417508	100	-0.02975397	0.130666666
184	16-03-05	500	10.0739436	19.6990251	0.31191714	0.0870531	80	-0.02975397	0.113961757
185	16-03-05	500	10.0739436	19.0177178	0.27181814	0.06667932	60	-0.02975397	0.094084265
186	16-03-05	500	10.0739436	18.2950818	0.23120059	0.04739103	40	-0.02975397	0.075265822
187	16-03-05	500	10.0739436	17.6156334	0.20906979	0.03748947	30	-0.02975397	0.065605451
188	16-03-05	500	10.0739436	16.8113255	0.18193503	0.02120679	20	-0.02975397	0.049719409
189	16-03-05	500	10.0739436	16.7287708	0.17901906	0.01920055	18	-0.02975397	0.047762037
190	16-03-05	500	10.0739436	16.6931234	0.17083081	0.01480898	16	-0.02975397	0.043477442
191	16-03-05	500	10.0739436	16.2861964	0.16250677	0.0124622	14	-0.02975397	0.041187826
192	16-03-05	500	10.0739436	16.0130639	0.15585654	0.00979209	12	-0.02975397	0.038582763

Line No.	Date	Controller Air Flow Set Point, SLPM @ 15C, 100 kPaa	Air Mass Flow Rate, g/s	Average Flow Loop Temperature , °C (Ai5)	Average Flow Loop Pressure, psig (Ai6)	Average Pressure Differential, psi (Ai7)	Kobold Rotameter Water Flow rate SLPH	Differential Pressure Correction	CORRECTED Average Pressure Differential, psi (Ai7)
193	16-03-05	500	10.0739436	15.9523575	0.14964753	0.00673613	10	-0.02975397	0.035601233
194	16-03-05	500	10.0739436	15.8294625	0.13978283	0.00385266	8	-0.02975397	0.032788006
195	16-03-05	500	10.0739436	15.6389186	0.12899381	0.00107652	6	-0.02975397	0.030079486
196	16-03-05	500	10.0739436	15.3079758	0.12011441	-0.00198877	4	-0.02975397	0.027088864
197	16-03-05	500	10.0739436	15.1727966	0.07645906	-0.00939432	2	-0.02975397	0.019863715
198	16-03-10	400	8.05915491	22.9632788	0.40103457	0.114087	140	-0.02875722	0.13936467
199	16-03-10	400	8.05915491	22.8878416	0.3805326	0.10362372	120	-0.02875722	0.129156261
200	16-03-10	400	8.05915491	22.2527924	0.35189561	0.09222039	100	-0.02875722	0.118030708
201	16-03-10	400	8.05915491	21.7796359	0.32112073	0.08299127	80	-0.02875722	0.1090264
202	16-03-10	400	8.05915491	21.1169827	0.28708512	0.06794093	60	-0.02875722	0.094342671
203	16-03-10	400	8.05915491	20.3294782	0.24853984	0.05106542	40	-0.02875722	0.077878235
204	16-03-10	400	8.05915491	19.7742576	0.22780867	0.04129585	30	-0.02875722	0.068346639
205	16-03-10	400	8.05915491	18.9496264	0.2026028	0.03243617	20	-0.02875722	0.059702777
206	16-03-10	400	8.05915491	18.2994307	0.19503836	0.02977785	18	-0.02875722	0.057109205
207	16-03-10	400	8.05915491	17.9181222	0.19248776	0.02760925	16	-0.02875722	0.054993438
208	16-03-10	400	8.05915491	17.7064303	0.18002889	0.02434399	14	-0.02875722	0.051807715
209	16-03-10	400	8.05915491	17.4233305	0.17573178	0.02240706	12	-0.02875722	0.049917966
210	16-03-10	400	8.05915491	17.0780134	0.16957683	0.02087138	10	-0.02875722	0.048419688
211	16-03-10	400	8.05915491	16.7201538	0.16366231	0.01877977	8	-0.02875722	0.046379028
212	16-03-10	400	8.05915491	16.4990656	0.15115245	0.01500221	6	-0.02875722	0.042693488
213	16-03-10	400	8.05915491	16.2199775	0.13975842	0.0115351	4	-0.02875722	0.039310837
214	16-03-10	400	8.05915491	15.6978082	0.12265337	0.0095976	2	-0.02875722	0.037420527

Line No.	*Gage Pressure Correction, psi*	*CORRECTED Gauge Pressure, psi*	*Daily Mean Station Pressure, kPaa*	*CORRECTED Absolute Pressure at P0, kPaa*	Average Pressure Gradient, Pa/m	Water Density, g/cc	Water Volumetric Flow Rate, m3/s	Vsl, m/s	*Pressure at P1, Beginning of dP Section, kPaa*
1	-0.01836367	0.193805101	92.62	93.95628617	499.424457	0.99892251	5.56155E-06	0.01035585	93.8040226
2	-0.01836367	0.187727979	92.62	93.91438442	471.618051	0.99896272	5.00519E-06	0.00931989	93.7705984
3	-0.01836367	0.178676488	92.62	93.85197438	442.151726	0.99902056	4.4488E-06	0.00828387	93.717172
4	-0.01836367	0.163163757	92.62	93.7450141	414.609818	0.9990712	3.8925E-06	0.00724801	93.6186087
5	-0.01836367	0.149599979	92.62	93.65149186	350.643377	0.99916306	3.33613E-06	0.00621201	93.5445884
6	-0.01836367	0.138096351	92.62	93.57217434	343.731303	0.99923007	2.77992E-06	0.00517633	93.4673782
7	-0.01836367	0.130570818	92.62	93.52028579	285.184963	0.99926955	2.22385E-06	0.0041409	93.4333392
8	-0.01836367	0.120021134	92.62	93.44754572	252.944746	0.99933848	1.66777E-06	0.00310546	93.3704284
9	-0.01836367	0.105216066	92.62	93.34546478	246.959136	0.9994105	1.11177E-06	0.00207016	93.2701724
10	-0.01836367	0.095490576	92.62	93.27840752	247.846241	0.99932397	5.55931E-07	0.00103517	93.2028446
11	-0.01639183	0.312457794	93.22	95.37439649	1043.09841	0.99822368	1.66963E-05	0.03108929	95.0563787
12	-0.01639183	0.340088868	93.22	95.56491275	1163.86094	0.99814941	1.94805E-05	0.03627354	95.2100771
13	-0.01639183	0.359093967	93.22	95.69595291	1281.13078	0.99808543	2.22648E-05	0.04145813	95.3053643
14	-0.01639183	0.378954443	93.22	95.83289088	1353.78513	0.99806604	2.50484E-05	0.04664131	95.4201515
15	-0.01639183	0.404451374	93.22	96.00869222	1465.12875	0.99805632	2.78319E-05	0.05182418	95.5620066
16	-0.01639183	0.42325904	93.22	96.13837108	1547.80696	0.99812817	3.06129E-05	0.05700249	95.6664787
17	-0.01569702	0.506564355	94.31	97.80276123	1989.65913	0.9979024	3.89706E-05	0.07256504	97.1961578
18	-0.01569702	0.477246155	94.31	97.60061224	1847.36437	0.99797915	3.34008E-05	0.06219382	97.0373914
19	-0.01569702	0.434808309	94.31	97.30800329	1614.05467	0.99821046	2.78276E-05	0.05181618	96.8159135
20	-0.01569702	0.388760197	94.31	96.99050156	1402.48533	0.99835867	2.22588E-05	0.04144679	96.5629146
21	-0.01569702	0.337131865	94.31	96.63452421	1184.70102	0.99851628	1.66914E-05	0.03108018	96.2733349
22	-0.01569702	0.279153341	94.31	96.23476229	932.933609	0.99872638	1.11253E-05	0.02071576	95.9503313
23	-0.01569702	0.201464157	94.31	95.69909536	627.258154	0.99901577	5.56103E-06	0.01035488	95.5078581
24	-0.01569702	0.204086437	94.31	95.71717598	634.785433	0.99901686	5.56102E-06	0.01035487	95.5236438
25	-0.01569702	0.18764387	94.31	95.60380448	580.053069	0.99909699	4.44846E-06	0.00828323	95.426959
26	-0.01569702	0.164556926	94.31	95.44462001	479.873582	0.99918688	3.33605E-06	0.00621186	95.2983171
27	-0.01569702	0.144445259	94.31	95.30595006	434.458293	0.99928585	2.22381E-06	0.00414083	95.1734933
28	-0.01569702	0.102733816	94.31	95.01834966	357.073782	0.99937012	5.55906E-07	0.00103512	94.9094857
29	-0.01707723	0.23642733	93.88	95.51016644	891.045157	0.99881939	8.34318E-06	0.01553538	95.2385063
30	-0.01707723	0.463091778	93.88	97.07301781	1944.86124	0.99846224	2.78206E-05	0.05180311	96.4800723
31	-0.01707723	0.418742699	93.88	96.76723091	1757.51802	0.99857439	2.22539E-05	0.04143783	96.2314022
32	-0.01707723	0.363569449	93.88	96.38681135	1520.62515	0.9987312	1.66878E-05	0.0310735	95.9232061
33	-0.01707723	0.296698531	93.88	95.92573637	1213.41438	0.99889895	1.11234E-05	0.02071218	95.555793
34	-0.01707723	0.253224911	93.88	95.62598576	1011.51257	0.99902098	8.3415E-06	0.01553224	95.3175978
35	-0.01707723	0.213539776	93.88	95.35235675	838.396818	0.99911977	5.56045E-06	0.0103538	95.096748
36	-0.01707723	0.211359018	93.88	95.33732043	832.551891	0.99915181	5.56027E-06	0.01035347	95.0834936
37	-0.01707723	0.195923516	93.88	95.23089264	769.945509	0.99920734	4.44797E-06	0.00828232	94.9961532
38	-0.01707723	0.173005543	93.88	95.07287322	664.375011	0.99927903	3.33574E-06	0.00621129	94.8703199
39	-0.01707723	0.145671	93.88	94.88440154	691.986471	0.99938994	2.22358E-06	0.0041404	94.6734301
40	-0.01707723	0.094174518	93.88	94.5293333	476.34534	0.99933986	5.55923E-07	0.00103515	94.3841061
41	-0.01707723	0.452053851	93.88	96.99691131	1987.40821	0.99881457	2.22486E-05	0.04142787	96.3909942
42	-0.01707723	0.402014735	93.88	96.6518916	1752.72974	0.99891004	1.66849E-05	0.03106793	96.1175228
43	-0.01707723	0.332489202	93.88	96.17251305	1421.25269	0.99904833	1.11217E-05	0.02070909	95.7392043
44	-0.01707723	0.274308752	93.88	95.77135884	1170.81098	0.9991544	8.34039E-06	0.01553017	95.4144043
45	-0.01707723	0.234812284	93.88	95.4990307	1034.34193	0.9992334	5.55982E-06	0.01035263	95.1836825
46	-0.01707723	0.21862624	93.88	95.38742792	968.244746	0.99927318	4.44768E-06	0.00828177	95.0922314
47	-0.01707723	0.191627905	93.88	95.2012744	849.485237	0.99932775	3.33558E-06	0.00621099	94.942285
48	-0.01707723	0.156412104	93.88	94.95846145	726.828094	0.99941473	2.22352E-06	0.0041403	94.7368675
49	-0.01707723	0.108111236	93.88	94.62542697	588.90401	0.99947612	5.55847E-07	0.00103501	94.4458831
50	-0.01675989	0.544433233	92.64	96.39386714	2409.99228	0.99833907	2.7824E-05	0.0518095	95.6591134
51	-0.01675989	0.495735473	92.64	96.05809608	2196.01755	0.99840542	2.22577E-05	0.04144485	95.3885785
52	-0.01675989	0.437668478	92.64	95.65772416	1946.06837	0.99862705	1.66896E-05	0.03107674	95.0644106
53	-0.01675989	0.367118763	92.64	95.17128387	1643.62481	0.99886796	1.11237E-05	0.02071283	94.6701787
54	-0.01675989	0.273274787	92.64	94.52422966	1275.54505	0.99916653	5.56019E-06	0.01035332	94.135344
55	-0.01675989	0.31456966	92.64	94.80895781	1427.54545	0.99903592	8.34138E-06	0.01553201	94.3737305
56	-0.01675989	0.261978596	92.64	94.44634242	1242.71371	0.99920725	5.00397E-06	0.00931761	94.0674663
57	-0.01675989	0.245646486	92.64	94.33373252	1178.64869	0.99925611	4.44775E-06	0.00828191	93.9743884
58	-0.01675989	0.234481419	92.64	94.25674938	1143.32363	0.99930422	3.8916E-06	0.00724632	93.9081751
59	-0.01675989	0.209194401	92.64	94.0823954	1029.1353	0.99933964	3.33554E-06	0.00621092	93.7686346
60	-0.01675989	0.196059834	92.64	93.99183255	1009.09763	0.9993795	2.7795E-06	0.00517556	93.6841808
61	-0.01675989	0.17316485	92.64	93.83397164	889.058194	0.99943541	2.22348E-06	0.00414021	93.5629173
62	-0.01675989	0.157620135	92.64	93.72679083	811.082836	0.99943783	1.6676E-06	0.00310515	93.4795095
63	-0.01675989	0.142258128	92.64	93.62086979	812.537734	0.99947549	1.11169E-06	0.00207002	93.3731449
64	-0.01675989	0.122837683	92.64	93.48696582	724.696279	0.99936401	5.55909E-07	0.00103513	93.2660218

Line No.	Gage Pressure Correction, psi	CORRECTED Gauge Pressure, psi	Daily Mean Station Pressure, kPaa	CORRECTED Absolute Pressure at P0, kPaa	Average Pressure Gradient, Pa/m	Water Density, g/cc	Water Volumetric Flow Rate, m3/s	Vsl, m/s	Pressure at P1, Beginning of dP Section, kPaa
65	-0.01675989	0.472606244	92.64	95.89862005	1448.22225	0.99828512	4.45208E-05	0.08289968	95.4570889
66	-0.01675989	0.443471832	92.64	95.69773828	1328.76511	0.99841328	3.89507E-05	0.07252791	95.292627
67	-0.01675989	0.41947212	92.64	95.53226026	1238.99592	0.99845793	3.33848E-05	0.062164	95.1545176
68	-0.01675989	0.393896192	92.64	95.35591424	1132.58206	0.99846988	2.78203E-05	0.05180271	95.0106148
69	-0.01675989	0.360210411	92.64	95.12365078	1015.83308	0.99850983	2.22554E-05	0.04144051	94.8139456
70	-0.01675989	0.325469067	92.64	94.88410922	878.776852	0.99856392	1.66906E-05	0.0310787	94.6161894
71	-0.01675989	0.290182732	92.64	94.64080994	736.587381	0.99864518	1.11262E-05	0.02071745	94.4162406
72	-0.01675989	0.268170458	92.64	94.48903531	671.004402	0.99873772	8.34387E-06	0.01553665	94.2844608
73	-0.017	0.244429214	92.64	94.32533943	596.563603	0.99878742	5.5623E-06	0.01035725	94.1434603
74	-0.017	0.239659269	92.64	94.29245066	573.112095	0.99880516	5.00598E-06	0.00932136	94.1177214
75	-0.017	0.230160548	92.64	94.22695698	552.914944	0.99884124	4.4496E-06	0.00828535	94.0583853
76	-0.017	0.22272189	92.64	94.17566743	527.828427	0.99885967	3.89333E-06	0.00724955	94.0147441
77	-0.017	0.219691804	92.64	94.15477499	502.014335	0.99888341	3.33706E-06	0.00621375	94.0017218
78	-0.017	0.210320063	92.64	94.09015684	484.451828	0.99891926	2.78078E-06	0.00517794	93.9424581
79	-0.017	0.201535885	92.64	94.02958993	459.066224	0.99896508	2.22452E-06	0.00414216	93.8896307
80	-0.017	0.190887518	92.64	93.95616944	422.830765	0.99899614	1.66834E-06	0.00310653	93.8272576
81	-0.017	0.179655581	92.64	93.87872523	393.763929	0.99904969	1.11217E-06	0.00207091	93.7586753
82	-0.017	0.168322742	92.64	93.80058531	370.536998	0.99909884	5.56057E-07	0.0010354	93.6876167
83	-0.01848099	0.524793982	92	95.6184545	2502.46275	0.99868643	1.66886E-05	0.03107489	94.8555085
84	-0.01848099	0.456882212	92	95.15020285	2220.14963	0.99892398	1.11231E-05	0.02071167	94.473328
85	-0.01848099	0.385741931	92	94.65969062	1925.58879	0.99905722	8.3412E-06	0.01553168	94.0726209
86	-0.01848099	0.343915571	92	94.37129786	1780.66296	0.99923546	5.55981E-06	0.0103526	93.8284128
87	-0.01848099	0.329712673	92	94.27336888	1728.34056	0.99926444	5.00368E-06	0.00931707	93.7464358
88	-0.01848099	0.311859602	92	94.15027196	1668.19108	0.99931677	4.44748E-06	0.00828141	93.6416771
89	-0.01848099	0.292585687	92	94.01737831	1602.51636	0.99937128	3.89134E-06	0.00724584	93.5288063
90	-0.01848099	0.263777822	92	93.81874808	1455.96983	0.99939276	3.33536E-06	0.00621059	93.3748548
91	-0.01848099	0.246560869	92	93.70003719	1410.14907	0.99944309	2.77933E-06	0.00517523	93.2701137
92	-0.01848099	0.224429732	92	93.547443	1332.82885	0.99948221	2.22337E-06	0.00414002	93.1410927
93	-0.01848099	0.201182914	92	93.38715619	1157.87877	0.99952168	1.66746E-06	0.00310489	93.0341444
94	-0.01848099	0.1763141	92	93.21568572	1002.59226	0.99957179	1.11159E-06	0.00206982	92.9100173
95	-0.01848099	0.158896675	92	93.09559257	954.385362	0.99945259	5.5586E-07	0.00103504	92.8046214
96	-0.01685419	0.563289005	92	95.88387769	2895.26936	0.99875648	1.66874E-05	0.03107271	95.0011736
97	-0.01685419	0.482132408	92	95.32430295	2555.42155	0.99903086	1.11219E-05	0.02070945	94.545211
98	-0.01685419	0.423041363	92	94.9168702	2305.67713	0.99931693	8.33903E-06	0.01552764	94.2139199
99	-0.01685419	0.377431862	92	94.60239269	2112.25168	0.99927556	5.55958E-06	0.01035219	93.9584135
100	-0.01685419	0.363633692	92	94.5072543	2021.99134	0.99929948	5.00351E-06	0.00931675	93.8907935
101	-0.01685419	0.342862906	92	94.36403973	1940.84674	0.99933872	4.44739E-06	0.00828123	93.7723182
102	-0.01685419	0.32553905	92	94.24459175	1878.99125	0.99937633	3.89132E-06	0.0072458	93.6717286
103	-0.01685419	0.302058858	92	94.08269583	1773.91266	0.99942135	3.33526E-06	0.00621041	93.5418688
104	-0.01685419	0.280739344	92	93.93569778	1648.02159	0.99945941	2.77928E-06	0.00517514	93.4332522
105	-0.01685419	0.254285992	92	93.75330191	1524.96239	0.99948783	2.22336E-06	0.00414	93.2883744
106	-0.01685419	0.230087164	92	93.58645099	1460.53776	0.99951926	1.66747E-06	0.0031049	93.1411651
107	-0.01685419	0.204370457	92	93.4091343	1254.11928	0.99955273	1.11161E-06	0.00206986	93.0267809
108	-0.01685419	0.187349744	92	93.29177648	1114.41118	0.99959076	5.55783E-07	0.00103489	92.952017
109	-0.01685419	0.414598513	92	94.85865674	2335.38656	0.99936247	5.5591E-06	0.01035129	94.1466486
110	-0.01685419	0.460460781	92	95.17487709	2469.93517	0.99925701	8.33953E-06	0.01552857	94.4218481
111	-0.01685419	0.527306905	92	95.63578111	2741.89973	0.99915285	1.11205E-05	0.02070692	94.7998361
112	-0.02019	0.571932515	92.73	96.67347469	3063.71197	0.99877979	1.6687E-05	0.03107198	95.7394162
113	-0.02019	0.542893243	92.73	96.47324891	2949.73884	0.99889359	1.39043E-05	0.02589037	95.5739383
114	-0.02019	0.495206952	92.73	96.14445193	2707.08493	0.99898179	1.11224E-05	0.02071047	95.3191212
115	-0.02019	0.433844381	92.73	95.72135701	2444.2835	0.99910637	8.34079E-06	0.01553091	94.9761486
116	-0.02019	0.391103194	92.73	95.42665653	2344.14539	0.99923052	5.55983E-06	0.01035266	94.7119781
117	-0.02019	0.372797557	92.73	95.30043916	2249.93236	0.99924822	5.00376E-06	0.00931723	94.6144842
118	-0.02019	0.350199768	92.73	95.1446274	2148.08186	0.99926965	4.44769E-06	0.0082818	94.4897244
119	-0.02019	0.329679062	92.73	95.00313713	2031.19961	0.99930701	3.89159E-06	0.0072463	94.383869
120	-0.02019	0.307558799	92.73	94.85061792	1913.10172	0.99933632	3.33555E-06	0.00621094	94.2673552
121	-0.02019	0.280435453	92.73	94.66360245	1777.71662	0.99936605	2.77954E-06	0.00517563	94.1216157
122	-0.02019	0.252723439	92.73	94.47252811	1600.31554	0.99940162	2.22355E-06	0.00414035	93.984627
123	-0.02019	0.227760206	92.73	94.30040662	1544.45758	0.99942573	1.66762E-06	0.00310519	93.8295354
124	-0.02019	0.199865156	92.73	94.10807025	1385.12942	0.99943052	1.11174E-06	0.00207012	93.6857747
125	-0.02019	0.181618215	92.73	93.98225759	1294.81088	0.99940465	5.55887E-07	0.00103509	93.5874982
126	-0.01975691	0.554555401	94.25	98.07365949	2554.36526	0.99832116	2.78245E-05	0.05181043	97.2948896
127	-0.01975691	0.512278491	94.25	97.7821602	2376.51986	0.99841632	2.22575E-05	0.04144439	97.0576115
128	-0.01975691	0.459490336	94.25	97.41818587	2152.60471	0.99861948	1.66897E-05	0.03107697	96.7619039

Line No.	*Gage Pressure Correction, psi*	*CORRECTED Gauge Pressure, psi*	*Daily Mean Station Pressure, kPaa*	*CORRECTED Absolute Pressure at P0, kPaa*	Average Pressure Gradient, Pa/m	Water Density, g/cc	Water Volumetric Flow Rate, m3/s	Vsl, m/s	*Pressure at P1, Beginning of dP Section, kPaa*
129	-0.01975691	0.383318579	94.25	96.8929816	1828.356	0.99889088	1.11234E-05	0.02071235	96.335556
130	-0.01975691	0.318041726	94.25	96.4428977	1648.07298	0.99904863	8.34127E-06	0.01553181	95.9404364
131	-0.01975691	0.28591295	94.25	96.22136979	1526.27346	0.99918114	5.56011E-06	0.01035317	95.7560425
132	-0.01975691	0.272692955	94.25	96.13021792	1477.70227	0.99920876	5.00396E-06	0.00931759	95.6796989
133	-0.01975691	0.253842718	94.25	96.00024554	1402.54548	0.99925263	4.44777E-06	0.00828194	95.5726402
134	-0.01975691	0.233605432	94.25	95.86070946	1333.55327	0.99928112	3.89169E-06	0.00724649	95.4541383
135	-0.01975691	0.226207419	94.25	95.80970015	1302.46155	0.99930535	3.33565E-06	0.00621113	95.4126082
136	-0.01975691	0.205015378	94.25	95.66358103	1195.39058	0.99933989	2.77961E-06	0.00517576	95.2991327
137	-0.01975691	0.183416449	94.25	95.51465642	1169.15791	0.99935177	2.22366E-06	0.00414056	95.1582058
138	-0.01975691	0.15909806	94.25	95.34698112	1070.45399	0.99939933	1.66767E-06	0.00310527	95.0206232
139	-0.01975691	0.144202972	94.25	95.24427949	1024.27223	0.99944904	1.11172E-06	0.00207008	94.9320014
140	-0.01975691	0.126583115	94.25	95.12279058	896.537385	0.99937665	5.55902E-07	0.00103511	94.849456
141	-0.01673086	0.225089022	94.25	95.80198881	1043.61036	0.99914729	5.5603E-06	0.01035352	95.4838149
142	-0.01673086	0.216574586	94.25	95.74328177	1007.4209	0.99916431	5.00418E-06	0.00931801	95.4361413
143	-0.01673086	0.191659195	94.25	95.57149015	908.868818	0.99923937	3.89185E-06	0.0072468	95.294396
144	-0.01673086	0.155845947	94.25	95.32455781	854.568279	0.99928679	2.77976E-06	0.00517604	95.0640187
145	-0.01673086	0.124224081	94.25	95.10652504	750.403701	0.999378	1.6677E-06	0.00310534	94.8777434
146	-0.01673086	0.107294998	94.25	94.98979901	647.734232	0.99935841	1.11182E-06	0.00207027	94.7923191
147	-0.01673086	0.211157441	94.25	95.70593055	905.782061	0.99903115	5.56094E-06	0.01035472	95.4297775
148	-0.01673086	0.195355602	94.25	95.59697687	855.991236	0.99912962	4.44832E-06	0.00828296	95.3360039
149	-0.01673086	0.203459886	94.25	95.65285591	836.82598	0.99912647	5.00437E-06	0.00931836	95.397726
150	-0.01673086	0.181013275	94.25	95.49808653	735.135764	0.99918736	3.89205E-06	0.00724717	95.2739598
151	-0.01673086	0.155640537	94.25	95.3231415	671.831523	0.99922626	2.77993E-06	0.00517635	95.1183148
152	-0.01673086	0.130520895	94.25	95.14994157	554.648957	0.99933147	1.66778E-06	0.00310548	94.9808413
153	-0.01673086	0.113073303	94.25	95.02964043	590.590429	0.99934179	1.11184E-06	0.0020703	94.8495824
154	-0.01673086	0.192711991	94.25	95.57874918	676.678931	0.99907998	5.56067E-06	0.01035422	95.3724446
155	-0.01673086	0.185653255	94.25	95.53007919	634.91574	0.99908938	5.00456E-06	0.00931871	95.3365073
156	-0.01673086	0.166457283	94.25	95.39772297	540.059185	0.99914766	3.89221E-06	0.00724746	95.2330708
157	-0.01673086	0.142631775	94.25	95.23344609	469.666493	0.99919677	2.78001E-06	0.0051765	95.0902551
158	-0.01673086	0.123277505	94.25	95.0999984	417.234812	0.99927274	1.66788E-06	0.00310567	94.9727927
159	-0.01673086	0.109535106	94.25	95.00524455	453.45722	0.99932094	1.11187E-06	0.00207034	94.8669954
160	-0.01536921	0.301586039	92.54	94.61943574	1038.00466	0.99834	1.66944E-05	0.03108567	94.3029709
161	-0.01536921	0.19357517	92.54	93.87470079	561.350658	0.99881341	5.84026E-06	0.01087483	93.7035573
162	-0.01536921	0.186390593	92.54	93.82516314	550.92769	0.99890558	5.56164E-06	0.01035602	93.6571974
163	-0.01536921	0.252456152	92.54	94.28068517	823.735107	0.998616	1.11265E-05	0.02071805	94.0295464
164	-0.01536921	0.225626644	92.54	94.09569571	692.056846	0.99872969	8.34393E-06	0.01553677	93.8847028
165	-0.01536921	0.165379127	92.54	93.68028908	479.378685	0.99905221	3.89258E-06	0.00724815	93.534137
166	-0.01686848	0.391290154	92.04	94.73794561	1413.15512	0.99779453	3.3407E-05	0.06220533	94.3071056
167	-0.01686848	0.359933494	92.04	94.52174144	1264.27949	0.99803494	2.78325E-05	0.05182529	94.1362904
168	-0.01686848	0.329092401	92.04	94.3090921	1095.13865	0.99816409	2.22631E-05	0.04145487	93.9752084
169	-0.01686848	0.284943179	92.04	94.00468322	889.408044	0.998357	1.66941E-05	0.03108514	93.7335222
170	-0.01686848	0.23872165	92.04	93.68598578	692.734995	0.99857179	1.1127E-05	0.02071897	93.4747861
171	-0.01686848	0.214489398	92.04	93.5189044	584.889539	0.9987117	8.34408E-06	0.01553705	93.3405844
172	-0.01686848	0.188878214	92.04	93.34231529	483.570548	0.99883088	5.56206E-06	0.0103568	93.1948852
173	-0.01686848	0.182061206	92.04	93.29531202	461.892864	0.99888417	5.00559E-06	0.00932062	93.154491
174	-0.01686848	0.176045002	92.04	93.25383029	424.944618	0.99892003	4.44925E-06	0.0082847	93.124274
175	-0.01686848	0.165896815	92.04	93.18385854	398.54007	0.99897418	3.89288E-06	0.00724872	93.0623524
176	-0.01686848	0.158823403	92.04	93.13508736	373.381339	0.9990098	3.33664E-06	0.00621297	93.0212516
177	-0.01686848	0.150704021	92.04	93.07910423	356.5761	0.99905845	2.7804E-06	0.00517722	92.970392
178	-0.01686848	0.14452484	92.04	93.03649877	333.319368	0.99907507	2.22428E-06	0.00414171	92.934877
179	-0.01686848	0.134175129	92.04	92.96513751	307.227116	0.99911802	1.66814E-06	0.00310615	92.8714707
180	-0.01686848	0.12235946	92.04	92.88366848	289.67888	0.9991706	1.11203E-06	0.00207066	92.7953517
181	-0.01686848	0.089064253	92.04	92.65409803	213.29673	0.99923574	5.5598E-07	0.00103526	92.5890685
182	-0.01686848	0.38313274	92.04	94.68170024	1291.11884	0.99810718	3.33965E-05	0.06218585	94.2880665
183	-0.01686848	0.356124782	92.04	94.49548037	1182.04202	0.99815058	2.78292E-05	0.05181929	94.1351017
184	-0.01686848	0.321429138	92.04	94.25625391	1030.92541	0.99823023	2.22616E-05	0.04145212	93.9419474
185	-0.01686848	0.282227344	92.04	93.98595754	851.108842	0.99836547	1.6694E-05	0.03108488	93.7264731
186	-0.01686848	0.242518595	92.04	93.71216571	680.872693	0.99850354	1.11278E-05	0.02072039	93.5045826
187	-0.01686848	0.220882967	92.04	93.56298805	593.482653	0.99862826	8.34478E-06	0.01553835	93.3820482
188	-0.01686848	0.194355342	92.04	93.38008008	449.773709	0.9987694	5.5624E-06	0.01035744	93.2429539
189	-0.01686848	0.191504615	92.04	93.36042432	432.066853	0.99878348	5.00609E-06	0.00932156	93.2286966
190	-0.01686848	0.183499578	92.04	93.30522959	393.307378	0.99878953	4.44983E-06	0.00828578	93.1853188
191	-0.01686848	0.175361787	92.04	93.24911952	372.59496	0.99885768	3.89334E-06	0.00724956	93.1355235
192	-0.01686848	0.168860353	92.04	93.20429213	349.028931	0.99890238	3.337E-06	0.00621363	93.0978809

Line No.	*Gage Pressure Correction, psi*	*CORRECTED Gauge Pressure, psi*	*Daily Mean Station Pressure, kPaa*	*CORRECTED Absolute Pressure at P0, kPaa*	Average Pressure Gradient, Pa/m	Water Density, g/cc	Water Volumetric Flow Rate, m3/s	Vsl, m/s	*Pressure at P1, Beginning of dP Section, kPaa*
193	-0.01686848	0.162790263	92.04	93.16243887	322.057301	0.99891219	2.7808E-06	0.00517798	93.0642507
194	-0.01686848	0.153146286	92.04	93.09594364	296.608172	0.99893193	2.2246E-06	0.0041423	93.0055143
195	-0.01686848	0.142598666	92.04	93.02321781	272.106251	0.99896221	1.6684E-06	0.00310663	92.9402586
196	-0.01686848	0.133917943	92.04	92.96336422	245.052363	0.99901384	1.11221E-06	0.00207098	92.8886531
197	-0.01686848	0.091239367	92.04	92.66909543	179.691931	0.99903446	5.56092E-07	0.00103547	92.6143113
198	-0.01713707	0.408815177	91.86	94.67878065	1260.72625	0.99751571	3.89857E-05	0.07259317	94.2944129
199	-0.01713707	0.388771926	91.86	94.54058243	1168.37854	0.9975334	3.34158E-05	0.06222162	94.1843695
200	-0.01713707	0.36077568	91.86	94.34754832	1067.73411	0.99768033	2.78424E-05	0.05184371	94.0220196
201	-0.01713707	0.330689384	91.86	94.1401033	986.278982	0.99778715	2.22715E-05	0.04147053	93.8394085
202	-0.01713707	0.297415312	91.86	93.91067857	853.44644	0.997933	1.67012E-05	0.03109835	93.6504815
203	-0.01713707	0.259732471	91.86	93.65085539	704.5052	0.99810051	1.11323E-05	0.02072875	93.4360672
204	-0.01713707	0.239465154	91.86	93.51111224	618.2801	0.99821478	8.34824E-06	0.01554479	93.3226122
205	-0.01713707	0.214823254	91.86	93.34120634	540.085653	0.99837853	5.56458E-06	0.01036149	93.1765461
206	-0.01713707	0.207428069	91.86	93.29021653	516.62357	0.99850258	5.0075E-06	0.00932418	93.1327093
207	-0.01713707	0.204934538	91.86	93.27302364	497.483835	0.99857323	4.45079E-06	0.00828758	93.1213517
208	-0.01713707	0.192754435	91.86	93.18904183	468.665022	0.99861174	3.8943E-06	0.00725135	93.0461562
209	-0.01713707	0.188553465	91.86	93.16007614	451.569902	0.99866252	3.3378E-06	0.00621513	93.0224024
210	-0.01713707	0.182536232	91.86	93.11858732	438.016118	0.99872326	2.78133E-06	0.00517896	92.9850458
211	-0.01713707	0.176754045	91.86	93.07871914	419.555822	0.99878482	2.22493E-06	0.00414291	92.9508058
212	-0.01713707	0.164524097	91.86	92.99439365	386.215536	0.99882212	1.66863E-06	0.00310707	92.876645
213	-0.01713707	0.153385003	91.86	92.91758959	355.615265	0.99886844	1.11237E-06	0.00207128	92.8091703
214	-0.01713707	0.136662671	91.86	92.80228912	338.515071	0.99895276	5.56138E-07	0.00103555	92.6990833

Line No.	Pressure at P2, End of dP Section, kPaa	dP Section Average Pressure for Fluid Properties, kPaa	Test Section Average Air Flow Rate, Actual m3/s	Test Section Average Superficial Air Velocity, Vsg, m/s = Q/A	Loop Test Section AverageAir Density, kg/m3	Flow Loop Diff. Section Inlet Air Density, kg/m3	Flow Loop Diff. Section Outlet Air Density, kg/m3	Flow Loop Diff. Section Inlet Air Velocity, m/3	Flow Loop Diff. Section Outlet Air Velocity, m/3
1	93.4233637	93.6136932	0.01250213	23.2795265	1.12808907	1.13038263	1.12579551	23.2322921	23.3269534
2	93.4111334	93.5908659	0.01249426	23.26487	1.12879976	1.13096751	1.126632	23.2202776	23.3096339
3	93.3801661	93.5486691	0.01248383	23.2454394	1.12974331	1.13177824	1.12770838	23.2036442	23.2873854
4	93.3025951	93.4606019	0.01248113	23.2404126	1.12998766	1.13189805	1.12807728	23.2011881	23.27977
5	93.2773297	93.4109591	0.01246053	23.2020568	1.13185567	1.13347485	1.13023649	23.1689125	23.2352961
6	93.2053879	93.336383	0.01244968	23.1818533	1.1328421	1.13443202	1.13125219	23.1493638	23.2144342
7	93.2159726	93.3246559	0.01243858	23.161186	1.13385297	1.13517342	1.13253252	23.1342445	23.1881903
8	93.1776352	93.2740318	0.01242238	23.1310169	1.13533182	1.13650516	1.13415848	23.1071362	23.154947
9	93.0819413	93.1760568	0.01241013	23.1082081	1.13645244	1.13760035	1.13530453	23.0848904	23.1315729
10	93.0139374	93.108391	0.01244938	23.181302	1.13286905	1.13401828	1.13171981	23.1578096	23.2048421
11	94.2613342	94.6588564	0.01252851	23.3286379	1.12571422	1.13044169	1.12098676	23.2310784	23.4270203
12	94.322988	94.7665325	0.01252981	23.3310535	1.12559767	1.13086591	1.12032944	23.2223637	23.4407654
13	94.3288926	94.8171284	0.01253627	23.3430804	1.12501774	1.13081072	1.11922476	23.2234971	23.4639016
14	94.3883031	94.9042273	0.01252871	23.3290041	1.12569655	1.13181613	1.11957697	23.2028673	23.4565199
15	94.4452926	95.0036496	0.01251757	23.3082678	1.12669803	1.13331988	1.12007618	23.1720805	23.4460654
16	94.4867478	95.0766133	0.01249334	23.2631586	1.1288828	1.13588651	1.12187909	23.1197214	23.4083867
17	95.6796494	96.4379036	0.01412759	26.3061957	1.14091013	1.14988067	1.13193959	26.1009737	26.5146703
18	95.6293393	96.3333653	0.01412588	26.3030193	1.14104791	1.14938694	1.13270887	26.1121856	26.496663
19	95.5856889	96.2008012	0.0140921	26.2401154	1.14378328	1.15109668	1.13646987	26.0734009	26.4089756
20	95.4939471	96.0284308	0.01408155	26.2204711	1.14464019	1.15101114	1.13826925	26.0753386	26.3672282
21	95.3703615	95.8218482	0.01407205	26.2027744	1.14541326	1.15081013	1.14001638	26.079893	26.3268193
22	95.2392539	95.5947926	0.01404903	26.1599209	1.1472896	1.15155663	1.14302257	26.0629868	26.2575788
23	95.029765	95.2688116	0.0140114	26.0898396	1.1503714	1.15325788	1.14748491	26.0245393	26.1554683
24	95.0398135	95.2817287	0.01400915	26.0856614	1.15055565	1.15347685	1.14763445	26.0195991	26.1520601
25	94.9848454	95.2059022	0.01399451	26.0583939	1.15175959	1.15443384	1.14908534	25.9980296	26.1190392
26	94.9325598	95.1154384	0.01397751	26.0267387	1.15316043	1.15537761	1.15094325	25.9767931	26.0768768
27	94.8423513	95.0079223	0.01395798	25.9903742	1.15477388	1.15678631	1.15276144	25.9451594	26.0357469
28	94.6373258	94.7734058	0.01396039	25.9948591	1.15457464	1.15623243	1.15291685	25.957588	26.0322374
29	94.5593561	94.8989312	0.01412542	26.3021588	1.14108524	1.14516836	1.13700212	26.2083778	26.3966133
30	94.9977086	95.7388904	0.01586037	29.5327173	1.14329577	1.15214683	1.13444472	29.3058402	29.7631345
31	94.8918306	95.5616164	0.01585701	29.5264509	1.14353841	1.15155341	1.13552342	29.3209421	29.7348608
32	94.7641931	95.3436996	0.01584523	29.5045257	1.14438819	1.15134387	1.13743251	29.3262783	29.6849532
33	94.6309344	95.0933637	0.01583227	29.4803818	1.14532542	1.15089502	1.13975582	29.3377155	29.6244425
34	94.5466278	94.9321128	0.01581682	29.4516085	1.14644437	1.15109967	1.14178908	29.3324998	29.5716884
35	94.457726	94.777237	0.01580645	29.4322994	1.1471965	1.1510639	1.14332909	29.3334112	29.5318566
36	94.4489266	94.7662101	0.01579613	29.413096	1.14794549	1.15178888	1.14410209	29.3149477	29.5119038
37	94.4093044	94.7027288	0.0157851	29.3925617	1.14874747	1.15230672	1.14518822	29.3017738	29.4839138
38	94.3639365	94.6171282	0.01577034	29.3650638	1.14982317	1.15290005	1.14674629	29.2866938	29.4438544
39	94.1460013	94.4097157	0.015757	29.3402305	1.15079637	1.15401089	1.14758186	29.2585028	29.422416
40	94.021038	94.202572	0.01581379	29.4459744	1.14666373	1.14887342	1.14445404	29.3893394	29.5028281
41	94.8762013	95.6335977	0.01752299	32.6285895	1.14979707	1.1589032	1.14069093	32.372209	32.8890634
42	94.7816007	95.4495617	0.01752168	32.6261424	1.1498833	1.15793025	1.14183636	32.3994097	32.856071
43	94.6559324	95.1975684	0.0175144	32.6125845	1.15036134	1.15690644	1.14381625	32.4280817	32.7991988
44	94.5220179	94.9682111	0.01751287	32.6097293	1.15046206	1.15586733	1.1450568	32.4572341	32.7636642
45	94.3953122	94.7894974	0.01751143	32.6070617	1.15055618	1.15534081	1.14577156	32.4720258	32.7432255
46	94.3542399	94.7232356	0.01750568	32.5963502	1.15093427	1.15541775	1.14645079	32.4698633	32.7238263
47	94.2948115	94.6185482	0.01749952	32.5848808	1.15133938	1.15527868	1.14740008	32.473772	32.6967525
48	94.1828827	94.4598751	0.01748596	32.5596211	1.15223259	1.15561137	1.1488538	32.464423	32.6553791
49	93.9970233	94.2214532	0.01749784	32.5817441	1.15145022	1.15419291	1.14870754	32.5043207	32.6595371
50	93.822229	94.7406712	0.01963183	36.5553314	1.12891555	1.13985957	1.11797153	36.2043564	36.9131779
51	93.7147847	94.5516816	0.0196481	36.5856291	1.12798066	1.13796466	1.11799667	36.2646431	36.9123481
52	93.5811268	94.3227687	0.01961557	36.5250536	1.12985138	1.13873518	1.12096757	36.2401046	36.8145191
53	93.4174159	94.0437973	0.01957913	36.4572044	1.1319541	1.13949352	1.12441469	36.2159868	36.7016568
54	93.1631298	93.6492369	0.01952941	36.3646247	1.13483591	1.14072653	1.1289453	36.1768408	36.5543682
55	93.2856624	93.8296964	0.01955195	36.4065901	1.1335278	1.14010011	1.12695549	36.1967179	36.6189103
56	93.120276	93.5938711	0.01952127	36.3494612	1.13530932	1.14105411	1.12956453	36.166455	36.5343289
57	93.0760281	93.5252083	0.01951129	36.3308876	1.13588973	1.14134515	1.13043431	36.1572327	36.5062186
58	93.0367394	93.4724573	0.01949759	36.305369	1.13668813	1.14198676	1.13138951	36.1369183	36.4753975
59	92.9842327	93.3764337	0.01949887	36.3077635	1.13661317	1.14138719	1.13183915	36.155901	36.4609071
60	92.9150515	93.2996162	0.0194932	36.2972036	1.13694384	1.14163013	1.13225756	36.148207	36.4474335
61	92.8852815	93.2240994	0.01947731	36.2676034	1.13787177	1.1420073	1.13373624	36.1362681	36.3998968
62	92.8613061	93.1704078	0.01948711	36.2858564	1.13729938	1.14107248	1.13352629	36.1658726	36.4066389
63	92.7538326	93.0634887	0.01948716	36.2859494	1.13729647	1.14108067	1.13351227	36.1656132	36.4070891
64	92.7136619	92.9898419	0.0195666	36.4338716	1.13267902	1.13604308	1.12931497	36.3259834	36.5424026

Line No.	Pressure at P2, End of dP Section, kPaa	dP Section Average Pressure for Fluid Properties, kPaa	Test Section Average Air Flow Rate, Actual m3/s	Test Section Average Superficial Air Velocity, Vsg, m/s = Q/A	Loop Test Section AverageAir Density, kg/m3	Flow Loop Diff. Section Inlet Air Density, kg/m3	Flow Loop Diff. Section Outlet Air Density, kg/m3	Flow Loop Diff. Section Inlet Air Velocity, m/3	Flow Loop Diff. Section Outlet Air Velocity, m/3
65	94.3532609	94.9051749	0.00624149	11.6219229	1.12982076	1.13639115	1.12325038	11.5547272	11.6899046
66	94.2798487	94.7862378	0.00623534	11.6104762	1.13093465	1.13697659	1.1248927	11.5487776	11.6728375
67	94.210161	94.6823393	0.00623718	11.6139078	1.13060048	1.13623876	1.12496221	11.5562769	11.6721163
68	94.1473663	94.5789906	0.00624264	11.6240757	1.12961152	1.13476665	1.12445638	11.5712686	11.677367
69	94.0396826	94.4268141	0.00624814	11.6343141	1.12861743	1.13324455	1.12399032	11.5868105	11.6822089
70	93.94639	94.2812897	0.00625151	11.6405916	1.1280088	1.13201564	1.12400196	11.599389	11.6820879
71	93.8548173	94.135529	0.00625155	11.6406591	1.12800226	1.13136595	1.12463856	11.6060499	11.6754753
72	93.7730245	94.0287427	0.00624732	11.632794	1.12876492	1.13183468	1.12569516	11.6012435	11.6645165
73	93.6887624	93.9161114	0.00624856	11.6351025	1.12854096	1.1312729	1.12580903	11.6070047	11.6633367
74	93.6808981	93.8993097	0.00624742	11.6329778	1.12874708	1.13137257	1.1261216	11.6059821	11.6600994
75	93.6369563	93.8476708	0.00624621	11.6307237	1.12896584	1.13150068	1.12643099	11.604668	11.6568968
76	93.6124359	93.81359	0.00624608	11.6304787	1.12898962	1.13141039	1.12656886	11.6055941	11.6554702
77	93.619089	93.8104054	0.00624317	11.625067	1.12951519	1.13181872	1.12721167	11.6014071	11.6488235
78	93.5732113	93.7578347	0.0062419	11.6226972	1.12974549	1.13197013	1.12752085	11.5998554	11.6456293
79	93.5397327	93.7146817	0.00623856	11.6164816	1.13034998	1.13246015	1.12823982	11.594836	11.6382081
80	93.5049781	93.6661178	0.00623751	11.6145179	1.13054109	1.13248603	1.12859615	11.5945711	11.6345336
81	93.4585503	93.6086128	0.00623379	11.6076001	1.13121487	1.1330283	1.12940143	11.5890219	11.6262379
82	93.4051952	93.546406	0.00623083	11.6020748	1.13175358	1.13346199	1.13004517	11.5845876	11.6196149
83	92.9481436	93.9018261	0.02325918	43.3096243	1.12610382	1.13754072	1.11466692	42.874187	43.7539972
84	92.7811407	93.6272344	0.02321416	43.2257855	1.12828796	1.13848411	1.11809181	42.8386597	43.6199719
85	92.6049465	93.3387837	0.02321695	43.2309837	1.12815229	1.13702192	1.11928267	42.8937495	43.5735626
86	92.4712002	93.1498065	0.02316391	43.1322301	1.13073526	1.13897279	1.12249773	42.8202798	43.448759
87	92.429103	93.0877694	0.02316202	43.1287068	1.13082763	1.13882909	1.12282617	42.8256827	43.4360497
88	92.37019	93.0059336	0.02315023	43.1067566	1.13140346	1.13913718	1.12366973	42.8141002	43.4034415
89	92.3073761	92.9180912	0.02313727	43.0826162	1.13203741	1.13947786	1.12459697	42.8012996	43.3676552
90	92.2651217	92.8199883	0.02314755	43.101769	1.13153438	1.13829855	1.1247702	42.8456429	43.3609756
91	92.195305	92.7327093	0.02313513	43.0786365	1.13214199	1.13870298	1.12558101	42.8304257	43.3297409
92	92.1252171	92.6331549	0.02313229	43.0733508	1.13228092	1.13848959	1.12607226	42.8384536	43.3108383
93	92.1516148	92.5928796	0.02311333	43.0380387	1.13320994	1.13861042	1.12780947	42.8339075	43.2441248
94	92.1458464	92.5279319	0.02309086	42.9962011	1.13431262	1.13899666	1.12962858	42.8193825	43.1744861
95	92.0771936	92.4409075	0.02320142	43.2020732	1.12890724	1.13334899	1.1244655	43.0327584	43.3727256
96	92.7944134	93.8977935	0.02501474	46.5785488	1.12761691	1.14086738	1.11436643	46.0375676	47.1323951
97	92.5974812	93.5713461	0.0249558	46.4688023	1.13028003	1.14204367	1.11851638	45.9901494	46.9575233
98	92.456544	93.3352319	0.02484306	46.258876	1.13540932	1.14609843	1.12472021	45.8274417	46.6985109
99	92.3484656	93.1534396	0.02491891	46.4001126	1.13195327	1.1417349	1.12217163	46.0025869	46.8045685
100	92.3496416	93.1202176	0.02491203	46.3872946	1.13226606	1.14163563	1.12289648	46.006587	46.7743555
101	92.2930143	93.0326662	0.02490897	46.3815969	1.13240515	1.14140828	1.12340201	46.0157508	46.7533069
102	92.2395706	92.9556496	0.02490346	46.3713368	1.1326557	1.14138106	1.12393035	46.0168484	46.7313291
103	92.1898012	92.865835	0.02489516	46.3558809	1.13303335	1.14128147	1.12478523	46.0208636	46.6958116
104	92.1771382	92.8051952	0.02488305	46.3333321	1.13358476	1.14125627	1.12591325	46.0218801	46.6490283
105	92.1260555	92.7072149	0.02488746	46.3415498	1.13338374	1.14048865	1.12627883	46.0528554	46.6338865
106	92.0279503	92.5845577	0.02489547	46.3564569	1.13301927	1.13983085	1.12620769	46.0794328	46.636832
107	92.0708973	92.5488391	0.02487759	46.3231627	1.13383362	1.13968897	1.12797826	46.0851691	46.5636271
108	92.1026182	92.5273176	0.02485083	46.2733484	1.13505421	1.1402641	1.12984433	46.0619247	46.486722
109	92.3666284	93.2566385	0.02660664	49.5427362	1.13587559	1.14671601	1.12503517	49.0743867	50.0201114
110	92.5392755	93.4805618	0.02661838	49.5645993	1.13537455	1.14680701	1.1239421	49.0704925	50.0687579
111	92.7099735	93.7549048	0.02660989	49.5487864	1.13573689	1.14839508	1.12307871	49.0026348	50.1072493
112	93.4042698	94.571843	0.02659816	49.5269433	1.13623779	1.15026565	1.12220993	48.9229462	50.1460406
113	93.3256617	94.4498	0.02656977	49.474083	1.1374518	1.15098971	1.12391389	48.8921701	50.0700146
114	93.2557942	94.2874577	0.02656466	49.4645661	1.13767064	1.15011867	1.12522261	48.9291983	50.0117791
115	93.1131277	94.0446381	0.02655751	49.4512489	1.13797702	1.14924866	1.12670537	48.9662391	49.9459628
116	92.9252819	93.81863	0.02654061	49.4197805	1.13870163	1.14954443	1.12785883	48.9536402	49.8948834
117	92.8995967	93.7570404	0.026546	49.4298216	1.13847032	1.14888206	1.12805857	48.9818639	49.8860485
118	92.8524669	93.6710956	0.02655557	49.4476421	1.13806002	1.14800598	1.12811407	49.0192436	49.8835946
119	92.8356985	93.6097837	0.02654668	49.4310839	1.13844124	1.14785533	1.12902716	49.025677	49.8432515
120	92.8091984	93.5382768	0.02654585	49.4295398	1.13847681	1.1473506	1.12960302	49.047244	49.8178419
121	92.7666487	93.4441322	0.02655065	49.4384865	1.13827078	1.14652341	1.13001815	49.0826304	49.7995404
122	92.7648743	93.3747507	0.02654346	49.4250902	1.1385793	1.14601592	1.13114268	49.1043655	49.7500321
123	92.6523574	93.2409464	0.02656279	49.4610805	1.13775081	1.14493293	1.13056869	49.1508131	49.77529
124	92.6300358	93.1579053	0.02658267	49.4981076	1.13689972	1.14334184	1.1304576	49.2192121	49.7801818
125	92.6005996	93.0940489	0.02662105	49.56958	1.13526047	1.14127797	1.12924297	49.3082195	49.833726
126	95.3479648	96.3214272	0.02107189	39.2367839	1.14738017	1.15897605	1.13578429	38.844209	39.6373748
127	95.2462396	96.1519255	0.02107376	39.2402648	1.14727839	1.15808497	1.1364718	38.8740972	39.6133961
128	95.1211991	95.9415515	0.02104109	39.1794327	1.14905972	1.1588848	1.13923463	38.8472674	39.5173273

Line No.	Pressure at P2, End of dP Section, kPaa	dP Section Average Pressure for Fluid Properties, kPaa	Test Section Average Air Flow Rate, Actual m3/s	Test Section Average Superficial Air Velocity, Vsg, m/s = Q/A	Loop Test Section AverageAir Density, kg/m3	Flow Loop Diff. Section Inlet Air Density, kg/m3	Flow Loop Diff. Section Outlet Air Density, kg/m3	Flow Loop Diff. Section Inlet Air Velocity, m/3	Flow Loop Diff. Section Outlet Air Velocity, m/3
129	94.941992	95.638774	0.02099302	39.0899274	1.15169075	1.16008146	1.14330004	38.8071953	39.3768095
130	94.6842832	95.3123598	0.02099185	39.0877547	1.15175476	1.15934444	1.14416509	38.8318657	39.3470386
131	94.5927243	95.1743834	0.02095626	39.021477	1.15371101	1.16076193	1.1466601	38.7844455	39.2614236
132	94.5534015	95.1165502	0.0209546	39.0183828	1.1538025	1.16063373	1.14697128	38.7887295	39.2507716
133	94.5036269	95.0381335	0.02094848	39.00699	1.15413949	1.16063052	1.14764847	38.7888366	39.2276112
134	94.4377105	94.9459244	0.02095324	39.0158504	1.15387739	1.16005372	1.14770107	38.8081234	39.2258131
135	94.4198784	94.9162433	0.0209463	39.002944	1.15425922	1.16029543	1.14822302	38.800039	39.2079823
136	94.3880118	94.8435723	0.02094271	38.9962489	1.15445739	1.16000258	1.14891221	38.8098343	39.1844629
137	94.2670794	94.7126426	0.02096475	39.0372835	1.15324387	1.15866915	1.14781858	38.8544976	39.2217973
138	94.2047284	94.6126758	0.02095867	39.0259706	1.15357817	1.15855212	1.14860421	38.8584223	39.1949701
139	94.1513061	94.5416537	0.02094369	38.9980803	1.15440317	1.15916952	1.14963683	38.8377255	39.1597649
140	94.1661196	94.5077878	0.02099549	39.0945368	1.15155496	1.15571811	1.14739181	38.9537099	39.2363857
141	94.6883802	95.0860976	0.01749419	32.5749573	1.15169012	1.1565073	1.14687294	32.4392733	32.7117811
142	94.66829	95.0522156	0.01749319	32.5730867	1.15175626	1.15640832	1.1471042	32.44205	32.7051863
143	94.6016606	94.9480283	0.01747956	32.5477216	1.15265385	1.1568587	1.148449	32.42942	32.6668894
144	94.4126709	94.7383448	0.01749663	32.5794954	1.1515297	1.15548821	1.14757118	32.4678833	32.6918775
145	94.3057894	94.5917664	0.01748006	32.5486486	1.15262102	1.15610571	1.14913632	32.4505417	32.6473506
146	94.2986192	94.5454691	0.01749824	32.5824991	1.15142354	1.1544298	1.14841727	32.4976506	32.6677919
147	94.7393948	95.0845862	0.01578785	29.3976653	1.14854804	1.15271768	1.14437839	29.2913273	29.5047783
148	94.6835716	95.0097878	0.01576409	29.3534411	1.15027845	1.15422794	1.14632897	29.2530009	29.4545734
149	94.7599014	95.0788137	0.01575385	29.3343647	1.15102649	1.15488725	1.14716573	29.2363006	29.4330889
150	94.7136429	94.9938013	0.01574462	29.3171774	1.15170128	1.15509791	1.14830465	29.2309686	29.4038962
151	94.6062481	94.8622815	0.01575107	29.3291887	1.15122962	1.15433679	1.14812245	29.2502423	29.4085624
152	94.5580906	94.7694659	0.01572292	29.2767798	1.15329046	1.15586278	1.15071814	29.2116257	29.3422252
153	94.3994372	94.6245098	0.01574253	29.3132808	1.15185438	1.15459416	1.14911459	29.2437221	29.3831712
154	94.8566832	95.1145639	0.0140135	26.0937616	1.15019849	1.15331698	1.14708	26.0232058	26.164701
155	94.8525776	95.0945425	0.01401338	26.0935309	1.15020866	1.15313533	1.14728199	26.0273053	26.1600943
156	94.8214403	95.0272555	0.01400388	26.0758488	1.15098862	1.15348149	1.14849575	26.0194943	26.1324478
157	94.7322776	94.9112663	0.01400411	26.0762635	1.15097031	1.15314087	1.14879975	26.0271801	26.1255325
158	94.6547783	94.8137855	0.01399135	26.0525056	1.15201991	1.1539519	1.15008792	26.0088874	26.0962702
159	94.5213725	94.694184	0.01399103	26.0519213	1.15204575	1.15414817	1.14994333	26.0044646	26.0995514
160	93.5118088	93.9073899	0.01260355	23.4683637	1.11901195	1.12372574	1.11429816	23.3699189	23.5676415
161	93.2756986	93.4896279	0.01254743	23.363868	1.12401677	1.12658883	1.12144472	23.3105273	23.4174534
162	93.237283	93.4472402	0.01252893	23.3294189	1.12567654	1.12820571	1.12314737	23.2771199	23.3819534
163	93.4016995	93.715623	0.01256608	23.3986033	1.12234817	1.12610775	1.11858859	23.3204856	23.4772461
164	93.3572204	93.6209616	0.01255103	23.3705636	1.12369474	1.12686032	1.12052916	23.304911	23.4365872
165	93.1687569	93.351447	0.01250118	23.2777448	1.12817542	1.13038328	1.12596757	23.2322789	23.323389
166	93.2300057	93.7685557	0.0109152	20.3245899	1.10751331	1.1138742	1.10115242	20.2085244	20.4419964
167	93.1726627	93.6544765	0.01088755	20.2730971	1.11032635	1.11603852	1.10461418	20.1693341	20.3779332
168	93.140499	93.5578537	0.01087584	20.2512894	1.11152201	1.11648043	1.10656359	20.1613511	20.3420337
169	93.0556198	93.394571	0.01085909	20.2201057	1.11323621	1.11727641	1.10919601	20.1469875	20.2937566
170	92.9467868	93.2107865	0.01083826	20.1813215	1.11537562	1.11853468	1.11221655	20.1243236	20.2386431
171	92.8947845	93.1176844	0.01081996	20.1472506	1.11726182	1.11993626	1.11458738	20.0991384	20.1955937
172	92.8263101	93.0105977	0.01080639	20.1219787	1.11866503	1.12088151	1.11644855	20.0821886	20.1619267
173	92.8024385	92.9784648	0.01079809	20.1065154	1.11952536	1.12164484	1.11740588	20.0685218	20.1446532
174	92.8003833	92.9623286	0.0107917	20.0946315	1.12018744	1.12213887	1.11823601	20.0596865	20.1296986
175	92.7585871	92.9104698	0.010785	20.0821499	1.12088367	1.122716	1.11905134	20.0493748	20.1150324
176	92.7366622	92.8789569	0.01078012	20.0730511	1.12139175	1.12310977	1.11967373	20.0423453	20.1038511
177	92.6986114	92.8345017	0.01077336	20.0604665	1.12209524	1.12373775	1.12045272	20.0311451	20.0898739
178	92.6808226	92.8078498	0.01077231	20.0585168	1.1222043	1.12374028	1.12066833	20.0311	20.0860087
179	92.6373037	92.7543872	0.01076764	20.0498306	1.12269048	1.12410765	1.12127331	20.0245536	20.0751714
180	92.5745599	92.6849558	0.01076204	20.0393913	1.12327533	1.12461325	1.12193741	20.015551	20.0632884
181	92.4264948	92.5077817	0.01076508	20.045046	1.12295845	1.1239452	1.12197171	20.0274479	20.0626752
182	93.303982	93.7960242	0.00904868	16.8490382	1.11330558	1.11914584	1.10746532	16.7611115	16.9378923
183	93.234155	93.6846284	0.00905297	16.8570278	1.11277792	1.1181286	1.10742723	16.7763603	16.9384748
184	93.1561811	93.5490642	0.00905402	16.8589847	1.11264875	1.1173216	1.1079759	16.7884772	16.9300869
185	93.0777621	93.4021176	0.00904717	16.8462246	1.11349152	1.11735832	1.10962472	16.7879255	16.90493
186	92.9856247	93.2451037	0.00903999	16.8328547	1.11437594	1.11747698	1.11127489	16.7861429	16.8798273
187	92.9296986	93.1558734	0.00902755	16.8096981	1.11591107	1.11862041	1.11320173	16.7689844	16.85061
188	92.9001386	93.0715463	0.00901074	16.7783878	1.11799349	1.12005247	1.1159345	16.7475442	16.8093452
189	92.8993774	93.064037	0.0090089	16.7749643	1.11822165	1.12020014	1.11624316	16.7453365	16.8046971
190	92.8855418	93.0354303	0.00901056	16.7780588	1.11801541	1.11981663	1.11621419	16.7510713	16.8051333
191	92.8515334	92.9935285	0.00900196	16.7620525	1.11908301	1.12079178	1.11737425	16.736497	16.7876862
192	92.8318527	92.9648668	0.00899624	16.7513976	1.11979482	1.12139702	1.11819262	16.727464	16.7753998

Line No.	Pressure at P2, End of dP Section, kPaa	dP Section Average Pressure for Fluid Properties, kPaa	Test Section Average Air Flow Rate, Actual m3/s	Test Section Average Superficial Air Velocity, Vsg, m/s = Q/A	Loop Test Section AverageAir Density, kg/m3	Flow Loop Diff. Section Inlet Air Density, kg/m3	Flow Loop Diff. Section Outlet Air Density, kg/m3	Flow Loop Diff. Section Inlet Air Velocity, m/3	Flow Loop Diff. Section Outlet Air Velocity, m/3
193	92.8187802	92.9415154	0.00899661	16.7520887	1.11974862	1.12122732	1.11826992	16.7299957	16.7742402
194	92.779441	92.8924777	0.00899753	16.7538072	1.11963377	1.1209962	1.11827133	16.733445	16.774219
195	92.7328605	92.8365596	0.00899702	16.7528449	1.11969808	1.12094879	1.11844737	16.7341527	16.7715789
196	92.7018754	92.7952643	0.00899071	16.7410934	1.12048406	1.12161171	1.1193564	16.7242621	16.7579585
197	92.477351	92.5458312	0.00901071	16.7783482	1.11799613	1.1188234	1.11716885	16.765942	16.7907727
198	93.3334935	93.8139532	0.00730327	13.5990169	1.10349908	1.10915055	1.0978476	13.5297256	13.6690216
199	93.293837	93.7391033	0.00730724	13.6064084	1.10289962	1.10813845	1.09766078	13.5420827	13.6713481
200	93.2081979	93.6151088	0.00730123	13.5952037	1.10380859	1.10860645	1.09901074	13.536366	13.654555
201	93.0876715	93.46354	0.00730135	13.5954396	1.10378943	1.10822838	1.09935048	13.5409839	13.6503352
202	92.9999888	93.3252351	0.00729574	13.5849959	1.10463799	1.10848775	1.10078824	13.5378154	13.6325063
203	92.8990968	93.167582	0.00728853	13.5715666	1.10573105	1.10891749	1.10254462	13.5325692	13.6107894
204	92.8513621	93.0869872	0.00728104	13.5576192	1.10686857	1.10967032	1.10406683	13.5233883	13.5920238
205	92.7648954	92.9707208	0.00726962	13.5363592	1.108607	1.11106131	1.10615268	13.5064577	13.5663935
206	92.7389414	92.9358254	0.00725616	13.5112994	1.11066317	1.1130161	1.10831023	13.4827363	13.5399838
207	92.742172	92.9317619	0.00724699	13.4942124	1.11206954	1.11433827	1.10980081	13.4667389	13.5217982
208	92.688942	92.8675491	0.00724672	13.4937218	1.11210997	1.11424883	1.10997111	13.4678199	13.5197236
209	92.678218	92.8503102	0.00724102	13.4830908	1.11298684	1.11504969	1.11092399	13.458147	13.5081273
210	92.6511921	92.8181189	0.00723492	13.4717382	1.11392475	1.11592807	1.11192143	13.4475537	13.4960098
211	92.6310224	92.7909141	0.00722812	13.459072	1.11497305	1.11689431	1.1130518	13.43592	13.4823039
212	92.5822734	92.7294592	0.00722739	13.4577195	1.11508511	1.11685504	1.11331518	13.4363925	13.4791144
213	92.5381221	92.6736462	0.00722477	13.4528496	1.11548876	1.11712003	1.11385749	13.4332052	13.4725516
214	92.4410688	92.570076	0.00721981	13.4435982	1.11625641	1.11781204	1.11470077	13.424889	13.4623596

Line No.	*Loop Test Section Water Density, g/cm3*	*Loop Test Section Air Viscosity Pa-s*	*Loop Test Section Water Viscosity, Pa-s*	**Apparent Friction Factor, fiSG (incl KE)**	**Apparent Friction Factor, fiSG (NO KE)**	**Superficial Gas Reynolds Number, ReSG**	**Superficial Liquid Reynolds Number, ReSL**	**Effective relative Roughness, e**
1	0.998922507	1.80336E-05	0.00111085	0.04149824	0.04178454	38079.7746	243.512861	0.011445753
2	0.998962724	1.80212E-05	0.00111817	0.03915922	0.03942964	38106.0041	217.727352	0.009447247
3	0.999020564	1.8003E-05	0.00112907	0.03668332	0.03693695	38144.6724	191.66694	0.007508296
4	0.999071199	1.79865E-05	0.00113901	0.03434623	0.03458427	38179.5366	166.244656	0.005850048
5	0.999163058	1.79556E-05	0.00115809	0.02894719	0.02914859	38245.3391	140.147476	0.002681796
6	0.999230074	1.79319E-05	0.001173	0.02838169	0.02857927	38295.7783	115.305672	0.002406139
7	0.999269551	1.79175E-05	0.00118221	0.02340515	0.02356907	38326.5492	91.5254471	0.000410376
8	0.999338475	1.78914E-05	0.0011992	0.02067691	0.02082237	38382.4595	67.6719653	-0.000352605
9	0.999410504	1.78626E-05	0.00121834	0.02018388	0.02032604	38444.301	44.4055907	-0.000464994
10	0.999323966	1.7897E-05	0.00119554	0.02019843	0.02034119	38370.5563	22.6262788	-0.000464457
11	0.998223682	1.82222E-05	0.00100805	0.08752598	0.08811765	37685.8134	805.039304	0.074230357
12	0.998149409	1.82399E-05	0.0009991	0.09775885	0.09841831	37649.0878	947.622893	0.09188732
13	0.998085426	1.8255E-05	0.00099162	0.10764889	0.10837444	37618.0711	1091.16525	0.109570962
14	0.998066044	1.82595E-05	0.00098939	0.11387639	0.11464242	37608.7488	1230.32733	0.120932789
15	0.998056325	1.82618E-05	0.00098828	0.12343022	0.12425844	37604.067	1368.57179	0.138603358
16	0.998128169	1.8245E-05	0.00099658	0.13070216	0.13157652	37638.5988	1492.88875	0.152189043
17	0.997902402	1.82971E-05	0.00097121	0.12997527	0.13107724	42893.1757	1949.66858	0.15100705
18	0.997979147	1.82798E-05	0.00097956	0.12064033	0.12166456	42933.7963	1656.90536	0.133600961
19	0.998210455	1.82257E-05	0.00100635	0.10556223	0.10645833	43061.164	1343.99935	0.10598456
20	0.998358674	1.81893E-05	0.001025	0.09169486	0.09247486	43147.3169	1055.63321	0.081516586
21	0.998516275	1.81489E-05	0.00104634	0.07739101	0.07805126	43243.4398	775.577801	0.05782024
22	0.998726381	1.80917E-05	0.00107769	0.06088346	0.06140459	43380.1281	502.012565	0.033539172
23	0.999015766	1.80049E-05	0.00112799	0.0407965	0.04114803	43589.1045	239.81245	0.011012749
24	0.999016865	1.80046E-05	0.0011282	0.04130171	0.04165741	43589.9455	239.767929	0.01145518
25	0.99909699	1.79785E-05	0.00114406	0.03771433	0.03803962	43653.3142	189.156179	0.008476776
26	0.999186875	1.79478E-05	0.00116311	0.03110729	0.03137663	43727.9867	139.543271	0.004018922
27	0.999285849	1.7912E-05	0.00118593	0.02812995	0.02837406	43815.3813	91.2387615	0.002467863
28	0.999370124	1.78794E-05	0.00120722	0.02297994	0.02318103	43895.0504	22.4073055	0.000459324
29	0.998819386	1.80648E-05	0.00109288	0.0577997	0.05830095	43444.6899	371.276626	0.029499045
30	0.998462243	1.81629E-05	0.00103884	0.10035234	0.10143259	48611.2544	1301.9575	0.09680713
31	0.998574391	1.81334E-05	0.00105467	0.09064657	0.09162453	48690.3427	1025.94092	0.079865627
32	0.998731204	1.80902E-05	0.00107847	0.0784057	0.07925373	48806.4835	752.472333	0.059581079
33	0.998898953	1.80412E-05	0.00110654	0.06249589	0.06317433	48939.2516	488.924336	0.035869499
34	0.999020976	1.80032E-05	0.00112902	0.05204875	0.05261523	49042.5197	359.390193	0.022623148
35	0.999119771	1.79707E-05	0.00114879	0.04306706	0.04353733	49131.1429	235.470893	0.013202598
36	0.999151812	1.79598E-05	0.00115554	0.04279046	0.04325751	49160.9557	234.09493	0.012946456
37	0.999207339	1.79404E-05	0.0011677	0.03955533	0.03998755	49214.0785	185.326379	0.010103965
38	0.999279035	1.79144E-05	0.00118433	0.03408168	0.03445495	49285.6317	137.042533	0.006001131
39	0.999389938	1.78714E-05	0.00121256	0.03555188	0.03594152	49404.1675	89.2347677	0.007015906
40	0.999339859	1.78912E-05	0.00119944	0.02420072	0.02446947	49349.5961	22.5528001	0.001000648
41	0.998814566	1.80664E-05	0.00109201	0.0833412	0.08444297	54301.0793	990.854058	0.067705926
42	0.998910037	1.80379E-05	0.00110847	0.07344688	0.07442037	54386.803	732.107604	0.051932653
43	0.999048333	1.79944E-05	0.00113432	0.05948825	0.06027967	54518.1704	476.950753	0.031952879
44	0.999154405	1.7959E-05	0.00115608	0.04892349	0.04957699	54625.8235	350.98023	0.019234255
45	0.999233402	1.79311E-05	0.0011736	0.04316725	0.04374564	54710.6561	230.492446	0.013413706
46	0.999273176	1.79166E-05	0.00118292	0.04039084	0.04093264	54755.0787	182.941739	0.010926097
47	0.999327747	1.7896E-05	0.00119631	0.03538946	0.03586531	54818.1634	135.670208	0.007014024
48	0.999414733	1.78613E-05	0.00121935	0.03023253	0.03064034	54924.5622	88.7381096	0.003795031
49	0.999476119	1.78352E-05	0.00123711	0.02438647	0.0247177	55004.9075	21.8659615	0.001183687
50	0.998339067	1.81939E-05	0.00102254	0.08183469	0.08317988	59312.55	1322.72005	0.065323719
51	0.998405421	1.81772E-05	0.00103125	0.07446999	0.07569813	59367.1138	1049.24076	0.053598566
52	0.998627047	1.81189E-05	0.00106251	0.06605819	0.06714915	59558.0581	763.776954	0.041060497
53	0.998867957	1.80502E-05	0.00110121	0.05583418	0.05675829	59784.6566	491.289486	0.027375604
54	0.999166528	1.79544E-05	0.00115882	0.04335199	0.04407213	60103.6161	233.432901	0.013680747
55	0.999035919	1.79981E-05	0.00113201	0.04850932	0.04931375	59957.8128	358.4402	0.018880175
56	0.999207249	1.79401E-05	0.0011678	0.0422435	0.04294552	60151.4758	208.474737	0.012656238
57	0.999256108	1.79225E-05	0.00117901	0.04006586	0.04073217	60210.6294	183.547606	0.010743869
58	0.999304223	1.79046E-05	0.00119059	0.03888053	0.03952723	60270.8901	159.043049	0.009761044
59	0.999339642	1.7891E-05	0.00119948	0.03495561	0.03553831	60316.7173	135.311722	0.006805696
60	0.999379498	1.78753E-05	0.0012099	0.03427699	0.03484881	60369.8302	111.788787	0.00634365
61	0.999435406	1.78523E-05	0.00122534	0.03017749	0.03068168	60447.434	88.3044644	0.003860462
62	0.999437828	1.78513E-05	0.00122603	0.02748243	0.02794266	60450.9389	66.1905771	0.002523279
63	0.999475491	1.78351E-05	0.00123709	0.02753184	0.02799341	60505.734	43.7326994	0.002546528
64	0.999364014	1.78813E-05	0.00120584	0.0244134	0.02482538	60349.3331	22.4330305	0.001285343

Line No.	*Loop Test Section Water Density, g/cm3*	*Loop Test Section Air Viscosity Pa-s*	*Loop Test Section Water Viscosity, Pa-s*	**Apparent Friction Factor, fiSG (incl KE)**	**Apparent Friction Factor, fiSG (NO KE)**	**Superficial Gas Reynolds Number, ReSG**	**Superficial Liquid Reynolds Number, ReSL**	**Effective relative Roughness, e**
65	0.998285123	1.82073E-05	0.00101566	0.49172252	0.49260585	18858.319	2130.69048	0.716377604
66	0.998413277	1.81752E-05	0.00103228	0.45128997	0.45210138	18891.5549	1834.33271	0.666426451
67	0.998457926	1.81638E-05	0.00103832	0.42042046	0.42117773	18903.4715	1563.13653	0.626307189
68	0.998469878	1.81607E-05	0.00103997	0.38365139	0.38434419	18906.7095	1300.55316	0.576102326
69	0.998509831	1.81502E-05	0.00104553	0.34341201	0.34403418	18917.5824	1034.90926	0.517920518
70	0.998563918	1.81359E-05	0.00105324	0.29640877	0.29694762	18932.5283	770.500309	0.445343223
71	0.998645178	1.81139E-05	0.00106525	0.24783426	0.24828645	18955.5198	507.876401	0.364822188
72	0.998737716	1.80881E-05	0.0010796	0.22558074	0.22599306	18982.5695	375.841257	0.326054422
73	0.998787422	1.80738E-05	0.00108765	0.2000951	0.200462	18997.5359	248.706752	0.280294391
74	0.99880516	1.80687E-05	0.00109058	0.19211464	0.19246715	19002.9471	223.234612	0.265695045
75	0.998841244	1.80581E-05	0.00109665	0.18524579	0.18558603	19014.0889	197.333364	0.253038897
76	0.998859668	1.80526E-05	0.0010998	0.17667246	0.17699734	19019.8489	172.171844	0.237134861
77	0.998883411	1.80455E-05	0.00110391	0.16792315	0.16823214	19027.3322	147.025745	0.220800941
78	0.998919258	1.80347E-05	0.00111026	0.1619479	0.16224621	19038.8006	121.821599	0.209598632
79	0.998965077	1.80205E-05	0.00111859	0.15334278	0.15362556	19053.743	96.7310698	0.193417934
80	0.998996139	1.80108E-05	0.0011244	0.14096211	0.14122263	19064.074	72.1735116	0.170099479
81	0.999049686	1.79936E-05	0.00113473	0.13108635	0.13132907	19082.2721	47.6777	0.151544224
82	0.999098836	1.79774E-05	0.00114459	0.12318624	0.12341475	19099.4531	23.6334224	0.136788221
83	0.998686432	1.81025E-05	0.00107156	0.0602922	0.0616971	70450.7301	757.321783	0.033254185
84	0.998923984	1.80332E-05	0.00111111	0.0535615	0.05481152	70721.339	486.910051	0.024759678
85	0.999057217	1.79911E-05	0.00113624	0.04640977	0.04749724	70886.9483	357.107206	0.016828144
86	0.999235458	1.79299E-05	0.00117425	0.04299403	0.04400168	71128.6419	230.364482	0.013495387
87	0.999264444	1.79193E-05	0.00118103	0.04172543	0.04270411	71170.6676	206.138884	0.012337986
88	0.999316775	1.78997E-05	0.00119375	0.04028373	0.04122918	71248.7635	181.281449	0.011078295
89	0.999371284	1.78784E-05	0.00120776	0.03870812	0.0396172	71333.5359	156.780946	0.009770549
90	0.999392755	1.78698E-05	0.00121353	0.03512636	0.03595316	71368.0651	133.745439	0.007073262
91	0.999443094	1.78489E-05	0.00122761	0.03403001	0.03483154	71451.4657	110.176324	0.006327723
92	0.999482213	1.7832E-05	0.00123918	0.03215215	0.03291053	71519.125	87.3178334	0.005138335
93	0.999521679	1.78143E-05	0.00125148	0.02791842	0.02857753	71590.1322	64.8445855	0.002872844
94	0.999571785	1.77908E-05	0.00126817	0.02416044	0.02473155	71685.0046	42.6610304	0.001348806
95	0.999452593	1.78448E-05	0.0012304	0.02287412	0.02341825	71467.9953	21.9852264	0.000927502
96	0.99875648	1.80827E-05	0.00108262	0.06004397	0.06166784	75952.8222	749.588285	0.032985164
97	0.999030859	1.79997E-05	0.00113106	0.05309121	0.05452942	76303.3227	478.325644	0.024261993
98	0.999316931	1.78997E-05	0.00119375	0.04809815	0.04939906	76729.2778	339.902758	0.018652393
99	0.999275562	1.79152E-05	0.00118367	0.04390381	0.04509786	76662.8307	228.532615	0.01441274
100	0.999299476	1.79063E-05	0.00118946	0.042029	0.04317242	76701.1638	204.677335	0.012670408
101	0.999338722	1.78913E-05	0.00119929	0.04033681	0.04143536	76765.6374	180.444692	0.011182837
102	0.999376326	1.78764E-05	0.0012091	0.03905161	0.04011603	76829.3226	156.608095	0.010108477
103	0.999421354	1.78581E-05	0.00122141	0.03686598	0.03787183	76908.3078	132.882525	0.008393815
104	0.999459414	1.7842E-05	0.00123235	0.03424913	0.0351842	76977.6308	109.752462	0.006532869
105	0.99948783	1.78296E-05	0.00124088	0.03166725	0.03253339	77031.173	87.1983066	0.004908075
106	0.999519256	1.78154E-05	0.00125071	0.0303083	0.03113893	77092.2914	64.8846892	0.004139204
107	0.999552726	1.77999E-05	0.00126167	0.02600983	0.02672334	77159.6551	42.8807139	0.002100684
108	0.999590755	1.77815E-05	0.00127483	0.02311086	0.02374503	77239.5596	21.2189969	0.001062099
109	0.999362468	1.7882E-05	0.0012054	0.04228938	0.04360706	82291.3622	224.411938	0.012958957
110	0.999257008	1.79222E-05	0.00117923	0.04472089	0.04611118	82106.9716	344.088633	0.015253414
111	0.999152853	1.79592E-05	0.00115587	0.04968882	0.05122774	81937.8253	468.058229	0.020425636
112	0.998779793	1.80762E-05	0.00108635	0.05558512	0.05728994	81407.371	747.013235	0.027326147
113	0.99889359	1.80426E-05	0.00110565	0.05356612	0.05520962	81558.8316	611.648146	0.024875716
114	0.998981786	1.80154E-05	0.00112165	0.04914954	0.05066039	81681.9235	482.337731	0.01983186
115	0.999106371	1.7975E-05	0.00114609	0.04436658	0.04573423	81865.6442	354.038293	0.014906695
116	0.999230523	1.79319E-05	0.00117305	0.04256501	0.04387977	82062.4967	230.601429	0.013209051
117	0.999248218	1.79255E-05	0.00117714	0.04083653	0.04209926	82091.9055	206.819278	0.011663747
118	0.999269646	1.79176E-05	0.0011822	0.03896293	0.04016959	82128.0242	183.05344	0.010085724
119	0.999307014	1.79036E-05	0.00119126	0.03684337	0.0379851	82192.2443	158.953344	0.008426232
120	0.999336315	1.78923E-05	0.00119861	0.03468932	0.03576548	82243.9168	135.409731	0.006880259
121	0.999366053	1.78807E-05	0.00120632	0.03221263	0.03321362	82297.6311	112.120635	0.00528275
122	0.999401621	1.78663E-05	0.00121587	0.02898453	0.02988628	82363.5931	88.9917274	0.003496308
123	0.999425733	1.78564E-05	0.00122259	0.02794345	0.02881496	82409.6206	66.3770711	0.002992537
124	0.999430517	1.78543E-05	0.00122395	0.0250193	0.02580159	82418.9544	44.2020747	0.00176443
125	0.999404652	1.7865E-05	0.00121674	0.0233393	0.02407107	82369.698	22.2320547	0.001182068
126	0.99832116	1.81987E-05	0.00102014	0.07390683	0.07530724	64687.5198	1325.82425	0.052808307
127	0.998416315	1.81748E-05	0.0010326	0.0687295	0.07003466	64772.6864	1047.8638	0.045010092
128	0.998619481	1.81213E-05	0.00106127	0.0623178	0.06350255	64963.668	764.670122	0.035913692

Line No.	*Loop Test Section Water Density, g/cm3*	*Loop Test Section Air Viscosity Pa-s*	*Loop Test Section Water Viscosity, Pa-s*	**Apparent Friction Factor, fiSG (incl KE)**	**Apparent Friction Factor, fiSG (NO KE)**	**Superficial Gas Reynolds Number, ReSG**	**Superficial Liquid Reynolds Number, ReSL**	**Effective relative Roughness, e**
129	0.998890882	1.80437E-05	0.00110507	0.05299995	0.05400939	65243.0233	489.572561	0.024024478
130	0.999048626	1.79944E-05	0.00113436	0.04774046	0.04865344	65422.0392	357.698288	0.018141674
131	0.999181145	1.79498E-05	0.00116184	0.04426213	0.04510886	65584.5984	232.825215	0.014628053
132	0.999208758	1.794E-05	0.00116797	0.04284579	0.04366606	65620.1875	208.443231	0.013289065
133	0.999252628	1.79242E-05	0.00117803	0.04066086	0.04144004	65678.076	183.700864	0.011332979
134	0.999281121	1.79137E-05	0.0011848	0.03863456	0.03937612	65716.6721	159.820419	0.009641477
135	0.99930535	1.79046E-05	0.00119069	0.03773833	0.03846283	65750.0768	136.310208	0.008932303
136	0.999339886	1.78913E-05	0.00119936	0.03461377	0.03527921	65798.7985	112.770686	0.006650482
137	0.999351769	1.78867E-05	0.00120244	0.03380998	0.0344617	65815.9869	89.9861922	0.006112684
138	0.999399329	1.78677E-05	0.00121508	0.03093565	0.03153296	65886.0269	66.7871075	0.004358041
139	0.999449039	1.7847E-05	0.00122908	0.02960739	0.03017936	65962.4039	44.0178813	0.003637779
140	0.999376652	1.78768E-05	0.00120899	0.02580865	0.02630945	65852.4514	22.3746228	0.001889832
141	0.999147285	1.79614E-05	0.00115454	0.0436032	0.04418499	54618.3001	234.297086	0.013822236
142	0.999164315	1.79556E-05	0.0011582	0.04207663	0.04263843	54636.1432	210.202412	0.012408863
143	0.99923937	1.7929E-05	0.00117496	0.03794216	0.03844955	54717.0979	161.158348	0.008915394
144	0.999286786	1.79115E-05	0.00118619	0.03561059	0.03608869	54770.5364	114.023691	0.007170061
145	0.999378004	1.78762E-05	0.00120934	0.03123994	0.0316604	54878.623	67.104492	0.004356389
146	0.999358412	1.7884E-05	0.00120418	0.0268715	0.0272346	54854.811	44.9278711	0.002156387
147	0.999031151	1.8E-05	0.00113097	0.04663248	0.04713896	49051.3045	239.18014	0.016696442
148	0.999129621	1.79674E-05	0.00115082	0.04410227	0.04458127	49140.0717	188.043884	0.014182718
149	0.999126466	1.79685E-05	0.00115016	0.04312979	0.04359774	49137.0991	211.672109	0.013261283
150	0.999187364	1.79475E-05	0.00116323	0.03783798	0.03824941	49194.547	162.783651	0.008717637
151	0.99922626	1.79337E-05	0.00117196	0.03451372	0.03489023	49232.4806	115.407739	0.006290259
152	0.999331466	1.78946E-05	0.00119723	0.02843976	0.02875089	49340.1738	67.7828982	0.002759239
153	0.999341786	1.78905E-05	0.00119988	0.03028352	0.03061531	49351.3145	45.0890117	0.003706216
154	0.999079978	1.79841E-05	0.00114062	0.04406299	0.04444283	43639.6935	237.158163	0.014001394
155	0.999089376	1.7981E-05	0.00114252	0.04129732	0.04165378	43647.2479	213.087207	0.011452981
156	0.99914766	1.79613E-05	0.00115463	0.03503818	0.03534159	43694.9916	163.995786	0.006506475
157	0.999196768	1.79442E-05	0.00116532	0.03037212	0.03063627	43736.5942	116.065664	0.003608794
158	0.999272736	1.79168E-05	0.0011828	0.02692111	0.02715601	43803.6002	68.609846	0.001918978
159	0.999320944	1.78986E-05	0.00119459	0.02932421	0.02957982	43848.0793	45.2884535	0.003057385
160	0.998339998	1.81935E-05	0.00102271	0.08657299	0.08716628	37745.2218	793.50009	0.072629725
161	0.998813414	1.80662E-05	0.00109199	0.04659421	0.04691641	38011.1678	260.105028	0.016328046
162	0.998905576	1.80387E-05	0.00110785	0.04577805	0.04609442	38068.978	244.1735	0.015501153
163	0.998615995	1.81218E-05	0.0010609	0.0687119	0.06918366	37894.6012	509.954864	0.044368284
164	0.998729691	1.80903E-05	0.00107836	0.05764625	0.05804297	37960.5813	376.275278	0.029118961
165	0.999052206	1.79927E-05	0.00113525	0.03979685	0.04007241	38166.4267	166.795472	0.009978847
166	0.997794531	1.83203E-05	0.00096002	0.15951283	0.16032891	32129.0481	1690.62112	0.206147004
167	0.998034944	1.82664E-05	0.00098593	0.14293731	0.14366831	32223.864	1371.83927	0.174943254
168	0.998164094	1.82362E-05	0.00100091	0.12377943	0.12441326	32277.2813	1081.03753	0.139014704
169	0.998356999	1.81891E-05	0.00102494	0.1004442	0.10095981	32360.8044	791.770357	0.096401492
170	0.998571787	1.81335E-05	0.00105445	0.07810318	0.07850552	32459.974	513.076839	0.058530484
171	0.998711705	1.80952E-05	0.00107556	0.06585728	0.06619729	32528.7517	377.254915	0.03999876
172	0.998830885	1.80609E-05	0.00109496	0.05429667	0.05457807	32590.4497	247.04698	0.024716827
173	0.998884165	1.80451E-05	0.00110411	0.05184484	0.05211371	32619.0735	220.498661	0.021821589
174	0.998920027	1.80342E-05	0.00111046	0.04762363	0.04787102	32638.7364	194.878626	0.017162243
175	0.998974181	1.80175E-05	0.00112035	0.04461249	0.04484462	32669.0929	169.013692	0.014110847
176	0.999009795	1.80062E-05	0.00112706	0.04173431	0.04195185	32689.5096	144.005761	0.011420355
177	0.999058453	1.79905E-05	0.00113653	0.03982283	0.04003067	32718.0301	119.005163	0.0097629
178	0.999075072	1.79851E-05	0.00113985	0.03714582	0.03734015	32727.9516	94.9271151	0.007620261
179	0.999118024	1.79707E-05	0.00114862	0.03415248	0.03433168	32754.0235	70.6513618	0.005483688
180	0.999170602	1.79528E-05	0.0011598	0.03214492	0.032314	32786.8564	46.6470376	0.004209305
181	0.999235736	1.79296E-05	0.00117439	0.02332577	0.02345044	32829.1211	23.0338175	0.000146728
182	0.998107183	1.82497E-05	0.0009942	0.2111179	0.21187458	26877.8641	1632.50978	0.301059292
183	0.998150576	1.82394E-05	0.0009993	0.19303776	0.19373125	26892.9637	1353.4793	0.268193848
184	0.99823023	1.82203E-05	0.00100891	0.16810817	0.16871379	26921.139	1072.465	0.22194986
185	0.998365475	1.8187E-05	0.00102605	0.13857474	0.13907544	26970.484	790.917841	0.166407376
186	0.998503541	1.81516E-05	0.00104472	0.11058199	0.11098314	27023.0754	517.853105	0.11434236
187	0.99862826	1.81183E-05	0.00106277	0.09628659	0.09663655	27072.7534	381.794051	0.088742078
188	0.998769397	1.80788E-05	0.00108477	0.07266398	0.07292937	27131.859	249.366921	0.049723265
189	0.998783481	1.80748E-05	0.00108707	0.06974549	0.07000044	27137.9441	223.955715	0.045330876
190	0.998789527	1.8073E-05	0.00108807	0.06331388	0.063546	27140.577	198.889737	0.036100127
191	0.998857676	1.8053E-05	0.00109952	0.05993925	0.06015923	27170.6306	172.215114	0.031536281
192	0.998902378	1.80396E-05	0.00110732	0.05606728	0.0562734	27190.8505	146.573714	0.026563509

Line No.	*Loop Test Section Water Density, g/cm3*	*Loop Test Section Air Viscosity Pa-s*	*Loop Test Section Water Viscosity, Pa-s*	**Apparent Friction Factor, fiSG (incl KE)**	**Apparent Friction Factor, fiSG (NO KE)**	**Superficial Gas Reynolds Number, ReSG**	**Superficial Liquid Reynolds Number, ReSL**	**Effective relative Roughness, e**
193	0.998912192	1.80366E-05	0.00110906	0.05159128	0.05178149	27195.3527	121.952645	0.021202238
194	0.998931931	1.80306E-05	0.00111261	0.04736533	0.04754057	27204.4731	97.2513068	0.01656336
195	0.998962208	1.80212E-05	0.00111814	0.04330399	0.04346482	27218.6259	72.577712	0.012530596
196	0.99901384	1.80049E-05	0.00112785	0.03884286	0.03898774	27243.2421	47.9686765	0.008624509
197	0.999034461	1.79982E-05	0.00113185	0.02793602	0.02804243	27253.3529	23.8995117	0.001623747
198	0.997515714	1.83795E-05	0.00093274	0.31961413	0.32037245	21350.3584	2030.09169	0.482125818
199	0.997533404	1.83759E-05	0.0009344	0.29583922	0.29654245	21354.6319	1736.99298	0.444740544
200	0.997680326	1.83449E-05	0.00094853	0.27033698	0.27098042	21390.6292	1425.92443	0.403142461
201	0.997787152	1.83219E-05	0.00095928	0.2494967	0.25009191	21417.5584	1127.95414	0.367984322
202	0.997933003	1.82895E-05	0.00097466	0.21568389	0.21619961	21455.4089	832.613549	0.308761131
203	0.998100512	1.82511E-05	0.00099346	0.17773102	0.17815734	21500.6129	544.576019	0.239417156
204	0.998214776	1.8224E-05	0.00100705	0.15579486	0.15616928	21532.6259	402.918887	0.198345032
205	0.998378529	1.81836E-05	0.00102778	0.13594738	0.1362748	21580.3975	263.193619	0.160981165
206	0.998502582	1.81518E-05	0.00104461	0.13015624	0.13046957	21618.2476	233.059308	0.150118505
207	0.99857323	1.81331E-05	0.00105468	0.12538553	0.12568726	21640.5216	205.186317	0.141202847
208	0.998611743	1.81227E-05	0.00106033	0.11796291	0.11824733	21652.921	178.580535	0.127418182
209	0.998662517	1.81088E-05	0.00106797	0.11364481	0.11391889	21669.5222	151.974493	0.119466739
210	0.998723257	1.80919E-05	0.0010774	0.11023967	0.11050561	21689.8174	125.536738	0.113240812
211	0.998784819	1.80743E-05	0.00108731	0.10557126	0.10582605	21710.9001	99.5138649	0.104778539
212	0.998822123	1.80634E-05	0.00109351	0.09696633	0.09720099	21723.9573	74.212573	0.089457085
213	0.998868444	1.80497E-05	0.00110141	0.08909039	0.08930655	21740.4656	49.120229	0.075842357
214	0.998952761	1.80241E-05	0.00111642	0.08472634	0.0849323	21771.4383	24.2297067	0.068511688

Appendix 2 Chemical Safety Data Sheets (SDS)

The following data sheets are included (first page only):

1. Glycerol.
2. Rhodamine B.

SIGMA-ALDRICH

sigma-aldrich.com

SAFETY DATA SHEET

Version 5.3
Revision Date 06/27/2014
Print Date 07/04/2017

1. PRODUCT AND COMPANY IDENTIFICATION

Product name	:	Glycerol
Product Number	:	G7893
Brand	:	Sigma-Aldrich
Product Use	:	For laboratory research purposes.
Supplier	:	Sigma-Aldrich Canada Co. 2149 Winston Park Drive OAKVILLE ON L6H 6J8 CANADA
Manufacturer	:	Sigma-Aldrich Corporation 3050 Spruce St. St. Louis, Missouri 63103 USA
Telephone	:	+1 9058299500
Fax	:	+1 9058299292
Emergency Phone # (For both supplier and manufacturer)	:	+1-703-527-3887 (CHEMTREC)
Preparation Information	:	Sigma-Aldrich Corporation Product Safety - Americas Region 1-800-521-8956

2. HAZARDS IDENTIFICATION

Emergency Overview

Target Organs

Kidney

WHMIS Classification

Not WHMIS controlled.

GHS Classification
Skin irritation (Category 3)
Eye irritation (Category 2B)

GHS Label elements, including precautionary statements

Pictogram	none
Signal word	Warning
Hazard statement(s)	
H316	Causes mild skin irritation.
H320	Causes eye irritation.
Precautionary statement(s)	
P305 + P351 + P338	IF IN EYES: Rinse cautiously with water for several minutes. Remove contact lenses, if present and easy to do. Continue rinsing.

HMIS Classification

Health hazard:	0
Chronic Health Hazard:	*
Flammability:	1
Physical hazards:	0

Potential Health Effects

Inhalation	May be harmful if inhaled. May cause respiratory tract irritation.
Skin	May be harmful if absorbed through skin. May cause skin irritation.

SAFETY DATA SHEET

Creation Date 12-December-2006 **Revision Date** 26-May-2017 **Revision Number** 3

1. Identification

Product Name **Rhodamine B**

Cat No. : **AC296570000; AC296570010; AC296570100; AC296570250; AC296571000**

Synonyms C.I. 45170; Basic Violet 10

Recommended Use Laboratory chemicals.
Uses advised against Not for food, drug, pesticide or biocidal product use

Details of the supplier of the safety data sheet

Company
Importer/Distributor
Fisher Scientific
112 Colonnade Road,
Ottawa, ON K2E 7L6,
Canada
Tel: 1-800-234-7437

Acros Organics
One Reagent Lane
Fair Lawn, NJ 07410

Manufacturer
Fisher Scientific
One Reagent Lane
Fair Lawn, NJ 07410
Tel: (201) 796-7100

Emergency Telephone Number
For information **US** call: 001-800-ACROS-01 / **Europe** call: +32 14 57 52 11
Emergency Number **US:**001-201-796-7100 / **Europe:** +32 14 57 52 99
CHEMTREC Tel. No.**US:**001-800-424-9300 / **Europe:**001-703-527-3887

2. Hazard(s) identification

Classification

WHMIS 2015 Classification Classified as hazardous under the Hazardous Products Regulations (SOR/2015-17)

Acute oral toxicity	Category 4
Serious Eye Damage/Eye Irritation	Category 1

Label Elements

Signal Word
Danger

Hazard Statements
Harmful if swallowed
Causes serious eye damage

Appendix 3 Equipment Data Sheets

The following data sheets are included

1. Omega pressure transducer
2. Omega differential pressure transducer
3. Omega mass flow controller
4. Cole-Parmer rotameter (air)
5. Kobold rotameter (liquid)
6. LaVision Imager Intense CCD camera
7. New Wave Research Solo Nd:YAG Laser System

4 TO 20 mA OUTPUT
HIGH PERFORMANCE PRESSURE TRANSMITTERS
PIEZORESISTIVE DESIGN WITH HIGH TEMPERATURE PERFORMANCE

4 to 20 mA Output
0-10 inH_2O to 0-5000 psi
25 mb to 0-345 bar

PX409-100GI, shown actual size.

PX419-100GI, shown actual size.

Stock Delivery for most Ranges!

PX409 Series

NIST CE RoHS

PX429-015GI, shown actual size.

4 to 20 mA Specifications

Output: 4 to 20 mA
Supply Voltage: 9 to 30 Vdc maximum loop res Ω = (Vs-9)x50 [9 to 20 Vdc above 105°C (229°F)]
Accuracy (Combined Linearity, Hysteresis and Repeatability): ±0.08% BSL maximum
Zero Balance: ±0.5% FS typical 1% maximum (1% typical, 2% maximum for 2.5 psi and below)
Span Setting: ±0.5% FS typical 1% maximum (1% typical, 2% max for 2.5 psi and below). Calibrated in vertical direction with fitting down
Operating Temperature Range: -45 to 115°C (-49 to 240°F)
Compensated Temperature:
Ranges >5 psi: -29 to 85°C (-20 to 185°F)
Ranges ≤ 5 psi: -17 to 85°C (0 to 185°F)
Thermal Effects Zero (Over Compensated Range):
- **Ranges >5 psi:** ±0.5% span
- **Ranges ≤5 psi:** ±1.0% span

Thermal Effects Span (Over Compensated Range):
- **Ranges >5 psi:** ±0.5% span
- **Ranges ≤5 psi:** ±1.0% span

To Order

RANGE psi	RANGE bar	2 m (6') CABLE TERMINATION	MINI-DIN TERMINATION	TWIST-LOCK TERMINATION
4 to 20 mA OUTPUT, GAGE PRESSURE RANGES				
10 in-H_2O	25 mb	**PX409-10WGI**	**PX419-10WGI**	**PX429-10WGI**
1	69 mb	**PX409-001GI**	**PX419-001GI**	**PX429-001GI**
2.5	172 mb	**PX409-2.5GI**	**PX419-2.5GI**	**PX429-2.5GI**
5	345 mb	**PX409-005GI**	**PX419-005GI**	**PX429-005GI**
15	1.0	**PX409-015GI**	**PX419-015GI**	**PX429-015GI**
30	2.1	**PX409-030GI**	**PX419-030GI**	**PX429-030GI**
50	3.4	**PX409-050GI**	**PX419-050GI**	**PX429-050GI**
100	6.9	**PX409-100GI**	**PX419-100GI**	**PX429-100GI**
150	10.3	**PX409-150GI**	**PX419-150GI**	**PX429-150GI**
250	17.2	**PX409-250GI**	**PX419-250GI**	**PX429-250GI**
500	34.5	**PX409-500GI**	**PX419-500GI**	**PX429-500GI**
750	51.7	**PX409-750GI**	**PX419-750GI**	**PX429-750GI**
1000	69	**PX409-1.0KGI**	**PX419-1.0KGI**	**PX429-1.0KGI**
1500	103	**PX409-1.5KGI**	**PX419-1.5KGI**	**PX429-1.5KGI**
2500	172	**PX409-2.5KGI**	**PX419-2.5KGI**	**PX429-2.5KGI**
3500	241	**PX409-3.5KGI**	**PX419-3.5KGI**	**PX429-3.5KGI**
5000	345	**PX409-5.0KGI**	**PX419-5.0KGI**	**PX429-5.0KGI**
4 to 20 mA ABSOLUTE PRESSURE RANGES				
5	345 mb	**PX409-005AI**	**PX419-005AI**	**PX429-005AI**
15	1.0	**PX409-015AI**	**PX419-015AI**	**PX429-015AI**
30	2.1	**PX409-030AI**	**PX419-030AI**	**PX429-030AI**
50	3.4	**PX409-050AI**	**PX419-050AI**	**PX429-050AI**
100	6.9	**PX409-100AI**	**PX419-100AI**	**PX429-100AI**
150	10.3	**PX409-150AI**	**PX419-150AI**	**PX429-150AI**
250	17.2	**PX409-250AI**	**PX419-250AI**	**PX429-250AI**
500	34.5	**PX409-500AI**	**PX419-500AI**	**PX429-500AI**
750	51.7	**PX409-750AI**	**PX419-750AI**	**PX429-750AI**
1000	69	**PX409-1.0KAI**	**PX419-1.0KAI**	**PX429-1.0KAI**

__Ordering Examples: PX409-1.0KGI,__ 4 to 20 mA output, 1000 psi gage pressure range, 2m (6') cable termination. __PX429-015AI,__ 4 to 20 mA output, 15 psi absolute pressure, twist lock termination, __PT06F10-6S,__ mating twist lock connector (sold separately), and __DP25B-E,__ 4-digit meter, system with meter.
(See B-25h for information on meters).

WET/WET DIFFERENTIAL PRESSURE TRANSDUCER
UNI-DIRECTIONAL AND BI-DIRECTIONAL RANGES

0-1 to 0-100 psid Uni-Directional
±0.5 to ±50 psid Bi-Directional

PX2300 Series

MADE IN USA · 1 YEAR WARRANTY · CE

- 0.25% Accuracy
- NEMA 4 (IP65) Rating
- Wet/Wet Corrosive Environments
- Ideal for Measuring Pressure Drop Across Filters

OMEGA's PX2300 Series high-output, low differential pressure transducers are compatible with most media, from dry air to corrosive liquids. All wetted parts are stainless steel with elastomer seals. The electronics are housed in a NEMA 4 (IP65) enclosure. A high working pressure and high overpressure ratings ensure dependability in harsh industrial environments. These transducers are ideal for measuring pressure drop across filters and other process devices.

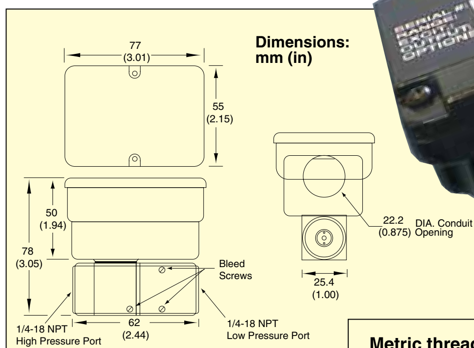

Metric thread adaptors and snubbers available, visit omega.com

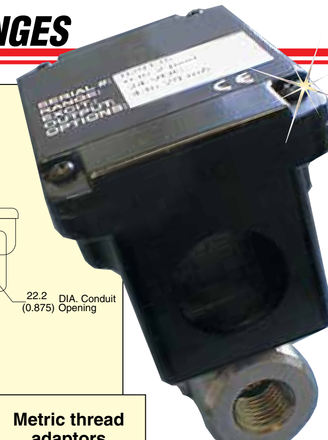

PX2300-1DI, shown smaller than actual size.

SPECIFICATIONS

Excitation: 24 Vdc nominal
Max: 30 + 0.004 x (loop resistance Ω) Vdc
Min: 11 + 0.02 x (loop resistance Ω) Vdc
Loop Resistance: 0 to 1000 Ω
Output: 4 to 20 mA
Accuracy: ±0.25% RSS FS at constant temperature (includes linearity, repeatability and hysteresis)
Linearity: ±0.20% FS
Hysteresis: 0.10% FS
Repeatability: ±0.05% FS
Operating Temperature Range: -18 to 80°C (0 to 176°F)
Compensated Temperature Range: -1 to 65°C (30 to 149°F)
Thermal Zero Effect: <±0.02% FS/°F
Thermal Span Effect: <±0.02% FS/°F
Sensor: Capacitive
Maximum Line Pressure: 250 psig
Maximum Overpressure:
High Side: 1 to 5 psi = 20 x FS, 10 to 25 psi = 10 x FS, 50 psi = 5 x FS, 100 psi = 2.5 x FS
Low Side: 2.5 x FS (shift recoverable)
The zero will shift slightly when high differential pressure is applied. The shift may be as much as ±10% FS with overpressure applied to the low port. (Other parameters will not shift.) The shift may be recovered by a positive overpressure or if the overpressure is always in one direction, the user may apply this pressure to pre-set the sensor. Subsequent overloads of less pressure will not cause any further shift.
Wetted Parts: Air and fluids compatible with 17-4 and 300 stainless steel, FKM, and silicone O-rings
Cavity Volume: 0.27/0.08" pos./neg. port
Case: NEMA 4 (IP65)
Pressure Port: ¼ NPT internal
Electrical Connection: Internal barrier strip with 22.2 mm (0.875") conduit opening
Response Time: 50 ms (water)
Weight: 410 g (14.4 oz)

To Order *Visit omega.com/px2300 for Pricing and Details*

RANGE (psid)	MODEL NO.	COMPATIBLE METERS
0 to 1	**PX2300-1DI**	DP41-E, DP25B-E, DP-7700
0 to 2	**PX2300-2DI**	DP41-E, DP25B-E, DP-7700
0 to 5	**PX2300-5DI**	DP41-E, DP25B-E, DP-7700
0 to 10	**PX2300-10DI**	DP41-E, DP25B-E, DP-7700
0 to 25	**PX2300-25DI**	DP41-E, DP25B-E, DP-7700
0 to 50	**PX2300-50DI**	DP41-E, DP25B-E, DP-7700
0 to 100	**PX2300-100DI**	DP41-E, DP25B-E, DP-7700
BI-DIRECTIONAL RANGE		
±0.5	**PX2300-0.5BDI**	DP41-E, DP25B-E, DP-7700
±1	**PX2300-1BDI**	DP41-E, DP25B-E, DP-7700
±2.5	**PX2300-2.5BDI**	DP41-E, DP25B-E, DP-7700
±5	**PX2300-5BDI**	DP41-E, DP25B-E, DP-7700
±10	**PX2300-10BDI**	DP41-E, DP25B-E, DP-7700
±25	**PX2300-25BDI**	DP41-E, DP25B-E, DP-7700
±50	**PX2300-50BDI**	DP41-E, DP25B-E, DP-7700

Comes complete with operator's manual.
Ordering Examples: PX2300-5BDI, *bi-directional range -5 to 5 psid transducer with current output.*
PX2300-1DI, *0 to 1 psid range transducer with current output.*

MASS AND VOLUMETRIC GAS FLOW CONTROLLERS

For Clean Gases

FMA-2613A shown smaller than actual size.

FMA-2601A shown smaller than actual size.

FMA-2600A Series

- 30+ Gas Calibrations, Including He, O_2, Neon, N_2O, N_2, Air, Argon, CO, CO_2, Methane, Ethane, H_2, Propane, Butane, iso-Butane, Ethylene, Acetylene, Krypton, Xenon, Sulfur Hexafluoride
- Pressure, Temperature, and Volumetric and Mass Flow Simultaneously Displayed
- Easy-to-Use Pushbutton Interface
- NIST Traceability Standard
- Full Scale Ranges from 0.5 SCCM to 3000 SLM
- Response Time of 50 to 100 ms Typical
- Turndown Ratio of 200:1
- Position Insensitive
- ±0.8% Reading Accuracy
- RS232 Standard

The FMA-2600A Series mass and volumetric flow controllers use the principle of differential pressure within a laminar flow field to determine and control mass flow rate. A laminar flow element (LFE) inside the meter forces the gas into laminar (streamlined) flow. Inside this region, the Poiseuille equation dictates that the volumetric flow rate be linearly related to the pressure drop. A differential pressure sensor is used to measure the pressure drop along a fixed distance of the LFE. This, along with the viscosity of the gas, is used to accurately determine the volumetric flow rate. Separate absolute temperature and pressure sensors are incorporated and correct the volumetric flow rate to a set of standard conditions. This standardized flow rate is commonly called the mass flow rate and is reported in units such as standard cubic feet per minute (SCFM) or standard liters per minute (SLM).

The controller uses a true proportional valve coupled to the flow body to control flow using the integral PID loop controller. Standard units include a 0 to 5 V output (4 to 20 mA optional) and RS232 communications. The gas-select feature and the setpoints can be adjusted from the front keypad or via RS232 communications. Volumetric flow, mass flow, absolute pressure, and temperature can all be viewed or recorded through the RS232 connection. It is also possible to multi-drop up to 26 units on the same serial connection to a distance of 46 m (150').

SPECIFICATIONS

Accuracy: ±(0.8% of reading + 0.2%FS)
Repeatability: ±0.2% FS
Turndown Ratio: 200:1
Control Response Time: 100 ms
Input Control Signal: 0 to 5 Vdc, RS232
Output Signal: 0 to 5 Vdc, RS232
Optional Input/Outputs: 4 to 20 mA, 0 to 10 Vdc
Operating Temperature: -10 to 50°C (14 to 122°F)
Zero Shift: 0.02%/ATM FS/°C
Span Shift: 0.02%/ATM FS/°C
Humidity Range: 0 to 100% RH, non-condensing
Excess Flow Rate: 2.4% FS
Wetted Materials: 303 and 302 SS, FKM, silicone RTV (rubber), glass-reinforced nylon, aluminum, brass, 410 SS, silicone, glass; >250 SLM: 416 SS and nickel replace brass

Maximum Pressure
Mass Flow Controllers: 145 psig
To Use in Volumetric Mode: Near atmosphere, 15 psig recommended maximum. Volumetric flowmeters and controllers not certified for accuracy at mass flow rates above the rated flow range of the meter. They are designed for near atmospheric pressure conditions only. The recommended maximum operating pressure is 15 psig

Cole-Parmer® Valved Acrylic Flowmeters for Bench or Panel Mount

Meter with valve provides flow control through a highly durable meter body

- Ideal for process plant applications on air sampling equipment, gas analyzers and chemical feed systems for water treatment
- Integrated precision valve allows precise manual flow across the full scale
- The flexible design allows for panel or bench mounting

Machined from solid acrylic blocks, these meters have integral metering tubes that provide precise readings even in aggressive plant environments. The meters' inlet/outlet ports and mounting studs are extended for easy panel installation. An alternate option is a tripod base (sold separately below) which allows for mobility from bench to bench.

Note: There are many additional types of acrylic flowmeters not listed here. Contact our Application Specialists for quotes on acrylic meters with special requirements.

2" Flowmeter 32460-18 shown with tripod base 32462-50

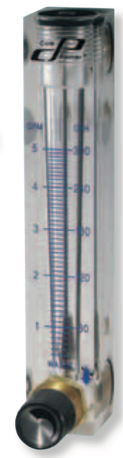

32461-08

GO to page(s) 602–670
For our selection of barbed and compression fittings.

Specifications

For LIQUIDS For GASES

Accuracy
2" and 50-mm flowmeters: ±5% full-scale
4" and 100-mm flowmeters: ±3% full-scale
5" and 127-mm flowmeters: ±2% full-scale

Repeatability: ±0.5% full-scale

Media type: liquids or gases

Connections
2", 4", 50-mm, and 100-mm flowmeters: 1/8" NPT(F)†
5" and 127-mm flowmeters: 1" NPT(F)

Maximum pressure: 100 psi

Max operating temp: 150°F (65°C)

Dimensions (not including valve stem):
2" and 50-mm flowmeters: 1"W x 4"H x 2 1/8"D
4" and 100-mm flowmeters: 1 3/8"W x 6 1/2"H x 2 1/8"D
5" and 127-mm flowmeters: 1 3/4"W x 10 7/8"H x 4 3/4"D

Materials of Construction

Part	2" and 50 mm	4" and 100 mm	5" and 127 mm
Body	Acrylic		
Fittings	Brass		PVC
Valve	Brass		
O-rings	Buna N		
Float (for air)	Glass (BG)	316 SS (SS)	

English-Unit Scales

For liquid applications				For air applications		
Cat. no.	**Float‡**	**Flow range**	**Price**	**Cat. no.**	**Flow range**	**Price**
Flowmeters with 2" scale						
R-32460-00	BG	0.2 to 2 GPH		R-32460-10	0.1 to 1 scfh	
R-32460-02	SS	0.4 to 5 GPH		R-32460-12	0.2 to 2 scfh	
R-32460-04	BG	1 to 10 GPH		R-32460-14	0.4 to 5 scfh	
R-32460-06	SS	2 to 20 GPH		R-32460-16	0.5 to 10 scfh	
R-32460-08	SS	4 to 40 GPH		R-32460-18	2 to 20 scfh	
—	—	—	—	R-32460-20	3 to 30 scfh	
—	—	—	—	R-32460-22	4 to 50 scfh	
—	—	—	—	R-32460-24	10 to 100 scfh	
—	—	—	—	R-32460-26	20 to 200 scfh	
Flowmeters with 4" scale						
R-32461-00	SS	1 to 10 GPH		R-32461-10	0.4 to 5 scfh	
R-32461-02	SS	2 to 25 GPH		R-32461-12	1 to 10 scfh	
R-32461-04	SS	4 to 50 GPH		R-32461-14	2 to 20 scfh	
R-32461-06	SS	6 to 60 GPH		R-32461-16	4 to 40 scfh	
R-32461-07†	SS	0.2 to 2.5 GPM		R-32461-18	10 to 100 scfh	
R-32461-08†	SS	0.4 to 5 GPM		R-32461-20	14 to 150 scfh	
—	—	—	—	R-32461-22	20 to 200 scfh	
—	—	—	—	R-32461-24†	0.5 to 5 scfm	
—	—	—	—	R-32461-26†	1 to 10 scfm	
Flowmeters with 5" scale						
R-32466-50	SS	1 to 10 GPM		R-32466-60	3 to 25 scfm	
R-32466-52	SS	2 to 20 GPM		R-32466-62	4 to 50 scfm	
—	—	—	—	R-32466-64	10 to 100 scfm	

†These models have dual scale: GPM/GPH, scfm/scfh, LPM/LPH; they also have 1/4" NPT(F) connections and use tripod base 32462-60 sold at right.

‡Float material key: BG = black glass, SS = stainless steel

Metric-Unit Scales

For liquid applications				For air applications		
Cat. no.	**Float‡**	**Flow range**	**Price**	**Cat. no.**	**Flow range**	**Price**
Flowmeters with 50-mm scale						
R-32460-30	BG	5 to 50 mL/min		R-32460-40	0.04 to 0.5 LPM	
R-32460-32	SS	10 to 100 mL/min		R-32460-42	0.1 to 1 LPM	
R-32460-34	SS	20 to 240 mL/min		R-32460-44	0.4 to 5 LPM	
—	—	—	—	R-32460-46	1 to 10 LPM	
—	—	—	—	R-32460-48	2 to 25 LPM	
—	—	—	—	R-32460-50	4 to 50 LPM	
—	—	—	—	R-32460-52	10 to 100 LPM	
Flowmeters with 100-mm scale						
R-32461-30	SS	4 to 50 mL/min		R-32461-50	0.4 to 5 LPM	
R-32461-32	SS	10 to 120 mL/min		R-32461-52	1 to 10 LPM	
R-32461-34	BG	25 to 225 mL/min		R-32461-54	2 to 20 LPM	
R-32461-36	SS	40 to 400 mL/min		R-32461-56	3 to 30 LPM	
R-32461-38	SS	40 to 660 mL/min		R-32461-58	4 to 50 LPM	
R-32461-40	SS	100 to 1500 mL/min		R-32461-60	10 to 100 LPM	
R-32461-42	SS	200 to 3000 mL/min		R-32461-62†	14 to 140 LPM	
R-32461-44†	SS	0.8 to 9 LPM		R-32461-64†	30 to 280 LPM	
R-32461-46†	SS	1.5 to 20 LPM		—	—	—
Flowmeters with 127-mm scale						
R-32466-54	SS	4 to 36 LPM		R-32466-66	100 to 700 LPM	
R-32466-56	SS	5 to 75 LPM		R-32466-68	100 to 1400 LPM	
—	—	—	—	R-32466-70	400 to 3400 LPM	

Tripod Bases

Durable acrylic base with three leveling screws and spirit level.

Catalog number	Description	Price
ED-32462-50	For one flowmeter with 2" or 50-mm scale	
ED-32462-55	For one flowmeter with 4" or 100-mm scale	
ED-32462-60	For one flowmeter with 1/4" connections	

Features

- Industrial and Sanitary Designs
- Body Sizes 1/2” Through 2”
- Reliable, Time Proven Glass Tube Design
- Flanged, Threaded or Tri-Clamp Fittings
- ±1.0% of Full Scale Accuracy
- Optional Surface Finishes for Food and Pharmaceutical Applications
- Optional Switches
- Special Calibrations for Compressed Gases and Viscous Media

The KDV series are high quality glass tube variable-area flowmeters (rotameters). This classic design is still the most widely used flowmeter style in the world today. The simple variable-area design makes the flowmeter a perfect choice when ease of installation and operation is a must.

The KDV features a tempered glass measuring tube which is inert to most chemicals. This tube is suitable for measurement of both liquids and gases. Liquid flow ranges are available from 0.01 to 0.1 GPH through 265 to 2645 GPH water. Gas flow ranges are available from 0.025 to 0.25 SCFH through 670 to 6700 SCFH air.

Custom Calibrations are Standard

Each KDV series is built specifically for the application. The KDV will arrive with a direct reading scale which is calibrated for your operating conditions. The KDV can be calibrated for viscous media, chemicals, and various compressed gases. The scale will be provided in any measuring units the user specifies when ordering. The application datasheet provided with the operating conditions will provide all the data required to properly factory calibrate the flowmeter.

A KDV for Every Application

The KDV is ideal for industrial and sanitary applications. The standard model is available with NPT threaded or flanged connections. Polished finishes and Tri-clamp® fittings for food and pharmaceutical applications are available.

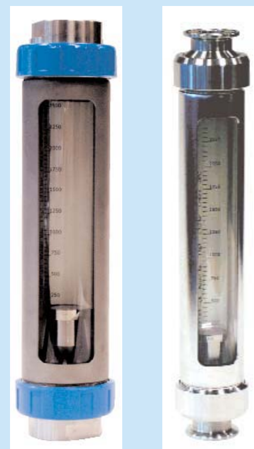

KDV Series Glass Tube Rotameter

Specifications

Flow Ranges
- **Water:** 0.01 to 0.1 through 265 to 2645 GPH
- **Air:** 0.025 to 0.25 through 670 to 6700 SCFH

Body Size: 1/2”, 1”, 1-1/2” and 2”

Maximum Operating Pressure:
- 1/2" through 1”: 145 PSIG
- 1-1/2": 131 PSIG
- 2": 102 PSIG

Process Temperature Range:
- **w/o Switch Contact:** -4˚F to 212˚F

Ambient Temp. Range:
- **With Proximity Switch:** -13˚F to 212˚F
- **With Reed Switch:** -4˚F to 185˚F

Wetted Materials
- **Measuring Tube:** Borosilicate Glass
- **Float:** 316 SS, Hastelloy®, aluminum, PTFE or PP, based on model code
- **Seals:** NBR, FKM, EPDM or FFKM
- **Fittings:** 316 SS or PVDF based on model code
- **Float Stops:** PVDF

Body Materials (Non-Wetted)
- **Tube Housing:** 316L SS
- **Union Nut:** Painted aluminum or 316 SS based on model code

Note: Electropolished finish for food and pharmaceutical applications available for all stainless steel surfaces.

Switch Specifications

The KDV can be fitted with up to two adjustable switches. Switch types available are bistable reed contacts and NAMUR proximity sensors.

Reed Contact: Bistable reed contact
Max. 12 VA, 30 VDC, 0.5 Amp
NEMA 3R/IP44

Proximity Sensor: Intrinsically safe output, NAMUR per DIN 19234 (use the REL-6003, -6004 or -6005 as a proximity sensor isolation relay/intrinsic safety barrrier)
NEMA 6/IP67

Electical Connection: Terminal box

Subject to change without prior notice.

LaVision

We count on Photons

Imager *intense*

most sensitive camera
for PIV systems

Imager Intense is a high sensitivity, high resolution digital camera used in the LaVision **FlowMaster** PIV system. It features an interline transfer chip with progressive scan readout. The camera delivers 12 bit digital images and it features a built in electronic shutter with exposure times as short as 500ns.

General System Specifications

Double Shutter	Two images with 500ns interframing time
Exposure time	500 ns ... 1 ms or 1ms...1000s (software selectable)
A/D-converter	12 bit @ 16 MHz
Serial link	coaxial (≤ 10 m) or fiber optic (≤ 300 m)

CCD Sensor

Number of pixels	1376 x 1040 pixels
Pixel size	6.45 µm x 6.45
Sensor format	2/3“
Full-well capacity	18.000 electrons
Spectral range	290 – 1100 nm
Max. QE	65 % @ 500 nm
Cooling type	2-stage Peltier, forced air (optional liquid)
CCD temperature	-12°C

CCD Control and A/D- Converter

Dynamic range	12 bit
A/D conversion factor	2 e- /count (high gain), 4 e- /count (low gain)
Readout (scan) rate	16 MHz
Readout noise	4-5 e- @ 16 MHz (high gain), 5-6 e- @ 16 MHz (low gain)

LaVisionUK Ltd
Downsview House/ Grove Technology Park
Grove/ Oxon/ OX12 9FF, United Kingdom
e-Mail: sales@lavision.com/ www.lavisionUK.com
Phone: +44-(0)-870-997-6532/ Fax: +44-(0)-870-762-6252

LaVision GmbH
Anna-Vandenhoeck-Ring 19
D-37081 Goettingen / Germany
E-Mail: Info@LaVision.com / www.LaVision.com
Tel. +49-(0)5 51-9004-0 / Fax +49-(0)551-9004-100

LaVision Inc.
211 W. Michigan Ave. / Suite 100
Ypsilanti, MI 48197 / USA
E-mail: sales@lavisioninc.com / www.lavisioninc.com
Phone: (734) 485 - 0913 / Fax: (240) 465 - 4306

Solo PIV

Nd:YAG Laser Systems

Solo PIV is a compact, dual laser-head system designed to provide a highly stable green light source for Particle Image Velocimetry (PIV) applications. It is ideally suited for most liquid and many air-based PIV experiments, and its small size provides excellent flexibility in setting-up such experiments.

Features

- **Small laser head requires minimum space**
- **Single power supply simplifies setup and enhances mobility**
- **High output energy**
  - 15 - 120 mJ at 532 nm
- **Highly flexible design with repetition rates**
  - From 1 to 15, 30, or 50 Hz, depending on model selected
- **Operating convenience provided through multiple triggering capabilities**
  - Continuous internal trigger
  - External TTL trigger
  - Single input pulse activating laser lamp and Q-switch
  - Separate pulses to control lamp & Q-switch independently for precise laser pulse timing control
- **Easy set up:**
  - Single power supply features internal, closed-loop cooling system
  - Operates on 95-240 VAC single phase source
- **Convenient operation made possible with:**
  - Remote positioning of a single power supply - saves valuable lab space
  - Local control panel on power supply with all system controls, including optional optical attenuator
- **Hi/Lo power switch permits energy reduction during optics alignment**

Reliable Operation

- Thermally compensated resonator assures stable operation.
- Requires minimal maintenance, increasing system up-time.
- Field-proven reliability permits users to concentrate on their applications, rather than on system upkeep.

Exceptional Performance

- Superior, proven design provides stable, high-energy output with excellent beam quality and pulse-to-pulse stability.
- Compact resonator design provides excellent beam pointing and energy stability.
- Predictable, high performance ensures that your work gets done faster.

NEW WAVE RESEARCH

Appendix 4 Calibration Certificates for Liquid Rotameters

Calibration sheets are included for the following:

1. 2-20 LPH
2. 16-160 LPH
3. 100-1000 LPH

Kontrollblatt
Durchflussmesser

Control sheet
flowmeter

KOBOLD

Kundenauftragsnummer - p/o N° 1470012315

Gegenstand / object	: Durchflussmesser / flowmeter	Messbereich Einheit / range unit	:	l/h
Geräte Typ / instrument type	: V31	Messbereich Qv min / range Qv min	:	2
Serien-Nr./TAG Nr. / serial-no./TAG N°	311.100	Messbereich Qv max / range Qv max	:	20
Umformertyp / converter type	: kein/non	Qv max Eichmedium / Qv max desired values	:	20 l/h
Druckverlust / pressure drop	:	Ausgang / output	:	kein/non . - 20 mA
		Prüfstand / testrig	:	1300

Die Meßgenauigkeit des Gerätes liegt bei örtlicher Anzeige innerhalb der Toleranz von +/- 1,60% v.Skalenendwert
at local indication the accuracy of the instrument is inside the measuring variation of +/- 1,60% of span

Bei dem elektrischen Ausgangssignal innerhalb der Toleranz von +/- vom Skalenendwert
at electrical output signal within the measuring variation of +/- of span

1	2	3	4	5	6	7
Durchflußanzeige Skalenwert / flow indication scale value	Durchflußwerte Sollwerte des Eichmediums / flow values (desired values) of the calibration product H2O / Luft (air)	Istwert des Eichmediums / actual value of the calibration product	Anzeigefehler empirisch in % vom Endwert / mistakes of indication empirically % of the end value in %	Sollwert des elektr. Ausgangssignals / desired value of the electrical output-signal in mA	Istwert des elektr. Ausgangssignals / actual value of the electrical output-signal in mA	Anzeigefehler elektrisch vom Endwert / mistakes of indication electrical of the end value in %
l/h	l/h	l/h				
0,00	0,00	0,00	0,00%	kein/non	kein/non	0,00%
2,00	2,00	2,02	0,10%			
4,00	4,00	4,04	0,20%			
6,00	6,00	6,16	0,80%			
8,00	8,00	8,07	0,35%			
10,00	10,00	10,07	0,35%			
12,00	12,00	12,00	0,00%			
14,00	14,00	14,10	0,50%			
16,00	16,00	16,18	0,90%			
18,00	18,00	18,29	1,45%			
20,00	20,00	20,10	0,50%			

Die Kalibrierung des oben angegebenen Messgerätes wurde gegen Normale durchgeführt,die sich auf nationale Standards zurückführen lassen.
The calibration of the above indicated instrument has been done against standards, which accuracy is traceble to National Standards.

Das angegebene Messgerät erfüllt die in unseren Spezifikationen angegebenen Genauigkeitsdaten.
The indicated instrument meets the accuracy data published in the specifications.

Qualitäts-Sicherung Datum/Stempel Unterschrift/signature	Kunden-Abnehmer Datum/Stempel Unterschrift/signature	aut./amtl. Abnehmer Datum/Stempel Unterschrift/signature	Datum / Unterschrift Date / signature
			Heinrichs Messtechnik GmbH, Robert-Perthel-Straße 9, D-50739 Köln, 22.07.2015

Kontrollblatt
Durchflussmesser

Control sheet
flowmeter

KOBOLD

Kundenauftragsnummer - p/o N°: 1470010093

Gegenstand / object	: Durchflussmesser / : flowmeter	Messbereich Einheit / range unit	: l/h
Geräte Typ / instrument type	: V31	Messbereich Qv min / range Qv min	: 16
Serien-Nr./TAG Nr. / serial-no./TAG N°	298.820	Messbereich Qv max / range Qv max	: 160
Umformertyp / converter type	: kein/non	Qv max Eichmedium / Qv max desired values	: 160 l/h
Druckverlust / pressure drop	:	Ausgang / output	: kein/non - 20 mA
		Prüfstand / testrig	: 1302

Die Meßgenauigkeit des Gerätes liegt bei örtlicher Anzeige innerhalb der Toleranz von +/- 1,60% v.Skalenendwert
at local indication the accuracy of the instrument is inside the measuring variation of 1,60% of span

Bei dem elektrischen Ausgangssignal innerhalb der Toleranz von +/- vom Skalenendwert
at electrical output signal within the measuring variation of of span

1	2	3	4	5	6	7
Durchflußanzeige Skalenwert	Durchflußwerte Sollwerte des Eichmediums	Istwert des Eichmediums	Anzeigefehler empirisch in % vom Endwert	Sollwert des elektr. Ausgangssignals	Istwert des elektr. Ausgangssignals	Anzeigefehler elektrisch vom Endwert
flow indication scale value	flow values (desired values) of the calibration product H2O / Luft (air)	actual value of the calibration product	mistakes of indication empirically % of the end value in %	desired value of the electrical output-signal in mA	actual value of the electrical output-signal in mA	mistakes of indication electrical of the end value in %
l/h	l/h	l/h				
0,00	0,00	0,00	0,00%	kein/non	kein/non	0,00%
16,00	16,00	15,95	-0,03%			
20,00	20,00	20,20	0,13%			
40,00	40,00	39,80	-0,13%			
60,00	60,00	59,60	-0,25%			
80,00	80,00	80,10	0,06%			
100,00	100,00	99,20	-0,50%			
120,00	120,00	119,80	-0,13%			
140,00	140,00	139,30	-0,44%			
160,00	160,00	159,80	-0,12%			

Die Kalibrierung des oben angegebenen Messgerätes wurde gegen Normale durchgeführt,die sich auf nationale Standards zurückführen lassen.

The calibration of the above indicated instrument has been done against standards, which accuracy is traceble to National Standards.

Das angegebene Messgerät erfüllt die in unseren Spezifikationen angegebenen Genauigkeitsdaten.

The indicated instrument meets the accuracy data published in the specifications.

Qualitäts-Sicherung Datum/Stempel Unterschrift/signature	Kunden-Abnehmer Datum/Stempel Unterschrift/signature	aut./amtl. Abnehmer Datum/Stempel Unterschrift/signature	Datum / Unterschrift Date / signature
			01.04.2014

Kontrollblatt
Durchflussmesser

Control sheet
flowmeter

KOBOLD

Kundenauftragsnummer - p/o N°	1470010093	Messbereich Einheit / range unit	: l/h
Gegenstand / object	: Durchflussmesser / : flowmeter	Messbereich Qv min / range Qv min	: 100
Geräte Typ / instrument type	: V31	Messbereich Qv max / range Qv max	: 1000
Serien-Nr./TAG Nr. / serial-no./TAG N°	298.821	Qv max Eichmedium / Qv max desired values	: 1000 l/h
Umformertyp / converter type	: kein/non	Ausgang / output	: kein/non - 20 mA
Druckverlust / pressure drop	:	Prüfstand / testrig	: 1303

Die Meßgenauigkeit des Gerätes liegt bei örtlicher Anzeige innerhalb der Toleranz von + / - 1,60% v.Skalenendwert
at local indication the accuracy of the instrument is inside the measuring variation of 1,60% of span

Bei dem elektrischen Ausgangssignal innerhalb der Toleranz von + / - vom Skalenendwert
at electrical output signal within the measuring variation of of span

1	2	3	4	5	6	7
Durchflußanzeige Skalenwert	Durchflußwerte Sollwerte des Eichmediums	Istwert des Eichmediums	Anzeigefehler empirisch in % vom Endwert	Sollwert des elektr. Ausgangssignals	Istwert des elektr. Ausgangssignals	Anzeigefehler elektrisch vom Endwert
flow indication scale value	flow values (desired values) of the calibration product	actual value of the calibration product	mistakes of indication empirically % of the end value	desired value of the electrical output-signal	actual value of the electrical output-signal	mistakes of indication electrical of the end value
	H2O / Luft (air)		in %	in mA	in mA	in %
l/h	l/h	l/h				
0,00	0,00	0,00	0,00%	kein/non	kein/non	0,00%
100,00	100,00	102,00	0,20%			
200,00	200,00	201,00	0,10%			
400,00	400,00	399,00	-0,10%			
600,00	600,00	601,00	0,10%			
800,00	800,00	798,00	-0,20%			
1000,00	1000,00	999,00	-0,10%			

Die Kalibrierung des oben angegebenen Messgerätes wurde gegen Normale durchgeführt,die sich auf nationale Standards zurückführen lassen.

The calibration of the above indicated instrument has been done against standards, which accuracy is traceble to National Standards.

Das angegebene Messgerät erfüllt die in unseren Spezifikationen angegebenen Genauigkeitsdaten.

The indicated instrument meets the accuracy data published in the specifications.

Qualitäts-Sicherung Datum/Stempel Unterschrift/signature	Kunden-Abnehmer Datum/Stempel Unterschrift/signature	aut./amtl. Abnehmer Datum/Stempel Unterschrift/signature	Datum / Unterschrift Date / signature
________________	________________	________________	01.04.2014

Appendix 5 Derivation of Rotameter Flow Equation for Gases

Description

A rotameter is an instrucment for measuring liquid or gas flow (Fig. A5.1.) It consists of a vertical metering tube with diameter increasing from bottom to top (also known as a variable area meter.) A "float" is placed insite the tuge to serve as a marker against an external scale. Fluid enters the bottom of the metering tube, exiting at the top. Flow rate is read from the position of the float against the external scale. The float can be made of metal or plastic material.

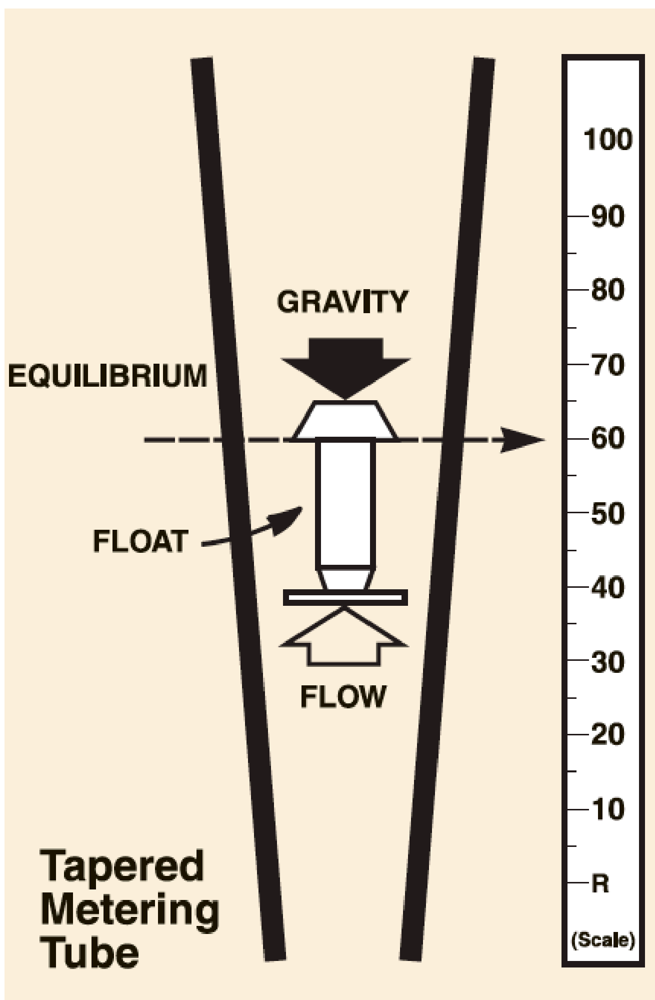

Figure A5.1 Rotameter Basic Structure (from Omega)

Principle of Operation

Drag forces from the upward flow of fluid and buoyancy forces from float-fluid density difference lift the float within the metering tube against gravity. The float reaches a static position when the fluid flowing past the float limits the upward drag force. At this point, the balance between upward and downward forces on the float is

$$F_d + F_b = F_g \tag{A5.1}$$

where drag force, buoyancy force and gravity force are given respectively by

$$F_d = \frac{C_D \rho_g A_s U_g^2}{2} \tag{A5.2}$$

$$F_b = V_s \rho_g g \tag{A5.3}$$

$$F_g = m_s g = V_s \rho_g g \tag{A5.4}$$

Substituting equations A5.2 through A5.4 into A5.1 gives

$$\frac{C_D \rho_g A_s U_g^2}{2} + V_s \rho_g g = V_s \rho_g g \tag{A5.5}$$

Solving for gas velocity, U_g,

$$U_g = \left[\frac{2}{C_D A_s} g V_s \frac{(\rho_s - \rho_g)}{\rho_g} \right]^{1/2} \tag{A5.6}$$

Now, for simplicity, assume the float has a circular cross section (i.e. a sphere or cylinder,) allowing us to say

$$A_s = \frac{\pi}{4} D_s^2 \tag{A5.7}$$

Substituting A5.7 into A5.6 yields

$$U_g = \left[\frac{8}{C_D \pi D_s^2} g V_s \frac{(\rho_s - \rho_g)}{\rho_g} \right]^{1/2} \tag{A5.8}$$

While rotameter floats come in various shapes, most of them exhibit a region of constant drag coefficient over a wide range of flow rates. For simplicity, assume it is a sphere. With its drag coefficient given in Fig. A5.2 below (from Schlichting, 1974):

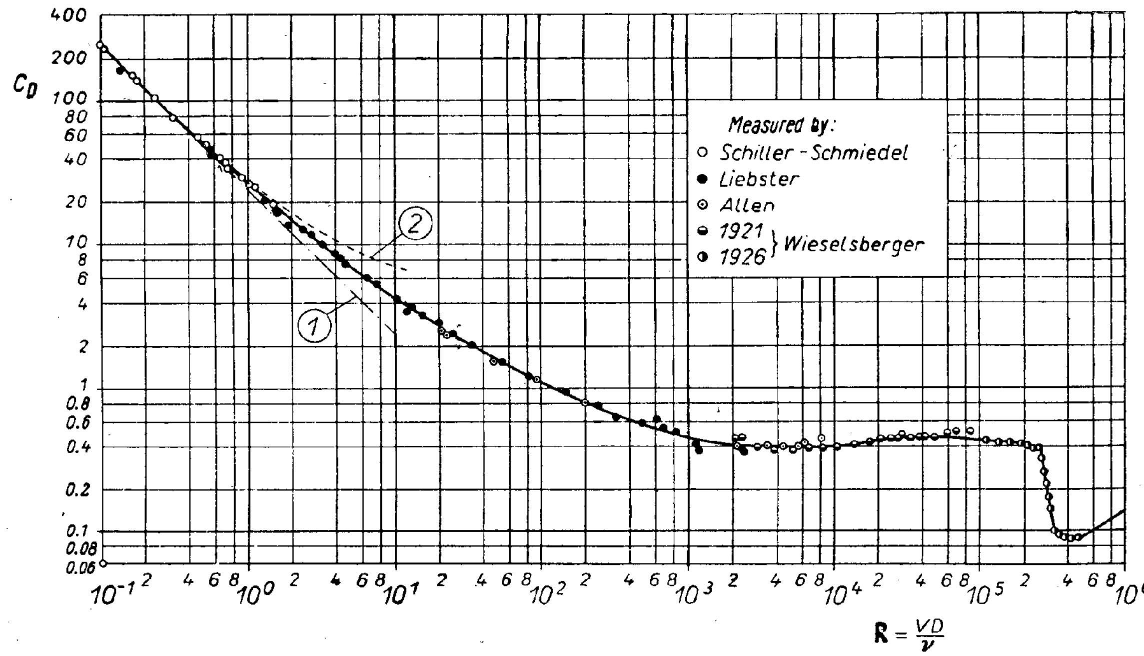

Figure A5.2 Drag Coefficient vs. Sphere Reynolds Number for Spheres.

Note that there is a range of Reynolds numbers for which C_D is constant. Making that assumption, we can develop the equations further. For gas flow, the float density will be greater than the gas density, i.e.

$$\rho_s - \rho_g \cong \rho_s \qquad \text{(A5.9)}$$

Then equation A5.8 can be simplified to,

$$U_g = k\left[\frac{V_s\rho_s}{\rho_g}\right]^{1/2} \qquad \text{(A5.10)}$$

where k represents some lumped constant terms,

$$k = \left[\frac{8g}{C_D\pi D_s^2}\right]^{1/2} \qquad \text{(A5.11)}$$

The volumetric flow rate, Q_g, can be expressed as

$$U_g = \frac{Q_g}{A_m} = k\left[\frac{V_s \rho_s}{\rho_g}\right]^{1/2} \tag{A5.12}$$

where A_m is the flow area between the tube and the float, i.e.

$$A_m = A_p - A_s = \frac{\pi}{4}\left(D_p^2 - D_s^2\right) \tag{A5.13}$$

Note that tube area, Dp increases with height in the rotameter. Rearranging to obtain an expression for volumetric flow rate,

$$Q_g = kA_m\left[\frac{V_s \rho_s}{\rho_g}\right]^{1/2} \tag{A5.14}$$

The density of the float can be expressed as

$$\rho_s = \frac{m_s}{V_s} \tag{A5.15}$$

and when substituted into A5.14 gives,

$$Q_g = kA_m\left[\frac{V_s m_s}{V_s \rho_g}\right]^{1/2} = kA_m\left[\frac{m_s}{\rho_g}\right]^{1/2} \tag{A5.16}$$

Assuming relatively low pressure operation, gas density can be well described by the ideal gas law,

$$\rho_g = \frac{PM}{RT} \tag{A5.17}$$

Substituting this into A5.16 above gives,

$$Q_g = kA_m\left[\frac{m_s RT}{PM}\right]^{1/2} \tag{A5.18}$$

Lumping constant terms by letting

$$k' = kA_m\left[m_s R\right]^{1/2} \tag{A5.19}$$

we find that

$$Q_g = k'A_m \left[\frac{T}{PM} \right]^{1/2} \tag{A5.20}$$

In a variable flow area rotameter, the annular flow area is a function of height (although not necessarily linear, i.e.

$$A_m = f(h) \tag{A5.21}$$

Thus, for a given temperature, pressure and gas, the flow rate can be indicated by the height of the float.

$$Q_g \propto h$$

Direct reading rotameters are calibration so that the scale indicates the flow rate correctly with a specified gas (usually air) under specified conditions (usually standard temperature and pressure.) In this case we can say,

$$Q_{std} = k'A_m \left[\frac{T_{std}}{P_{std} M_{air}} \right]^{1/2} \tag{A5.22}$$

At other than standard conditions, the flow rate is

$$Q_2 = k'A_m \left[\frac{T_2}{P_2 M_2} \right]^{1/2} \tag{A5.23}$$

This flow rate can be expressed using the calibrated scale by applying the following, as indicated in Fig A5.3.

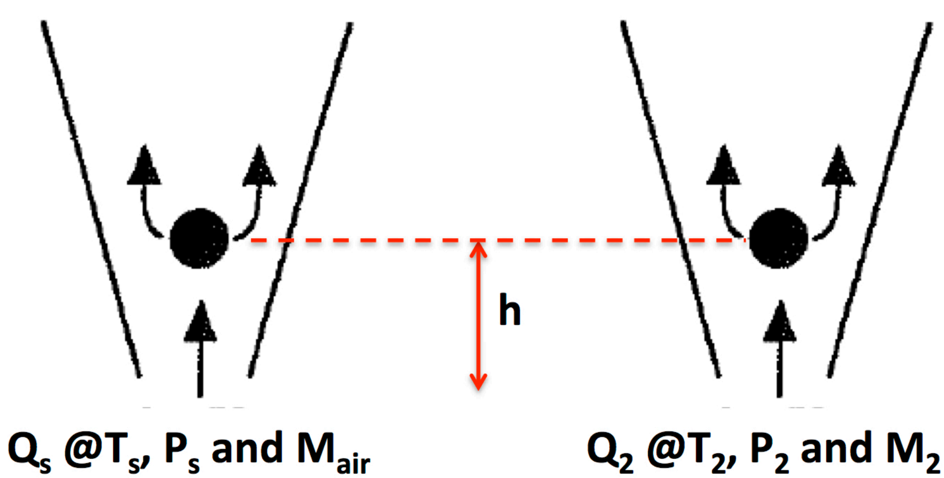

Figure A5.3 Equilibrium Conditions for Rotameter Float.

Note that the float will be at the same height (i.e. scale reading) when A_m is the same, therefore, by equating A_m in equations A5.2 and A5.23 we have

$$A_m = \frac{Q_{std}}{k'}\left[\frac{P_{std}M_{air}}{T_{std}}\right]^{1/2} = \frac{Q_2}{k'}\left[\frac{P_2M_2}{T_2}\right]^{1/2} \qquad (A5.24)$$

Rearranging to obtain an expression for Q2 gives,

$$Q_2 = \left[\frac{P_{std}M_{air}}{T_{std}}\frac{T_2}{P_2M_2}\right]^{1/2} Q_{std} \qquad (A5.26)$$

in which Q2 is the flow rate in actual volumes at T2 and P2 with gas of molecular weight M2 using the calibrated scale reading of Qstd.

While a useful result, the rate Q2 is commonly expressed at standard conditions. This is accomplished by again employing the real gas law,

$$\frac{P_2Q_2}{T_2} = \frac{P_{std}Q_{2std}}{T_{std}} \quad \therefore \quad Q_{2std} = \frac{T_{std}P_2}{P_{std}T_2}Q_2$$

Finally, substituting into equation A5.26,

$$Q_{std2} = \frac{T_{std}P_2}{P_{std}T_2}Q_2 = \frac{T_{std}P_2}{P_{std}T_2}\left[\frac{P_{std}M_{air}}{T_{std}}\frac{T_2}{P_2M_2}\right]^{1/2} Q_{std} \qquad (A5.27)$$

and finally (really this time) combining and simplifying terms,

$$Q_{std2} = \left[\frac{T_{std}^2P_2^2}{P_{std}^2T_2^2}\frac{P_{std}M_{air}}{T_{std}}\frac{T_2}{P_2M_2}\right]^{1/2} Q_{std}$$

$$Q_{std2} = \left[\frac{T_{std}P_2}{P_{std}T_2}\frac{M_{air}}{M_2}\right]^{1/2} Q_{std} \qquad (A5.28)$$

When measuring air, equation A5.28 reduces to

$$Q_{std2} = \left[\frac{T_{std}P_2}{P_{std}T_2}\right]^{1/2} Q_{std} \tag{A5.29}$$

Vendor-Supplied Equations

The derivation given is consistent with the equations recommended by vendors. For example, Cole Parmer (ref) gives the gas flow, corrected for temperature and pressure as,

$$Q_{std2} = Q_{std}\sqrt{\frac{P}{760}\frac{530}{T}} \tag{A5.30}$$

where Qstd is the rotameter scale reading at standard conditions with standard pressure is 760 mmHg (101.325 kPaa) and standard temperature is 530°R (21.3°C.) ABB (2003) gives the following,

$$Q_{2std} = Q_{std}\sqrt{\frac{G_1P_2T_1}{G_2P_1T_2}} \tag{A5.31}$$

where

Qstd is the indicated flow rate on the rotameter scale

G1 is specific gravity of calibration gas (usually air)

G2 is specific gravity of gas being measured

P1 is standard pressure (14.7 psia)

P2 is actual pressure

T1 is standard temperature (70°F)

T2 is actual temperature

Appendix 6 Extracting Data from Printed Graphs

In many cases where data was wanted for analysis it was unavailable in table form, often because the original source could not be obtained (e.g. early AERE internal reports.) However, the information was frequently published later in journals in graphic form. These graphic presentations could be scanned and tabular data then extracted with GraphClick, a software application for Macintosh OSX. When both graphic and tabular data were available together, an opportunity to assess the accuracy of the scanning method was available. This is especially important in the case of distorted images or logarithmic scales.

For an example of a scanned graph with linear scales, consider Figure A5.1 from Turner (1966) below:

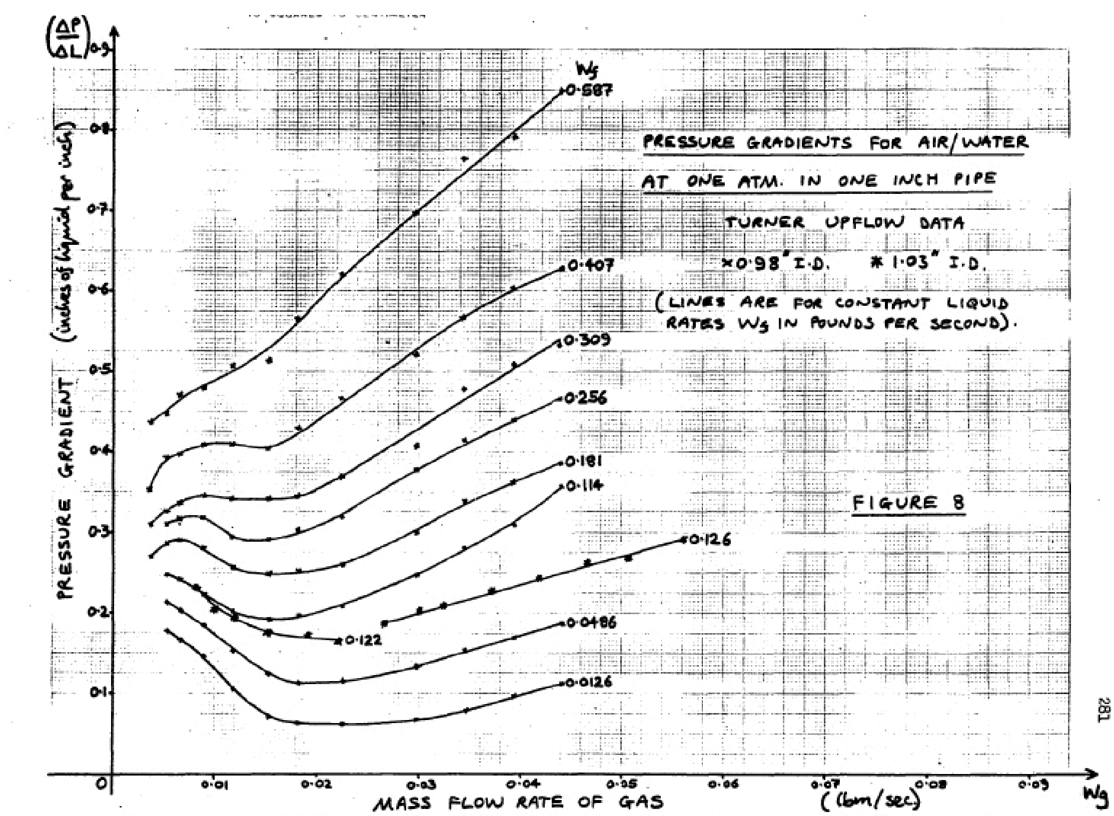

Figure A6.1 Original Graph of Pressure Gradient vs. Gas Flow from Turner (1966.)

This was plotted from data presented in a table in Turner's thesis. The measured data points are clearly visible. When selected data is scanned from the figure and compared with the original table (Turner's Table A-1) we find that the scanning process has retained the fidelity of the data (Figure A6.2.)

The average absolute error for these scanned data points was found to be 0.49%.

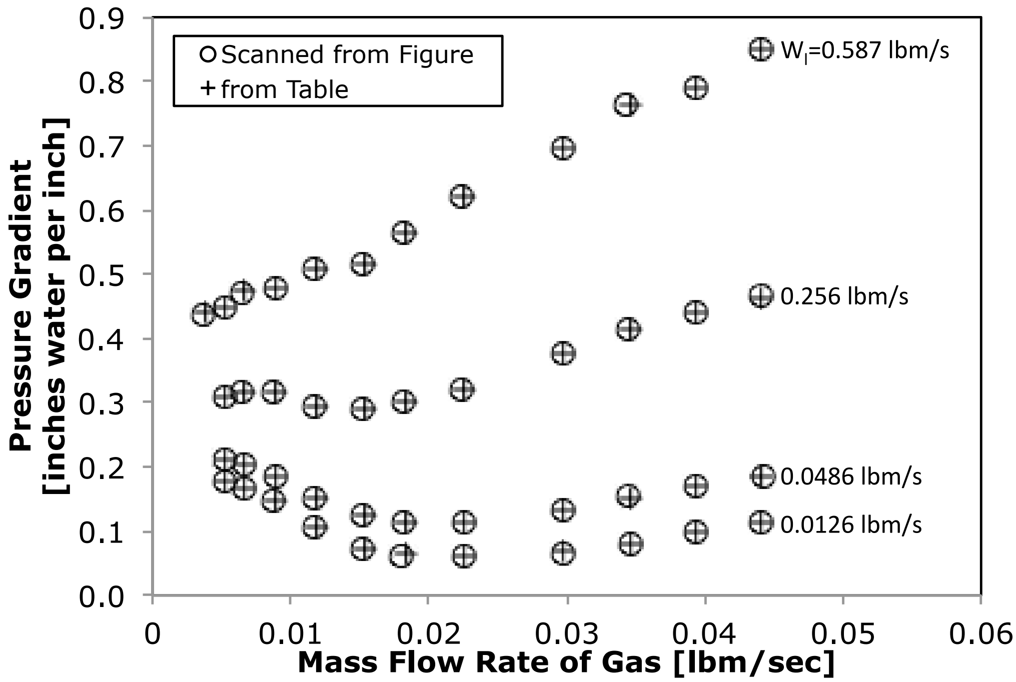

Figure A6.2 Scanned vs. Tabular Data from Turner's Fig. 8.

A more challenging example is that of a non-linear (e.g. logarithmic) scale, and where the axes are slightly tilted, such as the graph from Asali (1984) (Figure A5.3.)

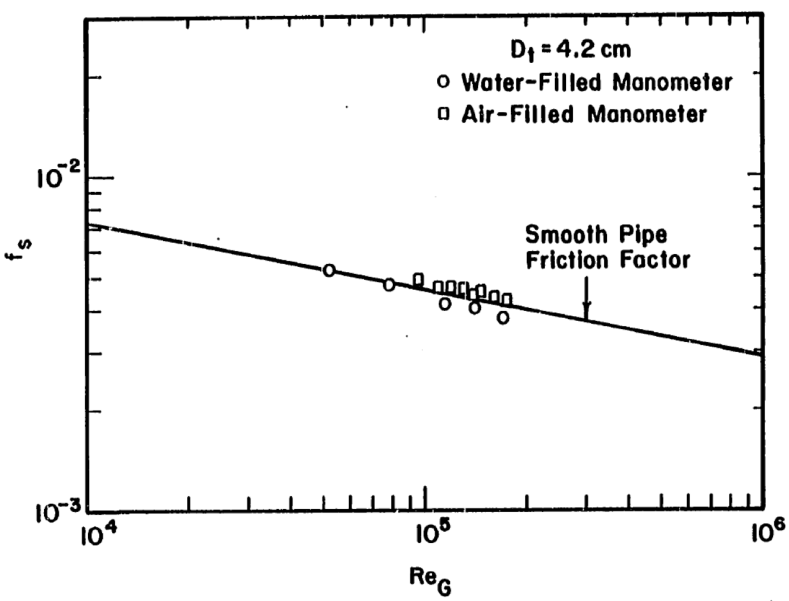

Figure 26. Pressure drop measurements for single-phase gas flow.

Figure A6.3 Original Graph of Friction Factor vs. Gas Reynolds Number from Asali (1984.)

When the data points in the figure are scanned and compared with those presented in Asali's thesis (his Table 16 for air-filled manometer) we find in Figure A6.4 that the correspondence exhibits only a small discrepancy; the average error in the value of f_s is only 0.71%.

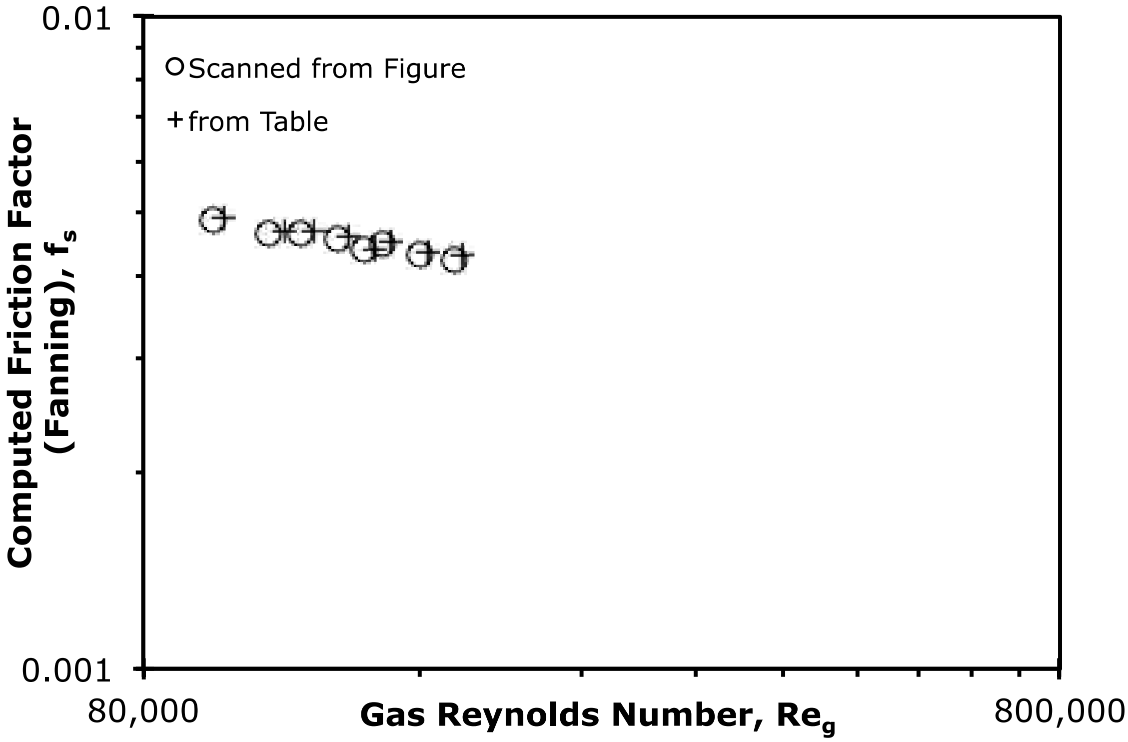

Figure A6.4 Comparison of Scanned vs. Tabular Data from Asali (1984.)

Appendix 7 Visual Basic for Applications (VBA) Code for Fluid Properties

```
Static Function Log10(x)
   Log10 = Log(x) / Log(10#)
End Function
Function CFJain(e, d, Nre)
'Calculate turbulent friction factor for rough pipe
'Inputs:  e, roughness
'         d, diameter
'       Nre, reynolds no.
'Outputs: f, friction factor
CFJain = (1.14 - 2 * Log10(e / d + 21.25 / Nre ^ 0.9)) ^ -2
End Function


Function FBlas(Re)
'Blasius friction factor for smooth pipe
'Inputs:  Reynolds number (dimensionless)
'Outputs:  friction factor, f (Moody)
'
FBlas = 0.3164 / Re ^ 0.25
End Function
Function FPrandtl(Re)
'Prandtl friction factor for smooth pipe (iterative)
'Inputs:  Reynolds number (dimensionless)
'Outputs:  friction factor, f (Moody)
'
f = FBlas(Re) 'initial guess
For i = 1 To 100
fnew = (2# * Log10(Re * f ^ 0.5) - 0.8) ^ -2#
diff = Abs(fnew - f) / fnew
f = fnew
If diff < 0.0001 Then GoTo done
Next i
done:
FPrandtl = fnew
End Function


Function CFZig(e, d, Re)
'Friction factor from Zigrang and Sylvester, 1982
'Inputs:  abs. roughness, e; pipe diameter, D; Reynolds Number, Re
'Outputs:  friction factor, lamda
'
'Note:  explicit calculation
'
Rough = e / d
Part1 = Rough / 3.7 + 14 / Re
Part2 = Rough / 3.7 - 5.2 / Re * Log10(Part1)
Part3 = -2# * Log10(Part2)
CFZig = 1# / Part3 ^ 2
End Function
```

```
Function AirVisc(T, P)
' Dry air viscosity from Kadoya et al, 1985
'Inputs:
'     Temperature, T, deg C
'     Pressure, P, kPaa
'Outputs:
'     Air viscosity, Pa-s x 1E-6
'NOTE:  This version good for P ~ 1 atm, and T from 250-300K; for higher pressures,
temps, include z factor in calculation of rhoair
'
T = T + 273.15 ' change to absolute temperature
Tr = T / 132.5
rhoair = P * 28.9644 / (8.3145 * T) ' air density at given T, P
P = P / 1000 ' change to MPa
rhored = rhoair / 314.3
NuoTr = 0.128517 * Tr + 2.60661 * Sqr(Tr) + (-1) + -0.709661 * Tr ^ (-1) +
0.662534 * Tr ^ (-2) - 0.197846 * Tr ^ (-3) + 0.00770147 * Tr ^ (-4)
NuoRhor = 0.465601 * rhored + 1.26469 * rhored ^ 2 - 0.511425 * rhored ^ 3 +
0.2746 * rhored ^ 4
AirVisc = 6.1609 * (NuoTr + NuoRhor)
End Function


Function WtrVisc(T, P)
'Pure Water viscosity from McCain et al book, 2011
'Inputs:
'     Temperature, T, deg C
'     Pressure, P, kPaa
'Output:
'     Water Viscosity, Pa-s
'
TK = T + 273.15 ' calculate temperature in Kelvin
rhow = WtrDens(T, P) 'need to obtain density of pure water
LNUW1 = 2885317# * TK ^ -2 - 11072.577 / TK - 9.0834095 + 0.030925651 * TK -
2.74071e-05 * TK ^ 2
LNUw2 = -1928385.1 / TK ^ 2 + 5621.6046 / TK + 13.82725 - 0.047609523 * TK +
3.5545041e-05 * TK ^ 2
LNUw = LNUW1 + rhow * LNUw2
WtrVisc = Exp(LNUw)
End Function


Function WtrDens(T, P)
'Pure Water density from McCain et al book, 2011
'Inputs:
'     Temperature, T, deg C
'     Pressure, P, kPaa
'Output:
'     Water Density, g/cm3
'
TH = T / 100 ' create term for intermediate use
```

```
PM = P / 1000 ' need to have pressure in MPa for this correlation
Rhow70 = (-0.127213 * TH ^ 2 + 0.645486 * TH + 1.03265) / (-0.070291 * TH ^ 2
+ 0.639589 * TH + 1)
Ew = (4.221 * TH ^ 2 + -3.478 * TH + 6.221) / (0.5182 * TH ^ 2 - 0.4405 * TH +
1)
Fw = (-11.403 * TH ^ 2 + 29.932 * TH + 27.952) / (0.20684 * TH ^ 2 + 0.3768 *
TH + 1)
Iw70 = 1 / Ew * Log(Ew + Fw)  'Log is actually the natural log function in VBA, i.e.
LN(x)<
Iw = 1 / Ew * Log(Ew * PM / 70 + Fw)
WtrDens = Rhow70 * Exp(Iw - Iw70)
End Function
```

Appendix 8 Test Matrix External Images Poster

(Larger format to be supplied in final version (the file is about 100MB!)